

Universidade Federal do Rio Grande – FURG

Instituto de Oceanografia

Programa de Pós-Graduação em Oceanologia

**RELAÇÃO ENTRE AS COMUNIDADES
FITOPLANCTÔNICAS E OS FLUXOS DE
DIÓXIDO DE CARBONO NO OCEANO
ATLÂNTICO SUL**

ANDRÉA DA CONSOLAÇÃO DE OLIVEIRA CARVALHO

Tese apresentada ao
Programa de Pós-Graduação em
Oceanologia, como parte dos requisitos
para a obtenção do Título de Doutor.

Orientador: *Prof. Dr.* RODRIGO KERR Duarte Pereira
Universidade Federal do Rio Grande (FURG), Brasil.

Coorientador: *Prof. Dr.* Carlos RAFAEL Borges MENDES
Universidade Federal do Rio Grande (FURG), Brasil.

Rio Grande, RS, Brasil

Setembro 2020

**RELAÇÃO ENTRE AS COMUNIDADES
FITOPLANCTÔNICAS E OS FLUXOS DE
DIÓXIDO DE CARBONO NO OCEANO
ATLÂNTICO SUL**

Tese apresentada ao Programa de Pós-Graduação em Oceanologia,
como parte dos requisitos para a obtenção do Título de Doutor

por

ANDRÉA DA CONSOLAÇÃO DE OLIVEIRA CARVALHO

Rio Grande, RS, Brasil

Setembro 2020

© A cópia parcial e a citação de trechos desta tese são permitidas sobre a condição de que qualquer pessoa que a consulte reconheça os direitos autorais do autor. Nenhuma informação derivada direta ou indiretamente desta obra deve ser publicada sem o consentimento prévio e por escrito do autor.

CARVALHO, ANDRÉA DA CONSOLAÇÃO DE OLIVEIRA
Relação entre as comunidades fitoplanctônicas e os fluxos de dióxido de carbono no oceano Atlântico Sul./ Andréa da Consolação de Oliveira Carvalho. – Rio Grande: FURG, 2020.
219 p.
Tese (Doutorado) – Universidade Federal do Rio Grande. Doutorado em Oceanologia. Área de Concentração: Oceanografia Biológica; Oceanografia Química.
1. Pigmentos fitoplanctônicos. 2. Ciclo do Carbono. 3. Pressão parcial do CO₂.



UNIVERSIDADE FEDERAL DO RIO GRANDE - FURG
IO – INSTITUTO DE OCEANOGRAFIA
PROGRAMA DE PÓS-GRADUAÇÃO EM OCEANOLOGIA
E-mail: ccpofgg@furg.br – home-page: www.ppgq.furg.br




ATA ESPECIAL DE DEFESA DE TESE DE DOUTORADO – 08/2020

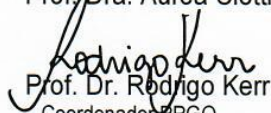
Às 09h do dia 28 de setembro do ano de dois mil e vinte, por videoconferência, reuniu-se a Comissão Examinadora da Tese de **DOUTORADO** intitulada "**Relação entre as comunidades fitoplanctônicas e os fluxos de dióxido de carbono no oceano atlântico sul**", da **Acad. Andréa da Consolação de O. Carvalho**. A Comissão Examinadora foi composta pelos seguintes membros: Prof. Dr. Rodrigo Kerr Duarte Pereira – Orientador/Presidente (IO/FURG), Prof. Dr. Carlos Rafael Borges Mendes – Co-orientador (IO/FURG), Profa. Dra. Eunice da Costa Machado (IO/FURG), Profa. Dra. Virginia Maria Tavano (IO/FURG), Prof. Dr. José Luiz Lima de Azevedo (IO/FURG) e Profa. Dra. Aurea Ciotti (IO/USP). Dando início à reunião, o Orientador e Presidente da sessão, Prof. Dr. Rodrigo Kerr Duarte Pereira, agradeceu a presença de todos e fez a apresentação da Comissão Examinadora. Logo após, esclareceu que a Candidata teria um tempo de 45 a 60 min para explanação do tema e cada membro da Comissão Examinadora um tempo máximo de 30 min para perguntas. A seguir, passou à palavra a Candidata, que apresentou o tema e respondeu as perguntas formuladas. Após ampla explanação, a Comissão Examinadora reuniu-se em reservado para discussão do conceito a ser atribuído a Candidata. Foi estabelecido que as sugestões de todos os membros da Comissão Examinadora, que seguem em pareceres em anexo, foram aceitas pelo Orientador/Candidata para incorporação na versão final da Tese. Finalmente, a Comissão Examinadora considerou a candidata **APROVADA**, por unanimidade. Nada mais havendo a tratar, foi lavrada a presente ATA que após lida e aprovada, será assinada pela Comissão Examinadora, pela Candidata e pelo Coordenador do Programa de Pós-Graduação em Oceanologia.

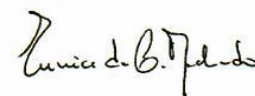

Prof. Dr. Rodrigo Kerr Duarte Pereira
Presidente



Prof. Dr. Carlos Rafael Borges Mendes


Prof. Dr. Jose Luiz Lima de Azevedo

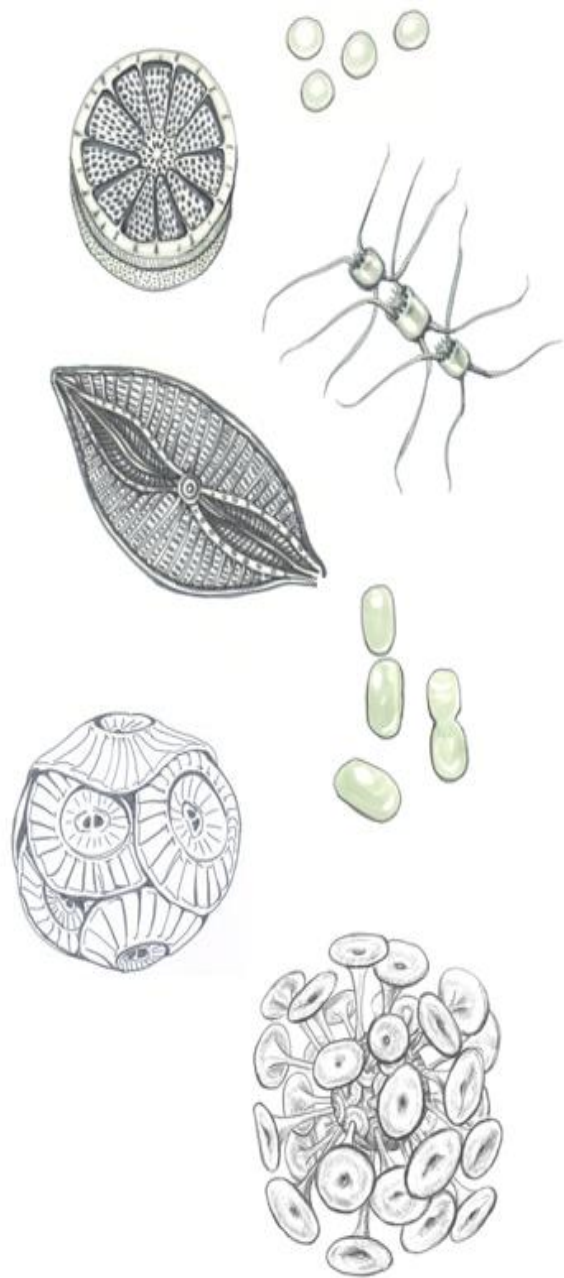

Prof. Dra. Aurea Ciotti


Prof. Dr. Rodrigo Kerr
Coordenador PPGO


Profa. Dra. Eunice Machado


Profa. Dra. Virginia Maria Tavano


Acad. Andréa da Consolação de O. Carvalho



*“I’ve learned that you are never too small
to make a difference”*

Greta Thunberg

Ilustrações: K. Krumhardt

Índice

Agradecimentos	x
Lista de Figuras	xii
Lista de Acrônimos e Abreviações	xvii
Resumo	xviii
Abstract	xx
Prefácio	xxii
Hipótese	xxvi
Capítulo I: Introdução.....	27
1.1 O aumento das concentrações do CO ₂ atmosférico e o ciclo do carbono no ambiente marinho	29
1.2 O fitoplâncton e seu papel na bomba biológica do carbono	32
1.3 Diferenciação dos grupos fitoplanctônicos	34
Objetivos	40
Capítulo II: Oceano Atlântico Sul.....	41
2.1 As províncias biogeoquímicas do oceano Atlântico Sul entre 20°S e 35°S.....	44
2.1.1 O sistema dominado por corrente de contorno oeste	45
2.1.2 O giro central do oceano Atlântico Sul	46
2.1.3 O sistema dominado por corrente de contorno leste.....	47
2.2 Plataformas continentais da Costa Sul-Sudeste do Oeste do Oceano Atlântico Sul (20°S a 50°S).....	49
2.2.1. A costa Sul-Sudeste brasileira	50
2.2.2. A Plataforma continental da Patagônia Argentina.....	51
Capítulo III: Dados e métodos.....	52
3.1 Análise dos parâmetros do sistema carbonato	56
3.1.1 Pressão parcial do CO ₂ (pCO ₂)	57
3.1.2 Alcalinidade total (A _T) e carbono inorgânico dissolvido total (C _T).....	59
3.2 Cálculos dos fluxos líquidos de CO ₂	60
3.3 Composição da comunidade fitoplanctônica.....	61
3.3.1 Análise de composição pigmentar por HPLC/CHEMTAX ..	62
3.4 Análises Estatísticas.....	64
3.5 Efeito da temperatura e da biologia no controle da pCO ₂	65

Capítulo IV: Distribuição do fitoplâncton nos vórtices anticiclônicos.....	67
4.1 Introduction	69
4.2 The FORSA Cruise	74
4.3 Data and Methods	75
4.3.1 <i>Physical and chemical data.....</i>	75
4.3.2 <i>Phytoplankton sampling and HPLC pigment analysis</i>	77
4.3.3 <i>Pigment indices.....</i>	79
4.3.4 <i>Chemotaxonomic analysis of HPLC data</i>	80
4.3.5 <i>Statistical analysis.....</i>	81
4.4 Results	82
4.4.1 <i>Hydrographical/environmental setting.....</i>	82
4.4.2 <i>Phytoplankton biomasses, pigment concentrations, and indices.....</i>	83
4.4.3 <i>Chemotaxonomic groups of phytoplankton</i>	86
4.4.4 <i>Phytoplankton association with environmental and physiological parameters.....</i>	89
4.5 Discussion	91
4.6 Conclusion.....	99
Capítulo V: Relação entre a captação de CO₂ e os grupos do fitoplâncton.....	100
5.1 Introduction	103
5.2 Biogeochemical provinces of the South Atlantic Ocean.....	106
5.3 Data and Methodology	110
5.3.1 <i>Cruise Sampling.....</i>	110
5.3.2 <i>Data for pCO₂ and FCO₂ calculations.....</i>	112
5.3.3 <i>Phytoplankton pigment analyses and chemotaxonomic groups.....</i>	114
5.3.4 <i>Statistical analysis.....</i>	116
5.4 Results	117
5.4.1 <i>Environmental physical conditions and phytoplankton biomass.....</i>	117
5.4.2 <i>Distribution of pCO₂ and net CO₂ fluxes in the South Atlantic Ocean</i>	120
5.4.3 <i>Phytoplankton group distribution in the South Atlantic Ocean</i>	121
5.4.4 <i>Relationships between environmental properties, CO₂</i>	

<i>dynamics and phytoplankton group biomasses</i>	123
5.5 Discussion	128
5.5.1 <i>Western boundary current dominated system (BRAZ)</i>	128
5.5.2 <i>South Atlantic subtropical gyre system (SATL)</i>	132
5.5.3 <i>Eastern boundary current dominated system (AFR)</i>	134
5.5.4 <i>Relevant phytoplankton groups associated with CO₂ uptake in the South Atlantic Ocean</i>	137
Capítulo VI: FCO₂ e o grupo do fitoplâncton dominante em áreas costeiras do Atlântico Sul e Sudeste	141
6.1 Introduction	143
6.2 Data and Methods	147
6.2.1 <i>Oceanographic Cruises</i>	147
6.2.2 <i>Calculations of pCO₂ and FCO₂</i>	148
6.2.3 <i>Controls on pCO₂^{sw}: temperature vs. biological effects</i>	149
6.2.4 <i>Determination of main phytoplankton groups</i>	151
6.2.5 <i>Statistical analysis</i>	153
6.3 Results	153
6.3.1 <i>SST, SSS, phytoplankton biomass and FCO₂ spatial variability</i>	153
6.3.2 <i>Dominant phytoplankton groups</i>	155
6.4 Temperature and biological controls on pCO₂^{sw}	158
6.5 Relationship between phytoplankton distribution and FCO₂	158
6.6 Discussion	161
6.6.1 <i>Physical and ecological processes along the southwestern South Atlantic shelves triggers contrasting biogeochemical behaviors</i>	161
6.6.2 <i>What is the role of biology on FCO₂ dynamics in SAO western coast?</i>	164
6.6.3 <i>Linking CO₂ uptake magnitudes and phytoplankton groups </i>	166
6.7 Remarks on future approaches	171
Capítulo VII: Síntese da Discussão e Conclusões	173
7.1 O impacto dos vórtices de mesoescala nas comunidades fitoplanctônicas no oceano Atlântico Sul através da ferramenta HPLC- CHEMTAX.	173

7.2 Grupos do fitoplâncton fortalecem a captação de CO₂ pelo oceano Atlântico Sul	176
7.3 Contraste entre as plataformas continentais do sudoeste do oceano Atlântico Sul em relação a magnitude do FCO₂ e os grupos dominantes do fitoplâncton.....	180
7.4 Considerações finais e direcionamentos futuros	181
ANEXO I.....	186
ANEXO II.....	194
Capítulo VIII:Referências Bibliográficas	201

Agradecimentos

Ao longo desses quatro anos, foram muitos os que me ajudaram a chegar na versão final desse documento escrito, mas, principalmente, em uma versão mais aprimorada da pessoa e da profissional que sou hoje. A todos os que contribuíram para que hoje eu tenha um pouco mais de conhecimento, experiências, disciplina, milhas náuticas navegadas, segurança, foco, dedicação, paciência e um olhar cada vez mais encantado pela ciência:

Ao meu orientador Rodrigo Kerr e ao meu coorientador Rafael Mendes, por todos os ensinamentos e disponibilidade. Agradeço a confiança depositada em mim e no meu trabalho, e todo o apoio direcionado para a minha formação acadêmica.

À minha banca de acompanhamento: Professora Virginia M. Tavano e Professor José Luiz L. Azevedo, pelas cuidadosas revisões, pela coautoria nos artigos elaborados durante o doutorado, pela presença nos seminários e por todas as valiosas considerações ao longo do meu trabalho.

Ao amigo e oceanógrafo Felipe Galdino (Chico) pela sua contribuição e coautoria no primeiro artigo publicado.

Aos tripulantes e as equipes científicas embarcadas nos diversos cruzeiros oceanográficos do GOAL e da rede BrOA, cujos dados foram utilizados para a realização desse trabalho, por todo o esforço amostral.

A todos os integrantes do CEOCEAN, professores, técnicos, pós-docs, mestrandos, doutorandos, alunos de graduação, pela convivência agradável e aprendizado ao longo desses anos.

Aos integrantes do Laboratório do Fitoplâncton e Micro-organismos Marinhos - LabFito pelo acolhimento e ensinamentos.

Em especial, ao *CARBON Team*, por todos os valiosos momentos de trocas de conhecimento em reuniões, workshops e confraternizações (presenciais e online). Pela dedicação de todos em prol do fortalecimento e evolução do grupo, e por ajudarem a manter o ânimo e a produtividade, principalmente durante esse período de isolamento.

A FURG e ao Programa de Pós-Graduação em Oceanologia.

A CAPES pelo fomento através da bolsa de doutorado.

À minha família: avós, pai, mãe, irmãs, cunhados, sobrinhos, tios e primos, por todo amor e carinho, mesmo à distância souberam se fazer presentes, em todos os momentos, incentivando, apoiando e torcendo pelo meu crescimento e sucesso.

Ao Josué, por seu amor e companheirismo em todos os momentos. Por toda a força, apoio e incentivo ao longo desses quatro anos, meu porto seguro nesta terra tão longe de casa.

A todos os meus amigos e colegas do trabalho e da vida (não vou citar nomes, pois certamente não incluiria todos) pela troca de experiências, pela agradável companhia do dia-a-dia, sempre dispostos elevar o ânimo nas horas difíceis, tornando tudo mais leve e agradável. E aos que mesmo estando longe, souberam estar sempre por perto, com o mesmo carinho e amizade.

A Deus, amor incondicional, sempre comigo.

Muito obrigada a todos que estiveram comigo nessa caminhada!

Lista de Figuras

- Figura 1.** Médias mensais da concentração global de CO₂ em período recente (esquerda) e no registro completo desde o início das medições no final da década de 70 (direita). Fonte: Modificada de ESRL NOAA.....**29**
- Figura 2.** Absorção de CO₂ antropogênico pelos oceanos globais. Nesta figura, as áreas onde o oceano absorveu dióxido de carbono produzido pelo homem são as áreas verdes e as áreas onde o oceano liberou CO₂ de volta para a atmosfera são as áreas em roxo. Figura adaptada do [State of the Climate Report \[2017\]](#), NOAA Climate.gov.....**30**
- Figura 3.** Esquema dos processos da bomba biológica. O fitoplâncton fixa o carbono inorgânico na zona eufótica através da energia solar (fotossíntese) e o transforma em carbono orgânico. Com a dissociação do ácido carbônico temos a formação dos íons carbonato e bicarbonato que irão compor a estrutura de diversos organismos, através da formação do carbonato de cálcio, e com sua morte, subsequente afundamento da matéria orgânica particulada (MOP) contribuirá para estoques de carbono nos sedimentos.....**33**
- Figura 4.** Diferenciação evolutiva dos grupos fitoplanctônicos. Figura adaptada de [Falkowski et al. \[2003\]](#).....**35**
- Figura 5.** Contribuição percentual dos diferentes grupos do fitoplâncton marinho em relação a diversidade de espécies identificadas. Diatomáceas, dinoflagelados e em menor percentual haptófitas e algas verdes são os grupos mais diversificados com aproximadamente, 40%, 40%, 10% e 6% de espécies descritas, respectivamente. Gráfico adaptado de [Simon et al. \[2009\]](#).....**36**
- Figura 6.** Uma comparação da faixa de tamanho (dimensão linear máxima) do fitoplâncton é apresentada na linha superior. Na linha inferior são apresentados alguns exemplos dos grupos citados acima, mostrando as diferenças de estrutura corporal de cada organismo. Adaptado de [Finkel et al. \[2010\]](#).....**37**
- Figura 7.** Mapa da área de estudo. O retângulo pontilhado em vermelho destaca a porção interna do giro subtropical do Atlântico Sul. Os retângulos pontilhados em amarelo destacam as regiões costeiras em destaque neste estudo, tanto na porção ocidental como na porção oriental dessa bacia oceânica. As setas em azul destacam a circulação oceânica superficial do giro subtropical do Atlântico Sul: na borda ocidental temos a Corrente do Brasil e a Corrente das Malvinas, que convergem em aproximadamente 35°S. Neste lado da bacia também temos as descargas da Lagoa dos Patos (estrela magenta) e do Rio da Prata (estrela azul) atuando como as principais fontes de água doce para a plataforma continental. Na parte sul do giro do Atlântico Sul, a Corrente do Atlântico Sul flui para leste em direção à borda ocidental, fundindo-se com a Corrente de Benguela. A região da retroflexão da Corrente das Agulhas é uma entrada importante das águas do oceano Índico para o Atlântico, e os vórtices das Agulhas, indicados pelas elipses alaranjadas são liberados preferencialmente nessa região. Fechando o circuito do giro do Atlântico Sul, o ramo sul da Corrente Equatorial Sul é mostrado por uma linha pontilhada e tracejada em azul. A batimetria do fundo é representada por tons de cores (escala a direita). Características batimétricas importantes, tais como a elevação do Rio Grande, a Cordilheira Meso-Atlântica e a Cordilheira Walvis, estão indicadas no mapa.....**42**
- Figura 8.** Províncias biogeoquímicas globais, adaptadas de [Longhurst \[2006\]](#). Fonte: <http://www.mar.dfo-mpo.gc>.....**44**
- Figura 9.** Mapa das estações oceanográficas dos cruzeiros transatlânticos que fizeram rotas entre o Brasil e a África. As estações oceanográficas ao longo das seções hidrográficas amostradas no Oceano Atlântico Sul são marcadas como símbolos de acordo com os seguintes cruzeiros neste estudo: H40_2009 (círculos vermelhos), TAI 2009_30 ° S (círculos azuis), TAI 2009_20 ° S (círculos amarelos), TAI 2011_1 (diamantes verdes), TAI 2011_2 (diamantes turquesa), A10 2011 (cruzes pretas) e FORSA 2015 (triângulos magenta). As linhas no mapa delimitam as províncias biogeoquímicas de acordo com [Longhurst \[2006\]](#) e foram sobrepostas usando o shapefile de [VLIZ \[2009\]](#).....**53**
- Figura 10.** Mapa das estações oceanográficas referentes aos cruzeiros costeiros trabalhados

nesta tese ([Capítulo VI](#)) Em amarelo temos as estações referentes ao banco de dados do cruzeiro PATEX IV ocorrido em outubro de 2007, em vermelho as estações do cruzeiro PATEX VI de outubro de 2008. Em verde as estações do cruzeiro que cobriu a plataforma sul e sudeste do Brasil (campanha MCTII) ocorrida entre dezembro de 2010 e janeiro de 2011 e por fim, a campanha EstARte Sul de outubro de 2014.54

Figura 11. Variação das proporções relativas das espécies do CO₂ aquoso (CO₂^{*}), carbonato (CO₃²⁻) e bicarbonato (HCO₃⁻) na água do mar com o pH na temperatura de 25°C. Mostrando que o pH na água do mar é determinado por mudanças relativas nas concentrações de CO₃²⁻ e HCO₃⁻, uma vez que as concentrações de HCO₃⁻ na água do mar são relativamente estáveis. Com o aumento no pH, temos o aumento da concentração de CO₃²⁻ (K₁ e K₂ são a primeira e segunda constantes de dissociação do ácido carbônico). Adaptado de [Xue & Cai \[2020\]](#).57

Figure 12. a. Mean surface Chl *a* concentration (mg m⁻³) in the region of the Agulhas Corridor (South Atlantic Ocean) composited from satellite images over 18 days, with a 4 km resolution. Red circles mark the position where the three Agulhas eddies (E₁, E₃ and E₅) were sampled during the cruise. The lower panels represent the 8-day compositions centered on the day of each core sampling in the eddy, where b. E₅ was sampled on July 9, 2015; c. E₃ was sampled on July 5, 2015; and d. E₁ was sampled on July 1, 2015. The satellite Chl *a* concentration is represented by the color bar. The dashed isolines of the SLA show the shape of the eddy, and the strong black dots mark the locations of the four sampling stations at each eddy. Note that the differences in the color scale emphasize the spatial structure of the Chl *a* concentration.75

Figure 13. Vertical profiles of the photopigment indices in a. E₁, b. E₃ and c. E₅. Colored lines refer to PPC_{TP} (red), PSC_{TP} (blue) and TChl *a*TP (green). Each station is represented by a symbol (circles for control stations, squares for border stations, triangles for midway stations and diamonds for center stations). The black bold line represents the average density profile.86

Figure 14. Depth distribution of the phytoplankton group biomasses for E₁ (TChl *a*), calculated through the CHEMTAX program at the four different zones (control, border, midway and center), and the respective density (dashed blue line) and fluorescence (green line) profiles. The black horizontal line represents the MLD depth.87

Figure 15. Depth distribution of the phytoplankton group biomasses for E₃ (TChl *a*), calculated through the CHEMTAX program at the four different zones (control, border, midway and center), and the respective density (dashed blue line) and fluorescence (green line) profiles. The black horizontal line represents the MLD depth.88

Figure 16. Depth distribution of the phytoplankton group biomasses for E₅ (TChl *a*), calculated through the CHEMTAX program at the four different zones (control, border, midway and center), and the respective density (dashed blue line) and fluorescence (green line) profiles. The black horizontal line represents the MLD depth.89

Figure 17. CCA ordination diagram of the absolute contributions of different phytoplankton groups at the sea surface. The arrows indicate the explanatory variables (e.g., salinity, temperature, TChl *a*, DIN, PO₄³⁻, SiOH₄⁻, PSCs, PPCs), grazing and senescence). Blue stars refer to the absolute contributions of the phytoplankton groups. The stations are separated according to distinct eddies, where the stations in yellow represent the surface, and those in green represent the DCM stations (circles correspond to E₁, triangles correspond to E₃, and squares correspond to E₅).90

Figure 18. Evolution of surface Chl *a* along the trajectories of the three eddies (E₁- red contour; E₃- green contour; E₅- magenta contour) over the bathymetric map of the South Atlantic basin. The gray line represents the ship track. The circle in each trajectory marks the location where the eddies were sampled in this work. The Chl *a* values represent the 8 day mean (composite) centered on the day of the eddy location based on the eddy fields in the SLA data. For each day, a grid of approximately three degrees (1.5°W – 1.75°E, 1.5°N – 1.5°S) from the eddy center was computed. To remove the Chl *a* data that were not within the eddy field, the values of Chl *a* located in areas with less than a 0.05 cm SLA were discarded. The eddy trajectories have been extracted from the Mesoscale Eddy Trajectory Atlas product (<https://www.avisio.altimetry.fr>) [[Chelton et al. 2011](#), [Schlax & Chelton 2016](#)].93

Figure 19. South Atlantic Ocean. (a) Biogeochemical provinces (black lines) according to Longhurst [2006], which were overlaid on the map using the shapefile overlay from VLIZ [2009].

The acronyms refer to the Longhurst provinces: Brazil (BRAZ), South Atlantic Gyral (SATL), Benguela (BENG) and East African (EAFR). Here, the last two provinces are referenced together as Africa (AFR). The freshwater discharges of the Patos Lagoon (yellow star) and, particularly, the La Plata River (black star) are highlighted. The oceanographic stations along the hydrographic sections sampled in the South Atlantic Ocean are marked as symbols according to the following cruises in this study: H40_2009 (red circles), TAI 2009_30°S (blue circles), TAI 2009_20°S (yellow circles), TAI 2011_1 (green diamonds), TAI 2011_2 (turquoise diamonds), A10 2011 (black crosses) and FORSA 2015 (magenta triangles). (b) Chlorophyll concentration climatology (2002-2020) with main surface circulation arrows. The data were obtained from MODIS Aqua Ocean Color (chlorophyll a concentration) Level-3, OCI Algorithm. Subtropical South Atlantic circulation is described: on the western boundary side are the Brazil Current and the Malvinas Current, which converge at approximately 35°S (with meridional seasonal variations). On the southern part of the South Atlantic Gyre, the South Atlantic Current flows eastward toward the eastern boundary side, merging with the Benguela current. The Agulhas eddies shed in the Agulhas retroflexion region are indicated by the orange ellipses. Closing the loop of the South Atlantic Gyre, the southern branch of the South Equatorial Current (sSEC) is shown by a dotted-dashed line.....108

Figure 20. Spatial distribution of environmental parameters for each cruise along the South Atlantic Ocean. a. Sea surface temperature (°C) b. Sea surface salinity c. Total Chlorophyll a (mg m⁻³).....117

Figure 21. Box plot (from bottom to top, the horizontal lines represent the minimum, first quartile, median, third quartile, and maximum values; the black dots represent the outliers) for each province (left to right: BRAZ, SATL and AFR) of the distribution of phytoplankton chemotaxonomic group biomasses indicated by the color legends at the bottom of the plots (Prasino- prasinophytes, Chloro- chlorophytes, Crypto- cryptophytes, Diatom- diatoms, Pelago- pelagophytes, Dino- dinoflagellates, Hapto- haptophytes, Syn- *Synechococcus* and Pro- *Prochlorococcus*). Note the difference in the y-scale at the AFR.....121

Figure 22. a. Canonical correspondence analysis (CCA) ordination diagram of the biomass of different phytoplankton groups at the sea surface in all seven cruises (see legend on top right for different cruise symbols) along the South Atlantic Ocean. The arrows indicate environmental variables (pointing in the direction in which the value of environmental variable increases; the angle indicates the correlation between variables) and point: sea surface temperature (T; °C), salinity, temperature-normalized CO₂ partial pressure (NpCO₂^{sw}), sea-air CO₂ partial pressure difference (ΔpCO₂) and total chlorophyll a (TChl a). Blue stars indicate the absolute contributions of phytoplankton groups. diatom = diatoms; dino = dinoflagellates; crypto = cryptophytes; prasino = prasinophytes; hapto = haptophytes; syn = *Synechococcus*; pelago = pelagophytes; chloro = chlorophytes; pro = *Prochlorococcus*. Stations are separated according to distinct ocean biogeochemical provinces by color (BRAZ-red, SATL-yellow and AFR-green) b. CCA ordination diagram of biomass contributions of different phytoplankton groups at the sea surface in the South Atlantic Gyral province (SATL). The first two ordination axes represent 95.2% of the total phytoplankton group variance and 32.6% of the phytoplankton group-environment relationship. Arrows indicate environmental variables: sea surface temperature (T°C), salinity, temperature-normalized CO₂ partial pressure (NpCO₂^{sw}), difference between seawater and atmospheric CO₂ partial pressures (ΔpCO₂) and total chlorophyll a (TChl a). Blue crosses indicate the absolute contributions of phytoplankton groups. diatom = diatoms; dino = dinoflagellates; Crypto = cryptophytes; prasino = Prasinophytes; hapto = haptophytes; Syn = *Synechococcus*; Pelago= Pelagophytes; chloro = Chlorophytes; Pro = *Prochlorococcus*. Stations are separated according to distinct cruises (see legend on top right).....124

Figure 23. a. Net FCO₂ (mmol m⁻² d⁻¹) distribution along the South Atlantic Ocean during the cruises investigated in this study. b. Chlorophyll a (TChl a, mg m⁻³) along the different cruise tracks evaluated in this study. On the right, the donut graphs represent the average phytoplankton group contributions to phytoplankton biomass along 20°S for a. BRAZ stations, b. SATL stations and c. AFR stations; along 30°S for d. BRAZ stations, e. SATL stations and f. AFR stations; and along 35°S for g. BRAZ stations, h. SATL stations and i. AFR stations. The gray shaded lines on the side table display the average FCO₂ and TChl a and the number of stations (n) used in each section (a to i) of the transects (20°S, 30°S and 35°S).....126

Figure 24. Schematic representation of the main biogeochemical systems of the South Atlantic basin. The western boundary current domain, which is influenced by the Brazil Current and the

subtropical gyre domain and the eastern boundary current domain, which are influenced by the Benguela Current. On top, the orange arrows indicate the magnitude of the carbon dioxide fluxes (FCO_2) in each province. The symbols representing the major phytoplankton groups (diatoms, haptophytes, prasinophytes, *Synechococcus* and *Prochlorococcus*) are distributed proportionally to their relevance in each domain by latitude. The main dynamical processes (presence of Agulhas eddies, upwelling and mesoscale variability) are also shown. The input of fresh water on the western side is marked.....137

Figure 25. Map of the study area with the distribution of the hydrographic stations of the four cruises (yellow- PATEX IV, red- PATEX VI, green- MCTII and blue-EstARte Sul) analyzed here. The main surface circulation is also represented highlighting the Brazil Current (red dashed line) and the Malvinas Current (Black dashed line) which confluence region occurs at approximately 35°S. From 20°S to 50°S we have important features marked in the map as the Cabo Frio upwelling, the Patos Lagoon estuarine system (PLE) at approximately 32°S and the La Plata River (LPR) discharge at approximately 35°S.....146

Figure 26. Distribution of a. sea surface temperature (SST); b. sea surface salinity (SSS); c. Log of Total of chlorophyll a (Log TChl a) and d. CO_2 net fluxes (FCO_2) from 20°S to 50°S. The gray dots represent the data measured in each cruise, and the red dots are the mean values from each 5° latitude bin. The boundaries of the main areas highlighted in the study region are marked by orange dotted lines: ACR- Abrolhos Campos Region (20°S-23°S); SBB- South Brazilian Bight (23°S-28°S); SBS – Southern Brazilian Shelf (28.5°S-35°S); BMC – Brazil-Malvinas Confluence region (~38°S) and PS – Patagonian shelf (40°S- 50°S).....154

Figure 27. Bar charts with the mean concentration of total chlorophyll a (TChl a) with the relative contribution of main phytoplankton groups for each 5° latitudinal bin between 20°-50°S. The dashed line, with red squares, represent the averaged value for sea–air CO_2 net fluxes (FCO_2) for each 5° latitudinal bin.....155

Figure 28. CCA ordination diagram of the absolute contributions of different phytoplankton groups at the sea surface. The black arrows indicate environmental variables (pointing in the direction in which the value of environmental variable increases; the angle indicates the correlation between variables) and point: sea surface temperature (SST; °C), sea surface salinity (SSS), CO_2 partial pressure at the seawater ($p\text{CO}_2^{\text{sw}}$), sea–air CO_2 fluxes (FCO_2) and phytoplankton biomass (TChl a) The absolute contributions of phytoplankton groups are indicated by their names: Diatoms; Dinoflagellates; Cryptophytes; Haptophytes; Green flagellates; Cyanobacteria and *Prochlorococcus*. Stations are separated by color according to distinct 5° latitudinal bin (see legend on top left for different latitudinal colors).....158

Figure 29. Correlation matrix diagram. The abiotic parameters used in this correlation were: sea surface temperature - SST, sea surface salinity - SSS, Total of Chlorophyll a - TChl a, CO_2 partial pressure at the seawater - $p\text{CO}_2^{\text{sw}}$, difference between seawater and atmospheric CO_2 partial pressure - $\Delta p\text{CO}_2$ and CO_2 net fluxes - FCO_2 and the phytoplankton groups: Diatoms, Dinoflagellates, Haptophytes, Cyanobacteria, *Prochlorococcus*, Green Flagellates and Cryptophytes). The colorbar indicates blue as positive correlations and red as negative correlations. The size of the dot in the diagram indicates the strength of the correlation.....159

Figure 30. Biogeochemical domains proposed in this study region, based on sea–air CO_2 fluxes (FCO_2 ; $\text{mmol m}^{-2} \text{d}^{-1}$) and dominance of phytoplankton groups. Note the increased CO_2 uptake magnitudes linked to increased phytoplankton size assemblages. The pizza graphs for each 5° latitudinal bin, with each color representing the phytoplankton group is shown at the legend on the right side. T/B ratio represents the temperature effect and biological effect index. The main phytoplankton groups (diatoms, haptophytes and cyanobacteria) are represented at the legend.....167

Lista de Tabelas

- Tabela 1.** Informações gerais sobre os cruzeiros abordados neste trabalho por ordem cronológica, incluindo o nome do cruzeiro, a área de cobertura, o período de amostragem (estação do ano), os dados utilizados (pigmentos fitoplanctônicos, temperatura da superfície do mar – SST, salinidade da superfície do mar – SSS, pressão parcial do CO₂: na atmosfera - $p\text{CO}_2^{\text{atm}}$, na superfície do mar - $p\text{CO}_2^{\text{mar}}$, na superfície do mar modelada - $m\text{pCO}_2^{\text{mar}}$, vento a 10m – U_{10}) e referências de trabalhos anteriores sobre estes cruzeiros.....**56**
- Table 2.** In this table, the stations sampled are listed in the first column and, in the second column, two depths (the first value corresponds to data at a 5 m depth, and the second (between brackets) is at a DCM depth) are listed. The subsequent columns show the value of each parameter measured for each depth: T (°C), salinity, DIN ($\mu\text{mol L}^{-1}$), PO_4^{3-} ($\mu\text{mol L}^{-1}$), SiOH_4^- ($\mu\text{mol L}^{-1}$), and TChl a (mg m^{-3}); in the last column, the MLD (m) for each station is listed.....**85**
- Table 3.** General information about the cruises used in this study, including the name of the cruise, the area covered, the sampling period (season), the data used and the references of earlier studies in the South Atlantic that previously used the data.....**112**
- Table 4.** Average physical and biogeochemical parameters for each South Atlantic cruise separated by provinces (Brazil, BRAZ; South Atlantic Gyral, SATL; and African - AFR). Sea surface temperature (SST; °C), sea surface salinity (SSS; psu), total chlorophyll a (TChl a; mg m^{-3}), seawater CO₂ partial pressure ($p\text{CO}_2^{\text{sw}}$; μatm), atmospheric CO₂ partial pressure ($p\text{CO}_2^{\text{atm}}$; μatm), temperature-normalized seawater CO₂ partial pressure ($Np\text{CO}_2^{\text{sw}}$; μatm), difference between seawater and atmospheric $p\text{CO}_2$ ($\Delta p\text{CO}_2$; μatm), wind speed at 10 meters (U_{10} ; m s^{-1}), CO₂ net fluxes (FCO_2 ; $\text{mol m}^{-2} \text{d}^{-1}$) and number of samples (n) within each cruise and province.....**119**
- Table 5.** General information about the cruises used in this study, including the name of the cruise, the coverage area, the sampling period (season), the data used (phytoplankton pigments, sea surface temperature – SST; sea surface salinity – SSS; Total Alkalinity – A_T ; Dissolved inorganic carbon – C_T ; CO₂ partial pressure in the seawater – $p\text{CO}_2^{\text{sw}}$ and in the atmosphere $p\text{CO}_2^{\text{air}}$ and wind speed at 10m – U_{10}) and references from previous work on these cruises.....**148**
- Table 6.** Mean values and standard deviation of Sea surface temperature - SST (°C), Sea surface salinity - SSS, Total of Chlorophyll a - TChl a and CO₂ fluxes (FCO_2). for each 5° latitudinal bin.....**154**
- Table 7.** Contribution of phytoplankton groups to total chlorophyll a (TChl a; %) for each 5° latitudinal bin. The bold values represent the dominant group for each bin and absent groups where marked with (-).....**157**
- Table 8.** Calculated effects of biology ($\Delta p\text{CO}_2^{\text{sw bio}}$) and temperature ($\Delta p\text{CO}_2^{\text{sw temp}}$) on seawater CO₂ partial pressure ($p\text{CO}_2^{\text{sw}}$) values for each latitudinal bin and the relative importance of the effects presented calculated by the difference (T-B) and by the ratio T/B.**158**

Lista de Acrônimos e Abreviações

A

AFR – Província Africana

A_T – Alcalinidade Total

B

BRAZ – Província do Brasil

BENG – Província de Benguela

C

C_T – Carbono Inorgânico dissolvido total

CHEMTAX – Chemotaxonomic software

CTD – Sistema Condutividade-Temperatura-Profundidade

Conductivity-Temperature-Depth

E

EAFR – Província do Leste Africano

F

FCO₂ – Fluxos Líquidos de CO₂

FORSA – Following Ocean Rings in the South Atlantic Ocean

G

Gt – Gigatoneladas (10⁹ Toneladas)

H

HPLC – High performance liquid chromatography

P

pCO₂ – Pressão parcial do CO₂

Pg – Petagramas (10¹⁵ gramas)

S

SATL – Província do giro central do Atlântico Sul

SBB – Southern Brazilian Bight

SBS – Southern Brazilian Shelf

T

TChl a – Total de clorofila a (clorofila a + DV clorofila a)

Resumo

O fitoplâncton marinho contribui para a absorção de dióxido de carbono (CO_2) atmosférico pelos oceanos através da mediação da fotossíntese na bomba biológica do carbono. No entanto, as comunidades fitoplanctônicas, que variam amplamente em relação à sua composição estrutural, respondem de maneira diferenciada com as variações ambientais e, também, podem diferir na sua capacidade de absorção de CO_2 . Desta forma, este estudo propõe avaliar o efeito da relação entre os processos físico-químicos e as comunidades fitoplanctônicas na variabilidade do fluxo líquido de CO_2 (FCO_2) na interface oceano-atmosfera em distintos regimes hidrográficos no oceano Atlântico Sul. Para isso, foram adotadas metodologias apropriadas: (i) para determinação dos parâmetros do sistema carbonato necessários para o cálculo do FCO_2 , i.e. pressão parcial do CO_2 ($p\text{CO}_2$), alcalinidade total e carbono inorgânico dissolvido total, e (ii) para determinação da composição pigmentar fitoplanctônica, através da cromatografia líquida de alta performance, combinada com análise quimio-taxionômica (ferramenta CHEMTAX), tendo em vista a caracterização das comunidades de fitoplâncton nas distintas áreas de estudo. Assim, foi possível determinar a relação existente entre a estrutura das comunidades fitoplanctônicas e a modulação das trocas de CO_2 na interface oceano-atmosfera nas regiões de estudo. No geral, a biomassa fitoplanctônica foi significativamente relacionada com a $p\text{CO}_2$ da água, e com o FCO_2 , no oceano Atlântico Sul. No entanto, na parte ocidental (sistema dominado pela corrente do Brasil) o valor médio encontrado para o FCO_2 foi de $-7.1 \text{ mmol CO}_2 \text{ m}^{-2} \text{ d}^{-1}$, e uma maior captação de CO_2 esteve associada a variações da temperatura e ao padrão de salinidade (parâmetros físico-químicos), apesar de uma clara dominância das diatomáceas nesta região. Maiores concentrações de haptófitas foram associadas ao aumento da captação de CO_2 na porção central do giro subtropical do Atlântico Sul onde o FCO_2 médio foi de $-9.8 \text{ mmol CO}_2 \text{ m}^{-2} \text{ d}^{-1}$. Já na porção oriental (sistema dominado pela corrente de Benguela) foram encontradas elevadas taxas de absorção de CO_2 atmosférico com FCO_2 médio de $-27.6 \text{ mmol CO}_2 \text{ m}^{-2} \text{ d}^{-1}$ associadas às haptófitas mas também a diatomáceas. Em uma investigação mais focada na porção central do Atlântico

Sul (dominada pelo giro subtropical do Atlântico Sul) foi observada a influência dos vórtices anticiclônicos das Agulhas na distribuição das comunidades fitoplanctônicas. Os resultados desse estudo mostraram o aumento da diversidade dos grupos e da biomassa fitoplanctônica no interior dessas estruturas de mesoescala em relação ao seu entorno, sendo diferenciadas pelo aparecimento principalmente de prasinófitas, pelagófitas e criptófitas. Isso foi evidenciado, principalmente, na estrutura (vórtice) mais jovem, ficando menos evidente essa diferenciação (interior vs entorno) à medida que as estruturas evoluíram ao longo das suas trajetórias. Nos estudos conduzidos em regiões costeiras do sudoeste do Atlântico Sul (20°S–50°S) observou-se que o FCO₂ variou amplamente entre as regiões que se comportaram, em geral, como fraca fonte (FCO₂ em média de $5.4 \pm 5.5 \text{ mmol CO}_2 \text{ m}^{-2} \text{ d}^{-1}$) e grande sumidouro de CO₂ (FCO₂ em média de $-20.8 \pm 6.8 \text{ mmol CO}_2 \text{ m}^{-2} \text{ d}^{-1}$). A pCO₂ na superfície do mar foi negativamente correlacionada com a clorofila *a* (índice de biomassa fitoplanctônica) e com uma maior abundância de diatomáceas nas regiões entre 40°S e 50°S. A região no entorno de 35°S marcou a transição de um importante gradiente zonal entre 20°S e 50°S. A porção norte da margem continental brasileira evidenciou uma emissão de CO₂ do oceano para a atmosfera, e esteve dominada por grupos de cianobactérias. Por outro lado, a porção mais ao sul apresentou maior influência da biologia e funcionou como um forte sumidouro de CO₂, sendo dominada por grupos funcionais do fitoplâncton de maior tamanho (diatomáceas). Com esta Tese, objetivamos associar a abundância de diferentes grupos do fitoplâncton e a absorção de CO₂ atmosférico em regiões de comportamentos dinâmicos distintos no Oceano Atlântico Sul. Mudanças globais afetam o fitoplâncton em todo o mundo. Entender como o fitoplâncton está relacionado à absorção de CO₂, é entender como as mudanças globais afetarão os processos biogeoquímicos oceânicos.

Palavras-Chave: Oceano Atlântico Sul, províncias biogeoquímicas, fitoplâncton, diatomáceas, cianobactérias, haptófitas, bomba biológica do carbono, absorção de CO₂, fluxo líquido de CO₂.

Abstract

Marine phytoplankton contributes significantly to atmospheric carbon dioxide (CO₂) uptake by the oceans through the mediation of photosynthesis in the biological carbon pump. However, phytoplankton vary widely functionally, in cell size and structure, and thus, respond differently to environmental variations and, also, may differ in their CO₂ absorption capacity. Thus, this study proposes to evaluate the effect of the relationship between physical-chemical processes and phytoplankton communities on the variability of the CO₂ net fluxes (FCO₂) at the ocean-atmosphere interface in different hydrographic regimes in the South Atlantic Ocean. Appropriate methodologies were adopted to accomplish this goal: (i) determination of the carbonate parameters, used for FCO₂ calculation, i.e. CO₂ partial pressure (*p*CO₂), total alkalinity and dissolved inorganic carbon and (ii) phytoplankton pigment analysis using high performance liquid chromatography combined with chemotaxonomic analysis (CHEMTAX). Thus, it was possible to determine the relationship between the structure of phytoplankton communities and the modulation of CO₂ exchanges at the ocean-atmosphere interface in the study regions. Phytoplankton biomass was significantly related to water *p*CO₂ and FCO₂ in the South Atlantic Ocean. However, in the western sector (western boundary current domain – Brazil current), the average value found for FCO₂ was $-7.1 \text{ mmol CO}_2 \text{ m}^{-2} \text{ d}^{-1}$, a higher CO₂ uptake was associated with temperature variations and with the salinity pattern (physical-chemical parameters), despite the clear dominance of diatoms in this region. Higher concentrations of haptophytes were associated with increased CO₂ uptake in the subtropical central gyre system where the average FCO₂ was $-9.8 \text{ mmol CO}_2 \text{ m}^{-2} \text{ d}^{-1}$. At the eastern sector (eastern boundary current domain – Benguela current) high rates of atmospheric CO₂ uptake were found with an average FCO₂ of $-27.6 \text{ mmol CO}_2 \text{ m}^{-2} \text{ d}^{-1}$ associated with haptophytes but also with diatoms. An investigation more focused on the central area of the South Atlantic (dominated by the subtropical gyre), the influence of the anti-cyclonic Agulhas eddies on the distribution of phytoplankton communities was observed. The results of this study showed an increase in group diversity and phytoplankton biomass within these structures in

relation to their surroundings. This pattern was evidenced, particularly, in the younger structure (eddy), this differentiation (interior vs surroundings) becoming less evident as the structures evolved along their trajectories. In studies conducted in coastal regions of the southwestern South Atlantic (20°S–50°S), it was observed that FCO_2 varied widely between regions that generally behaved as a weak source (with average FCO_2 of $5.4 \pm 5.5 \text{ mmol CO}_2 \text{ m}^{-2} \text{ d}^{-1}$) and a large CO_2 sink (with average FCO_2 of $-20.8 \pm 6.8 \text{ mmol CO}_2 \text{ m}^{-2} \text{ d}^{-1}$). The pCO_2 in the surface seawater was negatively correlated with chlorophyll *a* (phytoplankton biomass index) and with a greater abundance of diatoms in the regions between 40°S and 50°S. The region around 35°S marked the transition from an important zonal gradient between 20°S and 50°S. The northern portion of the Brazilian continental margin showed a CO_2 emission from the ocean into the atmosphere and was dominated by groups of cyanobacteria. On the other hand, the southernmost portion showed greater influence from biology and functioned as a strong CO_2 sink, being dominated by larger phytoplankton functional groups (diatoms). With this Thesis, we aim to associate the abundance of different groups of phytoplankton and the absorption of atmospheric CO_2 in regions of distinct dynamic behavior in the South Atlantic Ocean. Global changes affect phytoplankton worldwide. Understanding how phytoplankton is related to CO_2 uptake is to understand how global changes will affect oceanic biogeochemical processes.

Keywords: South Atlantic Ocean, biogeochemical provinces, phytoplankton, diatoms, cyanobacteria, haptophytes, biological carbon pump, CO_2 uptake, CO_2 net fluxes.

Prefácio

Os oceanos possuem um importante papel na regulação climática da Terra através da captação do dióxido de carbono (CO₂) em excesso na atmosfera. Isso se deve, em grande parte, à atuação do fitoplâncton na realização da fotossíntese, que é responsável por iniciar o processo da bomba biológica do carbono. Neste processo, estes micro-organismos marinhos convertem o carbono inorgânico em carbono orgânico, que posteriormente será exportado através da coluna de água, estocado nas massas de água, e sequestrado no fundo dos oceanos.

As mudanças climáticas globais têm impactado as comunidades do fitoplâncton marinho de forma direta e indireta, afetando tanto sua estrutura quanto o tamanho celular [[Hilligsøe et al. 2011](#)]. Estudos relacionando os efeitos do aumento da temperatura da superfície do mar na distribuição do fitoplâncton marinho mostram que o aumento da estratificação da camada eufótica, em

resposta ao aquecimento global, limita as trocas de nutrientes com a superfície e favorece comunidades fitoplanctônicas de menor tamanho. Estes organismos são capazes de crescer em condições de temperatura mais elevada e em regiões com menor concentração em nutrientes [Cermeño *et al.* 2008, Riebesell *et al.* 2009, Morán *et al.* 2010, Taucher & Oschlies 2011]. No entanto, o impacto acoplado dessas alterações na captação do CO₂ pelos oceanos ainda é um desafio e um assunto pouco abordado na literatura. Tal investigação, por sua vez, é de grande importância para entendermos o efeito biológico sobre a capacidade do oceano de absorver CO₂ atmosférico [Cao & Zhang 2017].

Até o momento, em comparação com a quantidade de experimentos envolvendo a captação do CO₂ usando espécies cultivadas em laboratório, existem relativamente poucos estudos abordando a captação de CO₂ pelo fitoplâncton em um ambiente natural [Tortell & Morel 2002, Beardall & Raven 2004, Reinfelder 2011, Takao *et al.* 2020], uma situação essencial para se obter informações sobre o sumidouro de CO₂ a longo prazo do oceano [Mercado & Gordillo 2011]. Portanto, este trabalho visa preencher uma lacuna importante do conhecimento ao buscar relacionar os diferentes grupos do fitoplâncton com os níveis de captação de CO₂ pelo oceano e, potencialmente, inferir como as mudanças globais afetarão os processos biogeoquímicos oceânicos.

No oceano Atlântico Sul, há ainda poucos estudos sobre a distribuição do fitoplâncton e sua relação com a captação de CO₂, e pouco se sabe sobre as possíveis vulnerabilidades da região face às mudanças globais. Esta tese foi motivada pela existência de um robusto banco de dados do Grupo de Oceanografia de Altas Latitudes (GOAL) e pela aquisição emergente de dados oriundos da Rede Brasileira de Pesquisa em Acidificação dos Oceanos (BrOA)

para diversas províncias biogeoquímicas do oceano Atlântico Sul. Esta base de informações oceanográficas conta com dados de pigmentos fitoplanctônicos e de parâmetros do sistema carbonato, pertinentes para a elaboração deste estudo numa abordagem espacialmente ampla e que integra diversos dados físicos e biogeoquímicos.

A estrutura desta tese segue o modelo de artigos científicos proposto pelo Programa de Pós-Graduação em Oceanologia (PPGO). Após o prefácio, as hipóteses a serem respondidas por esta tese são apresentadas. No Capítulo I temos uma Introdução ao tema abordado nesta tese, seguida pelos objetivos do estudo. No Capítulo II, temos a apresentação da área de estudo, o oceano Atlântico Sul, com todas suas subdivisões e particularidades. No Capítulo III serão apresentados os métodos utilizados para atingir os resultados esperados. Os resultados deste trabalho, por sua vez, serão apresentados na língua inglesa e na forma de artigos científicos nos Capítulos IV, V e VI. O Capítulo IV traz o primeiro artigo que aborda o impacto dos vórtices advindos da corrente das Agulhas na distribuição das comunidades do fitoplâncton no oceano Atlântico Sul. No Capítulo V, é apresentado o segundo manuscrito que aborda a relação entre os principais grupos do fitoplâncton com a magnitude dos fluxos de dióxido de carbono nas diferentes províncias biogeoquímicas do Atlântico Sul. No Capítulo VI temos um estudo mostrando o domínio de diferentes grupos do fitoplâncton e sua associação com a captação de dióxido de carbono nas Plataformas Sul e Sudeste do oeste do oceano Atlântico Sul. No capítulo VII, teremos uma síntese das principais discussões e conclusões sobre esses resultados. Em anexo, encontram-se os materiais suplementares dos manuscritos apresentados nos Capítulos IV e V. Por fim, no Capítulo VIII

encontram-se descritas as referências bibliográficas utilizadas nesta pesquisa. Com esta Tese, espera-se, ainda, incentivar e contribuir para novos estudos nesta linha de pesquisa na região. Estes devem potencializar a geração de dados biogeoquímicos em áreas-chave no oceano Atlântico Sul e focar no aprimoramento dos métodos necessários para elucidar o papel dos principais grupos do fitoplâncton na captação do CO₂.

Hipótese

A investigação das comunidades fitoplanctônicas dominantes e sua relação com a dinâmica do fluxo líquido de CO₂ (FCO₂), em regiões de regimes biogeoquímicos distintos do oceano Atlântico Sul, a partir de estudos preliminares na região, nos levaram a questionar o papel do fitoplâncton na captação de CO₂ em um contexto de gradientes naturais zonais nos regimes costeiros e oceânicos. Assim, as hipóteses testadas neste estudo foram:

(i) a atividade biológica tem maior influência que os fatores físicos (e.g. temperatura, salinidade) na distribuição da pressão parcial do CO₂ na superfície do mar ($p\text{CO}_2^{\text{mar}}$) nas regiões de estudo.

(ii) determinados grupos funcionais do fitoplâncton favorecem uma maior captação de CO₂ pelos oceanos nas diferentes províncias biogeoquímicas do Atlântico Sul.

Capítulo I: Introdução

Os ecossistemas marinhos têm feito um excelente papel em absorver o dióxido de carbono (CO₂) em excesso na atmosfera, ajudando a mitigar os efeitos do aumento das emissões de carbono antropogênico [Friedlingstein *et al.* 2019]. A transferência líquida de CO₂ entre a atmosfera, os oceanos e, os sedimentos ocorre, basicamente, pela ação dos mecanismos conhecidos como bomba de solubilidade e bomba biológica [Sarmiento *et al.* 2002]. Através da bomba de solubilidade (também conhecida como bomba física), o dióxido de carbono é transportado para o oceano profundo como resultado da subsidência de massas de água. Através da bomba biológica, o carbono inorgânico é fixado pela produtividade primária na zona eufótica. A matéria orgânica é oxidada por microorganismos e o carbono é transferido para o interior do oceano e posteriormente para os sedimentos. O fitoplâncton marinho atua, portanto, diretamente no ciclo biogeoquímico do carbono como

mediador chave da bomba biológica, através da fotossíntese [Basu & Mackey *et al.* 2018]. No entanto, variações nas características das comunidades fitoplanctônicas ocorrem em função das variáveis ambientais [Cullen *et al.* 2002] que resultam em efeitos biológicos locais diferenciados na pressão parcial do CO₂ na água do mar ($p\text{CO}_2^{\text{mar}}$) [Schloss *et al.* 2007, Litchman *et al.* 2015]. Assim, o papel do fitoplâncton na dinâmica do carbono marinho requer, primeiramente, nossa habilidade de explicar a distribuição dos grupos fitoplanctônicos dominantes em relação às condições bióticas e abióticas do ambiente [Arrigo *et al.* 1999].

Há ainda certas dificuldades e incertezas em como relacionar a dominância de determinado grupo do fitoplâncton com as mudanças na capacidade de absorção de CO₂ em determinada região, uma vez que o fitoplâncton é influenciado pela distribuição de temperatura na superfície do mar, pela intensidade e comportamento da luz na camada fótica dos oceanos, pela disponibilidade tanto de micro quanto de macro nutrientes e pela menor ou maior pressão de consumo do zooplâncton sobre a biomassa acumulada. Paralelamente, estes e outros parâmetros nos oceanos são afetados indiretamente pelo aumento dos níveis de CO₂ na atmosfera, que são associados à variabilidade nos processos físicos no oceano e na atmosfera e às alterações na dinâmica das correntes oceânicas. Com isso, visto a quantidade de processos oceanográficos relevantes ocorrendo simultaneamente em diferentes escalas espaço-temporais, bem como a resposta da composição das comunidades fitoplanctônicas às variações ambientais, torna-se um desafio observar potenciais mudanças em escala global a partir de medições *in situ* [Alvain *et al.* 2013]. Os efeitos concomitantes de mudanças em diversos

parâmetros oceanográficos, que regulam a variabilidade e o comportamento da sucessão das comunidades fitoplanctônicas, precisam ser melhor avaliados para compreendermos como alterações no sistema carbonato marinho podem atuar no enfraquecimento ou no reforço dos mecanismos da bomba biológica.

1.1 O aumento das concentrações do CO₂ atmosférico e o ciclo do carbono no ambiente marinho

O CO₂ é um gás de efeito estufa presente na atmosfera, essencial para a regulação climática do planeta. Com o aumento das atividades antrópicas, principalmente através da queima de combustíveis fósseis, a liberação desse gás para a atmosfera tem ocorrido de forma exponencial ao longo dos anos, atingindo níveis cada vez mais elevados e chegando a valores acima dos 400 ppm no ano de 2013. Esta tendência de aumento da concentração de CO₂ na atmosfera continua a ser observada na presente década (Fig. 1). Em 2020, a concentração média do CO₂ atmosférico para o mês de maio foi em torno de 417 ppm e para o mês de setembro foi próxima de 411 ppm (ESRL- NOAA).

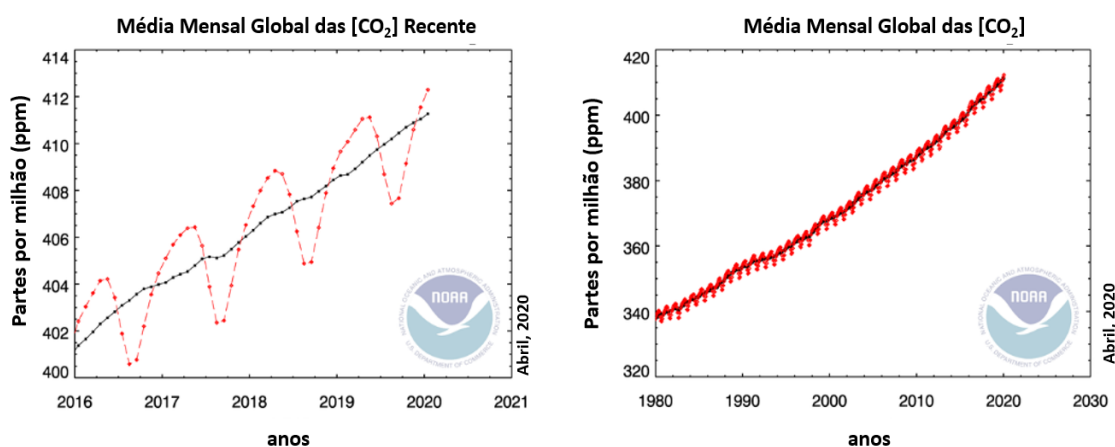


Figura 1. Médias mensais da concentração global de CO₂ em período recente (esquerda) e no registro completo desde o início das medições no final da década de 70 (direita). Fonte: Modificada de ESRL NOAA.

De acordo com o último balanço de carbono global, os oceanos globais absorvem em média 2,5 Gt de carbono antropogênico da atmosfera por ano, equivalente a aproximadamente 23% do total das emissões antropogênicas de CO₂ [Friedlingstein *et al.* 2019]. Porém, a absorção de CO₂ apresenta uma grande variabilidade espaço-temporal em cada região do oceano global, devido às suas propriedades hidrográficas e biogeoquímicas características e aos diferentes processos físicos e biológicos dominantes, o que resulta em áreas oceânicas com diferentes magnitudes na absorção do CO₂ atmosférico dependendo do período observado (Fig. 2).

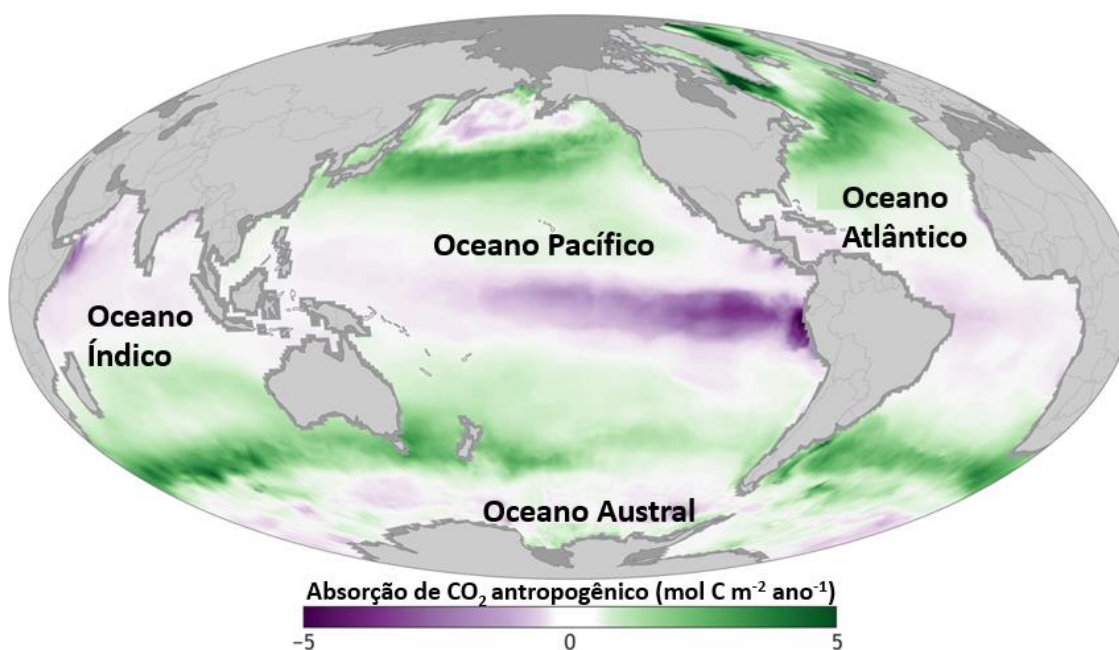


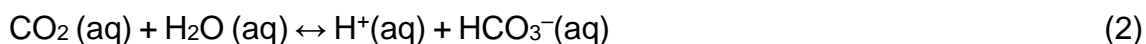
Figura 2. Absorção de CO₂ antropogênico pelos oceanos globais. Nesta figura, as áreas onde o oceano absorveu dióxido de carbono produzido pelo homem são as áreas verdes e as áreas onde o oceano liberou CO₂ de volta para a atmosfera são as áreas em roxo. Figura adaptada do [State of the Climate Report \[2017\]](#), NOAA Climate.gov.

O oceano Atlântico Sul, em geral, tem-se comportado como um sumidouro de CO₂ atmosférico, com absorção média estimada em $-0,3 \text{ Pg C ano}^{-1}$ [Takahashi *et al.* 2002]. Esforços mais recentes em obter medições do fluxo líquido de CO₂ (FCO₂), nessa região relativamente subamostrada dos

oceanos, encontraram o valor médio de -0.14 ± 0.04 Pg C ano⁻¹ para a região subtropical do oceano Atlântico Sul (entre 18°S e 44°S), já a região equatorial (entre 18°N e 18°S) apresentou o valor médio de $+0.12 \pm 0.04$ Pg C ano⁻¹ e a região subtropical do oceano Atlântico norte (entre 18°N e 49°N) apresentou o valor médio de -0.26 ± 0.06 Pg C ano⁻¹ [Schuster *et al.* 2013]. Uma investigação mais atual mostrou que a presença de vórtices no Atlântico Sul, provenientes da região do vazamento da Corrente das Agulhas, intensifica a absorção de CO₂ atmosférico [Orselli *et al.* 2018b]. A influência dessas estruturas de mesoescala no Atlântico Sul é também investigada nesta tese, focando-se na distribuição das comunidades fitoplanctônicas em relação à presença dos vórtices, motivando uma discussão sobre uma possível relação entre ambos os processos, i.e., fitoplâncton vs vórtices (ver Capítulo IV).

O FCO₂ na interface oceano-atmosfera depende de vários fatores, dentre eles: a solubilidade do CO₂ na água, a intensidade dos ventos na região, e da pressão parcial desse gás tanto no oceano ($p\text{CO}_2^{\text{mar}}$) quanto na atmosfera ($p\text{CO}_2^{\text{ar}}$). Sabe-se que a $p\text{CO}_2$ apresenta forte relação com a temperatura, com um aumento em torno de 4% na $p\text{CO}_2$ a cada 1°C [Takahashi *et al.* 2002]. A troca de CO₂ entre a atmosfera e o oceano ocorre por difusão. Na água do mar, o CO₂ dissolvido reage com a água e forma o ácido carbônico (H₂CO₃), que rapidamente se dissocia em íons bicarbonato (HCO₃⁻) e carbonato (CO₃²⁻) (Eq. 1-3). O carbono inorgânico dissolvido total (C_T) é, portanto, composto pelo somatório dessas espécies dissolvidas na água do mar: íon CO₂(aq), HCO₃⁻(aq) e CO₃²⁻(aq). A concentração de C_T na coluna de água geralmente aumenta com a profundidade, sendo maior em águas mais frias. O sistema carbonato atua no equilíbrio de reações bioquímicas como a fotossíntese, a respiração e o pH da

água do mar [Zeebe 2011].



O aumento das emissões antrópicas de CO₂ atmosférico e seu acúmulo contínuo na superfície dos oceanos está relacionado com o aumento da $p\text{CO}_2^{\text{mar}}$ e do C_T, juntamente com a diminuição do pH e do estado de saturação do carbonato de cálcio (Ω). Ao longo de décadas, ou mesmo de escalas temporais maiores, os efeitos desse aumento das concentrações de CO₂ pode configurar um estado de acidificação nos oceanos que tem potencial de impactar o fitoplâncton e, portanto, o ciclo de elementos biogeoquímicos em uma escala global [Doney *et al.* 2009, 2020]. Em relação às comunidades fitoplanctônicas, o efeito da acidificação dos oceanos ainda está em investigação, pois ao mesmo tempo que pode atuar prejudicando a formação de esqueletos e carapaças dos organismos calcificadores [Gattuso *et al.* 2015], pode ser vantajoso para determinados organismos fotossintéticos, pois a níveis mais elevados de CO₂ o consumo de C_T pode ser intensificado [e.g. Riebesell *et al.* 2013, Schulz *et al.* 2017].

1.2 O fitoplâncton e seu papel na bomba biológica do carbono

O fitoplâncton, realiza a fotossíntese, e possui um papel-chave na captação do CO₂ no ambiente marinho, sendo um mediador da bomba biológica [Basu & Mackey 2018]. A bomba biológica atua na transferência tanto do C_T

quanto do carbono orgânico [Sambrotto *et al.* 2014] (Fig. 3).

Este mecanismo é impulsionado pelas células fitoplanctônicas que realizam a fotossíntese, o que resulta na diminuição da $p\text{CO}_2^{\text{mar}}$, facilitando a absorção de CO_2 pelo oceano. Os consumidores e as bactérias decompositoras de matéria orgânica utilizam o carbono orgânico fixado através dos produtores primários na zona eufótica, e o transferem, em parte, para o interior dos oceanos. A partir do armazenamento e exportação do carbono na coluna de água, este pode ainda interagir com o sistema biológico e biogeoquímico bentônico e finalmente uma fração deste é sequestrada pelos sedimentos por um longo período de anos ou séculos, o que é importante para o ciclo do carbono, pois ajuda a manter os níveis de CO_2 atmosférico.

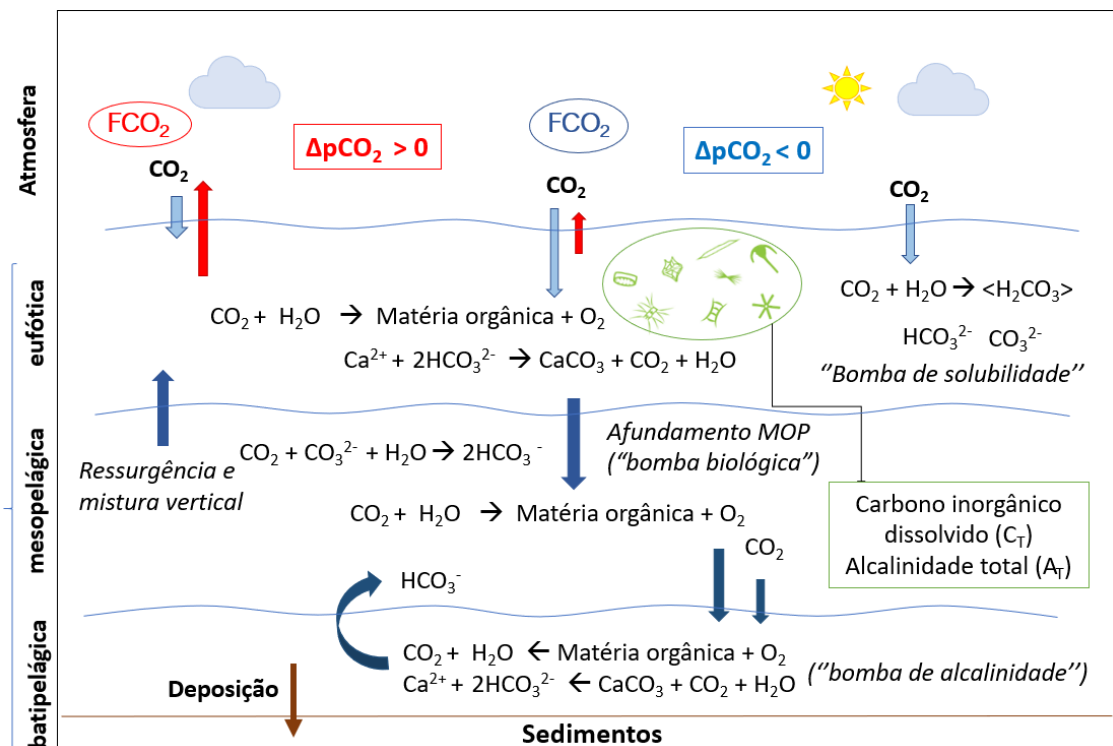


Figura 3. Esquema dos processos da bomba biológica. O fitoplâncton fixa o carbono inorgânico na zona eufótica através da energia solar (fotossíntese) e o transforma em carbono orgânico. Com a dissociação do ácido carbônico temos a formação dos íons carbonato e bicarbonato que irão compor a estrutura de diversos organismos, através da formação do carbonato de cálcio, e com sua morte, subsequente afundamento da matéria orgânica particulada (MOP) contribuirá para estoques de carbono nos sedimentos.

Portanto, através dos mecanismos da bomba biológica, uma parte do carbono perde o contato com a atmosfera por muitos anos e fica retido por mais tempo nos oceanos, ajudando a manter os níveis de CO₂ atmosférico mais baixos. Acredita-se que a bomba biológica tenha desempenhado um papel significativo nas flutuações do CO₂ atmosférico durante os períodos glacial-interglacial [Sigman & Boyle 2000] e que, atualmente, responde às variações contemporâneas no clima [Bopp *et al.* 2013, Boyd 2015]. No entanto, ainda não está claro como a bomba biológica responderá aos desequilíbrios climáticos globais no futuro. A importância da estrutura da comunidade do fitoplâncton para a bomba biológica é pouco compreendida e comumente negligenciada nos estudos climáticos relacionados ao ciclo do carbono [Kehfeld *et al.* 2005, Boyd *et al.* 2010]. Em um estudo recente, Jensen *et al.* [2017] fizeram o uso de modelagem para prever a futura distribuição global de duas espécies de fitoplâncton importantes para o funcionamento da bomba biológica: a diatomácea *Chaetoceros diadema* e o cocolitóforo *Emiliana huxleyi*. O modelo previu um declínio de ambas as espécies em relação às suas áreas de cobertura oceânica, o que resultaria em uma menor contribuição para o sequestro de carbono via bomba biológica. Embora a intensidade da bomba biológica do carbono esteja correlacionada com a composição da comunidade do fitoplâncton, a estrutura do ecossistema que direciona o processo permanece amplamente desconhecida [Guidi *et al.* 2016].

1.3 Diferenciação dos grupos fitoplanctônicos

O fitoplâncton é um grupo altamente diversificado de microalgas e

cianobactérias fotossintetizantes microscópicas, que atuam no acoplamento entre os processos atmosféricos e oceânicos. Os diversos grupos contribuem com quase 50% para a produção primária total da Terra, fixando cerca de 50 Gt de carbono por ano [Williams *et al.* 2002, Falkowski *et al.* 2003].

Cada grupo fitoplanctônico evoluiu para explorar condições ambientais diferentes, onde alguns adotaram preferências por condições mais estáveis e outros conseguem vantagens em ambientes de alta variabilidade [Aiken *et al.* 2000, Simon *et al.* 2009]. Neste diverso grupo de organismos unicelulares fotossintetizantes podemos distinguir três linhagens evolutivas (Fig. 4).

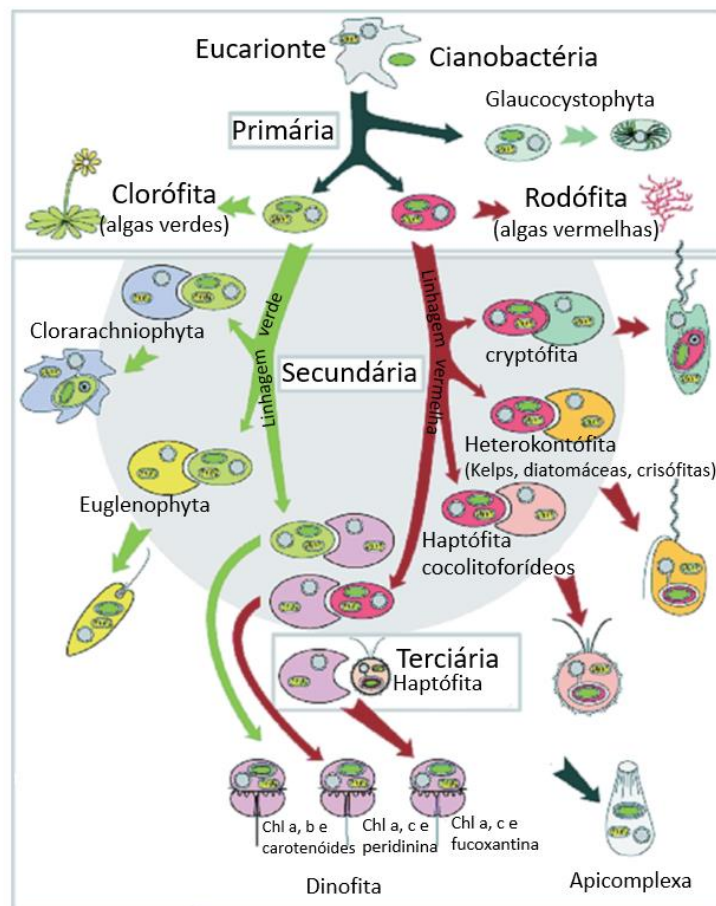


Figura 4. Diferenciação evolutiva dos grupos fitoplanctônicos. Neste esquema temos o caminho básico que conduziu a evolução de algas eucarióticas. O quadro superior mostra a simbiose primária de uma cianobactéria dando origem a ambas as linhagens de clorófitas (algas verdes) e rodófitas (algas vermelhas). No quadro inferior temos as sucessivas simbioses secundárias que deram origem à “linha verde” de algas e as simbioses secundárias na linha vermelha deram origem a todos os cromóforos, incluindo diatomáceas, criptófitas e haptófitas. Figura adaptada de Falkowski *et al.* [2003].

A primeira é composta pelos procariontes fotossintetizantes (cianobactérias). As demais são compostas por eucariontes (estruturas celulares mais complexas com núcleo, cloroplastos, mitocôndrias, e outras organelas), que descenderam de um ancestral comum apropriado por endossimbiose de uma cianobactéria em um hospedeiro heterotrófico. A cianobactéria apropriada tornou-se um cloroplasto. Os eucariontes se dividem em duas linhagens: a verde e a vermelha

Segundo estudos sobre a diversidade do fitoplâncton marinho, as diatomáceas, os dinoflagelados e, numa menor proporção, as haptófitas e as algas verdes, são os grupos de fitoplâncton eucariotos mais diversificados em termos de espécies descritas; em comparação aos demais grupos como as criptófitas e euglenófitas, que são menos diversificados [Simon *et al.* 2009] (Fig. 5).

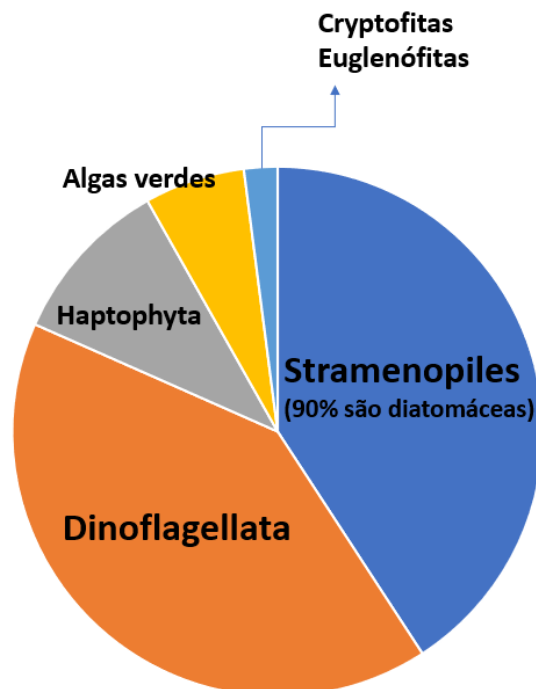


Figura 5. Contribuição percentual dos diferentes grupos do fitoplâncton marinho em relação a diversidade de espécies identificadas. Diatomáceas, dinoflagelados e em menor percentual haptófitas e algas verdes são os grupos mais diversificados com aproximadamente, 40%, 40%, 10% e 6% de espécies descritas, respectivamente. Gráfico adaptado de Simon *et al.* [2009]

A avaliação da diversidade global das cianobactérias é difícil, visto que dentre os vários gêneros já estudados, apenas poucos são conhecidos por serem estritamente marinhos [Dvorak *et al.* 2017]. Os organismos referentes a esses grupos fitoplanctônicos diferem no tamanho e na composição de suas paredes e revestimentos celulares, que influenciam suas velocidades de afundamento. E ainda, quanto às funções que desempenham no ambiente, por exemplo: fixadores de nitrogênio (cianobactérias diazotróficas), silicificadores (diatomáceas), calcificadores (coccolitóforos), dentre outros. Portanto, a eficiência da bomba biológica é função tanto da fisiologia quanto da estrutura da comunidade fitoplanctônica. Por outro lado, o tamanho (i.e., volume celular) dos organismos que compõem a comunidade fitoplanctônica é determinado por fatores ambientais como a temperatura da água, os nutrientes e a disponibilidade de luz, e pode variar em várias ordens de magnitude [Finkel *et al.* 2010, Hilligsøe *et al.* 2011] (Fig. 6).

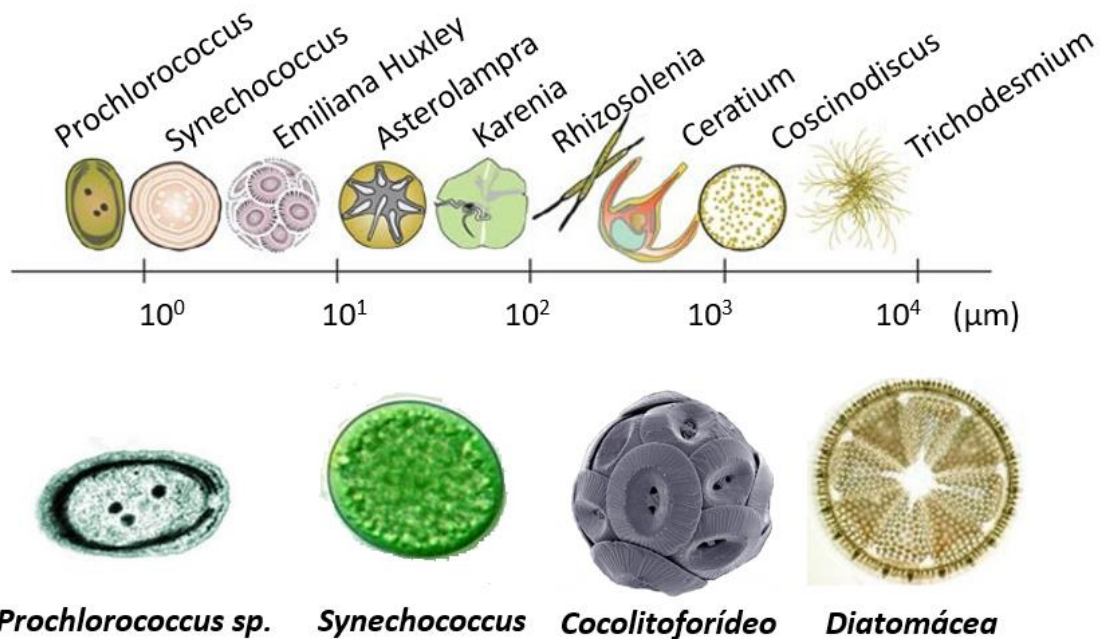


Figura 6. Uma comparação da faixa de tamanho (dimensão linear máxima) do fitoplâncton é apresentada na linha superior. Na linha inferior são apresentados alguns exemplos dos grupos citados acima, mostrando as diferenças de estrutura de revestimento de cada organismo. Adaptado de Finkel *et al.* [2010].

Assim, a estrutura da comunidade pode ser considerada um integrador de fatores ambientais [Claustre *et al.* 2005]. Devido à sua diversidade filogenética, é provável que diferentes táxons fitoplanctônicos respondam às mudanças climáticas de diferentes maneiras [Tortell *et al.* 2002, Finkel *et al.* 2010, Collins *et al.* 2014].

A seguir, será apresentada uma breve descrição dos principais grupos fitoplanctônicos que serão abordados neste trabalho:

a. Picoplâncton autotrófico (0,2–2 μm de diâmetro): inclui cianobactérias (e.g., *Prochlorococcus spp.* e *Synechococcus spp.*) e prasinófitas (algas verdes nanoplanctônicas; com clorofila *b*). Têm maior razão superfície/volume, o que promove melhor aquisição de nutrientes, podendo ter mais sucesso em regiões oligotróficas [Simon *et al.* 2009, Uitz *et al.* 2010]. Possuem baixas taxas de crescimento e baixas taxas de sedimentação. Acredita-se que estes grupos tenham uma menor contribuição para a exportação de carbono das camadas superficiais devido ao seu pequeno tamanho, velocidades lentas de afundamento (< 0,5 m/dia) e rápida reciclagem pela alça microbiana ainda na zona eufótica [Richardson *et al.* 2007].

b. Haptófitas (2–20 μm de diâmetro): também chamadas de primnesiófitas, são marcadas pela presença de um “flagelo” diferenciado (haptonema). Algumas haptófitas têm como característica a presença de pequenas placas achatadas (cocólitos) formadas por carbonato de cálcio. Portanto, podem ser potencialmente afetados pelo processo de acidificação dos oceanos, impedindo a capacidade de formação das suas placas calcárias e, conseqüentemente, podendo afetar a eficiência da bomba biológica [Collins *et al.* 2014]. Mudanças futuras na abundância relativa destes ou de outros taxa

fitoplanctônicos podem ter um impacto acentuado na produtividade total dos oceanos, afetando posteriormente a biogeoquímica oceânica, através de mudanças na captação, exportação, armazenamento e sequestro de carbono.

c. Diatomáceas (2–500 μm): organismos recobertos por uma carapaça (frústula) constituída por dióxido de silício (SiO_2). De acordo com a simetria celular, podem ser definidos dois grupos, as diatomáceas penadas (simetria bilateral) e as diatomáceas cêntricas (simetria radial). As diatomáceas possuem geralmente altas taxas de crescimento e são abundantes em regiões com maior concentração em nutrientes (e.g. zonas de ressurgência). Portanto, este grupo pode ser bastante afetado pelo aumento da temperatura dos oceanos, uma vez que a estratificação diminuiria a disponibilidade de nutrientes [Bopp *et al.* 2005]. As diatomáceas, pelo seu maior tamanho e densidade (presença das frústulas), são altamente eficientes no transporte vertical de carbono para maiores profundidades, formando agregados que afundam rapidamente [Passow *et al.* 2012].

d. Clorófitas (tamanhos variáveis): grupo de algas flageladas verdes (com clorofila *b*) bastante heterogêneo, presente em regiões transicionais e com grande variedade de formas de tamanho e hábitos. Seus representantes são comumente pertencentes ao picoplâncton (células de 0,2 a 2 μm) e nanoplâncton (células de 2 a 20 μm), e são considerados produtores primários chave de regiões oceânicas [Worden *et al.* 2004]

Objetivos

O objetivo geral desse estudo é avaliar o papel dos diferentes grupos de fitoplâncton na modulação do FCO₂ em distintos regimes hidrográficos do oceano Atlântico Sul. Assim, os seguintes objetivos específicos foram definidos:

- (i) caracterizar as comunidades fitoplanctônicas presentes em cada área de estudo, através da composição pigmentar, em termos de grupos funcionais do fitoplâncton;
- (ii) caracterizar o FCO₂ nas diferentes regiões de estudo, a partir de dados pretéritos de $p\text{CO}_2$, obtidos de maneira direta ou indireta, classificando-as como fonte ou sumidouro, e ainda quantificando a intensidade dos fluxos nas diferentes épocas amostradas; e
- (iii) correlacionar estes fluxos com as comunidades fitoplanctônicas, ou seja, analisar se a composição predominante de uma determinada comunidade favorece (ou não) a absorção de CO₂.

Capítulo II: Oceano Atlântico Sul

A área de estudo deste trabalho compreende o oceano Atlântico Sul entre as latitudes de 20°S e 50°S, abrangendo regiões costeiras e oceânicas que compõem um sistema complexo de interações biogeoquímicas (Fig. 7). O oceano Atlântico Sul é uma região de importância climática global onde vários estudos têm apontado para a sua relevância no entendimento da circulação oceânica no contexto da célula de revolvimento meridional do Atlântico [e.g. [Biastoch et al. 2009](#), [Lee et al. 2011](#), [Dong et al. 2015](#), [Lopez et al. 2017](#)], com destaque ainda para o papel da liberação de vórtices de mesoescala da região da retroflexão da corrente das Agulhas na dinâmica do transporte de sal, calor e outras propriedades biogeoquímicas [[Beal et al. 2016](#)]. Outros mecanismos, como os sistemas de ressurgências [[Campos et al. 2000](#), [Guenther et al. 2008](#)] e descargas fluviais proeminentes em áreas costeiras [[Burrage et al. 2008](#), [Marques et al. 2009](#)], também são responsáveis pela variabilidade do FCO₂ ao

longo das regiões da plataforma continental do oceano Atlântico Sul [Bianchi *et al.* 2005, Bianchi *et al.* 2009, Arruda *et al.* 2015, Ito *et al.* 2016]. Apesar de todos esses destaques, esta é ainda uma região do oceano global com poucos dados biogeoquímicos quando comparada a outras regiões oceânicas (e.g. oceano Atlântico Norte). Isto indica a necessidade de novos estudos, com aplicação integrada nas diversas áreas da oceanografia, a fim de preencher as lacunas atuais do conhecimento.

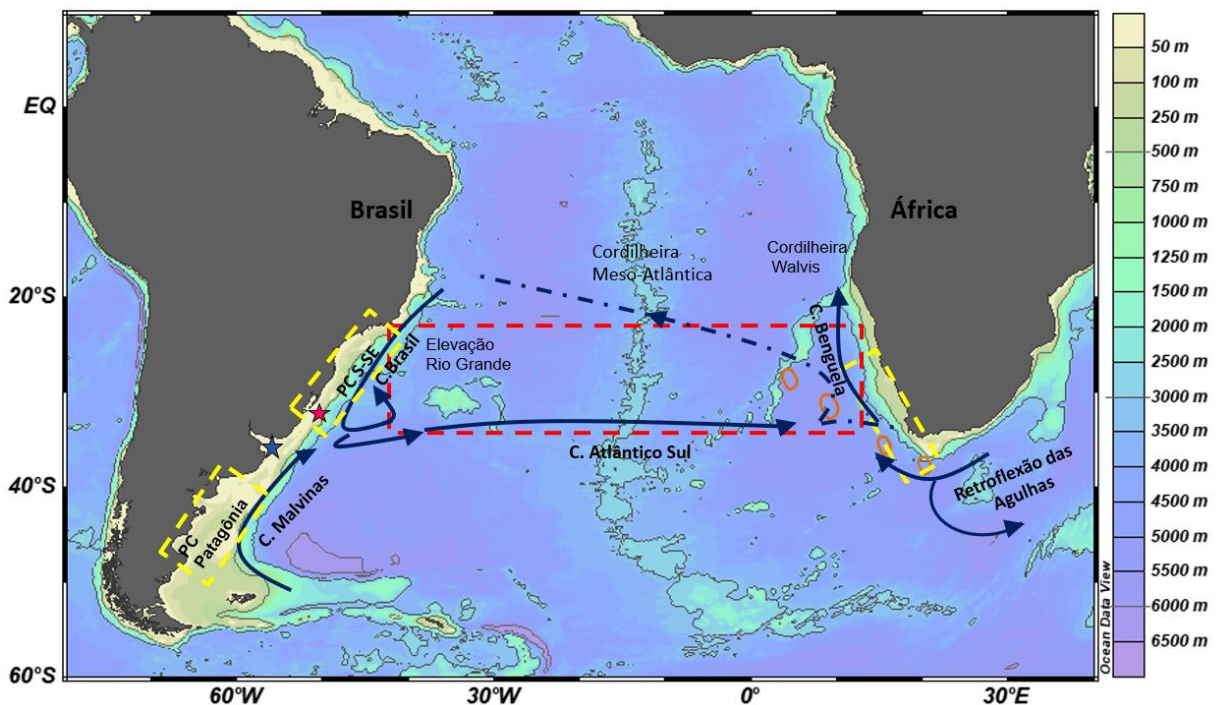


Figura 7. Mapa da área de estudo. O retângulo pontilhado em vermelho destaca a porção interna do giro subtropical do Atlântico Sul. Os retângulos pontilhados em amarelo destacam as regiões costeiras em destaque neste estudo, tanto na porção ocidental como na porção oriental dessa bacia oceânica. As setas em azul destacam a circulação oceânica superficial do giro subtropical do Atlântico Sul: na borda ocidental temos a Corrente do Brasil e a Corrente das Malvinas, que convergem em aproximadamente 35°S. Neste lado da bacia também temos as descargas da Lagoa dos Patos (estrela magenta) e do Rio da Prata (estrela azul) atuando como as principais fontes de água doce para a plataforma continental. Na parte sul do giro do Atlântico Sul, a Corrente do Atlântico Sul flui para leste em direção à borda ocidental, fundindo-se com a Corrente de Benguela. A região da retroflexão da Corrente das Agulhas é uma entrada importante das águas do oceano Índico para o Atlântico, e os vórtices das Agulhas, indicados pelas elipses alaranjadas são liberados preferencialmente nessa região. Fechando o circuito do giro do Atlântico Sul, o ramo sul da Corrente Equatorial Sul é mostrado por uma linha pontilhada e tracejada em azul. A batimetria do fundo é representada por tons de cores (escala a direita). Características batimétricas importantes, tais como a elevação do Rio Grande, a Cordilheira Meso-Atlântica e a Cordilheira Walvis, estão indicadas no mapa.

Em relação ao FCO₂, em geral, a climatologia global tem revelado que essa região dos oceanos atua como uma fonte de CO₂ ao norte de 30°S, estando o oceano aberto, em média, próximo ao equilíbrio com a atmosfera [Lefèvre & Moore 2000, Padin *et al.* 2010], e com uma zona de absorção (entre 0,3–0,6 Pg C ano⁻¹) abaixo dessa latitude [Takahashi *et al.* 2002]. Além das estimativas globais, estudos locais foram conduzidos na região para tentar compreender com mais detalhes a dinâmica do CO₂ [e.g. Ito *et al.* 2005, 2016, González Dávila *et al.* 2009, Padin *et al.* 2009, Gregor & Monteiro 2013, Lencina-Avila *et al.* 2016].

Trabalhos que abordam a dinâmica das comunidades fitoplanctônicas em ambientes costeiros no oceano Atlântico Sul [Schloss *et al.* 2007, Barlow *et al.* 2016, Lima *et al.* 2019] têm investigado e integrado importantes informações acerca das interações físico-químicas que afetam a estrutura do fitoplâncton. Em relação ao oceano aberto os estudos são mais escassos, no entanto, alguns trabalhos [e.g. Araujo *et al.* 2017] têm revelado padrões contrastantes na distribuição do fitoplâncton ao longo da bacia do Atlântico Sul.

Tendo em vista a complexidade dessa área de estudo, optamos por adotar a abordagem de Longhurst [2006] para melhor investigar cada um desses ambientes, que são diferenciados quanto aos aspectos físicos e biológicos e, conseqüentemente, quanto ao seu comportamento em relação à absorção de CO₂ e à distribuição das comunidades fitoplanctônicas.

A divisão do oceano em províncias proposta por Longhurst [2006] tem sido bastante útil e usada em diversos trabalhos para comparação de processos biogeoquímicos entre as regiões oceânicas [Oliver & Irwin 2008] (Fig. 8).

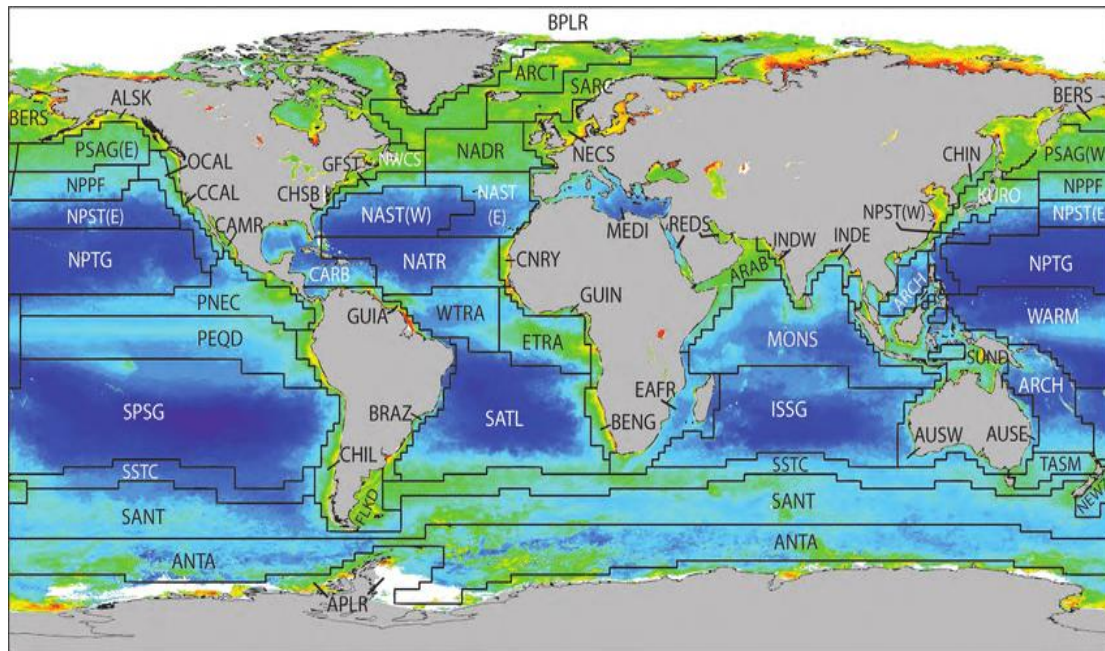


Figura 8. Províncias biogeoquímicas globais baseadas em Longhurst [2006]. Fonte: <http://www.mar.dfo-mpo.gc/>.

2.1 As províncias biogeoquímicas do oceano Atlântico Sul entre 20°S e 35°S

O oceano Atlântico Sul, mais especificamente a zona entre 20°S e 35°S, pode ser subdividido em três ambientes biogeoquimicamente distintos: (i) a província do Brasil (BRAZ), que é dominada pela corrente de contorno oeste (Corrente do Brasil) e influenciada por sistemas de ressurgência, pelo sistema frontal da confluência Brasil-Malvinas e, ainda, por eventos de mesoescala e descarga fluvial; (ii) a província do Giro do Atlântico Sul (SATL), que é regulada pela circulação anticiclônica do giro subtropical e influenciada, principalmente, pela liberação de vórtices provenientes da corrente das Agulhas, e por fim; (iii) a Província Africana (AFR) que, neste trabalho, é representada pela junção da província de Benguela (BENG) e da parte sul da província do Leste Africano (EAFR). Esta região é dominada pela Corrente de Benguela, uma corrente de

contorno leste, caracterizada pela presença de intensos sistemas de ressurgência, e influenciada pela retroflexão da Corrente das Agulhas.

2.1.1 O sistema dominado por corrente de contorno oeste

Este é o sistema biogeoquímico conhecido como província do Brasil (BRAZ). A região é dominada por um sistema de corrente de contorno oeste, Corrente do Brasil, que é reforçada por uma célula de recirculação de correntes entre o continente e a elevação do Rio Grande, e pela confluência do encontro da Corrente do Brasil com o fluxo norte da Corrente das Malvinas [Castro & Miranda 1998]. Outro aspecto importante dessa região é a presença do rio La Plata ($\approx 35^\circ\text{S}$), que em conjunto com a Lagoa dos Patos ($30^\circ\text{--}33^\circ\text{S}$), representam importantes fontes de água doce para as regiões da plataforma continental. Este aporte é controlado, principalmente, pela variabilidade do estresse do vento sob a superfície oceânica, que atua na alta variabilidade sazonal e interanual do deságue superficial [Piola *et al.* 2005].

Na porção sul da província BRAZ, a influência da convergência entre as correntes do Brasil e das Malvinas (dentro da faixa de latitude $35^\circ\text{--}45^\circ\text{S}$) [Garcia *et al.* 2008], assim como a presença do rio La Plata e da Lagoa dos Patos, possibilita o surgimento de elevadas biomassas de fitoplâncton, especialmente durante a primavera e inverno [Ciotti *et al.* 1995, 2010]. As medições de CO_2 nesta província apresentam uma forte variabilidade sazonal e espacial, com mudanças entre o comportamento de sumidouro e fonte de CO_2 da costa para as regiões *offshore*, respectivamente. O padrão é impulsionado, principalmente, por variações na distribuição superficial da $p\text{CO}_2^{\text{mar}}$ devido aos vários

mecanismos oceânicos atuantes na região [Ito *et al.* 2016].

Em relação aos grupos do fitoplâncton, Araujo *et al.* [2017] encontraram baixos valores de biomassa fitoplanctônica perto da costa brasileira, onde águas de baixa salinidade estavam associadas à presença de diatomáceas e nanoflagelados, enquanto a superfície do oceano aberto era dominada por procariontes. Outro estudo recente, na costa brasileira, associou positivamente a presença de haptófitas e cianobactérias, com temperatura e salinidade. Outros grupos como as criptófitas, dinoflagelados, prasinófitas e diatomáceas foram predominantes em regiões de maior estabilidade da coluna d'água e com maior teor em nutrientes, e negativamente associados à temperatura e salinidade [Lima *et al.* 2019]. Na região da confluência Brasil-Malvinas, massas de água ricas em nutrientes favorecem a presença de diatomáceas e dinoflagelados, porém baixos valores de biomassa podem ser encontrados, associados a altos índices de pastagem do fitoplâncton [Golçalves-Araujo *et al.* 2012].

2.1.2 O giro central do oceano Atlântico Sul

A porção central da circulação anticiclônica do oceano Atlântico Sul, excluindo as correntes de contorno que bordeiam as margens continentais, compõe o que é conhecido como província do Giro do Atlântico Sul (SATL). As águas oligotróficas do oceano aberto estão entre as províncias menos conhecidas do oceano Atlântico Sul [Longhurst 1998]. Essa região encontra-se permanentemente sob a influência dos ventos alísios [Reygondeau *et al.* 2013]. Estimativas do FCO₂ para essa região têm mostrado que essa província atua, principalmente, como um sumidouro de CO₂ atmosférico, tendo a temperatura

um importante controle na distribuição da $p\text{CO}_2^{\text{mar}}$ [Padin *et al.* 2010, Lencina-Avila *et al.* 2016, Orselli *et al.* 2018b]. A distribuição da clorofila *a* (Chl *a*) é marcada por uma mudança sazonal, com uma característica zonal permanente de alta clorofila na zona de convergência subtropical durante o verão austral que se move em direção ao equador durante o outono e atinge quase 25°S durante o inverno (julho-agosto). As concentrações elevadas de Chl *a* são mantidas durante o inverno e, de acordo com as condições da primavera e do verão, a floração oceânica do Atlântico Sul se move em direção ao polo, atingindo valores máximos de aproximadamente 1–2 mg de Chl *a* m⁻³ até fevereiro [Longhrust *et al.* 2006]. Os centros dos grandes giros subtropicais são regiões oligotróficas, portanto espera-se encontrar grupos fitoplanctônicos menores, com menores necessidades de nutrientes, como as cianobactérias picoplanctônicas [Marañón *et al.* 2003, Hartmann *et al.* 2012].

2.1.3 O sistema dominado por corrente de contorno leste

A província de BENG compreende a plataforma do sudoeste da África, incluindo o campo de ressurgência da Corrente de Benguela, que é dividida por uma barreira ambiental, a célula de ressurgência de Lüderitz a 26°S, em dois sistemas distintos: (i) o sistema de ressurgência do norte de Benguela, com baixa sazonalidade/variabilidade e (ii) o sistema de ressurgência do sul de Benguela, com ressurgências induzidas pelo vento na primavera e no verão [Duncombe Rae 2005, Hutchings *et al.* 2009]. Investigações dos padrões de distribuição da Chl *a* ao longo desses sistemas mostram maior biomassa na porção norte em comparação com a porção sul [Demarcq *et al.* 2007, Lamont *et al.* 2019]. Essa

região de fronteira oriental das águas superficiais do giro do Atlântico Sul atua como um sumidouro de CO₂, com forte variabilidade associada a eventos de ressurgência na região [González-Dávila *et al.* 2009].

A zona de retroflexão da Corrente de Agulhas, incluída na província costeira do EAFR, é uma região altamente energética, onde grandes vórtices de núcleo quente são liberados no Atlântico, com uma frequência média de liberação de vórtices que varia de 4 a 12 estruturas ao ano [Lutjeharms 2007]. Esses turbilhões possuem diâmetro médio de aproximadamente 300 km e têm vida útil muito longa, podendo ser identificados até 3,5 anos após sua liberação. Várias dessas estruturas não conseguem passar a barreira da Cordilheira Walvis, porém, algumas estruturas sobrevivem até atingir a região costeira brasileira [Azevedo *et al.* 2012, Pilo *et al.* 2015, Guerra *et al.* 2018]. Portanto, esses vórtices têm um papel importante na estrutura do giro subtropical do Atlântico Sul [Peterson & Stramma 1991] e, por esse motivo, são destacados ao longo desta tese.

O estudo recente de Orselli *et al.* [2018b] investigou o comportamento do CO₂ associado aos vórtices lançados pelo sistema de vazamento de Agulhas. O estudo destacou que essas estruturas de mesoescala intensificam o afundamento de CO₂ na região, podendo absorver em torno de 2,08 t de CO₂ ao longo de sua vida útil. Nesse estudo, o FCO₂ médio obtido para as bacias globais do Atlântico Sul foi de $-3,76 \text{ mmol CO}_2 \text{ m}^{-2} \text{ d}^{-1}$. Os autores também destacaram que a maior absorção de CO₂ ocorreu na bacia leste do oceano Atlântico Sul, com o mais intenso sumidouro de CO₂ encontrado próximo à região de vazamento de Agulhas. Tendo em vista esses resultados, o presente trabalho investigou a dinâmica dos grupos fitoplanctônicos nos mesmos vórtices

abordados em [Orselli et al. \[2018b\]](#), e os resultados serão apresentados no Capítulo VI. As maiores concentrações de biomassa fitoplanctônica foram encontradas na bacia oriental, influenciadas pelo sistema de ressurgência de Benguela e dominadas principalmente por flagelados (haptófitas e dinoflagelados).

2.2 Plataformas continentais da Costa Sul-Sudeste do Oeste do Oceano Atlântico Sul (20°S a 50°S)

As plataformas continentais são áreas de grande importância biogeoquímica pois, apesar de representarem uma pequena porção dos oceanos globais, possuem uma grande contribuição na produtividade primária [[Longhrust et al. 1995](#), [Laruelle et al. 2013](#)]. Por representarem uma região de interface entre os oceanos e o continente, apresentam influências distintas nos aportes de água doce, sedimentos, e carbono de origem terrígena. Essas regiões, por serem mais rasas, apresentam também grande variabilidade sazonal e recebem maiores impactos das atividades humanas, apresentando comportamentos bastante complexos em relação à dinâmica de CO₂ e à distribuição do fitoplâncton. Apesar de toda a sua relevância, as plataformas continentais são áreas ainda pouco estudadas, havendo ainda muita incerteza em relação à sua contribuição para o ciclo do carbono nos oceanos [e.g., [Cai et al. 2011](#), [Wanninkof et al. 2015](#), [Laruelle et al. 2018](#)]. A primeira estimativa de contribuição global das plataformas continentais resultou em valores em torno de 1 Pg C ano⁻¹ [[Tsunogai et al. 1999](#)]. Recentemente, as estimativas têm sido reportadas com valores variando de 0,2 a 0,4 Pg C ano⁻¹ [[Borges et al. 2005](#),

Laruelle *et al.* 2010, Roobaert *et al.* 2019]. Apesar dos avanços, há ainda muitas incertezas e um número limitado de observações nessas regiões, especialmente no Atlântico Sul.

2.2.1. A costa Sul-Sudeste brasileira

As regiões da plataforma continental e talude sul-sudeste brasileiros são geralmente caracterizadas como fonte de CO₂ para a atmosfera ao longo do ano [Ito *et al.* 2005]. Entretanto, podem ocorrer mudanças sazonais no comportamento do oceano aberto entre fonte e sumidouro de CO₂ [Ito *et al.* 2005, 2016]. Investigação recente na zona de quebra de plataforma continental sul-sudeste a identifica como região de fraca emissão de CO₂ para a atmosfera [Kerr *et al.* *In prep.*], sugerindo que estudos mais detalhados devam ser conduzidos de forma a compreender melhor a dinâmica da região.

A produção fitoplanctônica é limitada pela influência da corrente costeira relativamente pobre em nutrientes, sendo menor em pelo menos uma ordem de magnitude quando comparada aos sistemas de ressurgência do lado oriental [Longhurst 2006]. O consumo de carbono heterotrófico é substancialmente mais alto do que a produção autotrófica, exceto próximo aos sistemas de ressurgência estuarina locais [Brandini 2018], onde um ecossistema autotrófico baseado em diatomáceas e/ou dinoflagelados é alimentado por fontes pontuais de nutrientes [Villac *et al.* 2008]. Essa região pode ser marcada por alta variabilidade sazonal, com presença de plumas estuarinas, sistemas de ressurgências [Brandini *et al.* 2019] e, conseqüentemente, florações ocasionais de fitoplâncton ao longo da costa elevando a produtividade primária da região [Proença 2006]. A

comunidade fitoplanctônica é dominada por células de picoplâncton, principalmente cianobactérias e pico-eucariotos [Moser *et al.* 2016, Bergo *et al.* 2017].

2.2.2. A Plataforma continental da Patagônia Argentina

A quebra da plataforma continental da Patagônia Argentina é uma das regiões de maior absorção de CO₂ por unidade de área no oceano global [Bianchi *et al.* 2005, 2009]. Apresenta ainda grande variabilidade sazonal, tendo os menores fluxos líquidos de CO₂ no verão e os maiores na primavera, associados à predominância dos processos biológicos na distribuição da pressão parcial do CO₂ [Bianchi *et al.* 2009, Ferreira *et al.* 2013, Kahl *et al.* 2017]. Complementando o atual conhecimento sobre o sistema carbonato na região, estimativas recentes mostraram que esta é uma área de importante entrada de carbono antropogênico através da intrusão de águas intermediárias (Água Tropical e Água Central do Atlântico Sul) e, portanto, sujeita a estado de acidificação acelerado [Orselli *et al.* 2018a].

Esta é também uma das regiões mais produtivas dos oceanos, onde estudos sobre a variabilidade do fitoplâncton reportam importantes mudanças sazonais [Gonçalves-Araujo *et al.* 2016]. São áreas que apresentam predominantes florações de cocolitoforídeos no verão [Painter *et al.* 2010, Garcia *et al.* 2011, Souza *et al.* 2011] e diatomáceas na primavera [Golçalves-Araujo *et al.* 2016].

Capítulo III: Dados e métodos

Neste trabalho foram analisados dados hidrográficos, químicos e biológicos, previamente coletados, e parcialmente processados dos bancos de dados do Grupo de Oceanografia de Altas Latitudes (GOAL) e da Rede de Pesquisa Brasileira em Acidificação dos Oceanos (rede BrOA; www.broa.furg.br). Primeiramente, foram trabalhados os dados biológicos coletados em três vórtices distintos amostrados durante o cruzeiro transatlântico *Following Oceanic Rings in the South Atlantic* (FORSA) ocorrido em julho de 2015 (ver Capítulo IV). Em seguida, os dados de sete cruzeiros oceanográficos (Fig. 9), que percorreram rotas distintas entre o Brasil e a África entre as latitudes de 20°S e 35°S (ver Capítulo V), foram trabalhados de forma integrada caracterizando pela concentração de pigmentos a dominância dos grupos do fitoplâncton em cada província biogeoquímica definida anteriormente, e associando essa distribuição à magnitude dos fluxos de CO₂ medidos.

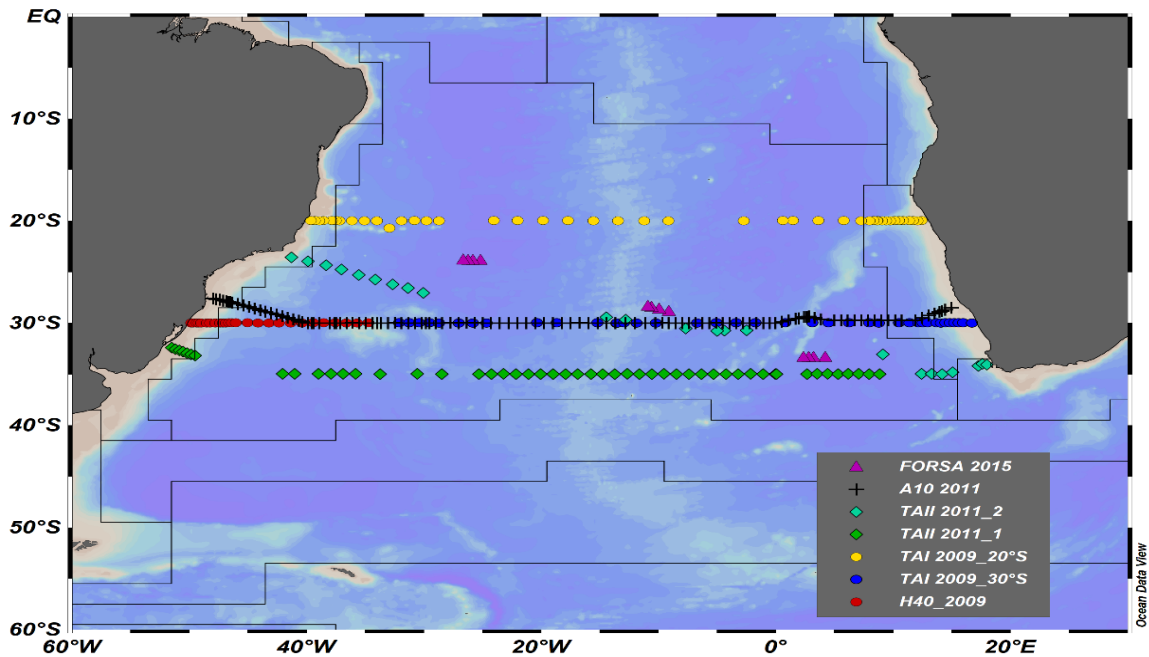


Figura 9. Mapa das estações oceanográficas dos cruzeiros transatlânticos que fizeram rotas entre o Brasil e a África. As estações oceanográficas ao longo das seções hidrográficas amostradas no Oceano Atlântico Sul são marcadas como símbolos de acordo com os seguintes cruzeiros neste estudo: H40_2009 (círculos vermelhos), TAI 2009_30 ° S (círculos azuis), TAI 2009_20 ° S (círculos amarelos), TAI 2011_1 (diamantes verdes), TAI 2011_2 (diamantes turquesa), A10 2011 (cruzes pretas) e FORSA 2015 (triângulos magenta). As linhas no mapa delimitam as províncias biogeoquímicas de acordo com Longhrust [2006] e foram sobrepostas usando o *shapefile* de VLIZ [2009].

Por fim, os dados dos cruzeiros ocorridos em regiões da plataforma continental sudoeste do Atlântico Sul entre 20°S e 50°S foram analisados no Capítulo VI. Dentre eles, dois cruzeiros que fizeram parte da série de amostragens na região da quebra de plataforma da Patagônia Argentina (*Patagonian Experiment – PATEX*) ocorridos nos anos de 2007 e 2008, e dois cruzeiros na costa sul e sudeste do Brasil, sendo um entre os anos de 2010 e 2011 (MCT II), e o outro ocorrido em 2014 no âmbito do projeto intitulado “Estudo dos processos físicos e biogeoquímicos que controlam a troca de carbono na interface ar-mar e Acidificação das águas na região do talude continental do Atlântico Sul” (EstARte-Sul) (Fig. 10). A tabela 1 reúne informações detalhadas sobre cada uma das campanhas oceanográficas mencionadas.

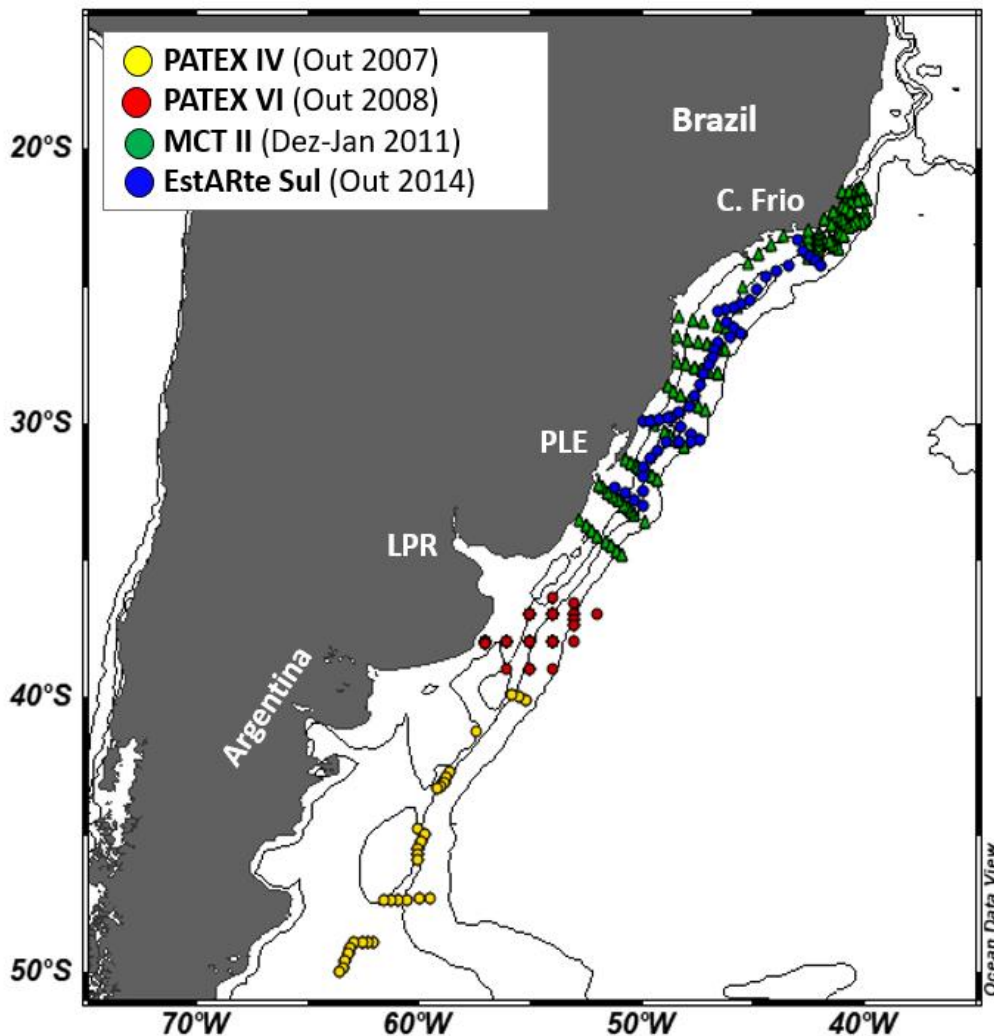


Figura 10. Mapa das estações oceanográficas referentes aos cruzeiros costeiros trabalhados nesta tese (Capítulo VI) Em amarelo temos as estações referentes ao banco de dados do cruzeiro PATEX IV ocorrido em outubro de 2007, em vermelho as estações do cruzeiro PATEX VI de outubro de 2008. Em verde as estações do cruzeiro que cobriu a plataforma sul e sudeste do Brasil (campanha MCTII) ocorrida entre dezembro de 2010 e janeiro de 2011 e por fim, a campanha EstARte Sul de outubro de 2014.

As metodologias trabalhadas nessa tese envolvem a determinação de parâmetros do sistema carbonato como a pressão parcial do CO_2 ($p\text{CO}_2$), a alcalinidade total (A_T) e o carbono inorgânico dissolvido total (C_T), para cálculo dos fluxos líquidos de CO_2 (FCO_2), e análises de pigmentos fotossintéticos do fitoplâncton, visando a caracterização das comunidades fitoplanctônicas. Neste capítulo, estas análises serão descritas de forma separada a fim de melhor detalhar cada etapa.

Tabela 1. Informações gerais sobre os cruzeiros abordados neste trabalho por ordem cronológica, incluindo o nome do cruzeiro, a área de cobertura, o período de amostragem (estação do ano), os dados utilizados (pigmentos fitoplanctônicos, temperatura da superfície do mar – SST, salinidade da superfície do mar – SSS, pressão parcial do CO₂: na atmosfera - $p\text{CO}_2^{\text{atm}}$, na superfície do mar - $p\text{CO}_2^{\text{mar}}$, na superfície do mar modelada - $m\text{pCO}_2^{\text{mar}}$, vento a 10m – U_{10}) e referências de trabalhos anteriores sobre estes cruzeiros.

Cruzeiro	Área de cobertura	Período de amostragem Estação do ano	Parâmetros medidos	Estações de coleta (n)	Referências
H40 2009 (30°S)	Seção meridional ao longo de 30°S indo de BRAZ até ~35°W SATL	12 Nov – 17Nov (2009) Primavera	Pigmentos fitoplanctônicos, SST, SSS, $m\text{pCO}_2^{\text{mar}}$, $p\text{CO}_2^{\text{atm}}$, U_{10}	26	Este estudo
TAI 2009 (30°S)	Seção meridional ao longo de 30°S indo de ~35°W SATL até AFR	24 Out – 16 Nov (2009) Primavera	Pigmentos fitoplanctônicos, SST, SSS, $m\text{pCO}_2^{\text{mar}}$, $p\text{CO}_2^{\text{atm}}$, U_{10}	39	Este estudo
TAI 2009 (20°S)	Seção meridional ao longo de 20°S até ~35°W SATL	1 Dez – 20 Dez (2009) Primavera	Pigmentos fitoplanctônicos, SST, SSS, $m\text{pCO}_2^{\text{mar}}$, $p\text{CO}_2^{\text{atm}}$, U_{10}	42	Este estudo
TAII 2011_1 (30°S)	Seção meridional ao longo de 30°S da BRAZ até AFR	25 Out – 23 Nov (2011) Primavera	Pigmentos fitoplanctônicos, SST, SSS, $m\text{pCO}_2^{\text{mar}}$, $p\text{CO}_2^{\text{atm}}$, U_{10}	52	Lencina-Avila et al. [2016]
TAII 2011_2	Seção SO-NE indo da AFR até BRAZ	4 Dez – 12 Dez (2011) Final da Primavera	Pigmentos fitoplanctônicos, SST, SSS, $m\text{pCO}_2^{\text{mar}}$, $p\text{CO}_2^{\text{atm}}$, U_{10}	23	Este estudo
A10 2011 (35°S)	Seção meridional ao longo de 35°S da BRAZ até AFR	28 Set – 29 Out (2011) Primavera	Pigmentos fitoplanctônicos, SST, SSS, $p\text{CO}_2^{\text{mar}}$, $p\text{CO}_2^{\text{atm}}$, U_{10}	117	Araújo et al. [2017] Orselli et al. [2019]
FORSA 2015	Seção SO-NE na SATL ao longo do corredor das Agulhas	27 Jun – 15 Jul (2015) Inverno	Pigmentos fitoplanctônicos, SST, SSS, $p\text{CO}_2^{\text{mar}}$, $p\text{CO}_2^{\text{atm}}$, U_{10}	12	Orselli et al. [2018b] Carvalho et al. [2019]
PATEX IV 2007	Quebra da Plataforma da Patagônia Argentina entre 35°S e 50°S	16 Out – 22 Out (2007) Primavera	Pigmentos fitoplanctônicos, SST, SSS, A_T , C_T , U_{10}	29	Orselli et al. [2018a]
PATEX VI 2008	Quebra da Plataforma da Patagônia Argentina entre 35°S e 50°S	13 Out – 18 Out (2008) Primavera	Pigmentos fitoplanctônicos, SST, SSS, A_T , C_T , U_{10}	37	Orselli et al. [2018a]
MCT II 2010/2011	Plataforma continental S-SE do Brasil entre 20°S e 30°S	6 Dez (2010) – 11Jan (2011) Verão	Pigmentos fitoplanctônicos, SST, SSS, $p\text{CO}_2^{\text{mar}}$, $p\text{CO}_2^{\text{atm}}$, U_{10}	109	Ito et al. [2016]
EstARte Sul 2014	Plataforma Continental S-SE do Brasil entre 20°S e 35°S	22 Out – 30 Out (2014) Primavera	Pigmentos fitoplanctônicos, SST, SSS, $p\text{CO}_2^{\text{mar}}$, $p\text{CO}_2^{\text{atm}}$, U_{10}	45	Carvalho-Borges et al. [2018] Kerr et al. In prep.

3.1 Análise dos parâmetros do sistema carbonato

Com um par de parâmetros do sistema carbonato (i.e., $p\text{CO}_2$, A_T , C_T e pH) é possível calcular os demais com certo erro associado [Millero *et al.* 2007]. Definindo brevemente, a $p\text{CO}_2$ é a fração molar do CO_2 em equilíbrio na fração total da amostra, ou seja, é a medida do grau de saturação da amostra de água com o CO_2 gasoso [Dickson 2010]. Portanto, se refere ao resultado da aplicação da Lei de Henry (Lei dos gases ideais) sobre o equilíbrio de dissolução de gases, a qual diz que a uma determinada temperatura, a concentração de um gás dissolvido na solução é proporcional à pressão parcial que o gás exerce em equilíbrio com a solução.

A A_T pode ser definida como o número de moles de hidrogênio equivalentes ao excesso de aceptores de prótons em 1 kg de água [Dickson 1981]. Para águas oceânicas (pH ~ 8; $A_T = 2300 \mu\text{mol kg}^{-1}$), a A_T pode ser expressa pela equação 4, que representa o somatório da alcalinidade carbonática (96%), do borato (3,7%) e da água (0,2%).

$$A_T = [\text{HCO}_3^-] + 2[\text{CO}_3^{2-}] + [\text{B}(\text{OH})_4^-] + [\text{OH}^-] - [\text{H}^+] \quad (4)$$

O C_T pode ser definido como a soma das formas de carbono inorgânico dissolvido (Eq. 5). Estas espécies químicas estão na água do mar nas proporções de CO_2 : HCO_3^- : CO_3^{2-} de 0,5: 86,5: 13, respectivamente [Zeebe & Wolf-Gladrow 2008]. As concentrações e as proporções relativas das diferentes formas químicas de CO_2 na água do mar são controladas pelo pH (Fig. 11).

$$C_T = [\text{CO}_2] + [\text{HCO}_3^-] + [\text{CO}_3^{2-}] \quad (5)$$

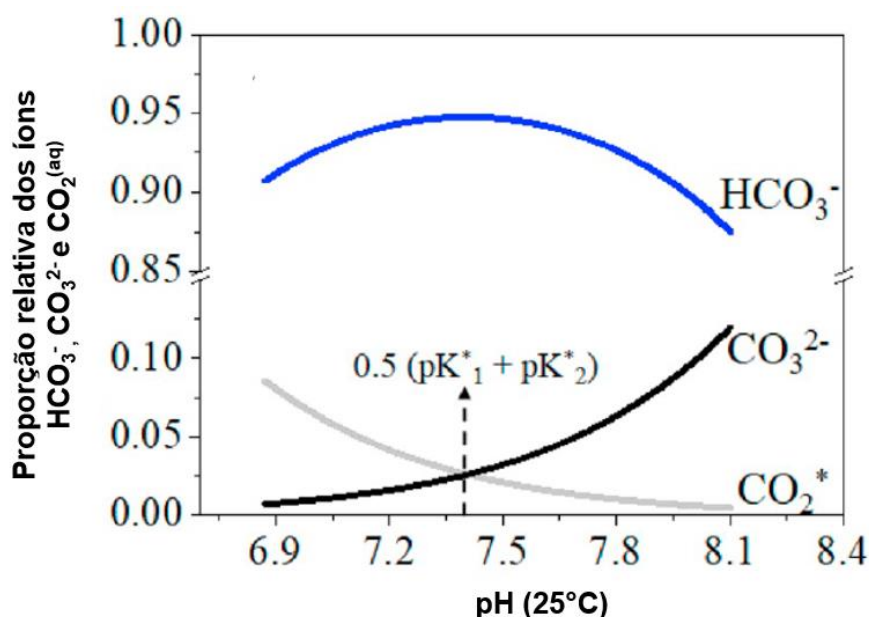


Figura 11. Variação das proporções relativas das espécies do CO₂ aquoso (CO₂^{*}), carbonato (CO₃²⁻) e bicarbonato (HCO₃⁻) na água do mar com o pH na temperatura de 25°C. Mostrando que o pH na água do mar é determinado por mudanças relativas nas concentrações de CO₃²⁻ e HCO₃⁻, uma vez que as concentrações de HCO₃⁻ na água do mar são relativamente estáveis. Com o aumento no pH, temos o aumento da concentração de CO₃²⁻ (K₁ e K₂ são a primeira e segunda constantes de dissociação do ácido carbônico). Adaptado de Xue & Cai [2020].

O pH, definido como a concentração do íon hidrogênio na água, é representado pela equação 6. A variável pH tem sido empregada para cálculos do sistema carbonato associada a diferentes significados, escalas e procedimentos analíticos, o que dificulta a utilização dessa variável para os cálculos. Medições de pH com pouca exatidão são um dos principais erros nos cálculos do sistema carbonato [Dickson 2010].

$$\text{pH} = -\log[\text{H}^+] \quad (6)$$

3.1.1 Pressão parcial do CO₂ (pCO₂)

As determinações da pressão parcial do CO₂ no oceano (pCO₂^{mar}) foram

feitas usando sistemas autônomos contínuos e rotinas de redução de dados. Quando não foi possível a medida direta e contínua, no caso dos cruzeiros PATEX IV e VI (Tab.1), a $p\text{CO}_2^{\text{mar}}$ foi calculada de maneira indireta, usando parâmetros do sistema carbonato (A_T e C_T) juntamente com dados de temperatura e salinidade, sendo esse método detalhado a seguir no item 3.1.2. Para os cruzeiros ocorridos em 2009 (i.e., H40 2009, TAI 2009 – 20°S e TAI 2009 – 30°S; Tab. 1) foi necessário modelar a $p\text{CO}_2^{\text{mar}}$ ($mp\text{CO}_2^{\text{mar}}$) usando um algoritmo (Eq. 7) desenvolvido para a região de estudo ($r^2 = 0,81$ e $\text{STD}_{\text{error}} = 6,74 \mu\text{atm}$) [Orselli *et al.* 2018b].

$$mp\text{CO}_2 = \alpha + \beta_1 T + \beta_2 S + \beta_3 \text{Chl } a \quad (7)$$

onde T, S e Chl a são as anomalias (diferença entre o dado observado e o dado médio) de temperatura, salinidade e clorofila a, respectivamente. E os coeficientes $\alpha = 353,05$, $\beta_1 = 4,91$, $\beta_2 = -9,6$ e $\beta_3 = -26,86$.

A pressão parcial do CO_2 na atmosfera ($p\text{CO}_2^{\text{atm}}$) foi medida diretamente durante a trajetória nos cruzeiros: TAI 2011_1, TAI 2011_2, A10 2011, FORSA 2015, MCT II 2010 e EstARte Sul 2014 (Tab.1). Quando não medida diretamente (i.e., cruzeiros H40 2009, TAI 2009 20°S e TAI 2009 30°S), esta foi obtida através do portal NOAA-ESRL (<https://www.esrl.noaa.gov/gmd/dv/data/>). Neste caso, dados de medidas discretas foram obtidos, e a média mensal da $p\text{CO}_2^{\text{atm}}$ para os meses de outubro, novembro e dezembro de 2009 da estação ABP (Arempebe, Bahia, Brasil) e CPT (Cape Point, África do Sul) foram determinadas. No caso dos cruzeiros PATEX IV e VI, a $p\text{CO}_2^{\text{atm}}$ foi obtida de dados da literatura para a região [Bianchi *et al.* 2009].

A $p\text{CO}_2^{\text{mar}}$ foi calculada e normalizada segundo [Takahashi et al. \[2009\]](#) em relação ao efeito da temperatura ([Eq. 8](#)), onde SST é a temperatura da superfície do mar e \overline{SST} representa sua média.

$$Np\text{CO}_2^{\text{mar}} = p\text{CO}_2^{\text{mar}} * \exp [0,0423 (SST - \overline{SST})] \quad (8)$$

3.1.2 Alcalinidade total (A_T) e carbono inorgânico dissolvido total (C_T)

Amostras para análise dos parâmetros A_T e C_T foram coletadas nos cruzeiros ocorridos na região da quebra de plataforma da Patagônia Argentina: PATEX IV (2007) e PATEX VI (2008) ([Tab. 1](#)). Estes parâmetros foram utilizados juntamente com os dados de salinidade e temperatura para a determinação da $p\text{CO}_2^{\text{mar}}$, utilizando o programa CO₂Sys v.2.1 desenvolvido por [Lewis et al. \[1991\]](#) e modificado por [Pierrot et al. \[2006\]](#). Foram ainda usadas as constantes de dissociação K_1 e K_2 de [Millero et al. \[2006\]](#), e constantes de sulfato e borato de [Dickson \[1990\]](#) e [Uppström \[1974\]](#), respectivamente.

As amostras de água da superfície do mar foram coletadas sem que houvesse a formação de bolhas, e fixadas com cloreto de mercúrio (HgCl_2) para cessar a atividade biológica. Em seguida, as amostras foram armazenadas em local escuro e arejado para posterior análise em laboratório.

A determinação da A_T foi realizada segundo [Dickson et al. \[2007\]](#) pelo método de titulação potenciométrica em cela fechada (SOP 3a – Alcalinidade Total da água do mar por titulação em cela fechada). Para esta análise a temperatura da amostra deve estar próxima da temperatura local, para isso fez-se uso de um banho termostático. Em seguida, em uma cela fechada, cujo

volume foi previamente calibrado, foi efetuada a titulação de uma quantidade conhecida de água do mar. A titulação foi feita com solução de ácido clorídrico (HCl) adicionado de cloreto de sódio (NaCl) com a finalidade de simular a força iônica da água do mar ($\sim 0,7 \text{ mol kg}^{-1}$), mantendo os coeficientes de atividade aproximadamente constantes durante a titulação. A cela fechada permite que o C_T seja estimado durante a mesma titulação, visto que a cela fechada permite assumir que o C_T permanece constante durante toda a titulação. O progresso da titulação é monitorado usando um eletrodo de pH e um termômetro. Inicialmente é adicionada uma quantidade maior de ácido ($\sim 3 \text{ mL}$), seguida de pequenos incrementos de ácido (0,1 a 0,2 mL). Ao final de cada adição, o volume de ácido e a força eletromotriz são monitorados para determinar o ponto de inflexão da curva de titulação. Assim, a A_T é calculada a partir desses dados usando um procedimento de mínimos quadrados com base em um ajuste de curva não linear [Dickson *et al.* 2007].

3.2 Cálculos dos fluxos líquidos de CO_2

O FCO_2 foi calculado a partir do produto da diferença de $p\text{CO}_2$ entre o oceano e atmosfera ($\Delta p\text{CO}_2 = p\text{CO}_2^{\text{mar}} - p\text{CO}_2^{\text{atm}}$) e os coeficientes de transferência gasosa (k) e de solubilidade do CO_2 na água do mar (K_0) (Eq. 9). Portanto, valores negativos de $\Delta p\text{CO}_2$ são indicativos de uma absorção de CO_2 da atmosfera pelo oceano e, inversamente, valores positivos são indicativos de liberação de CO_2 para a atmosfera. Neste estudo, utilizou-se a parametrização para o coeficiente de transferência gasosa (k) de Wanninkhof [2014] (Eq. 10) e o coeficiente de solubilidade do CO_2 (K_0) de Weiss [1974], calculado usando a

temperatura em Kelvin (T) (Eq. 11).

$$FCO_2 = k K_0 (\Delta pCO_2) \quad (9)$$

$$k = 0,251 U_{10}^2 (Sc/660)^{-0,5} \quad (10)$$

$$K_0 = \exp (-58,0931 + 90,5069 * (100/T) + 22,2940 * \ln(T/100) S^*(0,027766 - 0,025888 * (T/100) + 0,0050578 * (T/100)^2) \quad (11)$$

Os dados de velocidade do vento a 10 m (U_{10}) foram obtidos através do portal European Center for Medium-Range Weather Forecasts (ECMWF) (<http://data-portal.ecmwf.int/>) com resolução espacial de 1.5° de latitude e 1.5° de longitude. O número de Schimidt (Sc) que aparece na equação 10 foi calculado (Eq.12), usando a temperatura (t) em graus Celsius (°C). Para o oceano, os coeficientes adotados foram: A= 2116,8; B=136,25; C= 4,7353; D=0,092307 e E=0,000755.

$$Sc = A - Bt + Ct^2 - Dt^3 + Et^4 \quad (12)$$

3.3 Composição da comunidade fitoplanctônica

A composição da comunidade fitoplanctônica foi obtida pela análise dos pigmentos fitoplanctônicos determinados por cromatografia líquida de alta

eficiência (do inglês, *High Performance Liquid Chromatography* – HPLC). A contribuição relativa dos grupos fitoplanctônicos para a biomassa total (TChl *a*) foi calculada usando o programa quimio-taxonômico CHEMTAX v1.95. Esta metodologia é amplamente aceita e utilizada na determinação da estrutura das comunidades de fitoplâncton, sendo baseada no uso de pigmentos como biomarcadores taxonômicos dos grupos fitoplanctônicos.

3.3.1 Análise de composição pigmentar por HPLC/CHEMTAX

As amostras de água da superfície do mar coletadas para análise dos pigmentos fitoplanctônicos durante os diversos cruzeiros oceanográficos analisados nesse trabalho foram filtradas usando filtros Whatman GF/F (tamanho do poro 0,7 µm; 25 mm diâmetro). Os filtros foram imediatamente armazenados em nitrogênio líquido para posterior análise da composição pigmentar em laboratório.

As determinações por HPLC, na qual uma coluna cromatográfica efetua a separação simultânea de grupos de moléculas de diferentes polaridades, no caso os pigmentos presentes em cada amostra, foram realizadas no Laboratório do Fitoplâncton e Micro-organismos Marinhos – IO/FURG usando a metodologia de [Zapata et al. \[2000\]](#), otimizada e discutida por [Mendes et al. \[2007\]](#). A partir desta análise, cada pigmento é registrado em um gráfico, conhecido como cromatograma, de acordo com o seu tempo de retenção na coluna cromatográfica e espectro de absorvância. Esses cromatogramas são interpretados com dados da literatura [[Higgins et al. 2011](#)].

A metodologia descrita acima seguiu o seguinte protocolo: a extração dos pigmentos foi feita no escuro usando uma alíquota de 3 mL de metanol 95% tamponado a frio (2% acetato de amônio) contendo 0,05 mg L⁻¹trans-β-apo-8'-carotenal (Fluka) como padrão interno. As amostras foram sonicadas por 5 minutos em banho de gelo, mantidas a -20 °C por 1 h, e centrifugadas (3000 rpm) por 5 minutos a 3 °C usando uma centrífuga refrigerada (modelo 280-R Excelsa 4). O sobrenadante foi filtrado usando filtros Fluoropore PTFE (tamanho do poro 0,2 μm) para remoção de restos de filtro e de células do extrato. Antes da análise, uma alíquota da amostra (1000 μL) foi adicionada a 400 μL de água Milli-Q em vials de 2 mL, que foram em seguida colocados no rack de refrigeração (4 °C) do equipamento HPLC (Shimadzu *Prominence LC-20A Modular HPLC System*). Os procedimentos metodológicos para a análise de HPLC, usando uma coluna monomérica C8 com a fase móvel contendo piridina, estão descritos em [Zapata et al. \[2000\]](#). Os limites de detecção e quantificação do método de HPLC usado neste trabalho seguiram os procedimentos descritos e discutidos por [Mendes et al. \[2007\]](#). Os pigmentos foram identificados quanto ao espectro de absorvância e tempo de retenção no detector de fotodiodos (Shimadzu, SPD-M20A; 190–800 nm; 1 nm de acurácia) e/ou detector de fluorescência (Shimadzu, RF-10AXL; Ex. 430 nm/Em. 670 nm). A calibração e subsequente quantificação dos pigmentos foi feita no (ou próximo do) comprimento de onda de máxima absorção (e.g., clorofila *a* a 430 nm, fucoxantina a 448 nm, zeaxantina a 454 nm, e clorofila *b* a 470 nm). Os pigmentos foram quantificados pela integração dos picos de absorção usando o programa LC-Solution (Shimadzu), e todas as integrações dos picos foram conferidas manualmente e corrigidas quando necessário. O HPLC foi

previamente calibrado com padrões comerciais do *Institute for Water and Environment, Denmark* (DHI).

Utilizando a concentração dos pigmentos presentes em cada amostra, a contribuição relativa do principais grupos de microalgas para a TChl a foi calculada usando o programa quimio-taxonômico CHEMTAX v1.95, que utiliza os pigmentos acessórios classe-específicos em relação ao total de clorofila a [Mackey *et al.* 1996]. O CHEMTAX efetua uma análise fatorial e de algoritmos para melhor ajustar os dados em uma matriz inicial de proporções de pigmentos (razão entre um pigmento acessório marcador e a TChl a). Os procedimentos e cálculos de CHEMTAX estão descritos em Mackey *et al.* [1996]. As razões iniciais de pigmento das principais classes de algas usadas aqui foram derivadas de Higgins *et al.* [2011], com os grupos quimio-taxonômicos identificados/definidos de acordo com Jeffrey *et al.* [2011]. Com base nos pigmentos diagnósticos identificados, os grupos de algas são carregados no programa CHEMTAX (e.g. prasinófitas, clorófitas, criptófitas, diatomáceas, pelagófitas, dinoflagelados, haptófitas, *Synechococcus* e *Prochlorococcus*).

3.4 Análises Estatísticas

As análises de correlação entre os parâmetros bióticos (grupos fitoplanctônicos) e abióticos (variáveis ambientais) foram realizadas no programa R [R Core Team 2017] usando o pacote “corrplot” [Taiyun Wei & Viliam Simko 2017]. Matrizes de correlação e coeficiente de correlação de Pearson (r) foram calculados entre variáveis bióticas, representadas pelas biomassas dos grupos taxonômicos derivados do CHEMTAX (em mg m^{-3} do TChl a) e as variáveis

ambientais, incluindo temperatura da superfície do mar (SST), salinidade da superfície do mar (SSS), biomassa fitoplanctônica (TChl *a*), vento, pressão parcial do CO₂ na superfície do mar ($p\text{CO}_2^{\text{mar}}$), pressão parcial do CO₂ na superfície do mar normalizada pela temperatura ($Np\text{CO}_2^{\text{mar}}$), diferença de pressão parcial do CO₂ entre o oceano e a atmosfera ($\Delta p\text{CO}_2$), e o FCO₂. A relação dos grupos fitoplanctônicos com as variáveis ambientais foi investigada por análise de correspondência canônica (CCA) [Ter Braak & Prentice 1988], usando o programa CANOCO para Windows 4.5. Uma abordagem de Monte Carlo foi executada com base em 499 permutações sob um modelo reduzido ($p < 0,05$) para avaliar a significância da CCA. A análise de CCA também permitiu uma visão aprimorada dos padrões observados nas três províncias biogeoquímicas abordadas neste estudo.

3.5 Efeito da temperatura e da biologia no controle da $p\text{CO}_2$

Para investigação dos fatores que controlam a $p\text{CO}_2$ foi utilizada a abordagem proposta por Takahashi *et al.* [2002]. Neste contexto, foram calculados valores da $p\text{CO}_2^{\text{mar}}$ normalizados em relação ao efeito da temperatura, ou seja, usando a temperatura média (\overline{SST}) (Eq. 13). Em seguida, foi feito o cálculo usando um valor médio da $p\text{CO}_2^{\text{mar}}$ ($\overline{p\text{CO}_2^{\text{mar}}}$) para a região nas temperaturas observadas (SST) (Eq. 14).

$$p\text{CO}_2^{\text{mar}} \text{ na } \overline{SST} = p\text{CO}_2^{\text{mar}} * \exp [0,0423(\overline{SST} - SST)] \quad (13)$$

$$p\text{CO}_2^{\text{mar}} \text{ na } SST = \overline{p\text{CO}_2^{\text{mar}}} * \exp [0,0423(SST - \overline{SST})] \quad (14)$$

As mudanças na $p\text{CO}_2^{\text{mar}}$ relacionadas ao efeito da biologia ($\Delta p\text{CO}_2^{\text{bio}}$) e ao efeito da temperatura ($\Delta p\text{CO}_2^{\text{temp}}$) podem, então, ser assim obtidas (Eq. 15-16).

$$\Delta p\text{CO}_2^{\text{bio}} = (p\text{CO}_2^{\text{mar}} \text{ na } \overline{\text{SST}})_{\text{máx}} - (p\text{CO}_2^{\text{mar}} \text{ na } \overline{\text{SST}})_{\text{mín}} \quad (15)$$

$$\Delta p\text{CO}_2^{\text{temp}} = (p\text{CO}_2^{\text{mar}} \text{ na SST})_{\text{máx}} - (p\text{CO}_2^{\text{mar}} \text{ na SST})_{\text{mín}} \quad (16)$$

Para comparar a magnitude dos efeitos da temperatura (T) e da biologia (B), tanto a razão como a diferença entre $\Delta p\text{CO}_2^{\text{temp}}$ e $\Delta p\text{CO}_2^{\text{bio}}$ podem ser determinadas (Eq.17-18):

$$T-B = (\Delta p\text{CO}_2^{\text{temp}}) - (\Delta p\text{CO}_2^{\text{bio}}) \quad (17)$$

$$T/B = (\Delta p\text{CO}_2^{\text{temp}}) / (\Delta p\text{CO}_2^{\text{bio}}) \quad (18)$$

Em regiões com alta variabilidade sazonal e onde a atividade biológica é elevada, a razão T/B será menor que 1 ou a diferença T-B será negativa. Por outro lado, em regiões com atividade biológica fraca ou constante ao longo do ano, a razão T/B será maior que 1 ou a diferença T-B será positiva.

Capítulo IV: Distribuição do fitoplâncton nos vórtices anticiclônicos

O primeiro manuscrito, em síntese, trata da aplicação da metodologia de análise da composição pigmentar para determinação/quantificação dos grupos fitoplanctônicos durante a campanha oceanográfica *Following Oceanic Rings in the South Atlantic* – FORSA, cujo objetivo foi a investigação dos vórtices provenientes da região do vazamento da corrente das Agulhas que atingem o oceano Atlântico Sul. Este trabalho possibilitou observar a biomassa e a composição do fitoplâncton em vórtices com estágios de vida diferentes e, ainda, contribuiu para um melhor entendimento de como as comunidades fitoplanctônicas se estruturam em ambientes oligotróficos. De autoria de Andréa da Consolação de Oliveira Carvalho, Carlos Rafael Borges Mendes, Rodrigo Kerr, José Luiz de Lima Azevedo, Felipe Galdino e Virginia Maria

Tavano, intitulado “*The impact of mesoscale eddies on the phytoplankton community in the South Atlantic Ocean: HPLC-CHEMTAX approach*”, foi publicado no periódico “*Marine Environmental Research – Elsevier*” em dezembro de 2019.

Abstract

This study describes the pigment-based phytoplankton community within three South Atlantic anticyclonic eddies (at different ages) shed from the Agulhas Current retroflection crossing the South Atlantic Ocean. Seawater samples were collected over these mesoscale structures in June-July 2015 during the Following Ocean Rings in the South Atlantic (FORSA) cruise. Data on phytoplankton pigments, measured with high-performance liquid chromatography (HPLC), were processed using a chemical taxonomy (CHEMTAX) tool to determine and quantify phytoplankton taxonomic groups. In addition, physical (water column structure) and chemical (macronutrient) parameters were determined and related to the biological data. Our results showed that, in general, the community was composed mostly of small flagellates (haptophytes) and prokaryotes (*Prochlorococcus*) and that pelagophytes were prominent in the younger eddy. This ring, located in the eastern basin of the South Atlantic Ocean, represented a younger and stronger structure, with no evident deep chlorophyll maximum (DCM) depth and an evenly distributed biomass over a well-mixed upper layer, revealing a more diverse phytoplankton community. The weakened structures of the older western eddies presented a pronounced DCM depth below 100 m and similar phytoplankton community composition patterns marked by enhanced

Prochlorococcus contributions but also the important occurrences of haptophytes at the DCM depth and Synechococcus and chlorophytes at the surface. The community distributions in all three structures were associated with the distribution of nutrients and acclimation to light conditions. This study contributes to a better understanding of the phytoplankton distribution and its association with the presence of mesoscale anticyclonic eddies in an undersampled and complex region of the South Atlantic Ocean.

4.1 Introduction

Oceanic eddies are ubiquitous mesoscale structures with diameters of ten to hundreds of kilometers [e.g., [Zhang *et al.* 2014](#), [Angel-benavides *et al.* 2016](#)]. These eddies are particularly intense in western boundary currents such as the Agulhas Current in the Southwest Indian Ocean. These rotating structures present closed circulation, generating positive (negative) sea surface anomalies for anticyclonic (cyclonic) eddies. Eddies ordinarily transport waters with different characteristics from their surroundings, contributing to the redistribution of heat, salt, and momentum between different regions via the advection of physical, chemical, and biological properties.

Mesoscale eddies play a major role in ocean biogeochemistry as they modify the spatial distribution of biogeochemical properties through several mechanisms, such as isopycnal displacement, eddy pumping, eddy advection, eddy-induced Ekman pumping, stirring and trapping [e.g., [Siegel *et al.* 2011](#), [Gaube *et al.* 2013](#), [Angel-benavides *et al.* 2016](#), [McGillicuddy 2016](#)]. Mesoscale dynamics can influence both upper ocean phytoplankton biomass, normally

tracked as chlorophyll *a* (Chl *a*), and phytoplankton community distributions [Gaube *et al.* 2014]. Chlorophyll anomalies associated with eddies are usually related to mechanisms such as eddy stirring and trapping, which transport Chl *a* horizontally and modify its regional spatial distribution [Chelton *et al.* 2011, Lehahn *et al.* 2011]. Eddy-Ekman pumping is also responsible for greater biogeochemical impact by the vertical lowering of nutrients in anticyclonic eddies [He *et al.* 2016]. In these eddies, isopycnal displacement results in the sinking and deepening of the mixed layer and nutricline [Tilburg 2002, McGillicuddy 2015], which inhibits phytoplankton growth [Eden & Dietze 2009].

Near the tip of South Africa, anticyclonic eddies shed in the Agulhas retroflection zone carry warm and salty waters from the Indian Ocean to the South Atlantic [e.g., Duncombe Rae 1991, Lutjeharms 2007], which is associated with high positive sea level anomalies (SLAs) [McGillicuddy 2015]. As these mesoscale features stir the ocean, they generate physical perturbations in the water column, and nutrients can either be uplifted (which stimulates biological activity) or pulled down into the euphotic zone [Gao *et al.* 2017]. However, the intensity of the biological response sustained by eddies is variable [e.g., Bibby & Moore 2011]. The physical perturbations generated by the eddies are considered important mechanisms for the transport of large amounts of nutrients and thus contribute to increasing the concentrations of growth-limiting nutrients delivered into the euphotic zone. In this sense, the eddies may represent an important source of nutrients in oligotrophic regions of the open ocean and modify the phytoplankton community structure within these features, which vary as a function of nutrient availability and light distribution [e.g., Vaillancourt *et al.* 2003, Bibby *et al.* 2008].

Several studies have indicated that the occurrence of eddies plays an important ecological role in the dynamics of phytoplankton biomass and community composition [e.g., [Vaillancourt et al. 2003](#), [Condie & Condie 2016](#), [Barlow et al. 2017](#)]. In the North Pacific, a cyclonic eddy investigation showed a shift in species composition favoring the accumulation of larger phytoplankton species [[Vaillancourt et al. 2003](#)]. Using a coupled physical-biological model, [Chenillat et al. \[2016\]](#) investigated the contribution of eddies from the California Current System to the export of coastal production and found asymmetric behaviors between anticyclonic and cyclonic eddies in controlling biology, with cyclonic eddies playing a greater role in the redistribution and enhancement of biology. Through satellite observations and model simulation, [He et al. \[2017\]](#) reported a phytoplankton bloom in an anticyclonic eddy in the nutrient-depleted region of the southeastern Indian Ocean, which was attributed to the combined effect of eddy-Ekman pumping and winter mixing. Model simulations off the East Australian coast characterized cyclonic eddies as features of higher concentrations of both Chl *a* and large phytoplankton (i.e., diatoms) due to shallower mixed layers compared to anticyclonic eddies conditions [[Laiolo et al. 2016](#)]. [Morales et al. \[2017\]](#) found a mixture of coastal and oceanic diatom species around a front-eddy interaction due to both offshore and onshore advection, showing the contribution of eddies (and not just offshore advection) to the coastal environment as being the most commonly reported. In the Southern Ocean, the role of eddies in biogeochemical cycling still remains largely unresolved [[Moreau et al. 2017](#)]. For instance, studies conducted in the Scotia Sea found increased phytoplankton biomass in both anticyclonic [[Meredith et al. 2003](#)] and cyclonic eddies [[Kahru et al. 2007](#)]. Despite advances in knowledge

on the role played by eddies in phytoplankton, little is understood about changes in the phytoplankton community structure within mesoscale features in the global ocean, and even less is understood in the South Atlantic.

The African coast, which is under the influence of the eastern boundary upwelling system of the Benguela Current, provides a very productive biological environment due to a strong nutrient supply from a depth favored by offshore Ekman transport, which is driven by persistent equatorward winds [[Hutchings *et al.* 2009](#)]. Conditions become more oligotrophic westward of the South Atlantic basin. However, mesoscale eddies from the Agulhas retroflection, through a combination of horizontal and vertical dynamical processes (including horizontal eddy transport), play an important role in shaping and sustaining biological production, which contributes to the fertilization of oligotrophic waters in an otherwise nutrient-depleted subtropical gyre [e.g., [Lee & Williams 2000](#), [Oschlies 2002](#), [Lévy 2003](#), [Lehahn *et al.* 2011](#)]. However, the enhancement of productivity is difficult to demonstrate due to the paucity of observational data in the eddies of subtropical gyres.

Most of the oceanographic studies on anticyclonic eddies have focused on physical processes and ocean circulation modeling [e.g., [Wang *et al.* 2003, 2005, 2008](#)], whereas few studies have focused on biological processes associated with phytoplankton biomass and community structure [e.g., [Ning *et al.* 2004](#)]. The role of eddy dynamics on phytoplankton biomass distribution and production in oceans is unquestionable [e.g., [Jeffrey & Hallegraeff 1980](#), [Angel & Fasham 1983](#), [Falkowski *et al.* 1991](#), [McGillicuddy *et al.* 1998](#), [Machu & Garçon 2001](#), [Vaillancourt *et al.* 2003](#)]. The impact of eddies on surface chlorophyll and phytoplankton compositions remains an issue. In general, the spatial patterns of

Chl *a* are associated with the physical mechanism of vertical pumping and obey the following pattern: high Chl *a* and positive anomalies associated with the interior of anticyclonic eddies and low Chl *a* and negative anomalies associated within cyclonic eddies [e.g., [Angel-benavides et al. 2016](#)]. A recent investigation by [Villar et al. \[2015\]](#) showed that plankton transport by the Agulhas rings to the South Atlantic Ocean was related to complex nitrogen cycling driven by strong vertical mixing as the rings transited westward. However, details on the variability in phytoplankton biomass and community composition associated with formation processes and the evolution of eddies are not well elucidated.

In this study, we determined the vertical distribution of the chemotaxonomic groups of phytoplankton in three warm eddies shed from the Agulhas leakage into the South Atlantic Ocean. The identification of phytoplankton groups was made through pigment analysis by high-performance liquid chromatography (HPLC) combined with statistical techniques (i.e., chemical taxonomy, or CHEMTAX) to determine the composition and contribution of taxonomic groups to total biomass in phytoplankton samples. Furthermore, data on the vertical distribution of pigments also provide information on the light adaptation of the water column for the phytoplankton community, which contributes to the characterization of their physiological behavior in evolving anticyclonic eddies.

The study was designed to sample and analyze both the neighborhood and interior of mesoscale eddies propagating within the Agulhas Corridor, from southern Africa towards the west, in the interior of the South Atlantic. Within this context, the following specific questions have been posed: (1) How is the vertical distribution of phytoplankton pigments within the Agulhas anticyclonic eddies

released into the South Atlantic Ocean? (2) How is the phytoplankton community structured within and outside the influence of these eddies? (3) How variable are the phytoplankton communities for different ages of South Atlantic eddies?

4.2 The FORSA Cruise

The *Following Ocean Rings in the South Atlantic* (FORSA) was the first scientific cruise conducted by the Brazilian RV Vital de Oliveira (H-39). The vessel left Cape Town (South Africa) on June 27 towards Arraial do Cabo (Brazil) and arrived on July 15, 2015. Thus, this cruise allowed for a quasisynoptic view of mesoscale eddies crossing the South Atlantic Ocean through the Agulhas Corridor. The main goal of the FORSA cruise was to characterize the evolution of Agulhas eddies while crossing the South Atlantic Ocean.

Six mesoscale structures, known as Agulhas rings, were observed, and sampled during the FORSA cruise for physical, chemical, and biological data. Among these features, three eddies representative of the evolution along the basin (hereafter referred to as E₁, E₃ and E₅; [Fig.12](#)) were sampled for phytoplankton pigments since logistical time prevented the discrete sampling of all six eddies.

The eddies were tracked from the Agulhas Current retroflexion at approximately 40°W to investigate their spatial evolution. Further information about the FORSA cruise can be found [Orselli et al. \[2018b\]](#), who investigated the role played by these eddies in the sea-air CO₂ net flux.

The eddy E_1 , according to Orselli *et al.* [2018b], which is nearest the African coast, was the youngest sampled eddy (seven months old), while E_3 was 11 months old, and E_5 was the oldest (24 months old).

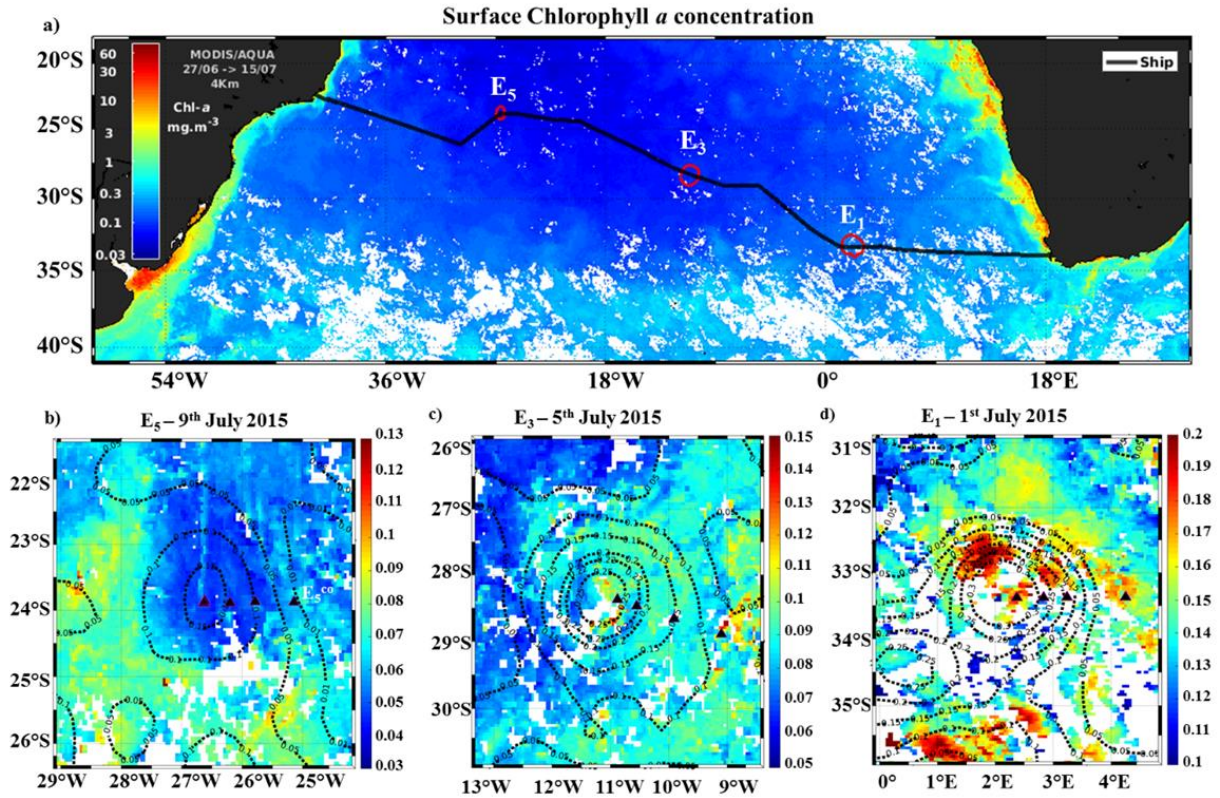


Figure 12. a. Mean surface Chl a concentration (mg m^{-3}) in the region of the Agulhas Corridor (South Atlantic Ocean) composited from satellite images over 18 days, with a 4 km resolution. Red circles mark the position where the three Agulhas eddies (E_1 , E_3 and E_5) were sampled during the cruise. The lower panels represent the 8-day compositions centered on the day of each core sampling in the eddy, where **b.** E_5 was sampled on July 9, 2015; **c.** E_3 was sampled on July 5, 2015; and **d)** E_1 was sampled on July 1, 2015. The satellite Chl a concentration is represented by the color bar. The dashed isolines of the SLA show the shape of the eddy, and the strong black dots mark the locations of the four sampling stations at each eddy. Note that the differences in the color scale emphasize the spatial structure of the Chl a concentration.

4.3 Data and Methods

4.3.1 Physical and chemical data

Four conductivity-temperature-depth (CTD) stations were positioned in strategic locations inside (three stations: close to the border, midway and close to the center of the eddy) and outside (one station) the eastern side of each sampled eddy (E₁, E₃ and E₅). CTD casts were performed across a transect from the outside of each eddy radiating inward through its border, midway and ending in the core. A more detailed description of the sampling strategy is further presented in Supplementary material (Anexo I, [Fig. S1](#), pg.186).

The CTD vertical profiles of temperature, salinity and fluorescence were obtained for each CTD station. The accuracies of the temperature, conductivity and pressure sensors (Sea-Bird Electronics Inc. SBE 9plus CTD) were $\pm 0.001^\circ\text{C}$, $\pm 0.0003 \text{ S m}^{-1}$ and 0.02%, respectively. The fluorescence profiles from the CTD stations were used to indicate Chl *a* biomass and then analyzed to choose the depths for phytoplankton analysis. The fluorescence probe was later calibrated with HPLC Chl *a* data, which was determined in the laboratory ($r^2=0.918$).

The surface mixed layer depth (MLD) was estimated from potential density profiles using the most common density threshold, which defines acceptable density variability within the mixed layer usually in a range of $\Delta=0.03 \text{ kg m}^{-3}$ from a near-surface value at a 10 m depth [[de Boyer Montégut et al. 2004](#)].

Seawater samples for macronutrient determination (e.g., dissolved inorganic nitrate (NO₃⁻) + nitrite (NO₂⁻) (DIN), phosphate (PO₄³⁻), and silicate (SiOH₄⁻) were sampled using plastic bottles, where each was rinsed at least three times with a sample prior to filling. The samples were immediately frozen without filtration and kept frozen at -20°C until the analysis was performed at the Laboratory of Biogeochemistry at the Federal University of Rio de Janeiro, Brazil. The dissolved inorganic nutrient analyses (NO₂⁻, NO₃⁻, SiOH₄⁻ and PO₄³⁻) were

performed following the spectrophotometric determination methods described in [Aminot & Chaussepied \[1983\]](#). The limits of detection for NO_3^- , NO_2^- , PO_4^{3-} and SiOH_4^- were 0.02, 0.11, 0.10 and 0.50 $\mu\text{mol L}^{-1}$, respectively.

4.3.2 Phytoplankton sampling and HPLC pigment analysis

In total, there were four phytoplankton sampling stations per eddy: a control station (E^{co}); a station outside of the eddy's influence; and three stations inside each eddy, which were located at the border (E^b), midway (E^m) and center (E^c) of the mesoscale structure (Anexo I, [Fig.S1](#), pg.186). At each station, seawater samples were taken from several depths (between the surface and 200 m) to characterize the vertical distribution of phytoplankton communities. Forty-two seawater samples were collected in total (i.e., 15 for E_1 , 17 for E_3 and 10 for E_5), with no replicates included; E_5 had the fewest samples due to logistic factors of the cruise. Seawater samples (1–2 L) were filtered onboard onto Whatman glass microfiber (GF/F) filters (nominal pore size of 0.7 μm and 25 mm in diameter) and under vacuum pressure (<5 inHg). The filters were immediately stored in liquid nitrogen until transportation to the laboratory, where they were preserved at -80°C .

In the laboratory, the filters were placed in a screw-cap centrifuge tube with 3 mL of 95% cold-buffered methanol (2% ammonium acetate) containing 0.05 mg L^{-1} trans- β -apo-8'-carotenal (Fluka) as an internal standard. The samples were sonicated for 5 min in an ice-water bath, stored at -20°C for 1 h, and then centrifuged at 1,100 g for 5 min at 3°C . The supernatants were filtered through Fluoropore polytetrafluoroethylene (PTFE) membrane filters (0.2 μm

pore size) to separate the extracts from the remains of the filter and cell debris. Immediately prior to injection, 1,000 μL of sample was mixed with 400 μL of milli-Q water in 2.0 mL amber glass sample vials, which were then placed in the HPLC cooling rack (4°C). The pigment extracts were analyzed using a Shimadzu HPLC comprising a solvent distributor module (LC-20AD) with a control system (CBM-20A), a photodiode detector (SPDM20A) and a fluorescence detector (RF-10AXL). The chromatographic separation of pigments was achieved using a monomeric C8 column (SunFire, 15 cm long, 4.6 mm in diameter, and 3.5 μm particle size) at a constant temperature of 25°C. The mobile phases were (A) methanol:acetonitrile:aqueous pyridine solution (0.25 M, pH adjusted to 5.0 with acetic acid; 50:25:25, v/v/v) and (B) methanol:acetonitrile:acetone (20:60:20, v/v/v). The solvent gradient followed that of [Zapata *et al.* \[2000\]](#), with a flow rate of 1 mL min⁻¹, injection volume of 100 μL , and runs of 40 min.

All of the studied pigments were identified from both absorbance spectra and retention times, and the concentrations were calculated from the signals in the photodiode array detector in comparison with the commercial standards obtained from the DHI (Institute for Water and Environment, Denmark). The peaks were integrated using the LC-Solution software, and all the peak integrations were checked manually and corrected when necessary. A quality assurance (QA) threshold procedure, through the application of limit of quantification (LOQ) and limit of detection (LOD), was applied to the pigment data, as described by [Hooker *et al.* \[2005\]](#), to reduce the uncertainty in pigments found in low concentrations. The LOQ and LOD procedures were performed according to [Mendes *et al.* \[2007\]](#). To correct for losses and volume changes, the concentrations of the pigments were normalized to the internal standard. The

HPLC method presently used allowed for the separation of all pigments, except for chlorophyll *b* (Chl *b*) and divinyl-Chl *b*, which exhibited the same retention times (coelution) and, consequently, were presented together as total Chl *b* (TChl *b*).

4.3.3 Pigment indices

As variations in irradiance alter pigment concentrations and the compositions of phytoplankton [Higgins *et al.* 2011], photopigment indices were derived according to Barlow *et al.* [2007] to assess the fluctuations in the contribution of total Chl *a* (TChl *a*) and carotenoids to the total pigment (TP) pool. Carotenoids were classified as either photosynthetic (photosynthetic carotenoid (PSC)=19'-butanoyloxyfucoxanthin + fucoxanthin + 19'-hexanoyloxyfucoxanthin + peridinin + prasinoxanthin) or photoprotective (photoprotective carotenoid (PPC)=violaxanthin + diadinoxanthin + alloxanthin + diatoxanthin + lutein + zeaxanthin + $\beta\epsilon$ -carotene + $\beta\beta$ -carotene). To determine the main differences in photoprotective and photosynthetic strategies, the ratios of specific pigments or pigment groups to the TPs were calculated for Chl *a*, photoprotective pigments, and photosynthetic pigments. Accordingly, these three photopigment indices were represented by $Tchl_{aTP}$, PSC_{TP} , and PPC_{TP} , respectively. These indices were used to investigate the phytoplankton pigment adaptations in response to environmental light across eddies and throughout the water column.

The HPLC analysis also allowed for the separation, identification and quantification of the three types of Chl *a* degradation products: chlorophyllide (chlide) *a*, pheophytin (phytin) *a* and pheophorbide (phide) *a*. The relative contents of the chlorophyll degradation products can be used as proxies for the

grazing pressure and senescence of phytoplankton cells [Jeffrey 1974]. In this way, the Chl *a* pigment contents were used to calculate the grazing index ($[\text{phide } a + \text{phytin } a] / [\text{TChl } a + \text{phide } a + \text{phytin } a + \text{chlode } a]$) and the senescence index ($[\text{chlode } a] / [\text{TChl } a + \text{phide } a + \text{phytin } a + \text{chlode } a]$).

4.3.4 Chemotaxonomic analysis of HPLC data

In this study, we employed the most widely tested inverse approach, the CHEMTAX v1.95 chemical taxonomy software [Mackey *et al.* 1996, Wright *et al.* 2009, 2010], which uses matrix factorization to optimize initial guesses of the ratios of accessory pigment to Chl *a* of the phytoplankton classes assumed to be present in the sample for the best fit with the bulk pigment concentrations. The bases for the calculations and procedures are fully described in Mackey *et al.* [1996]. Chl *a* was used to represent the biomass of all groups, except *Prochlorococcus*, for which DV Chl *a* was used. Therefore, in this work, the sum of Chl *a* + DV Chl *a*, named TChl *a*, was used as the phytoplankton biomass index and was also used in the pigment ratio calculations.

The initial pigment ratios of the major algal classes used here were compiled from Higgins *et al.* [2011] (Anexo I, Tab. S1, pg.189), with chemotaxonomic groups identified according to Jeffrey *et al.* [2011]. Based on the identified diagnostic pigments, nine algal groups were loaded into the CHEMTAX software: prasinophytes, chlorophytes, cryptophytes, diatoms, pelagophytes, dinoflagellates, haptophytes, *Synechococcus* and *Prochlorococcus*. The loaded pigments were Chl *a*, divinyl-Chl *a*, violaxanthin,

19'-butanoyloxyfucoxanthin, fucoxanthin, 19'-hexanoyloxyfucoxanthin, lutein, chlorophyll c_3 , prasinoxanthin, alloxanthin, zeaxanthin, peridinin and TChl b .

The same initial ratio was used for data on the three eddies, but to account for pigment ratio variation with irradiance and/or nutrient availability, data from these eddies were split into three bins according to eddy sampling depth (0–50 m, 51–100 m and 101–200 m) (see Anexo I, [Tab. S1](#), pg.189). A series of 60 pigment ratio matrices were generated by multiplying each ratio from the initial matrix by a random function to optimize the matrix, and 10% ($n=6$) of the generated ratios with lowest root mean square residual were averaged [[Wright et al. 2009](#)].

4.3.5 Statistical analysis

To explore the key factors underlying the phytoplankton distribution patterns, a canonical correspondence analysis (CCA) was performed according to [Ter Braak & Prentice \[1988\]](#). The response variables were represented by the biomasses of the CHEMTAX-derived taxonomical group (mg m^{-3} of TChl a), while the explanatory variables included sea surface temperature (SST), salinity, dissolved inorganic nitrogen ($\text{DIN}=\text{NO}_2^- + \text{NO}_3^-$), PO_4^{3-} , SiOH_4^- , TChl a , the grazing and senescence indices, and the photopigment indices (PPC_{TP} and PSC_{TP} , which were used as proxies for the phytoplankton light regime). To reduce the influences of the different scales in the datasets, all variables were previously log-transformed. A Monte Carlo test was further run based on 499 permutations under a reduced model ($p<0.05$) to evaluate the CCA significance.

4.4 Results

4.4.1 Hydrographical/environmental setting

The SST increases while the eddies cross the Agulhas Corridor towards lower latitudes. The SST increased from 17.7°C in the first eddy's center (E_1^c), which was located at approximately 33°S, to 22.4°C in the surroundings of E_5 , which was located at 23°S, as summarized in [table 2](#). However, while an increase in temperature was observed towards the core of E_1 , this pattern was not evident in either E_3 or E_5 . On the other hand, a deep chlorophyll maximum (DCM) was not actually detected in E_1 , as the Chl *a* values in the previously selected DCM depth were apparently not different from those at the surface (5 m) ([Tab. 2](#)). The surface salinity showed a slight increase from ~35.7 at E_1^c to ~36.5 at E_5^c . The water properties of E_3 were between those of E_1 and E_5 . Salinity in the core and surroundings of the first eddy was higher than that in the control station.

Regarding nutrient concentrations, the DIN ($\text{NO}_3^- + \text{NO}_2^-$) values were highest in E_1 but remained very low in the upper layers at all stations for E_3 and E_5 , increasing at DCM depths (close to the pycnocline) (see Anexo I, [Fig. S2](#), pg. [187](#)). In all three eddies, the concentrations of DIN, PO_4^{3-} and SiOH_4^- with depth were enhanced by approximately 2-fold in the midway and core stations of the eddies in relation to their respective control stations. However, except for E_1 , the PO_4^{3-} concentrations were near or below the LOD ($0.10 \mu\text{mol L}^{-1}$), while the SiOH_4^- levels were highest among the nutrients. In general, the nutrient concentrations gradually increased below 150 m towards the base of the MLD, and higher values were found towards the inner region of the eddies at the

midway and core stations when compared to the control or border stations of the eddies. The silicate-to-DIN (Si:N) ratios were higher within the mixing layer inside the eddies (see Anexo I, Fig. S2, pg. 187). Most of the study area was characterized by high Si and low DIN and PO_4^{3-} concentrations.

The estimated MLD sank from 97.3 m outside of eddy E_1^{co} to 200 m at E_1^{c} . Deepening in the MLD was less noticeable in both the older E_3 and E_5 eddies, where the MLD showed smaller differences between the control and eddy stations. The E_3^{b} depth was deeper (125 m) than the depth in the core E_3^{c} (93 m). The MLD decreased from 87 m in E_5^{b} to 79 m in E_5^{c} (Tab. 2).

4.4.2 Phytoplankton biomasses, pigment concentrations, and indices

The presence of macronutrients (mostly PO_4^{3-}) in the surface layers of E_1 allowed an increase in phytoplankton biomass (TChl *a*) in well-lit upper layers, which was almost uniformly distributed along the sampling depths (due to a deep MLD), resulting in the absence of a noticeable DCM. On the other hand, E_3 and E_5 showed a marked DCM depth greater than 100 m following the nutricline. Unlike what is normally observed in most anticyclonic eddies, in E_1 , there was an enhancement in TChl *a* towards the center of the eddy (E_1^{c}) in relation to the outer stations, reaching $\sim 0.30 \text{ mg m}^{-3}$ (see Tab. 2), although this was not apparent in E_3 and E_5 . In these eddies, the increase in TChl *a* was mostly pronounced at the DCM depths at both the midway and core stations. This pattern is probably due to enhanced DIN concentrations, especially at the DCM depths in E_3 and E_5 .

Table 2. In this table, the stations sampled are listed in the first column and, in the second column, two depths (the first value corresponds to data at a 5 m depth, and the second (between brackets) is at a DCM depth) are listed. The subsequent columns show the value of each parameter measured for each depth: T (°C), salinity, DIN ($\mu\text{mol L}^{-1}$), PO_4^{3-} ($\mu\text{mol L}^{-1}$), SiOH_4^+ ($\mu\text{mol L}^{-1}$), and TChl *a* (mg m^{-3}); in the last column, the MLD (m) for each station is listed.

Station	Depth	T(°C)	Salinity	DIN	PO_4^{3-}	SiOH_4^+	TChl <i>a</i>	MLD
E ₁ ^{co}	5 (30)*	16.46 (16.46)	35.35 (35.35)	0.39 (0.65)	0.21 (0.19)	0.50 (0.50)	0.08 (0.17)	97.3
E ₁ ^b	5 (120)*	17.68 (17.64)	35.69 (35.67)	0.71 (1.51)	0.21 (0.31)	0.50 (0.50)	0.16 (0.16)	140.9
E ₁ ^m	5 (15)*	17.68 (17.70)	35.69 (35.69)	1.78 (1.03)	0.27 (0.15)	0.50 (0.50)	0.21 (0.24)	198.5
E ₁ ^c	5 (90)*	17.69 (17.71)	35.69 (35.69)	0.20 (0.26)	0.16 (0.13)	0.82 (3.59)	0.27 (0.28)	200
E ₃ ^{co}	5 (120)	19.80 (17.92)	36.02 (35.80)	0.19 (0.28)	0.10 (0.10)	0.53 (0.55)	0.07 (0.21)	103.3
E ₃ ^b	5 (150)	20.60 (17.45)	36.27 (35.76)	0.39 (0.43)	0.10 (0.10)	0.50 (0.72)	0.07 (0.13)	125.1
E ₃ ^m	5 (110)	19.98 (16.98)	36.12 (35.66)	0.18 (1.04)	0.10 (0.10)	4.22 (6.12)	0.06 (0.27)	99.3
E ₃ ^c	5 (110)	19.68 (16.90)	36.05 (35.65)	0.18 (0.75)	0.10 (0.10)	3.01 (4.74)	0.10 (0.21)	93.4
E ₅ ^{co}	5 (115)	22.39 (20.07)	36.79 (36.35)	0.15 (0.19)	0.10 (0.10)	1.30 (1.61)	0.06 (0.17)	89.4
E ₅ ^b	5 (140)	22.12 (18.09)	36.49 (35.95)	0.13 (0.16)	0.10 (0.10)	2.16 (2.36)	0.04 (0.11)	87.4
E ₅ ^m	5 (140)	22.39 (17.92)	36.45 (35.94)	0.15 (0.94)	0.10 (0.10)	1.97 (3.20)	0.04 (0.17)	83.5
E ₅ ^c	5 (125)	22.41 (17.81)	36.45 (35.93)	0.13 (0.37)	0.10 (0.10)	2.58 (2.93)	0.04 (0.18)	79.5

*For E₁, despite no marked DCM depth being detected, the values in brackets represent the depth with the highest TChl *a* concentration.

A total of 20 phytoplankton pigments were identified by HPLC analysis. The highest mean pigment concentrations were found in the younger eddy (E₁). The main accessory pigments were 19'-butanoyloxyfucoxanthin (dominant in pelagophytes and present in some haptophytes) and 19'-hexanoyloxyfucoxanthin (major pigment in haptophytes and Type 2 dinoflagellates without peridinin) [Higgins *et al.* 2011], with mean concentrations of 48 ng L⁻¹ and 67 ng L⁻¹, respectively (see Anexo I, Tab. S2a, pg. 190). Another pigment with high mean concentration was DV Chl *a* (*Prochlorococcus* marker), with a mean contribution of 45 ng L⁻¹. Significant contributions of both zeaxanthin (prokaryote marker in general; dominant in cyanobacteria) and TChl *b* (one of the *Prochlorococcus* markers but also present in green Chl *b*-containing flagellates) (mean concentrations of 32 ng L⁻¹ and 38 ng L⁻¹, respectively) were also detected.

Similar pigment composition patterns were found in both E₃ and E₅: Chl *b* (flagellate marker; dominant in green algae) and DV Chl *a* (*Prochlorococcus* marker) were the main pigments at the DCM depth, with mean Chl *b* concentrations of 61 ng L⁻¹ for both eddies and DV Chl *a* concentrations of 57 and 44 ng L⁻¹, respectively, for E₃ and E₅. Significant contributions of other accessory pigments, such as zeaxanthin, 19'-butanoyloxyfucoxanthin and 19'-hexanoyloxyfucoxanthin, were also observed in all three eddies (Anexo I, Tab. S2b and S2c, pg.191 and 192).

Regarding the pigment indices, TChl_{ATP} was almost uniformly distributed throughout the depth at the E₁ stations, except for the outer E₁[∞] station, where it showed lower values at the surface (Fig. 13).

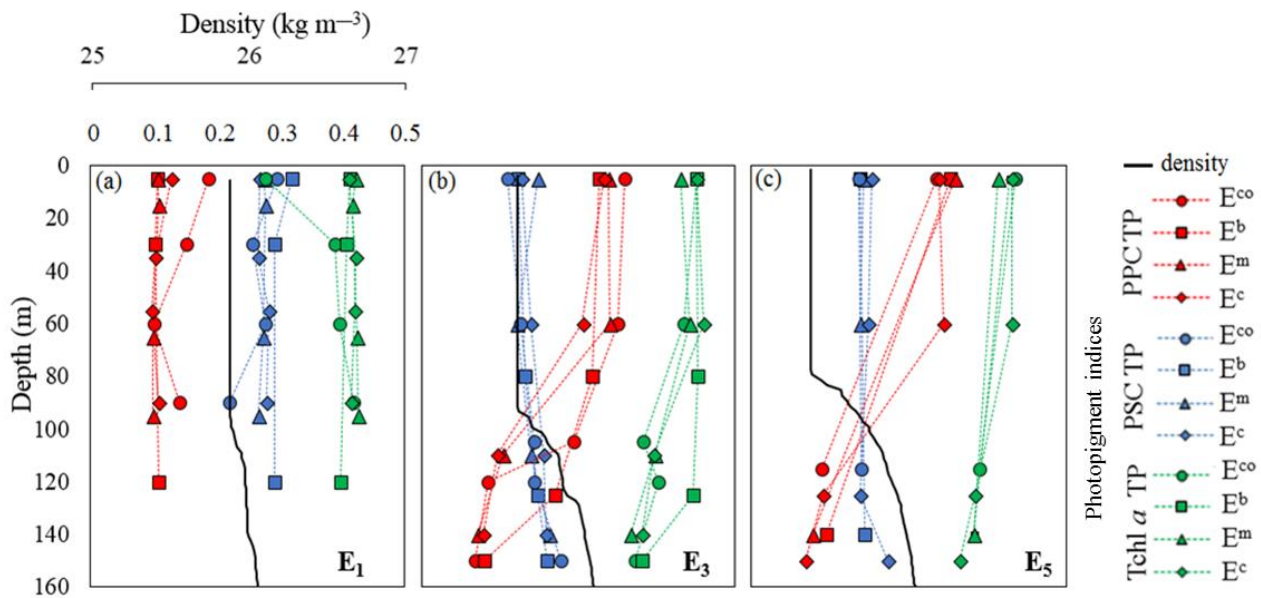


Figure 13. Vertical profiles of the photopigment indices in (a) E₁, (b) E₃ and (c) E₅. Colored lines refer to PPC_{TP} (red), PSC_{TP} (blue) and Tchl a_{TP} (green). Each station is represented by a symbol (circles for control stations, squares for border stations, triangles for midway stations and diamonds for center stations). The black bold line represents the average density profile.

Below 100 m, a decrease was observed in Tchl a_{TP} in both E₃ and E₅. The photosynthetic pigment indices (PSC_{TP}) were higher than the photoprotective indices (PPC_{TP}) at all depths in E₁, indicating regions of high productivity characterized by the dominance of large phytoplankton cells, while in E₃ and E₅, PPC_{TP} presented higher concentrations than PSC_{TP}, which is a pattern normally associated with lower productivity and smaller phytoplankton cells. However, an opposite trend was observed below 100 m, where PSC_{TP} was higher than PPC_{TP} (Fig.13).

4.4.3 Chemotaxonomic groups of phytoplankton

In this section, the vertical distributions of phytoplankton groups (contributions to Tchl a) are described for each of the three eddy stations. The percentage contribution of each group to the Tchl a can be found in [table S3](#)

(Anexo I, pg. 193). In the easternmost eddy (E_1), the phytoplankton community was dominated by flagellates (mainly haptophytes) and prokaryotes (mainly *Prochlorococcus*) (Fig.14). Small but persistent contributions of prasinophytes at the surface and pelagophytes with depth were observed at all stations. Diatoms (~3–4%) and dinoflagellates (~3–3.5%) appeared at the midway (Fig.14c) and core (Fig.14d) stations. Outside of the eddy's influence (E_1^{co}), a change was observed in the communities' relative contribution to Chl *a* with depth, where the surface was dominated by *Prochlorococcus* (49%), which decreased to 22% at 60 m, while haptophytes increased from a 25% contribution at the surface up to a 35% contribution at 60 m. This behavior was also observed in pelagophytes (7.9% at the surface to 18% at 60 m) and chlorophytes (2% at the surface to 12% at 60 m) at the same depth. At the stations within the eddy (E_1^b , E_1^m , and E_1^c), this variation with depth was not evident, as communities were more homogeneously distributed with depth.

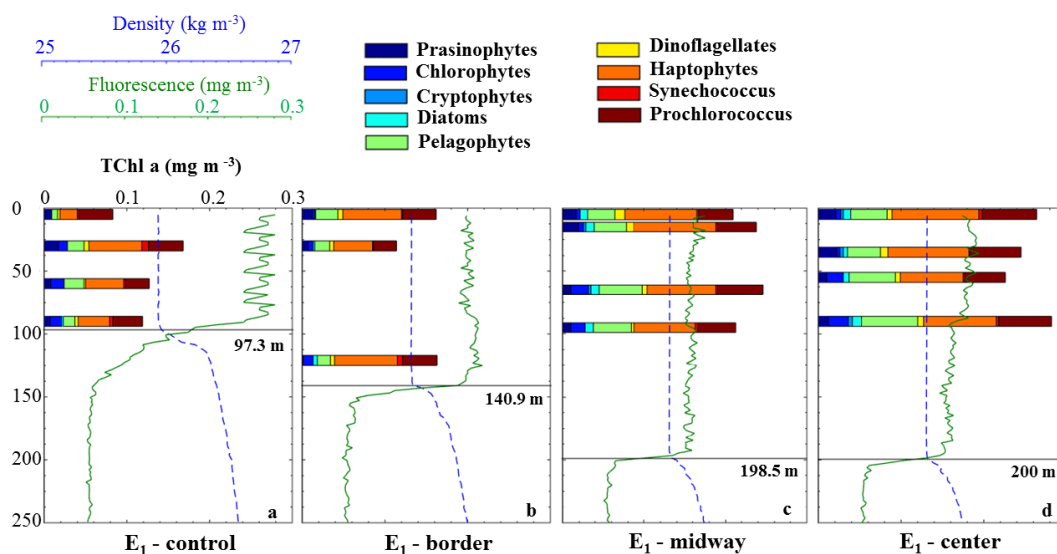


Figure 14. Depth distribution of the phytoplankton group biomasses for E_1 (TChl *a*), calculated through the CHEMTAX program at the four different zones (control, border, midway and center), and the respective density (dashed blue line) and fluorescence (green line) profiles. The black horizontal line represents the MLD depth.

Regarding the E₁ main chemotaxonomic groups, *Prochlorococcus* was dominant at the surface outside the eddy and was replaced by haptophytes with depth and inside the eddy. Both pelagophytes and haptophytes enhanced their concentrations, while prochlorophytes reduced their percentages towards the core. At both westernmost eddies (E₃ and E₅), an in situ fluorescence maximum was found at a 100 to 150 m depth, which coincided with the TChl *a* maximum obtained by the HPLC measurements.

The phytoplankton community structure at the intermediate E₃ station (with prominent DCM layers) was dominated by *Prochlorococcus* (representing >45%) at all depths (Fig.15). Haptophytes contributed >25% at stations within the eddy. Diatoms and dinoflagellates comprised a very small fraction of the phytoplankton community at the DCM depths at both the E₃^m (Fig.15c) and E₃^c (Fig.15d) stations. It is important to note low but consistent contributions of pelagophytes, chlorophytes and *Synechococcus* with DCM depth (approximately 110 m) at all stations.

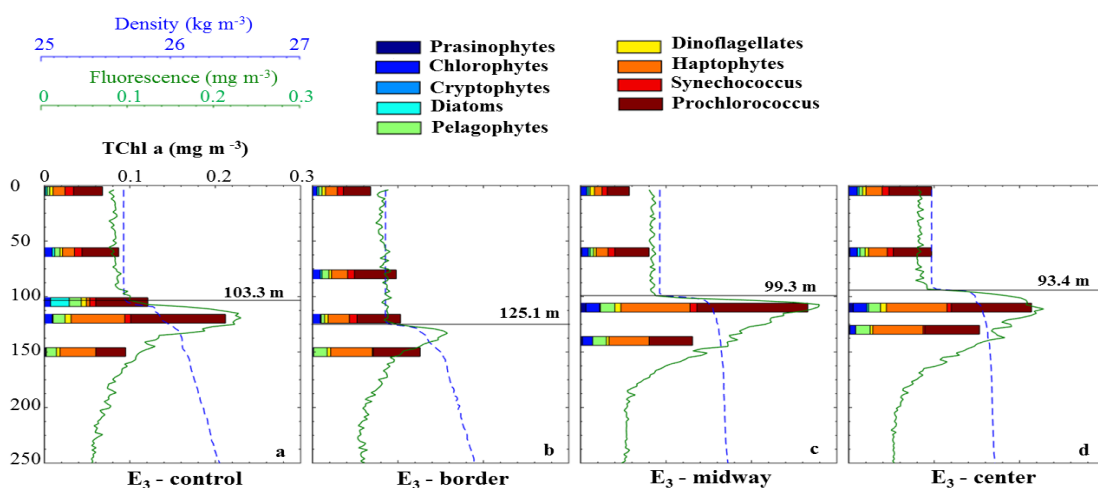


Figure 15. Depth distribution of the phytoplankton group biomasses for E₃ (TChl *a*), calculated through the CHEMTAX program at the four different zones (control, border, midway and center), and the respective density (dashed blue line) and fluorescence (green line) profiles. The black horizontal line represents the MLD depth.

In E₅, only the surface and DCM depths were sampled for phytoplankton community analysis, except for the core station (Fig.16). The main chemotaxonomic groups in this eddy were *Prochlorococcus* (~40%), followed by haptophytes (>20%). Unlike the other eddies, chlorophytes represented >10% at the surface within the eddy.

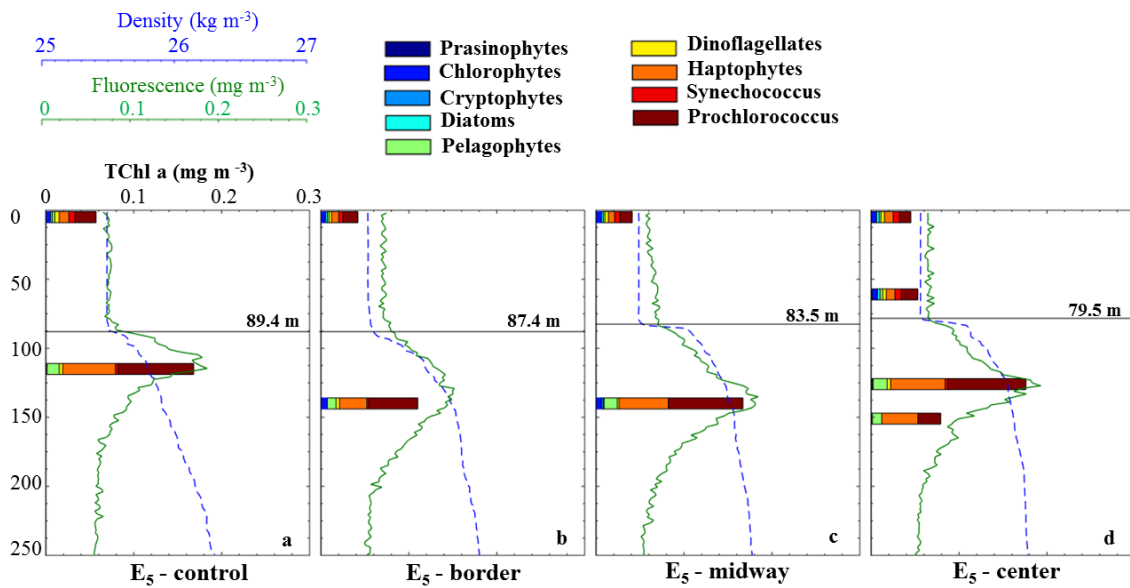


Figure 16. Depth distribution of the phytoplankton group biomasses for E₅ (TChl a), calculated through the CHEMTAX program at the four different zones (control, border, midway and center), and the respective density (dashed blue line) and fluorescence (green line) profiles. The black horizontal line represents the MLD depth.

4.4.4 Phytoplankton association with environmental and physiological parameters

A Monte Carlo F-ratio test on the CCA results showed that nine explanatory variables significantly contributed to explaining the spatial distribution of phytoplankton groups ($p < 0.02$): temperature, salinity, DIN, PO_4^{3-} , SiOH_4^- , PPC_{TP} , PSC_{TP} , TChl a, grazing and senescence (Fig.17). The first two ordinate CCA axes explained 86% of the total spatial distribution of phytoplankton groups

(59% and 27% in the first and second canonical axes, respectively), except for E_1 (represented by the circles), where the surface and DCM samples (green and yellow circles, respectively) were similar (i.e., without an evident DCM), the CCA revealed a notable separation between the surface (yellow symbols in Fig.17) and DCM (green symbols in Fig.17) samples, which was mainly associated with salinity, temperature and PPC_{TP} . On the other hand, particularly associated with the second axis, the CCA also showed that most flagellates (haptophytes, pelagophytes and prasinophytes) were positively correlated with the PO_4^{3-} concentration, which were dominant at the E_1 stations (circles in Fig.17).

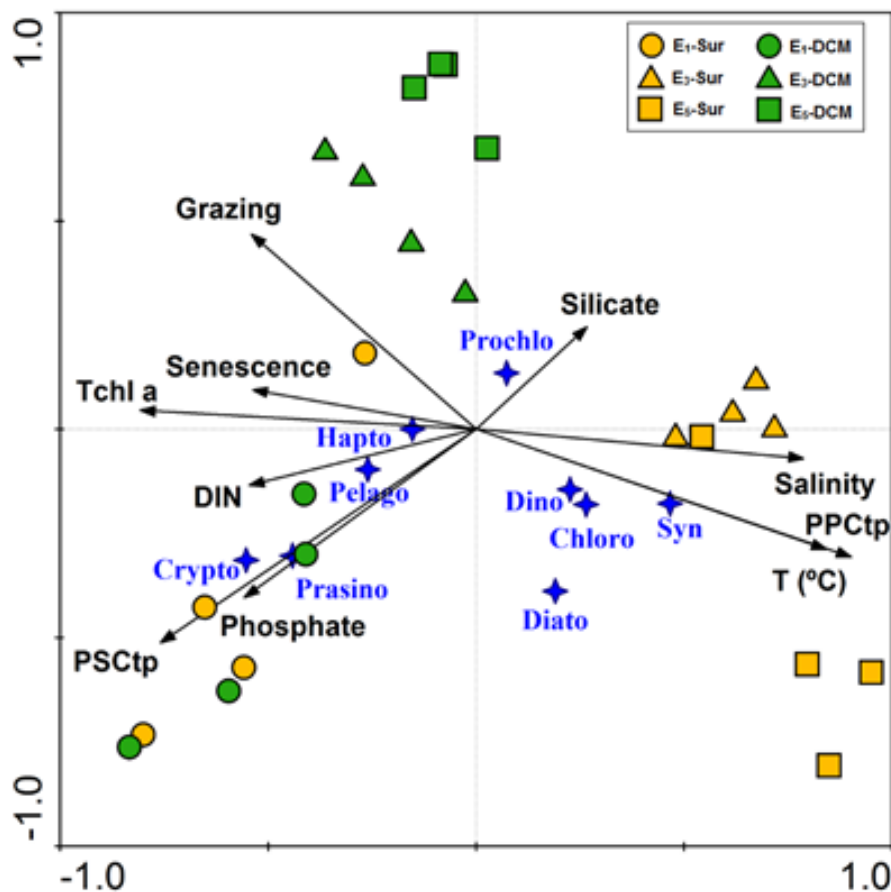


Figure 17. CCA ordination diagram of the absolute contributions of different phytoplankton groups at the sea surface. The arrows indicate the explanatory variables (e.g., salinity, temperature, TChl a, DIN, PO_4^{3-} , $SiOH_4^-$, PSCs, PPCs), grazing and senescence). Blue stars refer to the absolute contributions of the phytoplankton groups. The stations are separated according to distinct eddies, where the stations in yellow represent the surface, and those in green represent the DCM stations (circles correspond to E_1 , triangles correspond to E_3 , and squares correspond to E_5).

The results of the CCA analysis showed a clear distinction between E₁ (circles) and the other eddies (E₃ – triangles; E₅ – squares). E₁ showed no separation between the surface data (yellow) and DCM data (green) and was more associated with the PSC_{TP} and nutrient data (DIN and PO₄³⁻). The surface data of eddies E₃ (yellow triangles) and E₅ (yellow squares) were highly associated with PPC_{TP} and the physical parameters, such as salinity and temperature. The DCM data of these two eddies were related to factors such as TChl *a*, grazing, senescence and SiOH₄⁻. Regarding the phytoplankton groups, haptophytes and *Prochlorococcus* were allocated closer to the center of the axes in the CCA. These groups were the most abundant and occurred in all three eddies and therefore contributed less to explaining the data variability. In contrast, minor groups (dinoflagellates, chlorophytes, *Synechococcus* and diatoms) appeared at surface and contributed to the separation of the surface samples by the CCA. Pelagophytes were abundant in E₁; therefore, this group appears in the same square as the E₁ data. However, as it represents a major group, it is located near the center. Far from the center are the minor groups prasinophytes and cryptophytes, found mostly in E₁.

4.5 Discussion

The Agulhas rings sampled during the FORSA cruise followed northwestward trajectories during their lifetimes in the South Atlantic Ocean, crossed different biogeochemical environments, and departed from relatively productive waters near the African coast towards the oligotrophic waters of the

South Atlantic subtropical gyre, as has been previously investigated [e.g., [Lee & Williams 2000](#), [Oschlies 2002](#), [Lévy 2003](#), [McGillicuddy *et al.* 2003](#)]. In this way, this scenario allowed for the investigation of anticyclonic eddies at three different lifetime stages and, thus, represents the zonal evolution of the Agulhas rings throughout the South Atlantic basin. Recall that this research is not shown here in its entirety but complements other studies on this cruise [[Orselli *et al.* 2019b](#)].

An evident decay in the Agulhas rings towards the west was observed regarding the SLA. However, this property was more intense in the younger E₁ for a longer period than in the other eddies [[Orselli *et al.* 2018b](#)]. In [Orselli *et al.* \[2018b\]](#), after determining the lifetimes of these three eddies, E₁ and E₃ were considered in a determination of an ‘Agulhas True’ eddy, which represents the recent and young mesoscale structures shed by the Agulhas retroflection. The westernmost eddy E₅, however, was considered in the determination of an ‘Agulhas evolved’ structure, as it could have been modified by processes, such as splitting and merging, along its trajectory in the Atlantic basin [see supplementary material in [Orselli *et al.* 2018b](#)].

Despite the different lifetimes, the three rings evidenced well-defined anticyclonic structures, which were identified by the sinking of the isotherms. However, the youngest eddy E₁) presented a better defined structure in comparison with both E₃ and E₅, whose samplings occurred after they had crossed the Walvis Ridge, where they can interact with bathymetry (due to the intense barotropic component) and their structures can be altered [[Schouten *et al.* 2000](#)].

An eddy in its early life stages promotes the strong vertical and horizontal transport of heat and nutrients close to its formation area. During the aging process, it gradually softens its characteristics and eventually dies, releasing its

anomalous properties in a different environment [Williams 2011]. A corresponding decay in TChl *a* within these structures was also observed in this work as they departed from their site of origin (Fig.18). Together with aging, the bathymetric effect may act to enhance the mixing of the Indian Ocean waters of the ring into those of the South Atlantic, which should also be taken into account concerning the decrease in Chl *a* levels after crossing oceanic ridges [Schouten *et al.* 2000].

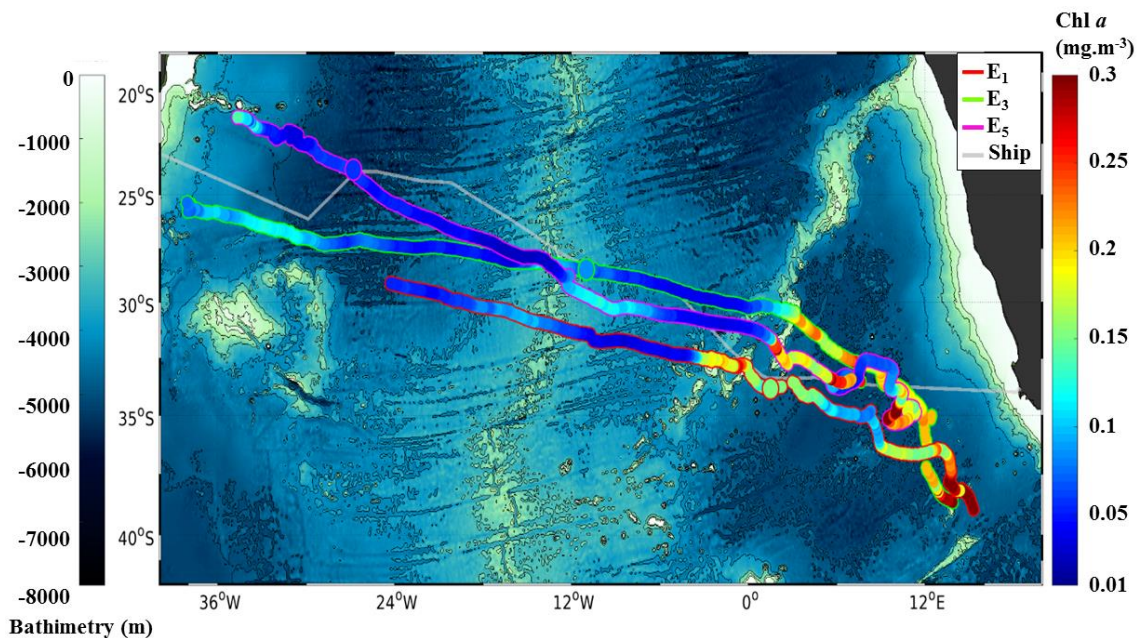


Figure 18. Evolution of surface Chl *a* along the trajectories of the three eddies (E_1 - red contour; E_3 - green contour; E_5 – magenta contour) over the bathymetric map of the South Atlantic basin. The gray line represents the ship track. The circle in each trajectory marks the location where the eddies were sampled in this work. The Chl *a* values represent the 8 day mean (composite) centered on the day of the eddy location based on the eddy fields in the SLA data. For each day, a grid of approximately three degrees ($1.5^\circ\text{W} - 1.75^\circ\text{E}$, $1.5^\circ\text{N} - 1.5^\circ\text{S}$) from the eddy center was computed. To remove the Chl *a* data that were not within the eddy field, the values of Chl *a* located in areas with less than a 0.05 cm SLA were discarded. The eddy trajectories have been extracted from the Mesoscale Eddy Trajectory Atlas product (<https://www.aviso.altimetry.fr>) [Chelton *et al.* 2011, Schlax & Chelton 2016].

The influence of oceanic mesoscale eddies on phytoplankton properties within the structure varies at different developmental stages [Liu *et al.* 2018], promoting changes in phytoplankton biomass and communities during the eddy

life cycle [Condie & Condie 2016]. As shown in figure 18, E₁ was sampled at an early life stage and relatively close to its formation area. Mesoscale processes modulate the dynamic supplies of nutrients to the euphotic layer through a combination of changes in mean advection, eddy advection and vertical mixing [Lévy *et al.* 2012]. Low phytoplankton concentrations in warm eddies are usually attributed to eddy-induced pumping, which transports nutrients downwards and leads to a decline in phytoplankton [Ning *et al.* 2008, Gaube *et al.* 2013]. However, in this work, the perturbations in the water column associated with the E₁ passage resulted in stronger and deeper [up to 200 m) mixing in the surface layer, which probably contributed to the enhancement of nutrients (particularly nitrogen and PO₄³⁻) and a relatively high phytoplankton biomass in relation to the control station (see Tab. 2). The Chl *a* values in the previously selected DCM depth for E₁ were apparently not different from those at the surface (5 m) (Table 1), which was likely due to a deep mixing layer within the eddy that caused the mixing and homogenization of the pigment across the upper layer. Therefore, the moderate availability of nutrients and deep mixing resulted in a non-distinct DCM in this eddy structure (see Fig.14), which would account for nearly the same [TChl *a*] in the mixing layer at the time of sampling. Thus, deep mixing within the ring may have limited phytoplankton growth, probably as a result of an insufficient amount of average light (over a greater depth), thereby preventing greater biomass accumulation. However, this light limitation was partly compensated for by a strategy of increasing the cell photosynthetic pigments under these conditions. In fact, E₁ showed higher photosynthetic characteristics in relation to the photoprotective pigment indices, as opposed to both older eddies (see Fig.

13), suggesting an investment in light-collecting capability under a low light regime (i.e., deep mixing).

Although a decrease in nutrients is most commonly associated with anticyclonic eddies, previous works [e.g., Villar *et al.* 2015, Dufois *et al.* 2016] have also observed strong vertical mixing within the anticyclonic eddies, leading to an increase in the surface TChl *a*. This apparent contradictory behavior observed in E₁ may be due to Ekman upwelling induced by wind, which results in an uplift of nutrients, as previously observed in anticyclonic eddies [Martin & Richards 2001, McGillicuddy *et al.* 2007]. The retention of nutrients in anticyclonic eddies along with the modulation of the mixed layer during wind events have been reported in previous studies as other factors controlling chlorophyll anomalies at the mesoscale [Lehahn *et al.* 2011, Li *et al.* 2014]. Villar *et al.* [2015] reported high NO₂⁻ concentrations (>0.5 mmol m⁻³) and vigorous deep mixing in a weakly stratified structure, which stimulates phytoplankton bloom in young Agulhas anticyclonic eddies.

At the time of E₃ and E₅ sampling, these eddies were in more advanced life stages and far from their releasing sites, as emphasized earlier. During their time of travel, the splitting and merging of these eddies with other structures along the way [Orselli *et al.* 2018b] may have influenced the distribution of biogeochemical properties, resulting in fluctuations in surface Chl *a* along their trajectories (see Anexo I, Fig. S2, pg.187). These continuous alterations may also be generated from changes in eddy properties, such as variations in eddy amplitude, scale, translation speed, linear rotation velocity, nonlinear degree and rotational angular velocity [Liu *et al.* 2018]. In this work, the conspicuous DCM depths detected in both E₃ and E₅, which were associated with the pycnocline,

enhanced phytoplankton biomass with depth, which is a very typical feature of oligotrophic environments. Indeed, light and nutrient availability were the main drivers of phytoplankton distribution with depth, and both can be affected by turbulent conditions [Cullen *et al.* 2002]. Thus, upwelling/downwelling in eddies have been proposed as the main factors influencing the growth and decline in phytoplankton in these structures, which modulates the biomass distribution at different vertical depths during eddy formation [Chen *et al.* 2007, Gaube *et al.* 2013, Chang *et al.* 2017]. Once the eddy is fully formed, the isopycnal movements are relatively stable in comparison to those recently formed [Chang *et al.* 2017]. Therefore, with nutrients limited to greater depths, the phytoplankton biomasses in E₃ and E₅ were mainly concentrated below 100 m.

The low biomasses found in these three warm Agulhas eddies (<0.3 mg m⁻³; particularly in the surface layers of the two older ones), as a result of a poor euphotic zone with respect to essential macronutrients, which leads to growth and biomass accumulation moving towards deeper waters, are corroborated by other studies [Ning *et al.* 2008, Chang *et al.* 2017]. In addition, the horizontal gradients in the biological data represented by the three eddy locations in this work are comparable with those in previous studies in the same region. For instance, Araujo *et al.* [2017] investigated the spatial distribution of pigments and the main taxonomic groups of phytoplankton in the subtropical South Atlantic Ocean along 30°S (from Africa to Brazil) during the early austral spring of 2011. They found that the highest Chl *a* concentration (>1 mg m⁻³) near the African coast and low Chl *a* levels (~0.1 mg m⁻³) were observed in both the subtropical gyre and near the Brazilian coast, corroborating what was found in the eddies sampled during the FORSA cruise.

Regarding the phytoplankton community structure, the easternmost eddy (E_1) showed a different pattern in relation to the other two, where the haptophytes were the dominant group throughout the water column (see Fig. 14). The success of these organisms in E_1 may be partly attributed to their ability to efficiently use nutrients at low concentrations, where larger groups are usually inhibited, but also because they benefit from strong mixing, which prevents fast sinking [Liu *et al.* 2009]. The pelagophytes also showed an important contribution to phytoplankton biomass in E_1 , unlike the two older eddies. In fact, this group was included in the CHEMTAX analysis because they comprise an important fraction of the phytoplankton population in the Indian Ocean [Not *et al.* 2008, Schlüter *et al.* 2011, Araujo *et al.* 2017]; therefore, this result indicates the possible influence of Indian waters in the South Atlantic. *Prochlorococcus*, on the other hand, showed a moderate contribution to surface waters surrounding E_1 but increased towards the eddy's core, where the mixed layers were deeper (see Fig. 14). The phytoplankton community in E_1 was dominated by small flagellates, with diatoms playing a very minor role in the assemblage. This group generally requires a high nutrient concentration for growth [Sarhou *et al.* 2005] and was most likely outcompeted by the smaller and motile flagellates and picocyanobacteria. Anticyclonic eddies have been previously shown to favor motile phytoplankton transported upwards i.e., flagellates, dinoflagellates, and coccolithophores) [Condie & Condie 2016]. Other previous studies that sampled inside anticyclonic eddies also identified the dominance of flagellates and dinoflagellates instead of diatoms [Rodríguez *et al.* 2003, Huang *et al.* 2010].

In the older westward eddies (E_3 and E_5), nearly half of the phytoplankton community was composed of *Prochlorococcus* spp., and the picoplankton

organisms were widely recognized as the most abundant phytoplankton in oligotrophic waters [Cullen *et al.* 2002]. Haptophytes and pelagophytes were found at the DCM depth in these eddies, where nutrients were more available. In the surface waters of both eddies, the occurrence of *Synechococcus* was observed which, together with *Prochlorococcus spp.*, comprised the two dominant picophytoplankton genera in the South Atlantic central gyre [Marañón 2005, Villar *et al.* 2015, Araujo *et al.* 2017]. Below the 100 m depth, under nutrient enhancement, the relative contribution of pelagophytes to the TChl *a* increased in these eddies. The community composition at the DCM depth observed in E₃ and E₅ agrees with those in previous studies in the South Atlantic [Odebrecht & Djurfeldt 1996, Araujo *et al.* 2017].

According to previous studies, flagellates (specifically dinoflagellates in the coastal zone) are typically the dominant phytoplankton group in the nutrient-rich upwelling-influenced surface waters of the African province [Barlow *et al.* 2007, Aiken *et al.* 2009, Araujo *et al.* 2017]. In this work, the contribution of this group was not excessive, except for a small percentage found at the surfaces of all three eddies. On the other hand, a higher percentage of other small flagellate groups (crysophytes, chlorophytes and prasinophytes), similar to that in the younger eddy, was observed in both E₃ and E₅, and this dominance can be mainly ascribed to low NO₃⁻ levels [Coupel *et al.* 2015].

Araujo *et al.* [2017] found a significant enhancement in the TChl *b* concentration at the DCM in the South Atlantic Ocean (in both the gyre and Brazilian provinces), which was related to the occurrence of distinct *Prochlorococcus* ecotypes that adapted to different light regimes (i.e., surface vs. Deep layers), indicating possible chromatic adaptation to higher proportions of

blue-green light at the bottom of the euphotic zone [McManus & Dawson 1994]. This same pattern in the higher contribution of TChl *b* at DCM depths was observed in both E₃ and E₅.

The Agulhas rings are expected to carry the thermohaline properties of the Agulhas Current into the Atlantic Ocean [Beal *et al.* 2006, Durgadoo 2017, Souza *et al.* 2018]. Based on our results, the contribution of these relatively warm, saltier and nutrient-rich waters initially supports phytoplankton communities, which change patterns over time as the rings advect through the South Atlantic Ocean. As eddies decline to more advanced stages, the differences in the phytoplankton community structure from those found in the youngest structures (e.g., E₁) become less clear (as seen in the older E₃ and E₅ structures).

4.6 Conclusion

The phytoplankton community structure estimated by pigment analysis in the three Agulhas eddies mainly showed a shift between haptophytes in the young E₁ eddy to the dominance of *Prochlorococcus* in the older E₃ and E₅ eddies following the decay of these mesoscale structures. Both nutrients and light availability play a key role in phytoplankton vertical distribution, and eddy dynamics can powerfully influence these mechanisms. Age also proved to be an important factor since older eddies, which represent weaker structures, showed more similarities with the external environment with respect to the phytoplankton biomass and community composition. The variability in phytoplankton communities across differently aged South Atlantic eddies tended to be smoothed from the youngest to oldest eddies. Lastly, this study highlights the

progressive transitions of eddies between a highly productive upwelling system region and oligotrophic open-ocean waters, reflecting phytoplankton biomass distribution and community characteristics.

Capítulo V: Relação entre a captação de CO₂ e os grupos do fitoplâncton

O segundo manuscrito contempla os dados de pigmentos fitoplanctônicos e dos fluxos líquidos de CO₂ de sete cruzeiros transatlânticos que fizeram rotas entre o Brasil e a África no período de 2009 a 2015. Ao abordar a dinâmica das principais províncias biogeoquímicas do oceano Atlântico Sul, este trabalho pretende fornecer uma visão mais global em relação ao comportamento de absorção do CO₂ atmosférico nesta região, e como isso pode estar relacionado com a dominância de determinadas comunidades fitoplanctônicas na região. De autoria de Andréa da Consolação de Oliveira Carvalho, Rodrigo

Kerr, Carlos Rafael Borges Mendes, José Luiz de Lima Azevedo e Virginia Maria Tavano, intitulado “*Phytoplankton strenghten CO₂ uptake in the South Atlantic Ocean*”, este trabalho foi submetido para publicação no periódico “*Progress in Oceanography – Elsevier*” em junho de 2020 e encontra-se atualmente em revisão.

Abstract

The influence of phytoplankton groups on carbon dynamics was investigated during six oceanographic spring cruises (three cruises were carried out in 2009, and another three were conducted in 2011) between the western (Brazil) and eastern (Africa) South Atlantic margins. A seventh cruise crossed the South Atlantic during the early winter of 2015. Sea surface temperature and salinity, oceanic and atmospheric partial pressure of CO₂ ($p\text{CO}_2$), chlorophyll *a* and other phytoplankton pigment data were gathered. Net CO₂ fluxes were calculated for each cruise, characterizing the ability of each region to take up atmospheric CO₂. We quantified phytoplankton chemotaxonomic groups using the HPLC/CHEMTAX approach. Thus, this study aimed to improve our understanding of the distribution of phytoplankton groups and their connection with the carbon biogeochemical cycle in the South Atlantic Ocean. Our results showed significant variations in both the zonal and meridional patterns of phytoplankton groups and the associated CO₂ uptake magnitudes. Diatoms and haptophytes dominated the coastal regions of Brazil and Africa, respectively, whereas the open ocean was dominated by haptophytes and the picoplanktonic cyanobacteria *Prochlorococcus* and *Synechococcus*. The CO₂ uptake capacity increased eastward from $-7.1 \text{ mmol CO}_2 \text{ m}^{-2} \text{ d}^{-1}$ on the Brazilian coast to -27.6

mmol CO₂ m⁻² d⁻¹ on the African coast. There was a significant negative relationship ($p < 0.05$) between the phytoplankton biomass and the difference in sea-air $p\text{CO}_2$ ($\Delta p\text{CO}_2$), with increasing CO₂ uptake corresponding to increases in the biomasses of diatoms and haptophytes. Therefore, according to our analysis, haptophytes and diatoms were the main phytoplankton groups related to a high uptake of CO₂ along the South Atlantic Ocean regions covered in this study. Thus, we encourage further investigations on their traits and vulnerabilities to future environmental change scenarios.

5.1 Introduction

Marine ecosystems, in general, are a major sink for atmospheric carbon dioxide (CO₂) and help to balance rising levels of CO₂ in the atmosphere [Sabine *et al.* 2004]. The combined effects of the solubility pump and the biological carbon pump are the main mechanisms of the net transfer of CO₂ from the atmosphere to the oceans and subsequent export of this CO₂ to sediments [Sarmiento & Gruber 2002]. The biological carbon pump contributes to approximately two-thirds of the vertical transport of carbon, while the remaining transport is attributed to the solubility pump [Passow & Carlson 2012]. Biologically mediated ocean-atmosphere CO₂ exchanges result from an equilibrium between photosynthetic activity in the surface layer, which takes up dissolved CO₂ and may lead to oceanic CO₂ uptake, and the production of organic matter and its transport to deeper layers, which releases CO₂ in the surface layers [Volk & Hoffert 1985]. Marine phytoplankton, photosynthetic unicellular organisms adrift in the ocean euphotic layers, act directly on the global carbon biogeochemical cycle as key

mediators of the biological carbon pump [Basu & Mackey 2018] through the fixation of inorganic carbon via photosynthesis. However, phytoplankton vary in morphology (size and shape) and physiology (growth, nutritional requirements, temperature, and light adaptations). As a result, many different taxonomic and functional groups play different biogeochemical roles (e.g., nutrient cycling and carbon export) [Quéré *et al.* 2006]. The biological effects on seawater CO₂ partial pressure ($p\text{CO}_2^{\text{sw}}$) vary according to the characteristics of the phytoplankton community [Litchman *et al.* 2015], which are driven by environmental (i.e., temperature, nutrients, light, etc.) and biological regulators (competition, grazing, etc.) [Cullen *et al.* 2002]. Primary production is also determined by interactions among the food web structure, and predators can have quantitatively important effects on CO₂ uptake [Spiers *et al.* 2016]. Thus, to understand the role of phytoplankton in marine carbon dynamics, we must describe the distribution of the dominant plankton groups in relation to biotic and abiotic environmental conditions [e.g., Arrigo *et al.* 1999].

The South Atlantic Ocean is an overall sink for atmospheric CO₂, with an average uptake trend of $-0.3 \text{ Pg C yr}^{-1}$ [e.g., Takahashi *et al.* 1997, Takahashi *et al.* 2002]. Recent efforts to assess the CO₂ uptake of a relatively undersampled subtropical region of the South Atlantic Ocean (South subtropics – 18°S to 44°S) revealed an average FCO₂ of $-0.14 \pm 0.04 \text{ Pg C yr}^{-1}$ [Schuster *et al.* 2013]. However, snapshot measurements conducted in the southern portion of the South Atlantic subtropical gyre along 35°S revealed an average sea air CO₂ net flux (FCO₂) of $-3.17 \pm 2.2 \text{ mmol CO}_2 \text{ m}^{-2} \text{ day}^{-1}$ in spring of 2011 [Lencina-Avila *et al.* 2016]. The recent study by Orselli *et al.* [2019] in a latitudinal gradient of the South Atlantic Ocean investigated the CO₂ behavior associated with ocean

eddies shed by the Agulhas leakage system. They found that those mesoscale structures intensify CO₂ sinking in the region, with an average FCO₂ of -3.76 mmol CO₂ m⁻² day⁻¹ for the overall South Atlantic Ocean basins. The authors also highlighted that the strongest CO₂ uptake occurred in the eastern basin of the South Atlantic Ocean, with the most intense CO₂ sink found near the Agulhas leakage region.

The scarcity of phytoplankton data in the South Atlantic Ocean has led to gaps in measurements, which are mainly limited to coastal environments [e.g., [Barlow *et al.* 2016](#), [Lima *et al.* 2019](#), [Schloss *et al.* 2007](#)]. To understand the physical-chemical interactions that affect the phytoplankton communities in the subtropical South Atlantic, [Araujo *et al.* \[2017\]](#) investigated the phytoplankton distribution along 30°S and found contrasting patterns along the basin. The highest phytoplankton biomass concentrations (in terms of total chlorophyll *a*) were found in the eastern basin, influenced by the Benguela upwelling system and dominated by flagellates (mainly haptophytes and dinoflagellates). However, in the western South Atlantic Ocean basin, the authors found low phytoplankton biomasses near the Brazilian coast, where low salinity waters were associated with the presence of diatoms and nanoflagellates, while the open-ocean surface was dominated by prokaryotes.

Few studies have provided a global- or basin-scale overview of the abundances and distribution of specific phytoplankton groups [e.g., [Guidi *et al.* 2009](#), [Mouw *et al.* 2016](#); [Swan *et al.* 2016](#)]. The majority of studies have investigated single species, making it difficult to extrapolate the findings to the community and ecosystem levels in natural complex environments [e.g., [Person *et al.* 2018](#), [Rivero-calle *et al.* 2015](#), [Taucher *et al.* 2015](#), [Wu *et al.* 2014](#)].

Advances in the use of coupled global biogeochemical modeling to investigate the link between phytoplankton communities and carbon parameters [e.g., [Behrenfeld et al. 2005](#), [Ciavatta et al. 2018](#), [Signorini et al. 2012](#)] will require new field measurements before this information can be introduced to improve biogeochemical models.

We gathered a robust (including novel and previous) *in situ* dataset of the phytoplankton pigment distribution and FCO₂ in the South Atlantic Ocean, and we investigated a possible relationship between the phytoplankton community composition patterns and the $p\text{CO}_2^{\text{sw}}$ levels. This study aimed to improve the current understanding of the role played by different phytoplankton groups in atmospheric CO₂ uptake in this complex region, which is a key region for understanding the climate. In addition, this study aimed to identify the main phytoplankton groups related to strengthening of CO₂ uptake magnitudes in distinct South Atlantic Ocean biogeochemical provinces.

5.2 Biogeochemical provinces of the South Atlantic Ocean

The South Atlantic Ocean was subdivided according to the biogeochemical provinces defined by [Longhurst \[2006\]](#) ([Fig. 19a](#)), which are based on the prevailing role of physical forcing as a regulator of the primary production distribution. As phytoplankton community distribution is directly influenced by environmental conditions, these biogeochemical provinces are useful for comparing and contrasting biogeochemical processes and biodiversity between ocean regions [[Oliver & Irwin 2008](#)]. The following provinces were sampled: Brazil (BRAZ), South Atlantic Gyral (SATL), Benguela (BENG) and East

Africa (EAFR). The last two provinces were grouped and renamed here as Africa (AFR) (Fig. 19a) due to the small number of samplings in each province. However, their differences will be highlighted and discussed further.

The BRAZ province is influenced by the western boundary of the Brazil Current, which is strengthened by a recirculation cell centered at 35°S and by the confluence of the Brazil Current with the northward flow of the Malvinas Current [Castro & Miranda 1998] (Fig. 19b). The La Plata River discharge (at approximately 35°S) (black star, Fig. 19a) together with the Patos Lagoon Estuarine System discharge (30°– 33°S) (yellow star, Fig. 19a) represent important sources of freshwater in the continental shelf zones. The La Plata River discharge (at approximately 35°S) (black star, Fig. 19a), together with the Patos Lagoon Estuarine system discharge (30°– 33°S) (yellow star, Fig. 19a), represent important sources of freshwater on the continental shelf zones that are mainly controlled by wind stress variability, although there is also a seasonal and interannual variability in the near surface flow, partly as a result of changes in precipitation rates in the region [e.g., Simionato *et al.* 2004, Piola *et al.* 2005, Dogliotti *et al.* 2016].

The influence of the convergence between the Brazil and Malvinas currents (within the latitude band 35°– 45°S) [Garcia *et al.* 2008] and both the La Plata River and Patos Lagoon discharge in the southern portion of the BRAZ province contribute to elevated *in situ* chlorophyll *a* concentrations, especially during spring and winter [Ciotti *et al.* 1995, Ciotti *et al.* 2010]. CO₂ measurements in this province highlight its strong seasonal and spatial variability, with shifts between CO₂ sink and source behavior from coast to offshore that are driven primarily by

variations in the surface $p\text{CO}_2^{\text{sw}}$ due to several oceanic mechanisms, such as coastal upwelling, eddy dynamics and biological uptake [Ito *et al.* 2016].

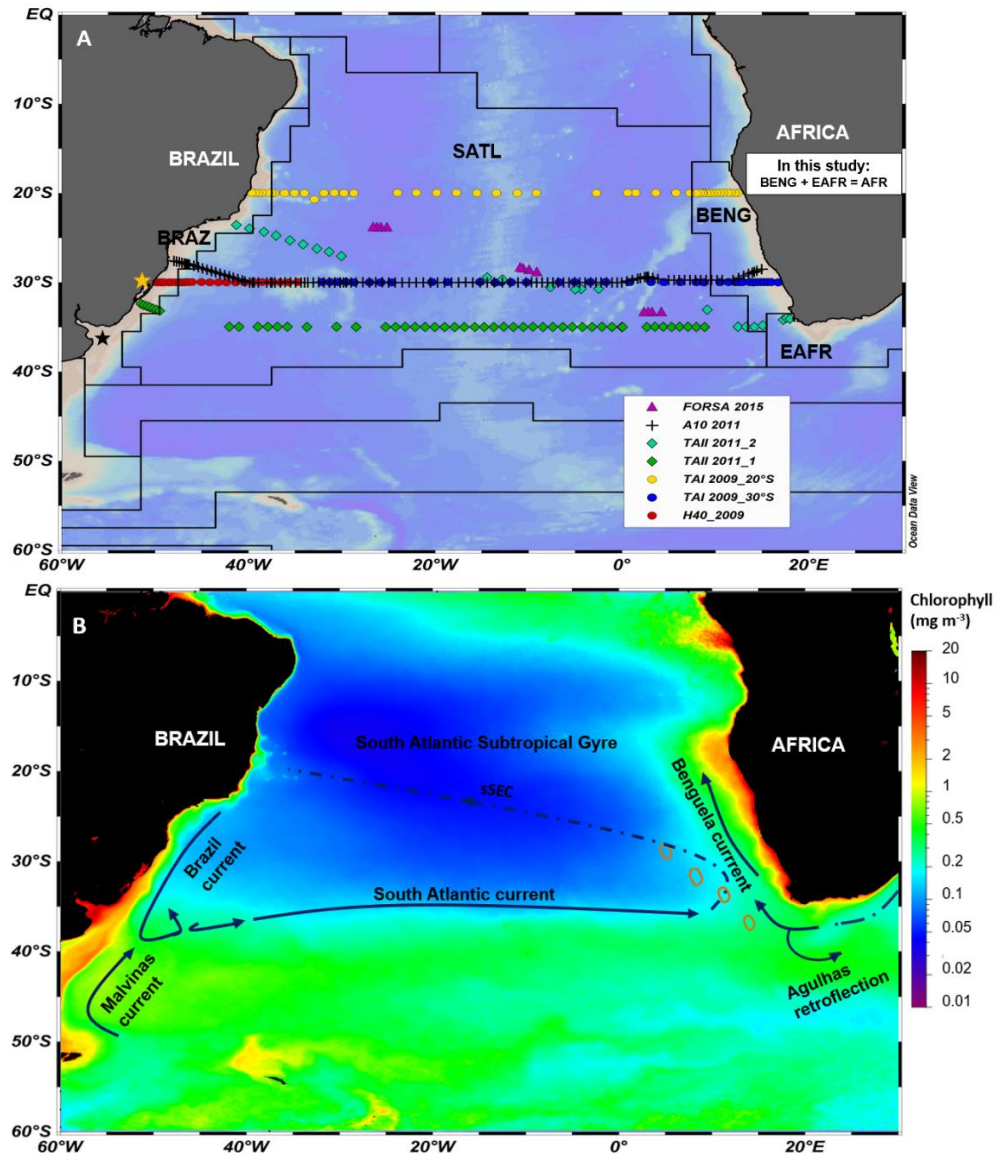


Figure 19. South Atlantic Ocean. **(a)** Biogeochemical provinces (black lines) according to Longhurst [2006], which were overlaid on the map using the shapefile overlay from VLIZ [2009]. The acronyms refer to the Longhurst provinces: Brazil (BRAZ), South Atlantic Gyral (SATL), Benguela (BENG) and East African (EAFR). Here, the last two provinces are referenced together as Africa (AFR). The freshwater discharges of the Patos Lagoon (yellow star) and, particularly, the La Plata River (black star) are highlighted. The oceanographic stations along the hydrographic sections sampled in the South Atlantic Ocean are marked as symbols according to the following cruises in this study: H40_2009 (red circles), TAI 2009_30°S (blue circles), TAI 2009_20°S (yellow circles), TAI 2011_1 (green diamonds), TAI 2011_2 (turquoise diamonds), A10 2011 (black crosses) and FORSA 2015 (magenta triangles). **(b)** Chlorophyll concentration climatology (2002-2020) with main surface circulation arrows. The data were obtained from MODIS Aqua Ocean Color (chlorophyll a concentration) Level-3, OCI Algorithm. Subtropical South Atlantic circulation is described: on the western boundary side are the Brazil Current and the Malvinas

Current, which converge at approximately 35°S (with meridional seasonal variations). On the southern part of the South Atlantic Gyre, the South Atlantic Current flows eastward toward the eastern boundary side, merging with the Benguela current. The Agulhas eddies shed in the Agulhas retroflexion region are indicated by the orange ellipses. Closing the loop of the South Atlantic Gyre, the southern branch of the South Equatorial Current (sSEC) is shown by a dotted-dashed line.

The SATL province comprises the central portion of the anticyclonic circulation of the South Atlantic (Fig. 19b), excluding the coastal boundary currents, which is persistently under the influence of the trade winds [Reygondeau *et al.* 2013]. The chlorophyll *a* distribution is marked by a seasonal shift, with a permanent zonal high chlorophyll feature at the subtropical convergence zone during the austral summer that moves equatorward during the fall and reaches almost 25°S during the mid-winter (July–August). The high chlorophyll *a* field is maintained during the winter, and according to spring and summer conditions, the oceanic South Atlantic bloom moves poleward, reaching its maxima at approximately 1–2 mg Chl *a* m⁻³ by February [Longhurst *et al.* 2006]. Net FCO₂ measurements have shown that this province is mainly a sink of atmospheric CO₂, with temperature as the main driver of $p\text{CO}_2^{\text{sw}}$ [Lencina Avila *et al.* 2016, Padin *et al.* 2010].

The BENG province comprises the southwestern Africa shelf, including the upwelling eddy field of the Benguela Current, which is split by an environmental barrier, the Lüderitz upwelling cell at 26°S, in two distinct systems: the Northern Benguela upwelling system, with low seasonal variations, and the Southern Benguela upwelling system, with wind-induced upwellings in spring and summer [Duncombe Rae 2005, Hutchings *et al.* 2009]. Investigations of the chlorophyll *a* distribution patterns along these systems show higher biomass in the north than in the south [Demarcq *et al.* 2007, Lamont *et al.* 2019]. The eastern boundary current domain of the South Atlantic gyre surface waters acts as a CO₂

sink, with strong variability associated with upwelling events in the region [González-Dávila *et al.* 2009].

The retroflection zone of the Agulhas Current (Fig. 19b), included in the EAFR coastal province, is a highly energetic region where large warm-core eddies are shed during Agulhas intrusions into the Atlantic, with a mean eddy liberation frequency of approximately 6 times/year [Lutjeharms 2007]. These unusually large (approximately 300 km) eddies have very long lifetimes and can be identified up to 3.5 years after their release, some surviving to reach the Brazilian coastal boundary [Guerra *et al.* 2009, Azevedo *et al.* 2012, Pilo *et al.* 2015, Guerra *et al.* 2018]. Therefore, these eddies have an important role in the structure of the South Atlantic subtropical gyre [Peterson & Stramma 1991].

5.3 Data and Methodology

5.3.1 Cruise Sampling

The South Atlantic Ocean was investigated seven times (Tab. 3), mainly during spring, with one survey conducted in early winter during June/July 2015 [the FORSA cruise, Orselli *et al.* 2018, Carvalho *et al.* 2019]. Hydrographic sections from 20°S to 35°S were performed, providing a robust spatial occupation of the study region. A total of 311 hydrographic conductivity-temperature-depth (CTD) stations provided measurements of physical parameters (temperature, salinity and pressure), where 31 oceanographic stations were located in the BRAZ province, 237 stations were located in the SATL province, and 43 stations were located in the AFR province (Fig. 19a).

Among the seven cruises presented, the FORSA cruise, which occurred in 2015, was the most atypical. This campaign aimed to sample the neighboring and interior of Agulhas eddies during their transition in the South Atlantic Ocean. However, as previously investigated by [Orselli *et al.* \[2018\]](#) and [Carvalho *et al.* \[2019\]](#), both the surface phytoplankton pigments and $p\text{CO}_2$ data available were within the scope of our investigation representing both zonal and meridional gradients of the South Atlantic Ocean and, thus, were included in our investigation. The other six cruises were not focused on eddy sampling; however, as these structures are common in these regions of the South Atlantic Ocean, it is possible that they may have been influencing factors even though they were not monitored.

Table 3. General information about the cruises used in this study, including the name of the cruise, the area covered, the sampling period (season), the data used and the references of earlier studies in the South Atlantic Ocean that previously used the data.

Cruise	Main area	Sampling period Season	Data used	References
<i>H40 2009</i> (30°S)	Meridional section along 30°S from BRAZ to ~35°W SATL	12 Nov – 17Nov Spring	Phytoplankton pigments, SST, SSS, $mpCO_2^{sw}$, pCO_2^{atm} , U_{10}	This study
<i>TAI 2009</i> (30°S)	Meridional section along 30°S from ~35°W SATL to AFR	24 Oct – 16 Nov Spring	Phytoplankton pigments, SST, SSS, $mpCO_2^{sw}$, pCO_2^{atm} , U_{10}	This study
<i>TAI 2009</i> (20°S)	Meridional section along 20°S from to ~35°W SATL	1 Dec – 20 Dec Late spring	Phytoplankton pigments, SST, SSS, $mpCO_2^{sw}$, pCO_2^{atm} , U_{10}	This study
<i>TAI</i> <i>2011_1</i> (30°S)	Meridional section along 30°S from BRAZ to AFR	25 Oct – 23 Nov Spring	Phytoplankton pigments, SST, SSS, $mpCO_2^{sw}$, pCO_2^{atm} , U_{10}	Lencina-Avila et al. [2016]
<i>TAI</i> <i>2011_2</i>	Southwestern- Northeastern section from AFR to BRAZ	4 Dec – 21 Dec Late Spring	Phytoplankton pigments, SST, SSS, $mpCO_2^{sw}$, pCO_2^{atm} , U_{10}	This study
<i>A10 2011</i> (35°S)	Meridional section along 35°S from BRAZ to AFR	28 Sep – 29 Oct Early spring	Phytoplankton pigments, SST, SSS, pCO_2^{sw} , pCO_2^{atm} , U_{10}	Araújo et al. [2017] Orselli et al. [2019]
<i>FORSA</i> <i>2015</i>	Southwestern- Northeastern section at SATL along the Agulhas corridor	27 June – 15 July Early winter	Phytoplankton pigments, SST, SSS, pCO_2^{sw} , pCO_2^{atm} , U_{10}	Orselli et al. [2018] Carvalho et al. [2019]

5.3.2 Data for pCO_2 and FCO_2 calculations

The pCO_2^{sw} and pCO_2 in the atmosphere (pCO_2^{atm}) were determined by autonomous underway measuring systems and data reduction routines, similar to those described by [Pierrot et al. \[2009\]](#), along the cruise tracks. For the cruises conducted in 2009 (H40 2009, TAI_2009) and 2011 (TAI_2011), pCO_2^{sw} was modeled ($mpCO_2^{sw}$) using the algorithm proposed by [Orselli et al. \[2018\]](#) for the region, with sea surface temperature (SST, in °C), sea surface salinity (SSS, in practical salinity) and total chlorophyll a (TChl a, in $mg\ m^{-3}$) anomalies used as the input parameters. This model is very representative of the zonal and meridional gradients of the South Atlantic Ocean and provides better quantification with smaller error and improved coefficients compared with those previously reported for the region, as reported in our manuscript ($r^2 = 0.81$ and

STD_{error} = 6.74 μatm). The analytical error for this estimative approach is comparable to the error found in other indirect measurements (e.g., calculated $p\text{CO}_2^{\text{sw}}$ using total alkalinity (TA) and total inorganic carbon (DIC) = 5.7 μatm) [Millero 2007]. The $p\text{CO}_2^{\text{atm}}$ for the TAI_2009 cruises (20°S and 30°S) was obtained using monthly means for the months of October, November and December (Station ABP) from NOAA-ESRL data (<https://www.esrl.noaa.gov/gmd/dv/data/>). For cruise TAI 2011_2 (December), the $p\text{CO}_2^{\text{atm}}$ was estimated using the average of TAI 2011_1 (October and November). The $p\text{CO}_2^{\text{sw}}$ values were normalized to the average temperature ($Np\text{CO}_2^{\text{sw}}$) of each cruise according to Takahashi *et al.* [2009; Eq. 19]:

$$Np\text{CO}_2^{\text{sw}} = (p\text{CO}_2^{\text{sw}}) \exp [0.0433(\overline{SST} - \text{SST}) - 4.35 \times 10^{-5} [(\overline{SST})^2 - (\text{SST})^2]] \quad (19),$$

where SST and \overline{SST} are the sea surface temperature and mean SST, respectively. $Np\text{CO}_2^{\text{sw}}$ values were used in the statistical analysis to evaluate the correlations between $p\text{CO}_2^{\text{sw}}$ and phytoplankton biomass.

The FCO_2 value was estimated as the difference between the $p\text{CO}_2$ of the seawater and the atmosphere ($\Delta p\text{CO}_2 = p\text{CO}_2^{\text{sw}} - p\text{CO}_2^{\text{atm}}$; thus, negative $\Delta p\text{CO}_2$ values likely indicate a CO_2 sink to the ocean, and positive $\Delta p\text{CO}_2$ values likely indicate a CO_2 source to the atmosphere), together with wind speed data (U_{10}), which were obtained through the European Center for Medium-Range Weather Forecasts portal (ECMWF; <http://data-portal.ecmwf.int/>) and had a spatial resolution of 1.5° latitude by 1.5° longitude. The $\Delta p\text{CO}_2$ parameter was used as a proxy to assess the association between FCO_2 and the phytoplankton groups, thereby avoiding the direct influence of the wind speed. The seawater CO_2

solubility coefficient [K_0 ; [Weiss 1974](#)] and updated parametrization of [Wanninkhof \[2014\]](#) for gas transfer velocity (k) were used to determine the FCO_2 (Eq. 20):

$$FCO_2 = k K_0 (\Delta pCO_2) \quad . \quad (20)$$

5.3.3 *Phytoplankton pigment analyses and chemotaxonomic groups*

Surface seawater samples were collected for phytoplankton pigment analysis and filtered through Whatman GF/F filters (nominal pore size of 0.7 μm ; 25 mm in diameter) for all cruises. Filters were immediately stored in liquid nitrogen for later high-performance liquid chromatography (HPLC) pigment analysis in the laboratory. Phytoplankton pigments were extracted in the dark with 3 mL of 95% cold-buffered methanol (2% ammonium acetate) containing 0.05 mg L^{-1} trans- β -apo-8'-carotenal (Fluka) as an internal standard. Samples were sonicated for 5 min in an ice-water bath, kept at -20°C for 1 h, and centrifuged at 1100 rpm for 5 min at 3°C in a model 280-R refrigerated centrifuge (Excelsa 4). The supernatants were filtered through Fluoropore PTFE membrane filters (0.2- μm pore size) to remove the remains of the filter and cell debris from the extract. Immediately prior to injection, 1000 μL of sample was mixed with 400 μL of Milli-Q water in 2.0-mL glass sample vials, and these were placed in the HPLC cooling rack (4°C) of the Shimadzu Prominence LC-20A Modular HPLC System. Methodological procedures for the HPLC analysis using a monomeric C8 column with a pyridine-containing mobile phase are fully described in [Zapata *et al.* \[2000\]](#). In addition, we used the detection limit and quantification procedure of [Mendes *et al.* \[2007\]](#). Pigments were identified from both the absorbance spectra and retention times of the signals in the photodiode

array detector (Shimadzu, SPD-M20A; 190–800 nm; 1 nm wavelength accuracy) or fluorescence detector (Shimadzu, RF-10AXL; Ex. 430 nm/Em. 670 nm). Calibrations and subsequent quantification of the pigments were performed at or close to the wavelength of maximum absorption (e.g., chlorophyll *a* at 430 nm, fucoxanthin at 448 nm, zeaxanthin at 454 nm, and chlorophyll *b* at 470 nm). Pigments were quantified by peak integration using LC-Solution software (Shimadzu), and all peak integrations were manually checked and corrected when necessary. The HPLC system was previously calibrated with pigment standards from DHI (Institute for Water and Environment, Denmark).

The relative contribution of microalgal groups to the overall biomass was calculated with CHEMTAX v1.95 chemical taxonomy software using the class-specific accessory pigments and total chlorophyll *a* [Mackey *et al.* 1996]. CHEMTAX uses a factor analysis and steepest-descent algorithm to best fit the data onto an initial matrix of pigment ratios (ratio between a marker accessory pigment and the total chlorophyll *a* – *TChl a*). The input matrix is loaded into the program with field measurements of pigment concentrations. For more information, the procedures and calculations of CHEMTAX are fully described in Mackey *et al.* [1996]. The initial pigment ratios of major algal classes used here were derived from Higgins *et al.* [2011], with chemotaxonomic groups identified according to Jeffrey *et al.* [2011]. The loaded pigments were chlorophyll *a* (Chl *a*), divinyl-Chl *a* (DV Chl *a*), violaxanthin, 19'-butanoyloxyfucoxanthin, fucoxanthin, 19'-hexanoyloxyfucoxanthin, lutein, chlorophyll c_3 , prasinoxanthin, alloxanthin, zeaxanthin, peridinin and total chlorophyll *b* (TChl *b*). Based on the identified diagnostic pigments, nine algal groups were loaded into the CHEMTAX

software: prasinophytes, chlorophytes, cryptophytes, diatoms, pelagophytes, dinoflagellates, haptophytes, *Synechococcus* and *Prochlorococcus*.

The same initial pigment ratio matrix was applied to data from the seven cruises (input and output matrices are shown in [Table S1 \(Anexo II, pág. 199\)](#); Supplementary material). Data from each cruise were run separately to minimize potential variations in the CHEMTAX optimization procedures. Chl *a* was used to estimate the biomass of all groups except *Prochlorococcus*, for which DV Chl *a* was used. Therefore, in this study, the sum Chl *a* + DV Chl *a*, named TChl *a*, was used as the phytoplankton biomass index. To optimize the input matrices, a series of 60 pigment ratio matrices was generated by multiplying each ratio of the initial matrix by a random function. The ten percent ($n = 6$) of the generated ratios with the lowest root-mean-square residuals were averaged, resulting in the output matrix ([Table S1; Anexo II pág. 194](#)) [[Wright et al. 2009](#)].

5.3.4 Statistical analysis

Statistical analysis was performed in R [[R Core Team 2017](#)] using the package “corrplot” [[Taiyun Wei & Viliam Simko 2017](#)]. Correlation matrices and Pearson-r parametric correlation coefficients were calculated between biotic variables, represented by the biomasses of the CHEMTAX-derived taxonomical groups (in mg m^{-3} of the TChl *a*), and environmental variables, including SST, SSS, TChl *a*, wind, $Np\text{CO}_2^{\text{sw}}$ and $\Delta p\text{CO}_2$. The relationship of the phytoplankton groups with environmental variables was investigated by canonical correspondence analysis [CCA; [Ter Braak & Prentice 1988](#)] using CANOCO software for Windows 4.5. A Monte Carlo approach was further employed based on 499 permutations under a reduced model ($p < 0.05$) to evaluate the CCA significance.

5.4 Results

5.4.1 *Environmental physical conditions and phytoplankton biomass*

The spatial distribution of surface temperature (Fig. 20a), salinity (Fig. 20b) and TChl *a* (Fig. 20c) along the cruise tracks revealed strong gradients in the properties across the South Atlantic Ocean, reflecting significant differences between biogeochemical provinces. In general, the province-averaged surface temperatures decreased from $22.7 \pm 2.6^{\circ}\text{C}$ in the western part of the South Atlantic Ocean basin at the BRAZ stations to $19.2 \pm 3.0^{\circ}\text{C}$ in the SATL stations, and it further decreased to $17.8 \pm 1.7^{\circ}\text{C}$ on the east coast of the South Atlantic Ocean at the AFR stations (Tab. 4). The SST along 20°S was high in the western area (Fig. 20a) and decreased toward the east. Greater variations in salinity were evidenced in the BRAZ province (35.5 ± 1.6), where the salinity values were lower at higher latitudes, reaching the lowest mean of 33.8 ± 1.9 at 35°S . Small salinity changes were measured in both the SATL (36.0 ± 0.6) and AFR (35.4 ± 0.2) provinces (Tab. 4).

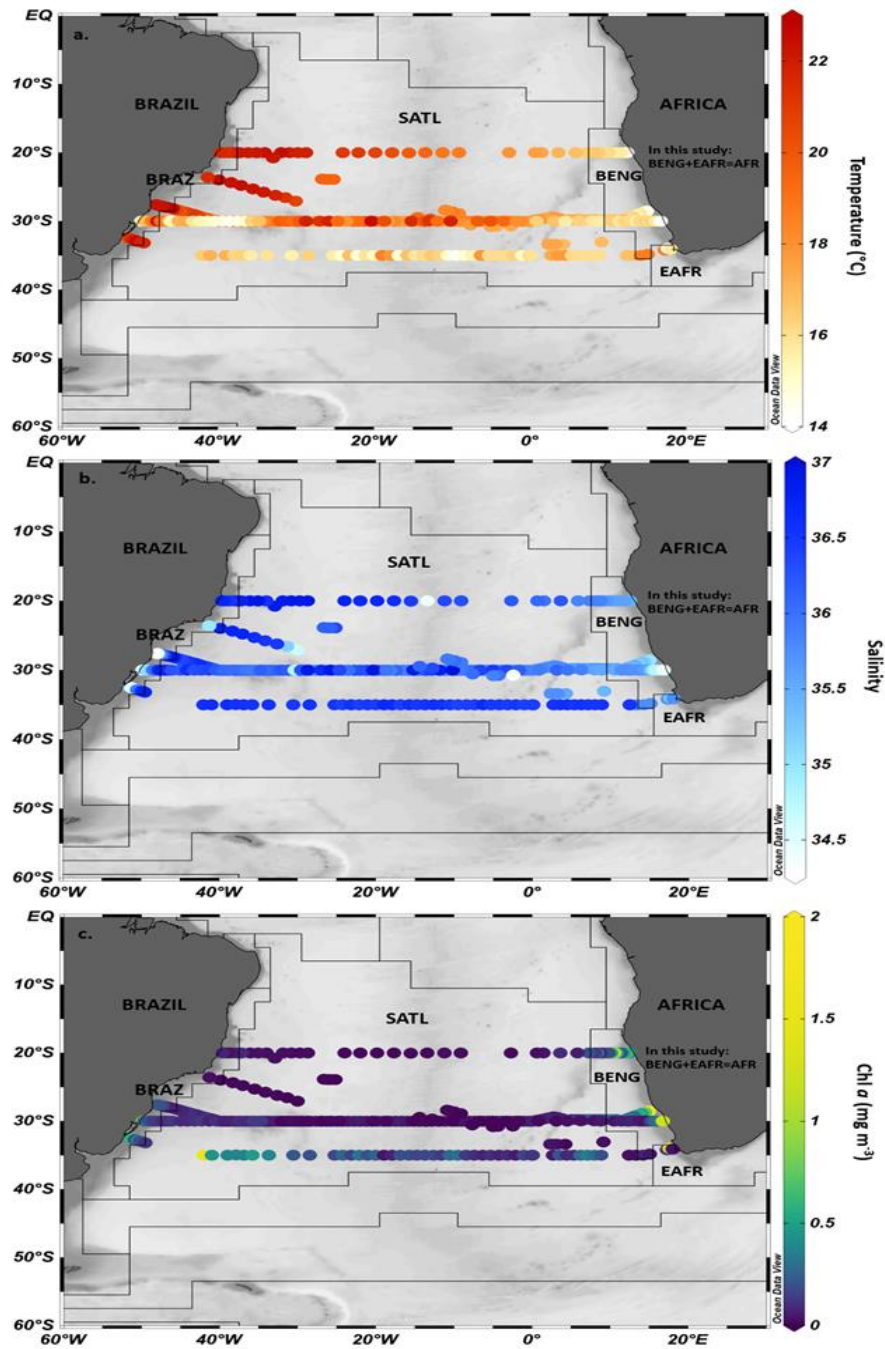


Figure 20. Spatial distribution of environmental parameters for each cruise along the South Atlantic Ocean. **(a)** Sea surface temperature ($^{\circ}\text{C}$). **(b)** Sea surface salinity. **(c)** Total chlorophyll *a* (mg m^{-3}). The biogeochemical provinces (black lines) according to Longhurst (2006) were overlaid on the maps using the shapefile overlay from VLIZ (2009). The acronyms refer to the Longhurst provinces: Brazil (BRAZ), South Atlantic Gyral (SATL), Benguela (BENG) and East African (EAFR). Here, the last two provinces are referenced together as Africa (AFR).

Table 4. Average physical and biogeochemical parameters for each South Atlantic cruise separated by provinces (Brazil, BRAZ; South Atlantic Gyral, SATL; and African - AFR). Sea surface temperature (SST; °C), sea surface salinity (SSS; psu), total chlorophyll *a* (TChl *a*; mg m⁻³), seawater CO₂ partial pressure ($p\text{CO}_2^{\text{sw}}$; μatm), atmospheric CO₂ partial pressure ($p\text{CO}_2^{\text{atm}}$; μatm), temperature-normalized seawater CO₂ partial pressure ($Np\text{CO}_2^{\text{sw}}$; μatm), difference between seawater and atmospheric $p\text{CO}_2$ ($\Delta p\text{CO}_2$; μatm), wind speed at 10 meters (U_{10} ; m s⁻¹), CO₂ net fluxes (FCO_2 ; mol m⁻² d⁻¹) and number of samples (*n*) within each cruise and province.

Cruise	Month	Province	SST	SSS	TChl <i>a</i>	$p\text{CO}_2^{\text{sw}}$	$p\text{CO}_2^{\text{atm}}$	$Np\text{CO}_2^{\text{sw}}$	$\Delta p\text{CO}_2$	U_{10}	FCO_2	<i>n</i>
H40 - 2009 (30°S)	Nov	BRAZ	22.8±1.2	35.2±0.8	0.2±0.1	374.2±2.2	386.6±0.0	368.8±17.4	-12.4±2.2	6.8±2.6	-5.4±3.5	8
		SATL	22.3±0.9	36.3±0.3	0.1±0.0	363.5±2.2	386.6±0.0	366.1±11.4	-23.1±2.2	6.0±2.5	-8.1±4.9	18
TAI 2009 (30°S)	Oct/Nov	SATL	19.2±1.0	35.9±0.2	0.1±0.1	353.4±8.4	386.4±0.2	345.5±12.5	-33.0±8.5	4.2±3.0	-8.7±5.5	26
		AFR	17.5±0.3	35.4±0.2	0.7±0.1	330.2±26.4	386.6±0.0	345.6±24.7	-56.4±26.4	10.4±0.6	-50.8±16.2	13
TAI 2009 (20°S)	Dec	BRAZ	27.4±0.4	37.0±0.2	0.1±0.1	370.1±1.8	386.8±0.0	319.0±5.7	-16.7±1.8	7.4±0.8	-7.7±1.3	5
		SATL	25.3±2.8	36.7±0.8	0.1±0.1	362.6±10.6	386.8±0.0	339.6±29.4	-24.3±10.8	5.7±1.6	-7.1±6.3	24
		AFR	19.5±0.9	35.5±0.2	0.7±0.4	329.3±13.3	386.8±0.0	389.2±11.9	-57.5±13.3	7.6±0.9	-28.0±6.6	14
TAI1 2011_1 (30°S)	Oct/Nov	BRAZ	19.2±0.5	33.8±1.9	0.4±0.3	372.8±14.5	379.3±1.1	331.0±15.1	-6.5±14.0	7.0±1.4	-20.9±9.1	7
		SATL	15.7±0.6	35.5±0.2	0.3±0.2	342.4±6.6	388.5±3.7	348.9±9.0	-46.1±6.7	7.5±2.0	-24.9±15.5	45
TAI1 2011_2	Dec	BRAZ	23.9±1.0	35.7±2.1	0.1±0.0	386.7±13.6	381.7±0.0	336.6±25.8	5.0±13.6	12.2±0.5	8.3±20.8	2
		SATL	20.8±3.5	35.7±2.8	0.1±1.2	372.0±0.0	381.7±0.0	368.2±34.2	-9.7±13.7	7.7±1.5	-6.1±6.3	16
		AFR	17.9±2.7	35.3±0.3	1.3±2.0	328.7±59.9	381.7±0.0	360.8±45.7	-53.0±59.9	5.5±2.2	-13.3±11.0	5
A10 2011 (35°S)	Sep/Oct	BRAZ	22.6±0.2	36.3±0.9	0.1±0.1	373.3±6.3	376.5±0.8	316.3±7.6	-3.2±6.7	9.6±0.9	-1.9±5.1	9
		SATL	18.4±1.0	36.0±0.3	0.1±0.0	349.8±7.8	382.1±2.8	351.2±15.3	-32.3±8.9	4.4±1.2	-6.1±3.6	97
		AFR	15.9±0.8	35.4±0.2	0.6±0.5	344.8±10.8	382.1±1.0	383.7±23.1	-37.4±11.5	4.5±0.5	-6.7±3.3	11
FORSA 2015	Jun/Jul	SATL	19.9±2.1	36.1±0.4	0.1±0.1	348.7±5.8	392.0±3.1	349.4±25.3	-43.3±7.7	6.8±0.6	-4.1±0.8	12

The TChl *a* concentration was used as a proxy for phytoplankton biomass and showed the highest mean concentration of $0.7 \pm 0.9 \text{ mg m}^{-3}$ in the AFR province. The maximum value of 4.8 mg m^{-3} was measured for this province near 35°S and 40°W (Fig. 20c). Specifically, the highest average of $1.3 \pm 2.0 \text{ mg m}^{-3}$ was observed in the AFR province, whereas the BRAZ and SATL provinces showed the lowest TChl *a* values of approximately 0.1 mg m^{-3} (Tab. 4).

5.4.2 Distribution of $p\text{CO}_2$ and net CO_2 fluxes in the South Atlantic Ocean

A high average $p\text{CO}_2^{\text{sw}}$ of $373.8 \pm 8.6 \text{ } \mu\text{atm}$ was found in the BRAZ province, while $p\text{CO}_2^{\text{sw}}$ was reduced to $352.5 \pm 11.6 \text{ } \mu\text{atm}$ in the SATL province and further decreased to an average of $333.5 \pm 25.8 \text{ } \mu\text{atm}$ in the AFR province (Tab. 4). The minimum $p\text{CO}_2^{\text{sw}}$ of $222.1 \text{ } \mu\text{atm}$ was observed along the east African coast (at 34°S and 17°E), and the maximum $p\text{CO}_2^{\text{sw}}$ of $399.7 \text{ } \mu\text{atm}$ was observed in the SATL province (at 30°W and 27°S). Regarding atmospheric CO_2 measurements, $p\text{CO}_2^{\text{atm}}$ was observed among different provinces, with mean values of $381.7 \pm 4.5 \text{ } \mu\text{atm}$ in BRAZ, $385.0 \pm 4.0 \text{ } \mu\text{atm}$ in SATL and $385.0 \pm 2.4 \text{ } \mu\text{atm}$ in AFR. The overall $\Delta p\text{CO}_2$ values revealed that the entire study region was undersaturated with CO_2 with respect to the atmosphere, independent of spatial and temporal variabilities. Negative sea-air $\Delta p\text{CO}_2$ values were found during all cruises except at a few stations in SATL (near 30°W) and one station in BRAZ (near 27°S) that showed CO_2 emission behavior; all the other cruises showed CO_2 sink behavior. Latitudinal variability was evident between the different cruises, with relatively high values of $p\text{CO}_2^{\text{sw}}$ at 20°S and low values of $p\text{CO}_2^{\text{sw}}$ at approximately 35°S (Tab. 4).

Small variations in U_{10} were found among the three sampled regions, with an average of $8.1 \pm 2.2 \text{ m s}^{-1}$ in BRAZ, $5.5 \pm 2.2 \text{ m s}^{-1}$ in SATL and $7.4 \pm 2.5 \text{ m s}^{-1}$ in AFR. Higher wind speeds were observed at higher latitudes. Although the three provinces acted as a sink for atmospheric CO_2 , the average FCO_2 increased by approximately threefold in the east side of the basin, from $-7.1 \pm 10.1 \text{ mmol CO}_2 \text{ m}^{-2} \text{ d}^{-1}$ in BRAZ to $-26.8 \pm 19.5 \text{ mmol CO}_2 \text{ m}^{-2} \text{ d}^{-1}$ in AFR, a value indicative of strong sink behavior (Tab. 4).

In the AFR province, large variations in $\Delta p\text{CO}_2$ values were observed that can be attributed to the dynamics of the Benguela upwelling system at the higher latitudes for the stations located at the BENG province and farther south (at approximately 35°S). The proximity to the Agulhas retroflexion (EAFR) is an influencing factor.

5.4.3 Phytoplankton group distribution in the South Atlantic Ocean

Among the nine phytoplankton groups identified in the South Atlantic Ocean, the groups or genera with the largest biomasses were haptophytes, diatoms, *Synechococcus* and *Prochlorococcus*. Biomass concentrations (TChl *a*) in the BRAZ and SATL provinces showed similar ranges, with maximum concentrations of approximately 0.5 mg m^{-3} , while in the AFR province, these concentrations increased by one order of magnitude and reached a maximum value of approximately 5.0 mg m^{-3} (Fig. 21, please note the different scale in the AFR panel).

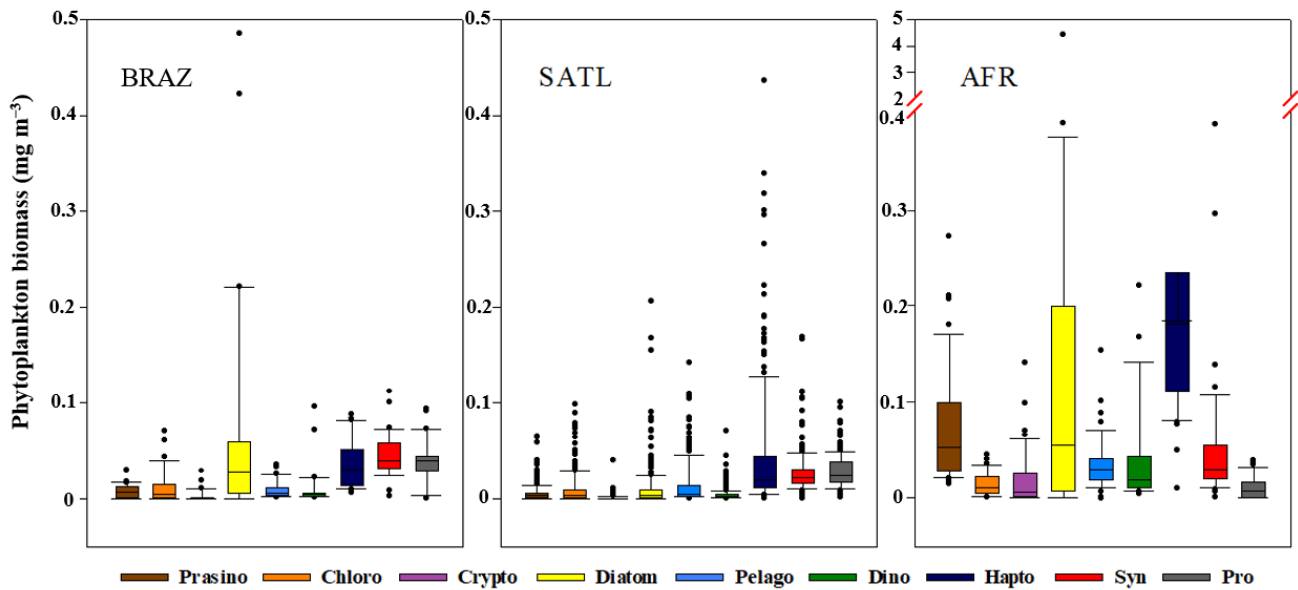


Figure 21. Box plot (from bottom to top, the horizontal lines represent the minimum, first quartile, median, third quartile, and maximum values; the black dots represent the outliers) for each province (left to right: BRAZ, SATL and AFR) of the distribution of phytoplankton chemotaxonomic group biomasses indicated by the color legends at the bottom of the plots (Prasino- prasinophytes, Chloro- chlorophytes, Crypto- cryptophytes, Diatom- diatoms, Pelago- pelagophytes, Dino- dinoflagellates, Hapto- haptophytes, Syn- *Synechococcus* and Pro- *Prochlorococcus*). Note the difference in the y-scale in the AFR panel.

Near the coastal waters, diatoms and haptophytes are the dominant groups (Fig. 21) and represent approximately $23 \pm 15\%$ and $17 \pm 5\%$ of the total biomass in BRAZ, respectively. For the AFR, diatoms and haptophytes represent $18.42 \pm 12.64\%$ and $38.52 \pm 9.15\%$ of the total biomass, respectively (Tab. S2). However, at the high latitudes of both South Atlantic Ocean coasts, diatoms were the prevailing group (Tab. S2). Considering the oligotrophic environment of the SATL, the major algal groups were the cosmopolitan haptophytes ($23.00 \pm 9.47\%$ TChl *a*) and the marine picocyanobacteria belonging to the genera *Synechococcus* ($24.01 \pm 10.31\%$ TChl *a*) and *Prochlorococcus* ($26.79 \pm 9.79\%$ TChl *a*), which dominate vast oceanic areas (Tab. S2).

5.4.4 Relationships between environmental properties, CO₂ dynamics and phytoplankton group biomasses

Because FCO₂ is a function of the difference between seawater and atmospheric pCO₂ ($\Delta p\text{CO}_2$), this parameter was used to identify significant correlations between physical and biological variables to understand the main factor driving CO₂ fluxes in the region. Pearson's correlation coefficient (r) showed that for the entire study region, the $\Delta p\text{CO}_2$ values were positively correlated with temperature ($r = 0.55$, $p < 0.05$) and negatively correlated with TChl *a* ($r = -0.63$, $p < 0.05$) (Anexo II, [Tab. S3a](#); [Fig. S2](#)).

Considering the provinces separately, at BRAZ, $\Delta p\text{CO}_2$ showed a significant correlation with salinity and wind ([Tab. S3b](#), Anexo II pág. 197). Most phytoplankton groups showed significant negative correlations with salinity and temperature (Anexo II, [Tab. S3b](#); [Fig. S1](#)) and no significant correlations with $\Delta p\text{CO}_2$, except for *Prochlorococcus*. This group showed significant negative correlation with $\Delta p\text{CO}_2$ ($r = -0.38$, $p < 0.05$) and strong positive correlations with both temperature (0.76 , $p < 0.05$) and salinity (0.71 , $p < 0.05$), unlike the other groups ([Tab. S3b](#), Anexo II pág. 197). South of 30°S at the BRAZ province, enhanced CO₂ uptake (FCO₂ = -20.1 ± 8.7) was observed at stations dominated by diatoms, while no significant correlations were found between the diatoms' biomass and $\Delta p\text{CO}_2$ ([Tab. S1](#), Anexo II pág. 194). However, in the SATL province, $\Delta p\text{CO}_2$ was positively correlated with temperature ($r = 0.64$, $p < 0.05$) and negatively correlated with TChl *a* ($r = -0.52$, $p < 0.05$), mainly due to the presence of pelagophytes and haptophytes ([Fig. S1](#), Anexo II pág. 199). In addition, in the AFR province, $\Delta p\text{CO}_2$ showed a significant negative correlation with TChl *a* ($r = -0.84$, $p < 0.05$) and the presence of diatoms ($r = -0.76$, $p < 0.05$) ([Tab. S3d](#), Anexo II pág. 198).

The correlation analysis showed that the sea surface temperature was an important driver of CO₂ variability in the South Atlantic Ocean (Anexo II; Fig. S1, Tab. S3a), as previously identified by Orselli et al. [2018] through an investigation of the FORSA 2015 cruise section only. However, in this study, TChl *a* also showed significant and strong correlations with $\Delta p\text{CO}_2$ for both the SATL and AFR provinces, but not for the BRAZ province (Anexo II; Fig. S1, Tab. S3b). In the BRAZ province, the temperature and salinity are probably the main factors driving the FCO₂. Indeed, more measurements must be taken to properly decipher the mechanisms of CO₂ uptake at this complex and variable province of the South Atlantic Ocean.

CCA analysis (Fig. 22a) was used to better understand the relationships between the biomass of the different phytoplankton groups and environmental variables. A clear split was observed between coastal (the red and green symbols in figure 22a indicate the BRAZ and AFR stations, respectively) and open ocean data (SATL stations are represented by yellow symbols in Fig. 22a).

In general, the dominant phytoplankton groups at the BRAZ stations (*Prochlorococcus* and *Synechococcus*) were mainly associated with physical variables, such as temperature and salinity. The AFR stations were associated with TChl *a* and a variety of phytoplankton groups, such as haptophytes, pelagophytes, diatoms and chlorophytes. There was a noticeable latitudinal pattern among the SATL samples (yellow symbols in Fig. 22a) in the CCA with low latitude cruises (TAI 2009 at 20°S - represented by yellow and red rectangles) that was mostly associated with temperature and salinity and with *Prochlorococcus* and *Synechococcus*. High-latitude data (A10 2011, represented by yellow stars) were mostly associated with $\text{NpCO}_2^{\text{sw}}$ and pelagophytes,

chlorophytes and haptophytes. The first two ordination axes represent 41.7% of the total phytoplankton group variance and 84.5% of the phytoplankton group-environment relationship.

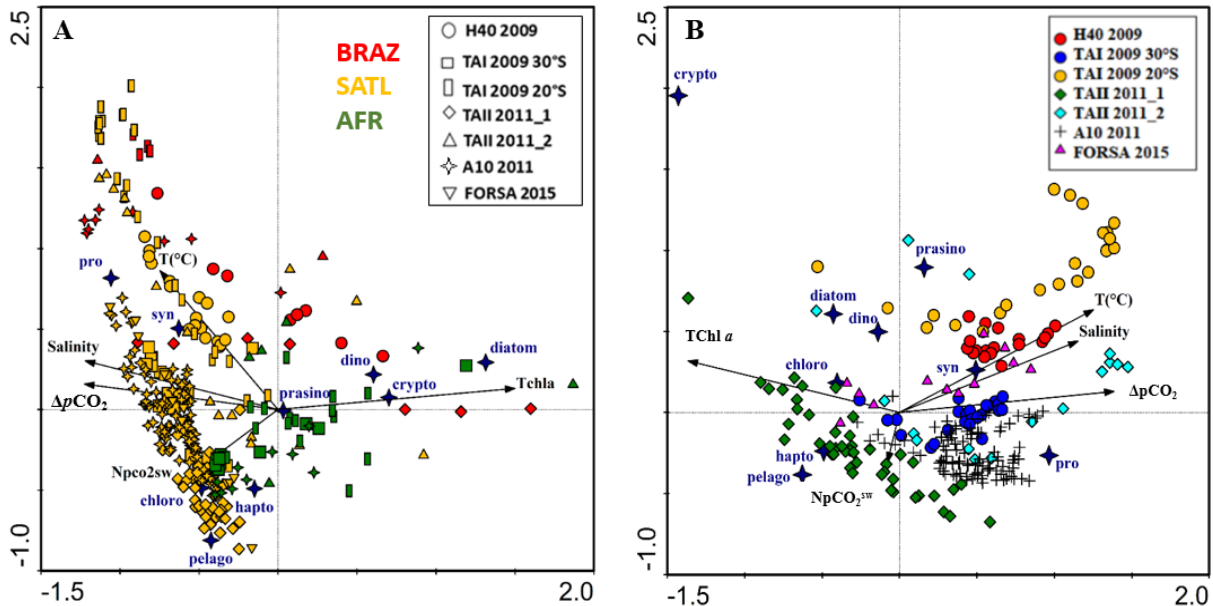


Figure 22. (a) Canonical correspondence analysis (CCA) ordination diagram of the biomass of different phytoplankton groups at the sea surface in all seven cruises (see legend at top right for different cruise symbols) along the South Atlantic Ocean. The arrows indicate environmental variables (pointing in the direction in which the value of environmental variables increases; the angle indicates the correlation between variables); the variables are as follows: sea surface temperature (T ; $^{\circ}\text{C}$), salinity, temperature-normalized CO_2 partial pressure ($\text{NpCO}_2^{\text{sw}}$), sea-air CO_2 partial pressure difference ($\Delta p\text{CO}_2$) and total chlorophyll a ($\text{Tchl } a$). Blue stars indicate the absolute contributions of phytoplankton groups. diatom = diatoms; dino = dinoflagellates; crypto = cryptophytes; prasino = prasinophytes; hapto = haptophytes; syn = *Synechococcus*; pelago = pelagophytes; chloro = chlorophytes; pro = *Prochlorococcus*. Stations are separated according to distinct ocean biogeochemical provinces by color (BRAZ-red, SATL-yellow and AFR-green). **(b)** CCA ordination diagram of biomass contributions of different phytoplankton groups at the sea surface in the South Atlantic Gyral province (SATL). The first two ordination axes represent 95.2% of the total phytoplankton group variance and 32.6% of the phytoplankton group-environment relationship. Arrows indicate environmental variables: sea surface temperature ($T^{\circ}\text{C}$), salinity, temperature-normalized CO_2 partial pressure ($\text{NpCO}_2^{\text{sw}}$), difference between seawater and atmospheric CO_2 partial pressures ($\Delta p\text{CO}_2$) and total chlorophyll a ($\text{Tchl } a$). Blue crosses indicate the absolute contributions of phytoplankton groups. diatom = diatoms; dino = dinoflagellates; Crypto = cryptophytes; prasino = Prasinophytes; hapto = haptophytes; Syn = *Synechococcus*; Pelago= Pelagophytes; chloro = Chlorophytes; Pro = *Prochlorococcus*. Stations are separated according to distinct cruises (see legend at top right).

Another CCA analysis was carried out using only SATL data, thus allowing a better understanding of the latitudinal pattern in the phytoplankton distribution in the South Atlantic Ocean (Fig. 22b). In figure 22b, yellow circles represent stations at 20°S (from the TAI 2009 cruise), which are most related to physical

drivers such as temperature and salinity. Red circles (Fig. 22b) refer to stations at 30°S (from H40 2009 cruise); stations in the west basin of the South Atlantic Ocean also showed a positive association with physical drivers. Cruise tracks at the high latitudes of 30°S and 35°S (represented by green diamonds and black crosses respectively, Fig. 22b), which were representative of stations in the eastern South Atlantic Ocean basin, were most associated with TChl *a*. The stations from cruise tracks that crossed a latitudinal gradient showed a varying behavior (TAII 2011_2 and FORSA 2015).

Along the SATL stations, Prasinophytes, *Synechococcus* and *Prochlorococcus* were positively associated with temperature, salinity and $\Delta p\text{CO}_2$ (Fig. 22b). Haptophytes, pelagophytes and chlorophytes were positively associated with TChl *a* and $Np\text{CO}_2^{\text{sw}}$, negatively associated with both temperature and salinity, and related to higher latitudes (at 35°S) (Fig 22b).

The distributions of FCO_2 and TChl *a* along the cruises revealed the latitudinal and longitudinal gradients detected in the South Atlantic Ocean (Fig. 23). Regarding FCO_2 , high uptake rates were generally found in the AFR province and at 35°S latitude. At 35°S, all three provinces showed a high capacity of ocean CO_2 uptake (Fig. 23).

The TChl *a* distribution indicated the highest biomass values at AFR and at the latitude of 35°S, where the FCO_2 values indicated high absorption of CO_2 . However, the phytoplankton community composition showed variations along the three provinces and was influenced by the increase in latitude. The shift in the percent contribution to total biomass among the main phytoplankton groups was compared by sectioning the transects 20°S, 30°S and 35°S among the three provinces (graphs on the right in Fig. 23). Comparing both coastal areas, in

BRAZ, diatoms and pelagophyte contributions increased greatly at high latitudes, while the percent contributions of *Prochlorococcus* and *Synechococcus* decreased. In AFR, the phytoplankton community was mostly dominated by haptophytes, with a small decrease at 35°S favoring an increase in diatoms. While diatoms and pelagophytes increased in coastal areas, mainly at high latitudes, haptophytes showed major increases in the SATL province with the decrease in *Prochlorococcus* and *Synechococcus*.

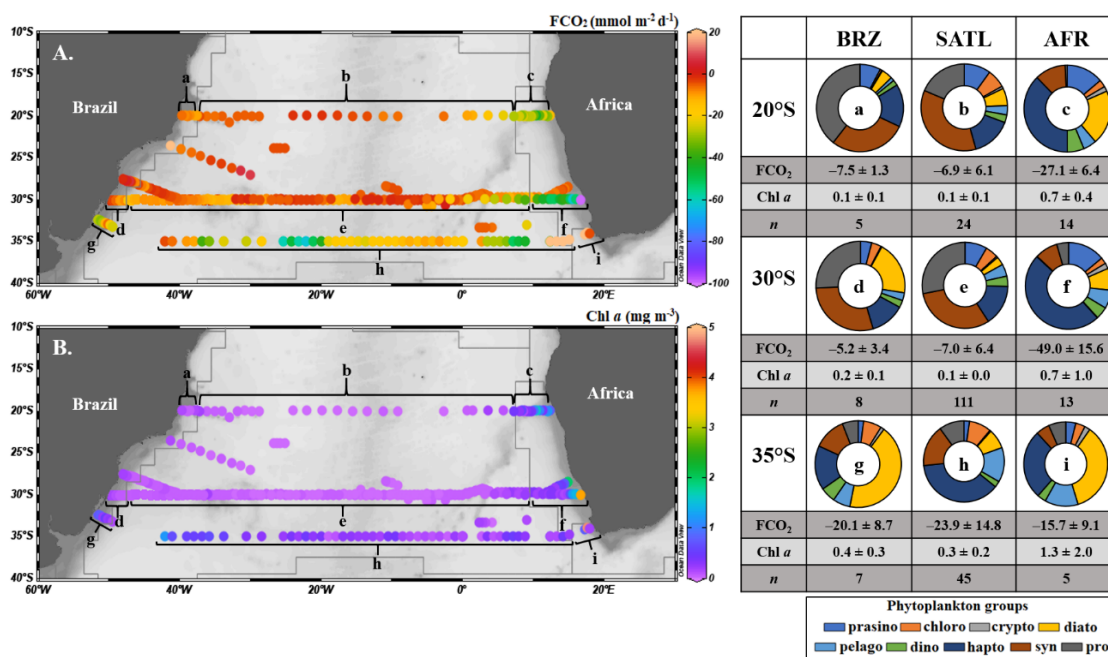


Figure 23. Net sea-air CO₂ fluxes (FCO₂, mmol m⁻² d⁻¹) and chlorophyll a (TChl a, mg m⁻³) distributions in the South Atlantic Ocean. **A.** FCO₂ and **B.** Chlorophyll a (TChl a, mg m⁻³) along the different cruise tracks evaluated in this study. On the right, the donut graphs represent the average phytoplankton group contributions to phytoplankton biomass along 20°S for (a) BRAZ stations, (b) SATL stations and (c) AFR stations; along 30°S for (d) BRAZ stations, (e) SATL stations and (f) AFR stations; and along 35°S for (g) BRAZ stations, (h) SATL stations and (i) AFR stations. The gray shaded lines on the side table display the average FCO₂ and TChl a and the number of stations (n) used in each section marked on left panels a and b (a to i) of the transects along 20°S, 30°S and 35°S.

At 35°S, the FCO₂ sinking rates were enhanced in both the BRAZ and SATL provinces. Notably, in the AFR sector at 30°S (donut graph f, Figure 23), the haptophyte contribution to the total biomass increased to almost half the phytoplankton community composition associated with the lowest FCO₂ value (–

49 mmol m⁻² d⁻¹). A different pattern was found in the AFR province at 35°S, where haptophytes ceased to be the dominant group, and the increases in diatoms and group diversity accompanied a decreased mean CO₂ sink rate (donut graph *i*, [Figure 23](#)) compared with the sink rate of lower latitudes.

5.5 Discussion

This discussion will focus on the spatial variability of phytoplankton groups and CO₂ properties subjected to distinct environmental conditions and the influence of different dynamic systems in the South Atlantic Ocean, rather than aspects related to seasonality or temporal variability (as the majority of the cruises were in spring). We address the three biogeochemical provinces (i.e., BRAZ, SATL and AFR) separately and consider the dominant characteristics and the environmental features of each region to elucidate the links between the dominant phytoplankton groups and the CO₂ behavior. Furthermore, we provide an overall view of the three systems together with our main findings and concerns regarding the association between the major phytoplankton groups in the South Atlantic Ocean and their connection to the atmospheric carbon sink fluxes at the different sites studied.

5.5.1 Western boundary current dominated system (BRAZ)

The sites sampled in the BRAZ province acted mainly as CO₂ sinks, with the weakest FCO₂ measured in BRAZ compared with the other biogeochemical provinces. Two stations in the transition zone between the coastal upwelling region of Abrolhos-Campos and a temperate area known as the South Brazil Bight (at approximately 23°S) showed CO₂ source behavior, which indicated that

the BRAZ province has a complex and highly dynamic structure that often alternates between sink and/or source behavior, which is similar to that of many other coastal regions [e.g., [Ito et al. 2005](#), [Cai et al. 2006](#), [Arruda et al. 2015](#)]. In previous studies, the southwestern subtropical Atlantic continental shelf between 20°S and 35°S was shown to act as a source of CO₂ to the atmosphere, with a marked seasonal difference of one order of magnitude between late spring and early summer [[Ito et al. 2016](#)]. The neighboring Argentinian continental shelf also transitions between source and sink regions [[Schloss et al. 2007](#), [Bianchi et al. 2009](#), [Kahl et al. 2017](#)] due to contrasts between light-limited areas under the influence of strong mixing by tidal fronts nearshore and highly stratified offshore waters favoring phytoplankton growth and the drawdown of CO₂.

Phytoplankton biomass in the BRAZ province was generally low but showed a slight increase with increased latitude. The main taxonomic groups also varied among the different BRAZ latitudinal physiographical regions. *Prochlorococcus*, a very small cyanobacterium (0.5 – 0.7 µm cell size diameter), was dominant at low latitudes near 20°S and showed a positive correlation with salinity and temperature ([Fig. S3b](#)); this result was expected since *Prochlorococcus* species are well adapted to low-nutrient and high-light conditions at low latitudes [[Biller et al. 2014](#)]. Conversely, the other phytoplankton groups showed negative correlations with temperature (lower biomass with increasing temperature) and salinity ([Tab. S3b](#)). *Synechococcus*, with a cell size of approximately 0.6 – 1.5 µm, also belongs to the small group of picocyanobacteria and was dominant at the surface at 30°S. Both *Synechococcus* and *Prochlorococcus* may have a common ancestor, although they have different physiological adaptations and photosynthetic pigments

[Dufresne *et al.* 2005]. While *Synechococcus* is present in almost all marine environments and has the ability to acclimate to changing temperatures, which may explain its greater geographical range [Mackey *et al.* 2013, Pittera *et al.* 2014], *Prochlorococcus* is a more versatile genus with respect to light conditions, showing adequate adaptations to both high and low light [Moore *et al.* 1998].

Diatoms are predominant near the coast and south of 30°S [e.g., Islabão *et al.* 2017]. This region is under the influence of the freshwater discharge from the Patos Lagoon mouth (near 32°S), which contributes to the northward spread of the relatively cold, fresh and nutrient-rich (mainly silicate and phosphate) La Plata plume water [Braga *et al.* 2008]. This was also the case at BRAZ sites near 35°S (Figure 5), where diatoms were the dominant group in the phytoplankton community. The highly energetic turbulent region has positive effects on diatom communities in the BRAZ province [Fernandes & Brandini 2004, Smayda & Trainer 2010]. In fact, the physical instability of shallow coastal waters tends to maintain vertical homogeneity, increasing the nutrient supply from deeper layers in the euphotic zone. Moreover, turbulence tends to slow the sinking of phytoplankton out of the euphotic zone, while land drainage further contributes to nutrient enrichment, favoring diatom growth [Margalef 1978]. Diatoms are not limited to high-turbulence, high-nutrient conditions but rather have specific adaptations that allow them to episodically thrive in stratified conditions [Kemp & Villareal 2018].

Salinity, which may be an influential parameter that either directly or indirectly shapes the phytoplankton community structure, appeared to be an important driver of $p\text{CO}_2$ mainly in association with the intrusion of continental discharge from both the Patos Lagoon and La Plata River. Most of the

phytoplankton groups in the BRAZ province were negatively correlated with salinity; among them, the diatoms presented the highest significant correlation (see [Table S3b](#); $r = -0.81$, $p < 0.05$), probably due to the influence of freshwater and nutrient inputs in this well-mixed coastal region [e.g., [Islabão et al. 2017](#)]. Continental discharge can be an important source of silica, an essential nutrient for diatom growth, and may also favor the growth of diatoms at the coast, where high concentrations ($> 10 \mu\text{mol kg}^{-1}$) of silicate (limiting nutrients for diatoms) are found [[Piola et al. 2000](#)].

The Patos Lagoon estuarine system (centered at approximately 32°S) works as an important source of nutrients and freshwater input [[Niencheski & Windom 1994](#)] and consequently influences the distribution and concentration of Chl *a* [[Ciotti et al. 2010](#)]. In addition, the frontal zone of confluence between the Brazil and Malvinas currents, at approximately 35°S , generates eddy processes that influence the Chl *a* pattern [[Pilo et al. 2015](#), [Angel-Benavides et al. 2016](#)], contributing to CO_2 variability. Local nutrient availability in the euphotic zone is also increased by the influence of the Subtropical Shelf Front at approximately 33°S [e.g., [Muelbert et al. 2008](#), [Piola et al. 2008](#)]. This frontal zone is relatively narrow and runs in the meridional direction as an extension of the Brazil-Malvinas Confluence. This front also marks the subsurface transition between the warm and salty subtropical shelf waters with the relatively cold and fresh subantarctic shelf waters [[Piola et al. 2000](#), [Souza et al. 2018](#)].

The Brazil-Malvinas convergence zone was reported as a sink of CO_2 with an uptake rate of $-4.1 \pm 4.0 \text{ mol m}^{-2} \text{ yr}^{-1}$ in the shelf waters and $-5.4 \pm 3.6 \text{ mol m}^{-2} \text{ yr}^{-1}$ in the oceanic domain, mainly during the summer from 2000-2008 [[Padin et al. 2010](#)]. These values are close to those found in the present study at 20°S

and 30°S; however, at 35°S, we report a much higher ocean CO₂ sink rate. Despite the enhanced CO₂ uptake at 35°S, which was concomitant with the dominance of diatoms, both the $p\text{CO}_2^{\text{sw}}$ and diatom abundances were significantly negatively correlated with salinity (Fig. S1; Anexo II, pág. 199). In this region, the physico-chemical parameters showed more relevance in driving FCO₂ dynamics.

5.5.2 South Atlantic subtropical gyre system (SATL)

The SATL province is one of the least studied provinces in the global oceans. It is a major anticyclonic subtropical gyre that is persistently under the influence of trade winds but has significant changes in its mixed layer depth due to seasonal variations in the wind and surface heat flux. SATL is mainly characterized by the depletion of nutrients [Longhurst 2006]. An investigation of the proportional contributions of varying phytoplankton size fractions to biomass and primary production in the Sargasso Sea revealed a major contribution of the picophytoplankton (*Prochlorococcus*, *Synechococcus* and picoeucaryotes) [Cotti-Rausch *et al.* 2020]. However, it is important to emphasize that the phytoplankton growth rates of subtropical gyres present large variability of these groups with small changes in biomass [Marañón *et al.* 2003, Marañón *et al.* 2005].

In the open ocean, the South Atlantic is thought to act as a CO₂ source to the atmosphere north of 30°S and uptake CO₂ south of 30°S [Takahashi *et al.* 2002]. However, the FCO₂ at the sampled SATL sites indicates that these sites had a CO₂ sink behavior stronger than that in the coastal BRAZ region, which presents higher spatial-temporal variability in the sea-air CO₂ fluxes than the adjacent open ocean. The $\Delta p\text{CO}_2$ of the SATL sites was mostly affected by

temperature but was also positively correlated with salinity and negatively associated with Chl *a* (see Anexo II; [Tab. S3c](#) and [Fig. S1](#)).

The phytoplankton biomass was enhanced south of 30°, and the phytoplankton community of the SATL mostly consisted of prokaryotes, as previously reported by [Araujo *et al.* \[2017\]](#). However, we observed an increase in haptophytes (e.g., coccolithophores) at 35°S, which was to the detriment of *Synechococcus*. Although little variation for both phytoplankton groups and CO₂ uptake was found between 20°S and 30°S, the SATL was the biogeochemical province with the highest mean CO₂ uptake capacity at 35°S, which was associated with a haptophyte-dominated phytoplankton community. This approximately 3-fold enhancement of the CO₂ absorption may be a consequence of the influence of the south Atlantic Subtropical Front, which represents a transition between subtropical and subantarctic waters. These frontal features represent strong meridional gradients in temperature, salinity, and biological characteristics [[Longhurst 1998](#)]. In fact, previous studies have reported similarity with the conditions of the SATL province, which is characterized by enhanced CO₂ uptake by coccolithophore phytoplankton, such as the haptophyte *Emiliana huxleyi*, in response to elevated atmospheric CO₂ under warm, stratified, and nutrient-limited high-light conditions [[Leonardos & Geider 2005](#), [Krumhardt *et al.* 2016](#)]. In the North Atlantic, the statistical analysis indicated that increasing CO₂ and temperature have accelerated the growth of coccolithophores [[Rivero-calle *et al.* 2015](#)], showing that these calcifying organisms may adapt to a high-CO₂ world [[Lohbeck *et al.* 2012](#)]. However, in the open ocean, haptophytes may also be represented by a diversity of noncalcifying pico/nanoplanktonic eucaryotes rather than coccolithophores [[Liu *et al.* 2009](#), [Cotti-Rausch *et al.* 2016](#)].

Oligotrophic regions of the open ocean may also be influenced by the biogeochemical properties transported by eddies [e.g., [McGillicuddy et al. 2007](#); [He et al. 2016](#)]. These features increase the concentrations of growth-limiting nutrients delivered into the euphotic zone and may modify the phytoplankton community structure [e.g., [Bibby et al. 2011](#), [Carvalho et al. 2019](#)]. The study of [Carvalho et al. 2019](#) showed variability in phytoplankton communities across Agulhas eddies of different ages crossing the South Atlantic Ocean. They also highlighted the progressive transition of eddies between highly productive upwelling systems and oligotrophic open-ocean waters, reflecting phytoplankton biomass distribution and community characteristics.

5.5.3 Eastern boundary current dominated system (AFR)

AFR is the most biogeochemically complex of all the provinces because of the influence of the eastern boundary upwelling system (BENG) and of the highly dynamic environment influenced by the deep and turbulent inflow from the Agulhas Current (EAFR). This western boundary current is characterized by border eddies, meanders and filaments carrying warm and salty waters from the Indian ocean, which can powerfully influence the phytoplankton distribution and CO₂ behavior in the South Atlantic Ocean [[Carvalho et al. 2018](#); [Orselli et al. 2019](#)]. Coastal upwelling regions, such as those located along the eastern boundaries of the Atlantic Ocean basins, make major contributions to the productivity of the global ocean [[Capone & Hutchins 2013](#)].

The biological drawdown of $p\text{CO}_2^{\text{sw}}$ in this region is controlled by the upwelling activity, with values ranging from 150-250 μatm [[González-Dávila et al. 2009](#)]. A complex pattern of supersaturated areas and areas with low CO₂

concentrations has been shown to be highly associated with temperature variability and ocean circulation [Hardman-Mountford *et al.* 2003], with the highest variability associated with the most significant upwelling cells [e.g., Santana-Casiano *et al.* 2009]. According to these authors, south of 20°S, the east Atlantic Ocean acts as a net sink of CO₂, and in the South African coastal area, the constant biologically mediated CO₂ drawdown reduces the *p*CO₂ drastically and maintains the *p*CO₂ below the atmospheric *p*CO₂ all year. In the present work, the lowest seawater *p*CO₂ was associated with the highest TChl *a* concentration, suggesting that the *p*CO₂ dynamics in this province were controlled by combined physical-biological processes. Previous studies have reported large interannual variability in CO₂ fluxes as the result of changes in the upwelling intensity [Gregor & Monteiro 2013], with major CO₂ sinks in summer due to the contribution of high photosynthetic activity to the net CO₂ flux [Chen & Borges 2009, Gonzales-Dávila *et al.* 2009]; although the region acts as a continuous CO₂ sink, some studies have found CO₂ source behavior in autumn [Gregor & Monteiro 2013].

In the south Benguela subsystem, upwelling has been shown to be restricted to spring and summer and located in important upwelling cells between 30°S and 34°S [Lutjeharms & Meeuwis 1987]. In our investigation, the high CO₂ uptake rate found at 30°S in the AFR province may have been associated with upwelling events (associated with the BENG region). The spatial influence of the upwelling regime may range between 150 and 200 km in width (on average), but the mixing area due to the presence of upwelling filaments may extend up to 625 km, representing an important characteristic of the Benguela region [Van Foreest *et al.* 1984, Lutjeharms & Meeuwis 1987, Lutjeharms & Stockton 1987]. Other

studies in this region have shown high primary productivity rates but relatively low CO₂ sinking [González-Dávila *et al.* 2009; Gregor & Monteiro 2013] compared with the CO₂ sink data of our study, which may be related to the balance between the net annual carbon uptake and the nearly equally large remineralization carbon fluxes from the sediments and subthermocline waters, resulting in decreased CO₂ sink rates [Gregor & Monteiro 2013].

In the eastern portion of the South Atlantic Ocean, south of 20°S (20°S–33°S), the FCO₂ was negative, and the area was a sink for CO₂, corroborating the results of previous studies that showed that intensive upwelling areas may not always be a source of CO₂ [Chen *et al.* 2004]. In upwelling regions, Lefèvre & Taylor [2002] found a negative correlation between the fugacity of CO₂ and SST, with a decrease in the fugacity of CO₂ with increasing temperature. However, the complex behavior of wind-induced physical processes plays a role in the AFR region because upwelling, filaments, and fronts, which change in intensity according to seasonal patterns, strongly control the local hydrography and affect the biological distribution and chemical composition. Therefore, the correlations found between the physical, biological, and water chemical parameters indicate that simple fugacity of CO₂–SST or fugacity of CO₂–chlorophyll relationships cannot be applied in this region.

The AFR province in the present study showed the highest phytoplankton biomasses, with Chl *a* acting as the main driver of FCO₂. The dominant phytoplankton groups (see Fig. 23, right panel) were represented by haptophytes (e.g., coccolithophores). As latitude increased, diatoms dominated the assemblage at 35°S, probably due to the enhanced nutrient concentrations and reduced vertical mixing. These ubiquitous groups (haptophytes and diatoms)

probably experience competitive interactions in the natural environment, and the result of competition between the two algal groups can potentially influence the biogeochemical processes in the ocean [Arrigo *et al.* 1999, Cermeño *et al.* 2008]. Haptophytes and diatoms generally adopt different growth strategies, as diatoms generally have high growth rates under suitable conditions (*r*-strategists) and haptophytes are characterized by slow growth rates (*K*-strategists) [Alexander *et al.* 2015], although some species of this group, such as *Emiliania huxleyi* and *Phaeocystis antarctica*, can form blooms [Paasche 2002]. Many haptophyte species have adopted a mixotrophic lifestyle [Poulton *et al.* 2017, Godrijan *et al.* 2020], which is beneficial in oligotrophic environments, whereas specialization as autotrophs or heterotrophs is advantageous over mixotrophy in eutrophic environments [Troost *et al.* 2005, Endo *et al.* 2018]. Thus, the ecological niche of the two groups is defined by nutrient utilization strategies in conjunction with their responses to the physical environmental conditions, such as turbulence and light. High nutrient concentrations [Schiebel *et al.* 2004] and low water-column stability [Li 2002] favor diatoms, while low nutrient concentrations and high water-column stability [Cavender-Bares *et al.* 2001, Haidar & Thierstein 2001] support increased haptophyte (e.g., coccolithophores) abundances.

5.5.4 Relevant phytoplankton groups associated with CO₂ uptake in the South Atlantic Ocean

The discrimination of the total biomass (TChl *a*) in terms of different phytoplankton groups highlights the utility of phytoplankton pigment data in assessing and monitoring the key phytoplankton groups and in understanding CO₂ dynamics. Diatoms and haptophytes were most related to the regions of high

CO₂ uptake, whereas the areas dominated by the picocyanobacteria *Prochlorococcus* and *Synechococcus* were associated with smaller CO₂ uptake magnitudes. The CO₂ uptake rate increased considerably at 35°S, mostly related to the increase in diatom biomass and probably due to enhanced nutrient concentrations. The dominance of haptophytes was associated with high CO₂ uptake at 30°S in the central and eastern basin, and they were later overtaken by diatoms at 35°S (Fig. 24).

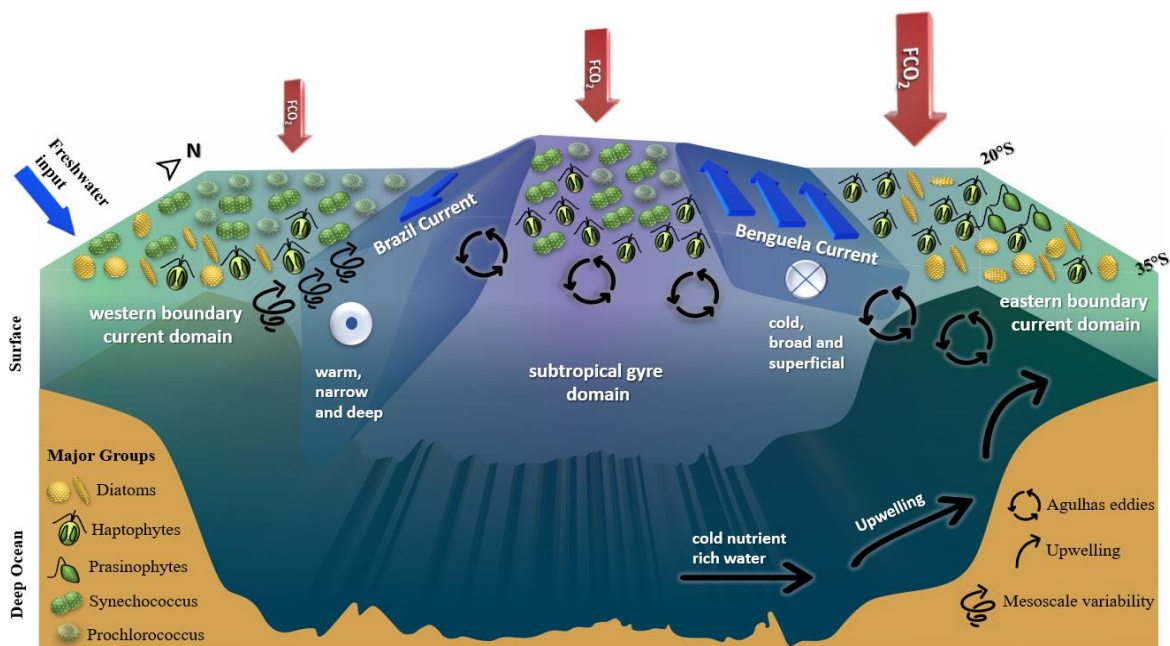


Figure 24. Schematic representation of the main biogeochemical systems of the South Atlantic basin. These are: (i) the western boundary current domain along the Brazilian margins, which is influenced by the Brazil Current; (ii) the South Atlantic subtropical gyre domain, which is influenced by mesoscales structures, such as the Agulhas eddies; and (iii) the eastern boundary current domain, which is influenced by the Benguela Current and meso- and submesoscale processes. On top, the red arrows indicate the magnitude and direction of the net sea-air carbon dioxide fluxes (FCO_2) in each province. The symbols representing the major phytoplankton groups (diatoms, haptophytes, prasinophytes, *Synechococcus* and *Prochlorococcus*) are distributed proportionally to their relevance in each domain by latitude. The main dynamic processes (presence of Agulhas eddies, upwelling and mesoscale variability) are also shown. The input of freshwater on the western side is marked.

Diatoms contribute approximately one-quarter of the global primary production. A mesocosm investigation of natural subtropical diatom assemblage's response to elevated pCO_2 showed enhanced diatom biomass in

high-nutrient conditions but with pronounced shifts in the diatom species composition, as not all diatoms benefitted equally from high CO₂ [Bach *et al.* 2019]. Haptophytes, which are a very diverse group including calcifiers (e.g., coccolithophores) and noncalcifying planktonic organisms, may be more efficient at adapting to a world ocean influenced by high-CO₂ conditions [Iglesias-Rodriguez *et al.* 2008, Lohbeck *et al.* 2012] due to their high competitive abilities under the stratified, warm, and nutrient-depleted conditions projected for future oceans. Nevertheless, with increasing atmospheric pCO₂, decreases in calcification may have a negative feedback effect on atmospheric CO₂ [Zondervan *et al.* 2001, Zhang & Cao 2016].

An investigation of the five global subtropical gyres showed that these regions are becoming more oligotrophic in response to changes in forcing factors (i.e., trends in warming and sea level height) [Signorini *et al.* 2015], which may influence the phytoplankton community, favoring the dominance of *Prochlorococcus* over haptophytes and weakening the CO₂ uptake capacity of the regions. Based on an estimate of the global ocean climatological net annual sea-air CO₂ flux, the SATL province was estimated to be a weak source of CO₂ to the atmosphere (+0.060 Pg C yr⁻¹) [Signorini & McClain 2009], although the subtropical gyres represent an overall sink for atmospheric CO₂ and show downward trends in net primary production [Signorini *et al.* 2015].

Model predictions have shown that the increase in atmospheric CO₂ (to approximately 650 ppm) may increase the global abundance of *Prochlorococcus* by more than 25% and expand their niches toward the poles as the waters increase in temperature [Flombaum *et al.* 2013]. Estimations of future global distributions of phytoplankton groups using environmental data of the RCP 8.5

IPCC scenario predict declines of 8% and 16%, respectively, for diatoms and coccolithophores [Jensen *et al.* 2017]. Despite those projections, there are still difficulties in predicting how different marine planktonic systems will respond to the future warming climate due to the problems of extrapolating potential rapid shifts at the global scale from *in situ* measurements [Alvain *et al.* 2013]. This is further complicated by the wide range of relevant processes operating at different scales and the unstable response/adaptation features involved in phytoplankton composition changes in response to climate variability.

Marine phytoplankton are fundamental components of atmospheric CO₂ uptake; hence, it is crucial to identify dominant phytoplankton groups and their associations with FCO₂. To date, few studies have proven the ability of different phytoplankton groups to take up CO₂ in the natural environment. Based on our estimates, we propose further investigations of the potential atmospheric CO₂ uptake efficiencies of both diatoms and haptophytes in the natural environment. We also encourage evaluations of the impacts of shifts in picocyanobacteria on $p\text{CO}_2^{\text{sw}}$ and, consequently, the ocean's ability to take up atmospheric CO₂.

Capítulo VI: FCO₂ e o grupo do fitoplâncton dominante em áreas costeiras do Atlântico Sul e Sudeste

O terceiro manuscrito aborda os aspectos biogeoquímicos das regiões da plataforma continental Sul e Sudeste do Brasil e da quebra da plataforma da Patagônia Argentina, fazendo um paralelo entre estes ambientes. A plataforma continental do Sul e Sudeste da América do Sul configura uma região com aspectos ecológicos e dinâmicos bastante complexos e ainda pouco compreendidos do ponto de vista integrado. Pouco se sabe acerca da variabilidade dos FCO₂ nessa região, principalmente na porção da costa do Brasil. E menos ainda é compreendido em relação à interação do fitoplâncton nos processos de captação de CO₂ atmosférico nessas regiões costeiras dos oceanos. Portanto, este trabalho tem como objetivo caracterizar o FCO₂ ao longo da plataforma continental sudoeste do Atlântico Sul, avaliando os efeitos

da temperatura e da biologia sobre a pressão parcial do CO₂ na superfície do mar. E ainda, associar esses aspectos aos grupos fitoplanctônicos dominantes, contribuindo assim para o entendimento sobre a influência da atividade biológica na absorção de CO₂ em áreas costeiras, interagindo com diferentes sistemas dinâmicos do sudoeste do Oceano Atlântico Sul. Este manuscrito, de autoria de Andréa da Consolação de Oliveira Carvalho, Carlos Rafael Borges Mendes, Rodrigo Kerr e Virginia Maria Tavano foi intitulado “***Contrasting zonal sea-air net CO₂ fluxes along southwestern Atlantic continental shelves and associated dominant phytoplankton groups***”, encontra-se em fase final de preparação e será submetido ao periódico “***Continental Shelf Research – Elsevier.***”

Abstract

Continental shelves are dynamic environments connecting the coastal and oceanic regimes, while playing an important role on carbon dioxide (CO₂) exchange between the ocean and the atmosphere. The coastal ocean is a transitional zone constantly influenced by processes from both the continent and adjacent open ocean (e.g. input of continental discharges, frontal systems, upwelling events, ocean current dynamics). Phytoplankton is a key component for understanding coastal carbon cycle, largely contributing with CO₂ uptake and carbon export via biological carbon pump. The dominant phytoplankton community in a natural environment is influenced by environmental variables linked with variations in sea–air CO₂ net fluxes (FCO₂). This study addresses the CO₂ uptake by the coastal ocean considering the dominance of different phytoplankton functional

types at the southwestern Atlantic Ocean (20°S-50°S). The study region was split into 6 latitudinal bins of 5° latitude each. A total of 219 oceanographic stations were characterized for both FCO₂ and phytoplankton pigment obtained through High Performance Liquid Chromatography technique, with further characterization of phytoplankton groups using CHEMTAX approach. Our results bring contrasting regions, marked by a transitional zone at approximately 35°S. North of 35°S, higher surface temperature and salinity combined with lower phytoplankton biomass and a cyanobacteria domain and FCO₂ source behavior. At the transitional zone (35°S- 40°S), salinity and temperature variations promoted a shift in dominant phytoplankton community structure and changed the FCO₂ behavior from CO₂ source to sink. Further south, between 40°S-50°S, lower temperature, and salinity, followed by higher phytoplankton biomass favors diatoms domain, associated with stronger CO₂ uptake rates. Understanding how the shift in phytoplankton domain affects the CO₂ uptake rates in this coastal region of the South Atlantic Ocean is essential to shed light on long-term FCO₂ modulation at the western South Atlantic margins.

6.1 Introduction

Coastal environments represent a relatively small but particularly important portion of the global ocean in terms of controls of the sea–air carbon dioxide (CO₂) fluxes (FCO₂) due to its high spatiotemporal variability of biogeochemical processes [Bauer *et al.* 2013]. However, these regions are often unattended in respect to FCO₂ data and neglected from global carbon budgets [Le Quéré *et al.* 2013, Friedlingstein *et al.* 2019]. In fact, continental shelves are

subject to many controversial discussions as they vary widely from CO₂ sink to source behaviors [e.g. [Cai et al. 2003](#), [Ito et al. 2005](#), [Cai et al. 2006](#), [Chen et al. 2009](#), [Laruelle et al. 2010](#), [Chen et al. 2013](#)]. Modulation of coastal FCO₂ is greatly influenced by human and land activities and coastal discharges [[Ito et al. 2005](#), [Jiang et al. 2008](#), [Chen & Borges 2009](#), [Bauer et al. 2013](#), [Ito et al. 2016](#)]. Zonal distribution of coastal seawater CO₂ partial pressure ($p\text{CO}_2^{\text{sw}}$) apparently does not strictly follow temperature, being strongly regulated by non-thermal factors such as net primary production and water mass mixing, both in ocean- and river-dominated margins [[Gruber et al. 2015](#), [Laruelle et al. 2017](#), [Cao et al. 2020](#)]. Many studies offer information about important coastal ecosystems individually, due to the challenging task to unravel the roles played by different mechanisms and properties in driving sea–air CO₂ exchanges in coastal waters [e.g. [Ito et al. 2016](#), [Bianchi et al. 2009](#)]. However, gathering data from different coastal regions together, and integrating their biogeochemical information, could provide a bigger picture to compose a global scenario, improving the conceptualization of the coastal carbon cycle, still a challenge and in progress to be better evaluated by the scientific community.

A recent global study provided a high-resolution monthly FCO₂ climatology that suggested a global coastal ocean carbon sink of $-0.20 \pm 0.02 \text{ Pg C year}^{-1}$ where the coastal zonal mean pattern of the FCO₂ agrees with that of the adjacent open ocean, except for the river influenced regions [[Roobaert et al. 2019](#)]. The influence of riverine nutrient inputs is a main driver for phytoplankton growth, which enhance primary productivity, lowering surface waters $p\text{CO}_2$ values. Thus, contributing to greater CO₂ uptake rates [[Eyre & Ferguson 2005](#), [Cao et al. 2011](#), [Jiang et al. 2013](#), [Saeck et al. 2013](#), [Barroso et al. 2016](#)].

The dynamics of coastal environments promotes interaction of biological and physical processes that act simultaneously favoring or even smoothing one another effects. Biological uptake and water masses mixing contribute significantly to variations of $p\text{CO}_2$ at the sea surface. Coastal phytoplankton biomass and community composition influence substantially the biological mediated CO_2 uptake [e.g. [Rixen et al. 2005](#), [Hilligsøe et al. 2011](#), [Shadwick & Thomas 2011](#), [Craig et al. 2015](#)]. However, the structure of phytoplankton communities can vary widely in function of environmental conditions [[Cullen et al. 2002](#), [Finkel et al. 2007](#), [Li et al. 2009](#)] following variations of salinity, nutrients and temperature associated with the distribution of distinct water masses [[Brandini et al. 2014](#), [Lima et al. 2019](#)]. [Gonçalves-Araujo et al. \[2012\]](#) emphasized the importance of both conservative and non-conservative properties of water masses for the structure of phytoplankton communities. Recently, [Lima et al. \[2019\]](#) demonstrated that the distribution of water masses is prone to be the main factor influencing the composition and horizontal distribution of phytoplankton groups on the outer continental shelf and slope of the subtropical Southwestern Atlantic.

At the western portion of the South Atlantic Ocean, contrasting environmental characteristics can be found at the continental margins from north to south. The Brazilian coast presents a narrow continental shelf from 20°S to 23°S at the region of Abrolhos-Campos (ACR), which is also characterized by the coastal upwelling of the cold and nutrient-rich South Atlantic Central Water (SACW) at Cabo Frio (see [Fig.25](#)). The continental shelf widens from 23°S to 28.5°S at the South Brazil Bight (SBB), and forms a typical western boundary current system with the oligotrophic Tropical Water (TW) of the Brazil Current,

which is enriched by the advection of the SACW [Castro & Miranda 1998] during intense wind stress events [Rodrigues & Lorenzetti 2001]. From 28.5°S to 35°S, the Southern Brazilian Shelf (SBS) receives strong influence of low-salinity waters from the Patos Lagoon Estuarine system (PLE) and the La Plata River (LPR) discharges [Soares & Möller Jr. 2001]. South of 35°S, the Brazil-Malvinas confluence (BMC) promotes a highly energetic region marked by a thermohaline frontal zone with the dynamic interaction of opposite flows of the Brazil Current and Malvinas Current [Pezzi *et al.* 2009, Matano *et al.* 2010]. On the other hand, the adjacent Patagonian Shelf (PS) presents a very wide portion of coastal margin, which can be subject to intense winds, strong seasonal variability and also by the advection of cold, nutrient-rich and relatively fresh waters [Bianchi *et al.* 2005, Bianchi *et al.* 2009, Piola *et al.* 2010].

As mentioned above, the Brazilian and the Argentinian margins together configure a biogeochemical zonal gradient with contrasting patterns [Acha *et al.* 2004] that may reflect in the distribution of both FCO₂ and biological activity. Depicting these different patterns is of main importance for understanding the role of the coastal ocean at the southwestern South Atlantic Ocean in the context of the global carbon cycle. In this study, we compiled a robust dataset from previous studies on both coastal areas of the Brazilian and the Argentinian margins, combining information from FCO₂ and the composition of main phytoplankton groups. Our work aims to increase the knowledge about the influence of the biological properties on the CO₂ uptake in coastal areas of different dynamic systems of the southwestern South Atlantic Ocean.

6.2 Data and Methods

6.2.1 Oceanographic Cruises

In this study, we gathered data from the south and southeast Brazilian continental shelves at approximately 20°S to 35°S during an early summer cruise occurred in 2010 [MCTII campaign; [Ito et al. 2005](#), [Ito et al. 2016](#)] and during a spring cruise in 2014 [EstARte; [Carvalho-Borges et al. 2018](#)]. For the Argentine continental shelf, we used data from approximately 35°S to 50°S sampled during two spring cruises performed in 2007 and 2008 [PATEX IV and VI, respectively; [Orselli et al. 2018a](#)] ([Fig.26](#)).

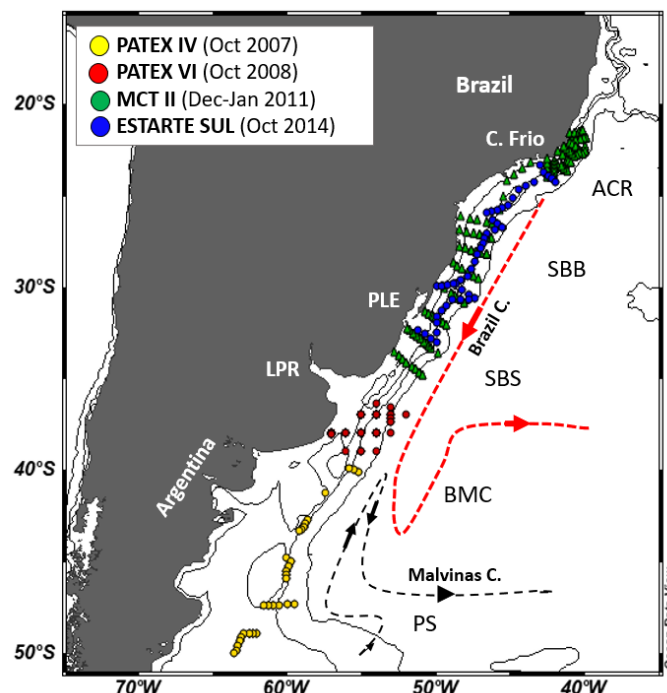


Figure 25. Map of the study area with the distribution of the hydrographic stations of the four cruises (yellow- PATEX IV, red- PATEX VI, green- MCTII and blue-EstARte Sul) analyzed here. The main surface circulation is also represented highlighting the Brazil Current (red dashed line) and the Malvinas Current (Black dashed line) which confluence region occurs between 35°S and 45°S at the Brazil Malvinas Confluence region (BMC). From 20°S to 50°S we have important features marked in the map as the Cabo Frio upwelling at the Abrolhos Campos region (ACR), the South Brazil Bight (SBB) between 23°S and 28.5°S and the Southern Brazilian Shelf (SBS) between 28.5°S and 35°S where we have the the Patos Lagoon estuarine system (PLE) at approximately 32°S and the La Plata River (LPR) discharge at approximately 35°S and south of 35°S we have the Patagonian shelf (PS) region.

A total of 219 oceanographic stations with physical, chemical, and biological parameters were analyzed (Tab. 5). The study area was divided in six latitudinal bins of 5° latitude, and data from each parameter measured was averaged for each latitudinal bin for better visualization, and comparison, of the FCO₂ patterns and the phytoplankton groups distribution.

Table 5. General information about the cruises used in this study, including the name of the cruise, the coverage area, the sampling period (season), the data used (phytoplankton pigments, sea surface temperature – SST; sea surface salinity – SSS; Total Alkalinity – A_T; Dissolved inorganic carbon – C_T; CO₂ partial pressure in the seawater – pCO₂^{sw} and in the atmosphere pCO₂^{air} and wind speed at 10m – U₁₀) and references from previous work on these cruises.

Cruise	Sampling region	Sampling period	Data	n	References
PATEX IV 2007	Argentinian shelf break between 35°S and 50°S	16 Oct – 22 Oct (2007) Spring	Phytoplankton pigments, SST, SSS, A _T , C _T , U ₁₀	29	Orselli <i>et al.</i> [2017]
PATEX VI 2008	Argentinian shelf break between 35°S and 50°S	13 Oct – 18 Oct (2008) Spring	Phytoplankton pigments, SST, SSS, A _T , C _T , U ₁₀	37	Orselli <i>et al.</i> [2017]
MCTII 2010/2011	Brazilian continental shelf S-SE between 20°S and 30°S	6 Dec (2010) – 11Jan (2011) Summer	Phytoplankton pigments, SST, SSS, pCO ₂ ^{sw} , pCO ₂ ^{air} , U ₁₀	109	Ito <i>et al.</i> [2016]
EstARte Sul 2014	Brazilian continental shelf S-SE between 20°S and 30°S	22 Oct – 30 Oct (2014) Spring	Phytoplankton pigments, SST, SSS, pCO ₂ ^{sw} , pCO ₂ ^{air} , U ₁₀	45	Carvalho- Borges <i>et al.</i> [2018] Kerr <i>et al.</i> In prep.

6.2.2 Calculations of pCO₂ and FCO₂

During both Brazilian coastal cruises, the seawater and atmospheric pCO₂ (pCO₂^{sw} and pCO₂^{air}, respectively) were measured continuously using a semi-autonomous system as described by Pierrot *et al.* [2009]. On the other hand, during both Patagonian shelf cruises, pCO₂ was calculated indirectly using the carbonate parameters measured by potentiometric titrations in a closed cell. Total alkalinity and total dissolved inorganic carbon were estimated following the methods developed by Dickson *et al.* [2007]. These were used as input parameters together with seawater surface temperature and salinity at the

CO₂Sys v.2.1 software developed by Lewis & Wallace [1998] and modified by Pierrot *et al.* [2006]. The atmospheric value for $p\text{CO}_2$ in this case was attributed from the regional literature [Bianchi *et al.* 2009].

The difference between seawater and atmospheric $p\text{CO}_2$ ($\Delta p\text{CO}_2 = p\text{CO}_2^{\text{sw}} - p\text{CO}_2^{\text{air}}$) was then calculated and used to obtain the FCO_2 values following the formula (Eq.21):

$$\text{FCO}_2 = k K_0 (\Delta p\text{CO}_2) \quad (21)$$

where k is the gas transfer velocity parametrization of Wanninkhof *et al.* [2014] and K_0 is the CO₂ solubility coefficient [Weiss *et al.* 1974]. The wind speed data (U_{10}) was obtained through the European Center for Medium-Range Weather Forecasts portal (ECMWF; <http://data-portal.ecmwf.int/>) and had a spatial resolution of 1.5° latitude by 1.5° longitude.

6.2.3 Controls on $p\text{CO}_2^{\text{sw}}$: temperature vs. biological effects

We used the method adapted from Takahashi *et al.* [2002] [e.g. Ito *et al.* 2005, Thomas *et al.* 2005] to evaluate the thermal and the biological effects on the $p\text{CO}_2^{\text{sw}}$. Although this approach is mainly used for comparing the seasonal effects of both temperature and biology on a particular environment, we found appropriate to use it here, though considering that we are not evaluating the seasonal effect but these effects for the correspondent sampling period (spring and early summer) at the study region. We calculated the temperature-normalized $p\text{CO}_2^{\text{sw}}$ ($\text{N}p\text{CO}_2^{\text{sw}}$) for a spatial averaged temperature (\overline{SST})

according to the equation (Eq.22).

$$p\text{CO}_2^{\text{sw}}(\text{at } \overline{SST}) = (p\text{CO}_2^{\text{sw}}) \exp [0.0433(\overline{SST} - \text{SST})] \quad (22)$$

\overline{SST} is the mean temperature for the period evaluated, and SST is the temperature observed during sampling. Then, we calculated the $p\text{CO}_2^{\text{sw}}$ value at a given in situ temperature (SST) using the equation (Eq. 23):

$$p\text{CO}_2^{\text{sw}}(\text{at SST}) = (\overline{p\text{CO}_2^{\text{sw}}}) * \exp [0.0433(\text{SST} - \overline{SST})] \quad (23)$$

and for each 5° latitudinal bin we calculated both the effect of temperature ($\Delta p\text{CO}_2^{\text{temp}}$) and biological ($\Delta p\text{CO}_2^{\text{bio}}$) changes using the difference between maximum and minimum values for $p\text{CO}_2$ calculated using SST for thermal effect and using \overline{SST} for biological effect (Eq.24-25):

$$\Delta p\text{CO}_2^{\text{temp}} = (p\text{CO}_2^{\text{sw}} \text{ at SST})_{\text{max}} - (p\text{CO}_2^{\text{sw}} \text{ at SST})_{\text{min}} \quad (24)$$

$$\Delta p\text{CO}_2^{\text{bio}} = (p\text{CO}_2^{\text{sw}} \text{ at } \overline{SST})_{\text{max}} - (p\text{CO}_2^{\text{sw}} \text{ at } \overline{SST})_{\text{min}} \quad (25)$$

To compare the relative effect of both T and B, the ratio (T:B) and the difference (T – B) between them was applied (Eq.26-27). Thus, meaning that when $T - B < 0$ or $T:B < 1$ the biological effect has greater magnitude and variability. Contrary, where biological effects are weaker or rather constant $T - B > 0$ or $T:B > 1$.

$$T - B = \Delta p\text{CO}_2^{\text{temp}} - \Delta p\text{CO}_2^{\text{bio}} \quad (26)$$

$$T/B = \Delta p\text{CO}_2^{\text{temp}}/\Delta p\text{CO}_2^{\text{bio}} \quad (27)$$

6.2.4 Determination of main phytoplankton groups

Phytoplankton pigments concentrations were measured using the High-Performance Liquid Chromatography (HPLC) system (Shimadzu Prominence LC-20A Modular HPLC System). Surface seawater samples for each cruise were filtered (Whatman GF/F filters; (nominal pore size of 0.7 μm ; 25 mm in diameter) and stored in liquid nitrogen previous from the analysis. At the laboratory, the filters were centrifuged with 3 mL of 95% cold-buffered methanol (2% ammonium acetate) containing 0.05 mg L⁻¹ trans- β -apo-8'-carotenal (Fluka) as an internal standard and then sonicated for 5 min in an ice-water bath, kept at -20 °C for 1 h, and centrifuged at 1100 rpm for 5 min at 3 °C in a model 280-R refrigerated centrifuge (Excelsa 4). The supernatants were filtered through Fluoropore PTFE membrane filters (0.2 μm pore size) to rid the extract from the remains of filter and cell debris. Immediately prior to injection, 1000 μL of sample was mixed with 400 μL of Milli-Q water in 2.0 mL glass sample vials, and these were placed in the HPLC cooling rack (4 °C) of the Shimadzu HPLC system. HPLC analysis was performed using a monomeric C8 column with a pyridine-containing mobile phase are fully described in [Zapata *et al.* \[2000\]](#). The detection limit and quantification procedure of this method were conducted according to [Mendes *et al.* \[2007\]](#). Pigments were identified from both absorbance spectra and retention times from the signals in the photodiode array detector (Shimadzu, SPD-M20A;

190–800 nm; 1 nm wavelength accuracy) or fluorescence detector (Shimadzu, RF-10AXL; Ex. 430 nm/Em. 670 nm). Calibrations, and subsequent quantification of the pigments, were done at or close to the wavelength of maximum absorption (e.g., chlorophyll *a* at 430 nm, fucoxanthin at 448 nm, zeaxanthin at 454 nm, and chlorophyll *b* at 470 nm). Pigments were quantified from peak integration using LC-Solution software (Shimadzu), but all peak integrations were manually checked and corrected where necessary. The HPLC system was previously calibrated with pigment standards from DHI (Institute for Water and Environment, Denmark). The relative contribution of microalgal groups to the overall biomass was calculated using CHEMTAX v1.95 chemical taxonomy software from the class-specific accessory pigments and total chlorophyll *a* [Mackey *et al.* 1996]. Procedures and calculations are fully described in Mackey *et al.* [1996]. The initial pigment ratios of major algal classes used here were derived from Higgins *et al.* [2011], with chemotaxonomic groups being identified according to Jeffrey *et al.* [2011].

Data from each cruise were run separately to minimize potential variations in the CHEMTAX optimization procedures. Chlorophyll *a* (Chl *a*) was used for estimating the biomass of all groups, except *Prochlorococcus*, for which Divinyl Chlorophyll *a* (DV Chl *a*) was used. Therefore, in this work, the sum Chl *a* + Dv Chl *a*, named Total of chlorophyll (TChl *a*), was used as phytoplankton biomass index. For optimization of input matrices, a series of 60 pigment ratio matrices was generated by multiplying each ratio of the initial matrix by a random function. Ten percent ($n = 6$) of the generated ratios with lowest root-mean-square residual were averaged resulting the output matrixes for each cruise evaluated) [Wright *et al.* 2009].

After evaluating each cruise separately, the chemotaxonomic groups were rearranged to promote an effective comparativeness among the different cruises. Seven phytoplankton functional groups were evaluated from 20°S to 50°S: diatoms (sum of diatoms A and B), dinoflagellates, haptophytes (including coccolithophores and *Phaeocystis*), cyanobacteria (including *Synechococcus* and *Trichodesmium*), *Prochlorococcus*, green flagellates (including prasinophytes) and cryptophytes. Thus, we could unify the different groups found for each cruise and better compare the four cruises together.

6.2.5 Statistical analysis

Correlation analysis and canonical correspondence analysis (CCA) were used to associate the biotic (phytoplankton groups) and environmental variables (SST, SSS, TChl *a*, $p\text{CO}_2^{\text{sw}}$ and FCO_2). The abiotic variables were normalized for the CCA and both analyses were performed using the software PAST 4.02 [Hammer *et al.* 2001].

6.3 Results

6.3.1 SST, SSS, phytoplankton biomass and FCO_2 spatial variability

The spatial distribution of SST, SSS, phytoplankton biomass (referred here as TChl *a*) and FCO_2 pointed out the biogeochemical contrasting zonal patterns along the southwestern South Atlantic Ocean (Fig. 26; Tab. 6). SST is at least 10°C higher between 20°S and 35°S when compared to the southern region

between 35°S and 50°S (Tab. 6).

While from 20°S to 35°S mean SST was 23.2 ± 1.7 °C, south of 35°S mean temperature values were down to 10.2 ± 3.4 °C. Salinity presented a smaller but yet significant variability range (Fig. 26b). The higher variability in SSS values occurred between 30°S and 35°S (34.0 ± 2.3). The SSS presented lower averages but less variable values south of 35°S. The concentration of TChl a was low in the northern part of the study area 20°S - 35°S (0.2 ± 0.4 mg m⁻³) and increased sharply south of 35°S (Fig. 26c).

Table 6. Mean values and standard deviation of sea surface temperature - SST (°C), Sea surface salinity - SSS, Total of Chlorophyll a - TChl a and CO₂ fluxes FCO₂. for each 5° latitudinal bin.

Latitudinal bin	Mean SST (°C)	Mean SSS	Mean TChl a (mg m ⁻³)	FCO ₂ (mmol m ⁻² d ⁻¹)
20°S-25°S	24.6 ± 1.4	36.0 ± 0.7	0.3 ± 0.6	5.4 ± 5.5
26°S-30°S	23.1 ± 1.0	35.7 ± 1.0	0.2 ± 0.1	8.1 ± 15.2
31°S-35°S	21.6 ± 1.0	34.0 ± 2.3	0.2 ± 0.2	3.2 ± 10.0
36°S-40°S	12.3 ± 3.2	33.9 ± 0.6	0.8 ± 0.6	-4.3 ± 11.6
41°S-45°S	7.5 ± 0.4	33.9 ± 0.1	1.6 ± 1.5	-20.7 ± 2.3
46°S-50°S	7.3 ± 0.5	33.7 ± 0.2	5.7 ± 5.0	-20.8 ± 6.8

A contrasting pattern was found for the FCO₂ behavior on the study region, shifting from mainly CO₂ source to sink at latitudes higher than 35°S (Fig. 26d). Between 20°S and 35°S, the FCO₂ is highly variable, although indicating an averaged behavior from a weak to moderated source of CO₂ to the atmosphere (Tab. 6). The FCO₂ distribution indicate that the shelf domain south of 35°S behaved as a CO₂ ingassing zone, changing from a moderate to stronger sink towards south.

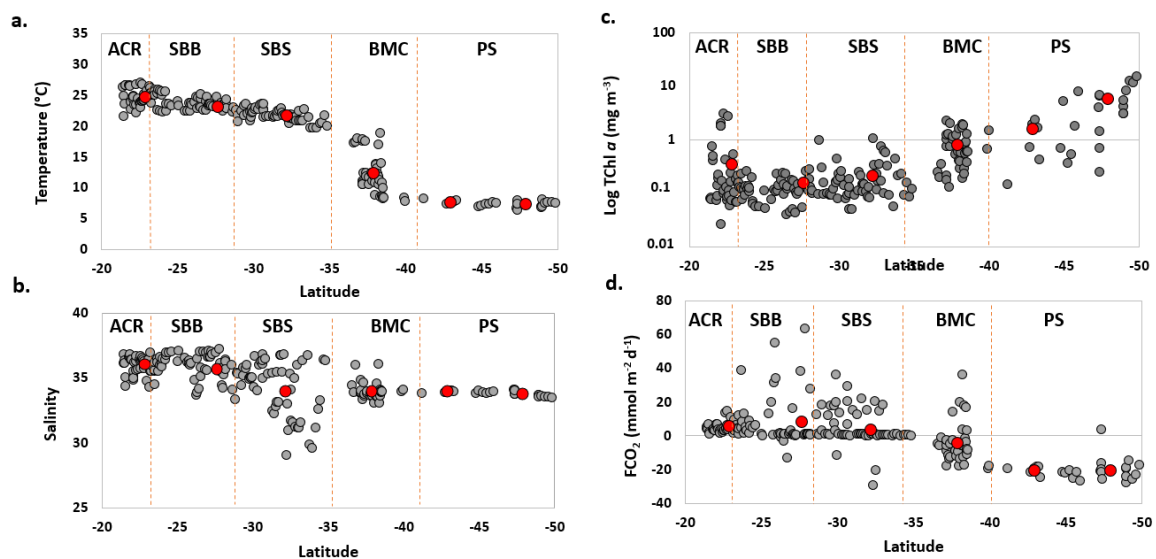


Figure 26. Distribution of **a.** sea surface temperature (SST); **b.** sea surface salinity (SSS); **c.** Log of Total of chlorophyll a (Log TChl a) and **d.** CO₂ net fluxes (FCO₂) from 20°S to 50°S. The gray dots represent the data measured in each cruise, and the red dots are the mean values from each 5° latitude bin. The boundaries of the main areas highlighted in the study region are marked by orange dotted lines: ACR- Abrolhos Campos Region (20°S-23°S); SBB- South Brazilian Bight (23°S-28°S); SBS – Southern Brazilian Shelf (28.5°S-35°S); BMC – Brazil-Malvinas Confluence region (~38°S) and PS – Patagonian shelf (40°S- 50°S).

6.3.2 Dominant phytoplankton groups

A noticeable separation of the phytoplankton distribution pattern was evident around 35°S (Fig. 27). The shelves north of 35°S, comprising the SBB and SBS biogeochemical provinces showed a variable phytoplankton composition and were dominated by cyanobacteria. In contrast, a predominance of diatoms was seen south of 35°S, which became the massively dominant group at higher latitudes.

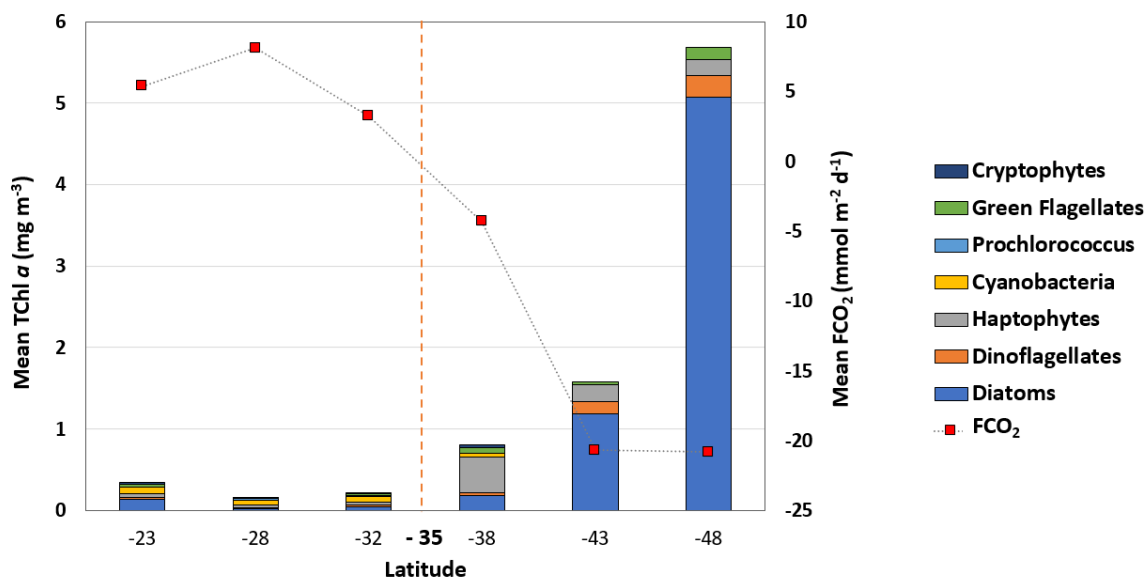


Figure 27. Bar charts with the mean concentration of total chlorophyll *a* (TChl *a*) with different colors (legend on the right) for the relative contribution of main phytoplankton groups for each 5° latitudinal bin between 20°-50°S. The dashed line, with red squares, represent the averaged value for sea–air CO₂ net fluxes (FCO₂) for each 5° latitudinal bin.

The drop in FCO₂ mean values south of 35°S occurs concomitantly with an increase in phytoplankton biomass (TChl *a*) (Fig. 27). The relative contribution (%) of each phytoplankton group's for TChl *a* is presented in table 7. Cyanobacteria contributed with approximately 40% to TChl *a* from 20°S to 35°S. Between 35° and 40°S, haptophytes were the main group contributing with approximately 42% of total biomass, followed by diatoms, which contributed with approximately 18% for TChl *a*. South of 40°S, diatoms become to represent more than 60% of total biomass (Tab. 7).

Table 7. Contribution of phytoplankton groups to total chlorophyll *a* (TChl *a*; %) for each 5° latitudinal bin. The bold values represent the dominant group for each bin and absent groups where marked with (–).

Latitudinal bin	Diatoms	Dinoflagellates	Haptophytes	Cyanobacteria	Prochlorococcus.	Green Flagellates	Cryptophytes
20°S-25°S	15.1 ± 16.8	5.5 ± 3.8	19.3 ± 9.9	39.4 ± 16.4	12.4 ± 13.3	6.3 ± 6.0	2.1 ± 3.1
25°S-30°S	9.0 ± 11.6	3.6 ± 1.9	22.9 ± 9.3	40.6 ± 12.1	20.2 ± 14.0	3.4 ± 4.6	0.2 ± 0.6
30°S-35°S	17.8 ± 11.2	6.9 ± 6.5	22.1 ± 7.9	37.1 ± 13.6	10.8 ± 10.7	4.4 ± 5.0	0.8 ± 1.4
35°S-40°S	26.2 ± 19.5	7.8 ± 11.9	42.7 ± 28.0	9.1 ± 11.3	–	10.0 ± 7.5	4.2 ± 3.7
40°S-45°S	59.9 ± 22.4	16.4 ± 12.5	18.9 ± 14.9	–	–	4.8 ± 5.0	–
45°S-50°S	77.0 ± 26.0	12.5 ± 15.4	6.6 ± 8.3	–	–	3.9 ± 3.7	–

6.4 Temperature and biological controls on $p\text{CO}_2^{\text{sw}}$

The effects of temperature and biology on $p\text{CO}_2^{\text{sw}}$ for each latitudinal bin are shown in [table 8](#). For the entire study region, the biological control on $p\text{CO}_2$ ($\Delta p\text{CO}_2^{\text{bio}}$) prevailed over the temperature effect ($\Delta p\text{CO}_2^{\text{temp}}$). The values for T – B were all negative and the values for T: B were all < 1. However, between 20°S and 35°S, despite the stronger biological effect, the temperature effect is also relatively high. Between 35°S and 40°S, there is a marked transitional region with the highest values for both $\Delta p\text{CO}_2^{\text{bio}}$ and $\Delta p\text{CO}_2^{\text{temp}}$, highlighting the strong influence of biology and temperature changes on $p\text{CO}_2$ across the highly dynamic Brazil-Malvinas confluence region. The relative importance of temperature over biology, calculated using the ratio T/B, shows a decrease in temperature effect over $p\text{CO}_2^{\text{sw}}$ southwards, however the difference T – B reveals the $p\text{CO}_2^{\text{sw}}$ variations modulated by biology even when temperature effect also displays a high control over $p\text{CO}_2^{\text{sw}}$.

Table 8. Calculated effects of biology ($\Delta p\text{CO}_2^{\text{bio}}$) and temperature ($\Delta p\text{CO}_2^{\text{temp}}$) on seawater CO_2 partial pressure ($p\text{CO}_2^{\text{sw}}$) values for each latitudinal bin and the relative importance of the effects presented calculated by the difference (T-B) and by the ratio T/B.

Latitudinal bin	$\Delta p\text{CO}_2^{\text{bio}}$	$\Delta p\text{CO}_2^{\text{temp}}$	T–B	T/B
20°S-25°S	147.89	93.33	–54.56	0.63
26°S-30°S	143.68	73.93	–69.75	0.51
31°S-35°S	131.52	64.40	–67.13	0.49
36°S-40°S	393.38	161.15	–232.23	0.41
41°S-45°S	51.60	11.20	–40.40	0.22
46°S-50°S	223.92	14.70	–209.22	0.07

6.5 Relationship between phytoplankton distribution and FCO_2

The relationship between the main phytoplankton groups (cryptophytes,

green flagellates, haptophytes, cyanobacteria, dinoflagellates, diatoms, and *Prochlorococcus*) and the environmental variables (SST, SSS, $p\text{CO}_2^{\text{sw}}$, FCO_2 , and TChl *a*) was investigated through the CCA analysis. The result of the CCA shows a clear separation between the lower and higher latitudes along the first axis (Fig.28).

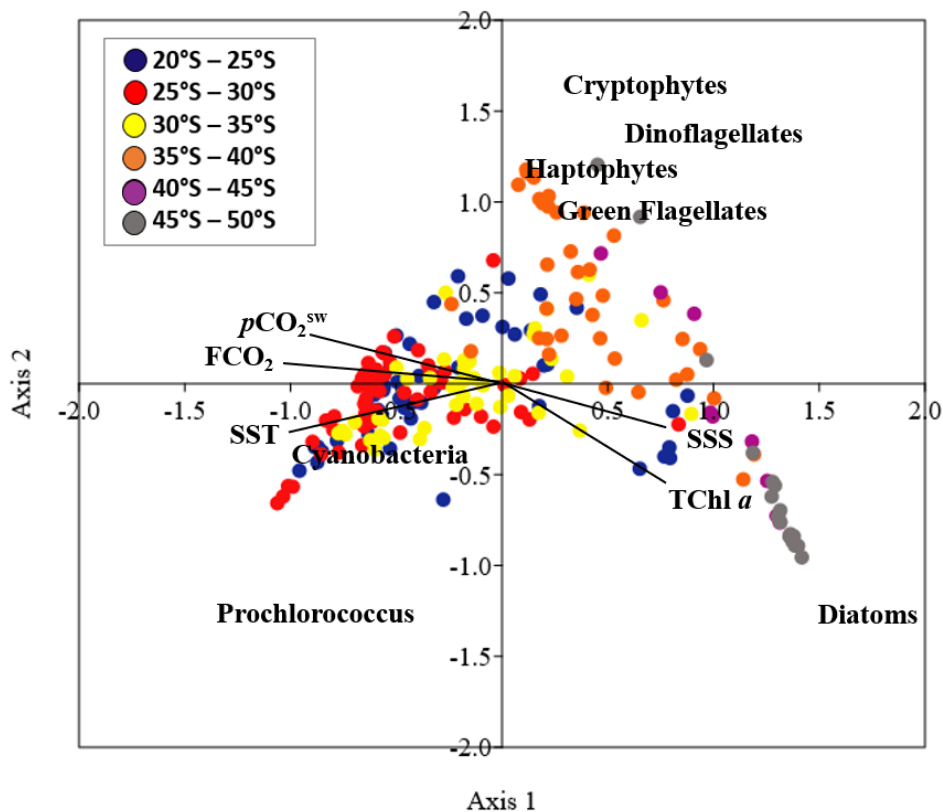


Figure 28. CCA ordination diagram of the absolute contributions of different phytoplankton groups at the sea surface. The black arrows indicate environmental variables (pointing in the direction in which the value of environmental variable increases; the angle indicates the correlation between variables) and point: sea surface temperature (SST; °C), sea surface salinity (SSS), CO_2 partial pressure at the seawater ($p\text{CO}_2^{\text{sw}}$), sea–air CO_2 fluxes (FCO_2) and phytoplankton biomass (TChl *a*). The absolute contributions of phytoplankton groups are indicated by their names: Diatoms; Dinoflagellates; Cryptophytes; Haptophytes; Green flagellates; Cyanobacteria and *Prochlorococcus*. Stations are separated by color according to distinct 5° latitudinal bin (see legend on top left for different latitudinal colors).

The first two ordination axes from the CCA explained 93% of the variance associated with the phytoplankton–environment relationship. Lower latitudes were associated with temperature and cyanobacteria and *Prochlorococcus*

whereas higher latitudes were positively associated with TChl *a*, salinity, and the presence of diatoms (specially between 45°S–50°S; grey dots at Fig. 29).

The correlation analysis revealed strong positive correlation between the FCO₂ and temperature ($r = 0.62$, $p < 0.001$), but also a significant negative correlation between FCO₂ and TChl *a* ($r = -0.43$, $p < 0.001$) (Fig. 30). An evident contrasting behavior is observed between two main phytoplankton groups of diatoms and cyanobacteria. While cyanobacteria dominates at lower latitudes with positive correlations with temperature, negative correlation with TChl *a* (lower phytoplankton biomass) and positive relation with FCO₂ (indicating CO₂ outgassing), diatoms showed the opposite behavior with negative correlation with temperature and FCO₂ (CO₂ uptake), and positive correlation with TChl *a* (higher biomass), establishing the niche preferences of those different phytoplankton groups.

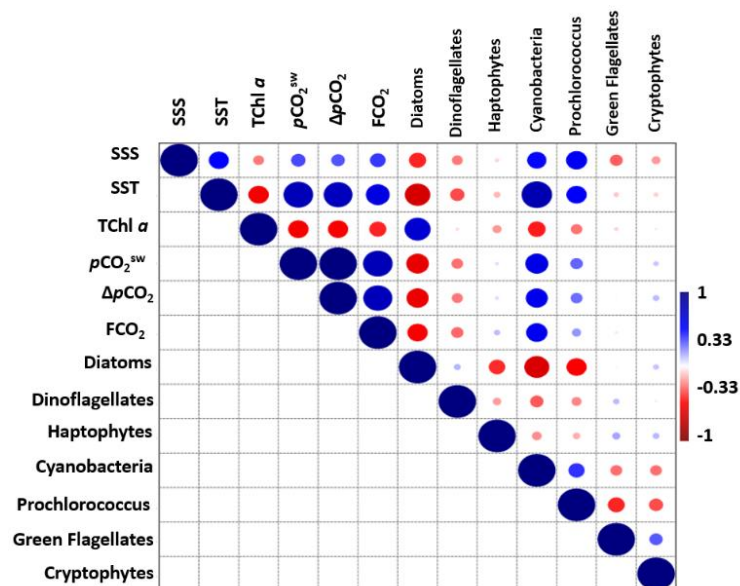


Figure 29. Correlation matrix diagram. The abiotic parameters used in this correlation were: sea surface temperature - SST, sea surface salinity - SSS, Total of Chlorophyll *a* - TChl *a*, CO₂ partial pressure at the seawater - $p\text{CO}_2^{\text{sw}}$, difference between seawater and atmospheric CO₂ partial pressure - $\Delta p\text{CO}_2$ and CO₂ net fluxes - FCO_2 and the phytoplankton groups: Diatoms, Dinoflagellates, Haptophytes, Cyanobacteria, *Prochlorococcus*, Green Flagellates and Cryptophytes). The colorbar indicates blue as positive correlations and red as negative correlations. The size of the dot in the diagram indicates the strength of the correlation.

6.6 Discussion

Marine coastal environments tend to exhibit greater variations of seawater properties on smaller time and space scales [e.g. [Terlouw et al. 2019](#), [Enochs et al. 2019](#), [Doney et al. 2020](#)] and thereby undergo more abrupt changes than the ocean [[Carstensen et al. 2018](#)]. Spatial distribution of biogeochemical parameters at the southwestern South Atlantic Ocean margins suggests a clear division of the studied area in two main biogeochemical domains, with opposite behaviors in relation to both the magnitude and direction of the FCO_2 . The northernmost domain (latitudes $< 35^\circ S$) acting as a CO_2 source to the atmosphere, while the domain south of $35^\circ S$ is marked as an ocean CO_2 sink. In addition, source regions were mostly dominated by cyanobacteria and sink regions were associated with the dominance of diatoms. Although acting differently in relation to the FCO_2 , the effect of biology on pCO_2^{sw} prevailed at the entire study area for the investigated periods (mainly spring). This observation prompts two questions for this discussion: what is the role of biology on FCO_2 modulation at both biogeochemical domains? And second, how changes in the dominant phytoplankton group can influence the FCO_2 magnitudes at these environments?

6.6.1 Physical and ecological processes along the southwestern South Atlantic shelves triggers contrasting biogeochemical behaviors

We showed that variations in dominant phytoplankton groups, affecting the FCO_2 magnitudes are occurring against a background of both natural and anthropogenically altered gradients over the southwestern South Atlantic

shelves. In addition, other potential environmental drivers interacting with phytoplankton and linked to the atmospheric CO₂ uptake by the ocean must be considered. So, before trying to answer the posed questions, we must understand what physical and ecological processes are driving the variability over the phytoplankton distributions and thus affecting the FCO₂ at each of the two main biogeochemical domains.

Overall, the northern domain (20°S – 35°S) is characterized by higher temperatures, broad salinity range and low TChl *a*, reflecting the dominance of oligotrophic Brazil Current waters. However, between 20°S and 25°S, the coastal intrusion of SACW brings nutrient supply from deep waters and overcome oligotrophic surface waters, promoting phytoplankton succession/growth [Margalef 1978]. Despite the usual high primary production, coastal upwelling regions are generally found as CO₂ sources [Borges *et al.* 2005] due to the high concentration of CO₂ brought up to surface from ocean's interior. The first response to upwelling is a CO₂ sink behavior due to nutrients supply at the euphotic zone, enhancing primary production followed by respiration, nutrient depletion, and CO₂ release at surface [Lefevre *et al.* 2002, Capone & Hutching 2013]. The fate that the SACW that upwells in this area is relatively young (compared to central waters in the center of the South Atlantic Gyre) and originated in the Brazil-Malvinas Confluence zone [Souza *et al.* 2018] brings additional challenges to better understanding the coupling of biological and chemical processes on changing the surface CO₂, which needs further investigation.

Further south (25°S – 30°S), the Brazilian coastline orientation forms an embayment and the offshore circulation is dominated by the Brazil current, a

southward flow shallow current carrying warm and salty tropical waters at surface [Silveira *et al.* 2000]. At this region, phytoplankton biomass is reduced due to oligotrophic environmental conditions [Longhrust 2006]. Between 30°S and 35°S, the freshwater discharge from the Patos Lagoon Estuary appears as an important feature for the region, occurring approximately at 32°S. This high CO₂ estuarine region [Coelho *et al.* submitted], as found in many coastal and estuarine systems associated with excess nutrient and organic carbon inputs from land sources [Feely *et al.* 2010, Cai *et al.* 2011], influence the phytoplankton distribution and FCO₂ along the adjacent continental shelf.

At the southern domain (35°S – 40°S), the La Plata River discharge (~36°S) represent a massive input of relatively cold and fresh waters, which enhances biological activity [Moore & Abbott 2000, Feely 2001]. Mixture of water masses promotes mixing of community composition [Demir-Hilton *et al.* 2011, Clay *et al.* 2016] as the environmental conditions start to change, transitioning to less warm and saline waters. The mixing with sub-Antarctic waters from the Malvinas Current at the Brazil-Malvinas confluence region (south of 38°S) can be evidenced by a high chlorophyll signal [Garcia *et al.* 2004]. This highly dynamical region is of great importance for the enhancement of phytoplankton biomass and variability in distribution of phytoplankton groups and, consequently, for the behavior change in CO₂ flux dynamics [Brandini *et al.* 2000, Painter *et al.* 2010, Gonçalves-Araujo *et al.* 2012, Arruda *et al.* 2015]. From 40°S to 50°S, adjacent to the Patagonian shelf, the lower seawater temperature and salinity, together with higher biomasses and biological activity, favor a stronger ocean CO₂ uptake. Recent study on the Patagonian open shelf reported this region as a CO₂ sink with dominance of the biological effect on $p\text{CO}_2^{\text{sw}}$, i.e., with the biological pump

acting as the main process controlling the CO₂ fluxes [Kahl *et al.* 2017]. According to Orselli *et al.* [2018a], the SACW is acidifying faster in the Patagonian shelf-break than in the South Atlantic Gyre domain. Although studies are still not very conclusive, and present certain degree of uncertainties, acidity conditions may potentially affect the phytoplankton dynamics at the region and consequently interfere in the FCO₂ behavior [Dutkiewicz *et al.* 2015, Mackey *et al.* 2015, Sommer *et al.* 2015] once this region presents a main control from biology on pCO₂^{sw}. Thus, comprehending the dynamical and ecological mechanisms driving FCO₂ is pivotal for the carbon biogeochemical of the southwestern South Atlantic Ocean.

6.6.2 What is the role of biology on FCO₂ dynamics in SAO western coast?

Our results showed that biology had a pivotal role on pCO₂^{sw} control at the entire study area. However, the FCO₂ behavior along the zonal gradient on the study region is in agreement with previous studies, with the lower latitude regions of the southwestern South Atlantic continental shelf acting as a moderate CO₂ source to the atmosphere [Ito *et al.* 2005, Padin *et al.* 2010, Arruda *et al.* 2015, Ito *et al.* 2016]. At some sites, CO₂ flux balances with high temperatures (which favors CO₂ emissions), specially at lowest latitudes, modulating FCO₂ the behavior as a source region. Contrarily, further south, the Patagonian mid/outer shelves have been acting as a strong CO₂ sink [Bianchi *et al.* 2009, Kahl *et al.* 2017].

The influence of biology ($\Delta p\text{CO}_2^{\text{bio}}$) showed a clear increase from north to south (see Fig. 27). Overall, at lower latitudes, phytoplankton biomasses were

lower, due to higher temperatures and oligotrophic conditions of the water masses, favoring the developments of small size phytoplankton assemblages, such as picoplanktonic cyanobacteria and haptophytes (see Fig. 27) [Marañón *et al.* 2015, 2018]. However, some peculiarities occur in the study region, such as an increase of the nutrient availability during spring between 20°S and 25°S, when the occurrence of upwelling at Cabo Frio (23°S; 42°W) is favored due to more intense occurrence of northeasterly winds [Castelão & Barth 2006]. At this region, we found a CO₂ source behavior with magnitudes in agreement with other previous measurements reported at the region [Ito *et al.* 2005]. FCO₂ measurements using eddy covariance methodology at the Cabo Frio upwelling region during austral winter in 2015, found contrasting magnitudes, the open ocean acting as CO₂ source and coastal region as CO₂ sink [Oliveira *et al.* 2019]. $\Delta p\text{CO}_2^{\text{bio}}$ was greater than $\Delta p\text{CO}_2^{\text{temp}}$ but, apparently, not strong enough to make the region act as a CO₂ sink. Indeed, at the Cabo Frio region, during downwelling periods, higher temperatures favors the dominance by smaller phytoplankton (pico and nanoplankton), while during SACW upwelling events, lower temperature, and higher nitrate contents, brings up the autotrophic microplankton and decreases autotrophic picoplankton and bacterioplankton abundances [Guenther *et al.* 2008]. This succession of phytoplankton communities must be enhancing the $\Delta p\text{CO}_2^{\text{bio}}$ on $p\text{CO}_2^{\text{sw}}$ observed here.

Between 25°S and 35°S, both $\Delta p\text{CO}_2^{\text{bio}}$ and $\Delta p\text{CO}_2^{\text{temp}}$ were smaller than the previous region. Although the $\Delta p\text{CO}_2^{\text{bio}}$ was always higher than $\Delta p\text{CO}_2^{\text{temp}}$, this area showed high temperature and low phytoplankton biomass and behaved as a CO₂ source to the atmosphere. This oligotrophic coastal zone is dominated by nutrient-poor waters [Brandini 1990, Castro *et al.* 2006], especially with low

nitrate concentrations, which limit the primary production in the region. Between 35°S and 40°S, both $\Delta p\text{CO}_2^{\text{bio}}$ and $\Delta p\text{CO}_2^{\text{temp}}$ are enhanced (see [Tab. 8](#)). However, the biology effect increases much more than the temperature effect, maintaining the $\Delta p\text{CO}_2^{\text{bio}}$ predominant for the $p\text{CO}_2^{\text{sw}}$ but still not enough to promote a CO_2 sinking condition. This increase in magnitudes of both effects at this region reflects the higher dynamic conditions generated by the mixing at the confluence region. In fact, measurements of FCO_2 along 35°S found that physical variables (salinity and temperature) were the main drivers of $p\text{CO}_2^{\text{sw}}$ variability in South America continental shelf [[Lencina-Ávila et al. 2016](#)]. They also demonstrate that surface waters originated from La Plata river plume (~36°S) influence the $p\text{CO}_2^{\text{sw}}$ distribution in the South American continental shelf.

At higher latitudes (40°S- 50°S), temperature showed a much smaller effect over biology on $p\text{CO}_2^{\text{sw}}$. [Kahl et al. \[2017\]](#) investigated the seasonal effects of biology and temperature on $p\text{CO}_2^{\text{sw}}$ at Patagonian shelf and found that CO_2 sinking regions were dominated by biology. According to their analysis, the high biological activity at the PS is stimulated by the intense wind and tidal mixing, in association with nutrient-rich waters upwelled from a strong boundary current. High nutrient fluxes sustain the phytoplankton growth resulting in an intense biological productivity that leads to high atmospheric CO_2 uptake rates comparable to some of the largest global CO_2 sinks.

6.6.3 Linking CO_2 uptake magnitudes and phytoplankton groups

Many studies have already contributed to an understanding of FCO_2 dynamics on the southwestern South Atlantic margins [e.g. [Ito et al. 2005](#), [Bianchi](#)

et al. 2009, *Ito et al.* 2016, *Lencina-Ávila et al.* 2016, *Kahl et al.* 2017, *Orselli et al.* 2018a, 2018b] and reported the importance of biology for the FCO₂ modulation. However, to the best of our knowledge, previous studies did not address the actual role of phytoplankton composition at each region to the carbon uptake in the surface. However, it is largely known that changes in dominant phytoplankton community exerts an important control over CO₂ dynamics [*Basu et al.* 2018, *Takao et al.* 2020]. Therefore, in order to shed light on the second issue raised in discussion, in this study we evaluated the connections between the different phytoplankton groups and CO₂ uptake magnitudes. At the entire study area, pCO₂^{sw} was negatively correlated with TChl *a*. However, the two main biogeochemical domains under investigation here showed strikingly different composition of phytoplankton assemblages (see [Fig. 30](#)). FCO₂ showed large zonal changes from small CO₂ source to strong sink, following the shifts in the dominance of the main phytoplankton groups, varying from small cyanobacteria (northern domain) to the massive dominance of diatoms (southern domain) ([Fig.30](#)).

As discussed before, the input of new nutrients by the upwelling region, also favored the presence of diatoms, even though the phytoplankton size structure in the oligotrophic southwestern Atlantic regions is dominated by picoplankton [e.g. *Maranón et al.* 2000]. Within this context, the diatoms were part of a highly diverse phytoplankton community of smaller groups comprised by cyanobacteria, haptophytes, green flagellates, and dinoflagellates. The phytoplankton assemblage along the subtropical coastal embayment of the South Brazil Bight (25°S – 30°S) was dominated by cyanobacteria. The coastal areas of SBB have been shown to be marked by the presence of cyanobacteria

Synechococcus [Brandini *et al.* 2019] and picoplankton cells [Gérikas Ribeiro *et al.* 2016, Moser *et al.* 2016, Bergo *et al.* 2017], and also by a highly diverse mixotrophic dinoflagellates nanoplankton community [Tenenbaum *et al.* 2006, Villac *et al.* 2008, Moser *et al.* 2017]. This phytoplankton structure pattern is typical of oligotrophic conditions, which favors the dominance of small phytoplankton [Zwirgmaier *et al.* 2008]. With scarce macro-nutrients, the carbon fluxes at these zones are mainly driven by smaller cells and heterotrophic bacteria, as commonly seen in oligotrophic plankton systems [Marañón *et al.* 2012].

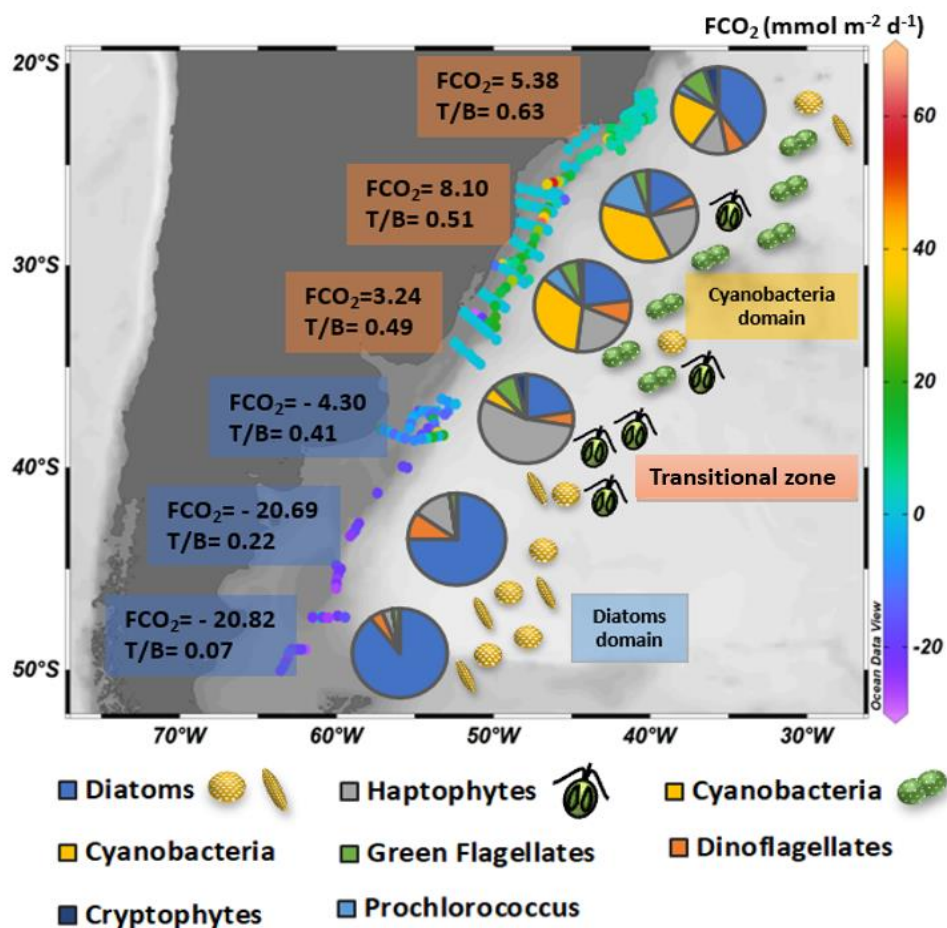


Figure 30. Biogeochemical domains proposed in this study region, based on sea–air CO₂ fluxes (FCO₂; mmol m⁻² d⁻¹) and dominance of phytoplankton groups. Note the increased CO₂ uptake magnitudes linked to increased phytoplankton size assemblages. The pizza graphs for each 5° latitudinal bin, with each color representing the phytoplankton group is shown at the legend on the right side. T/B ratio represents the temperature effect and biological effect index. The main phytoplankton groups (diatoms, haptophytes and cyanobacteria) are represented at the legend.

Between 35°S and 40°S, a dynamical transition zone, due to strong salinity and temperature contrasts promoted by the mixture of subtropical and subantarctic waters, favored phytoplankton growth with dominance of haptophytes. Haptophytes and diatoms experience competitive interactions in natural environments [Endo *et al.* 2018]. Often, after a diatom bloom, the depletion of nutrients, specially silica, favors the succession by haptophytes (i.e. Coccolithophores) [e.g. Iglesias-Rodrigues *et al.* 2002, Garcia *et al.* 2011]. Phytoplankton distribution at the Brazil-Malvinas confluence area have been previously studied [e.g. Souza *et al.* 2011, Gonçalves-Araujo *et al.* 2012, Ulibarrena & Conzonno 2015]. The presence of diatoms and dinoflagellates is mainly associated with the presence of sub-Antarctic waters, in contrast with nanoflagellates and cyanobacteria found at oligotrophic tropical waters [Gayoso & Podestá 1996, Gonçalves-Araujo *et al.* 2012], where grazing pressure must be responsible for low biomasses at this zone. Diatom bloom have been reported for this confluence zone associated with the complex mesoscale circulation of the confluence zone which may enhance the retention of cells in a geographic area [Gayoso & Podestá 1996, Garcia *et al.* 2004].

At higher latitudes (40°S – 50°S), along the Patagonian shelf region, diatoms prevailed (>60% abundance) over other groups. Although diatoms are a vast group with large size range, they are usually related to larger phytoplankton sizes [Litchman *et al.* 2009] and linked to lower $p\text{CO}_2^{\text{sw}}$. The contrast between the two main domains (cyanobacteria vs diatoms) was separated by a transitional zone roughly located between 35°S and 40°S and highly dominated by haptophytes (Fig. 31).

The phytoplankton distribution pattern showed an apparent decrease in

diversity (within the studied groups) with increase in latitude. It has been shown that the relatively higher seasonal variability of subpolar regions compared to more stable subtropical and tropical environments enhances competitiveness at higher latitudes, lowering diversity [Barton *et al.* 2010]. Different traits and adaptations of each dominant phytoplankton group (cyanobacteria, haptophytes, and diatoms) lead to success on particular environmental conditions and dynamics of the Southwestern south Atlantic contributing to different rates of seawater CO₂ uptake.

The prokaryotic picoplanktonic (<3µm) cyanobacteria are broadly distributed in marine and freshwater environments [Flobaum *et al.* 2013] due to their ability to succeed under nutrient stress and higher temperatures. Because of their abundance and high functional diversity, they drive the biogeochemical cycles of most biologically relevant elements [Jorgensen *et al.* 2006, Amin *et al.* 2012] and contribute to almost 25% of the global carbon fixation [Rosgaard *et al.* 2012, Durall & Lindblad 2015]. Projections of phytoplankton distribution in future climate scenarios predict higher global abundances and distributions of *Prochlorococcus* and *Synechococcus* due to future changes in ocean temperature [Flobaum *et al.* 2013], which can have a large impact on ocean carbon cycle.

Haptophytes, dominant at transitional zone (35°S – 40°S), contribute more to global biomass than photosynthetic prokaryotes such as *Prochlorococcus* and *Synechococcus* [Liu *et al.* 2009]. This group is usually negatively correlated with temperature and salinity and tend to show slower growth strategies, being adapted to intermediate to low nutrient concentrations [Endo *et al.* 2018]. Their behavior as mixotrophic flagellates may have benefited this groups under limiting

nutrients conditions [Unrein *et al.* 2013, Alexander *et al.* 2015].

Diatoms are responsible for total 40% of the ocean primary production and thus play a major role in driving the biological pump and shaping the carbon cycle [Sarhou *et al.* 2005]. Their great efficiency for CO₂ uptake is mainly due to the presence of an effective carbon fixation enzyme and carbon concentration mechanisms for higher CO₂ fixation capacity relative to phytoplankton groups [Badger *et al.* 1998, Reinfelder *et al.* 2011]. Another important advantage is the ability for nutrients storage in large vacuoles [Raven *et al.* 1987]. Completely opposite to cyanobacteria, diatoms are associated with nutrient-rich environments and are usually negatively correlated with temperature and salinity [Watermann *et al.* 1999].

6.7 Remarks on future approaches

There are few studies about $p\text{CO}_2^{\text{sw}}$ distribution (especially at the southern and southeastern Brazilian continental shelf) addressing the environmental drivers of $p\text{CO}_2^{\text{sw}}$ variation at the Southwestern Atlantic Ocean. Regarding the distribution of the phytoplankton groups, many of the reported studies were carried out mostly during spring/summer seasons, as is the case in the present study, mostly conducted in spring. However, an integrated understanding about the phytoplankton succession and competition mechanisms over the seasons is lacking. In addition, the study area is a complex region with influence of different frontal zones [Acha *et al.* 2004] and distinct local features interacting simultaneously (i.e. eddies, upwelling, entrainment, water mixing, etc.). Thus, further investigations are essential to unravel the connection between the main

phytoplankton groups with the seawater CO₂ uptake at different coastal regions. In this context, we believe that understanding the phytoplankton geographical distribution and different functional group traits is key finding to associate with CO₂ uptake magnitudes, as previously pointed out [Arrigo *et al.* 2005, Beaugrand *et al.* 2010, Endo *et al.* 2018]. Ongoing climate change will potentially result in a 2-fold increase in surface ocean pCO₂ by the end of the century [Cabr e *et al.* 2015]. Changes in phytoplankton communities due to high CO₂ or higher seawater temperature conditions will affect the oceans capacity to mitigate the impacts of growing releases of anthropogenic carbon emissions. Controlled experiments are being successful in elucidating some of the most ubiquitous species responses to environmental changes [e.g. Iglesias-Rodriguez *et al.* 2008, Bach *et al.* 2019, Ji *et al.* 2020]. However, understanding the conditions and processes by which different phytoplankton groups absorb CO₂ on a natural environment is challenging since the variables that interact with phytoplankton also affects CO₂ dynamics.

There are still many gaps to be filled towards a precise attribution of the role of phytoplankton in the modulation of the FCO₂. Studies probing the combined effects of physico-chemical parameters (i.e. salinity, temperature, and nutrient) on phytoplankton and their implications for CO₂ dynamics would be essential. We suggest that future studies in the region should evaluate the interaction among the natural dominant species/groups under multiple stressors to elucidate their potential impacts on the phytoplankton community. A complete analysis of the marine food web is also desirable to understand the CO₂ feedbacks along with the effects of biological interactions such as competition and grazing on the biological carbon pump.

Capítulo VII: Síntese da Discussão e Conclusões

Aqui serão destacados os principais pontos de discussão e conclusões dos artigos científicos apresentados entre os Capítulos IV a VI.

Primeiramente, os artigos serão abordados individualmente, e por fim, teremos um fechamento geral concluindo a Tese através da verificação das hipóteses formuladas e considerações finais.

7.1 O impacto dos vórtices de mesoescala nas comunidades fitoplanctônicas no oceano Atlântico Sul através da ferramenta HPLC-CHEMTAX.

A interação entre os processos físicos e biológicos foi investigada em três vórtices de mesoescala no oceano Atlântico Sul, em diferentes estágios

evolutivos, provenientes da região do vazamento das Agulhas. O impacto da evolução dessas estruturas na distribuição do fitoplâncton nessa região foi discutido ao longo de suas trajetórias. O decaimento dos vórtices reflete na maneira como estes interagem com o entorno. Os vórtices das Agulhas transportam consigo as propriedades da Corrente das Agulhas, interligando os oceanos Índico e Atlântico Sul. Assim, estas estruturas transportam águas relativamente mais salinas, mais quentes e ricas em nutrientes entre estes oceanos. Essas propriedades termohalinas, inicialmente, propiciam melhores condições para sustentar as comunidades fitoplanctônicas nas proximidades da região de liberação dos vórtices, porém, os padrões de distribuição do fitoplâncton aprisionado nestas estruturas mudam ao longo do tempo, à medida que os anéis avançam pelo oceano Atlântico Sul e interagem com o entorno.

O vórtice analisado no estágio mais jovem possibilitou uma estrutura de águas bem misturadas, sem profundidade marcada de máximo de clorofila *a*. Além disso, os nutrientes ficaram mais concentrados em superfície, favorecendo uma maior diversidade de grupos do fitoplâncton no interior dos vórtices. As estruturas com estágios mais avançados apresentaram uma profundidade máxima de clorofila *a* bem marcada, e a diversidade foi diminuindo à medida que foram avançando em deslocamento dentro do oceano Atlântico Sul. Este comportamento foi também observado ao se reconstruir, a partir de imagens de satélite, as trajetórias das estruturas de mesoescala analisadas *in situ*. As imagens da clorofila *a* na superfície do mar, ao longo da trajetória dos vórtices, permitiram confirmar essa evolução e, também, observar como estas estruturas interagem com a batimetria, sendo que a feição da cordilheira Walvis impacta fortemente na distribuição e, potencialmente, na composição dos grupos

fitoplanctônicos.

A distribuição do fitoplâncton nos três vórtices analisados foi associada à distribuição de nutrientes e luz. Movimentos verticais, como bombeamento de nutrientes da superfície para camadas inferiores, podem levar a uma diminuição da biomassa ao longo do tempo, e a um declínio na diversidade dos grupos do fitoplâncton. Uma mistura profunda dentro do vórtice pode ter limitado o crescimento do fitoplâncton, provavelmente como resultado da insuficiente quantidade de luz, evitando assim maior acúmulo de biomassa nos vórtices anticiclônicos analisados. No entanto, esta limitação de luz foi parcialmente compensada por uma estratégia em aumentar os pigmentos fotossintetizantes sob essas condições. Foi observado que o fitoplâncton no vórtice mais jovem apresentou concentrações mais elevadas de pigmentos fotossintéticos, sugerindo um investimento na capacidade de coleta de luz sob um regime de luz baixa. Nos vórtices em estágios mais avançados o fitoplâncton apresentou maiores concentrações de pigmentos fotoprotetores.

Embora vórtices anticiclônicos sejam comumente associados com uma diminuição nos nutrientes, outros trabalhos corroboram com a observação de forte mistura vertical dentro de estruturas anticiclônicas, levando a um aumento do TChl *a* na superfície. As baixas biomassas encontradas nestes três vórtices ($< 0,3 \text{ mg m}^{-3}$), particularmente nas camadas superficiais dos dois mais antigos, é resultado de uma zona eufótica pobre, em relação aos macronutrientes essenciais, o que leva ao deslocamento/acumulação de biomassa em direção a águas mais profundas, formando um evidente pico de clorofila *a* em profundidade.

A estrutura da comunidade fitoplanctônica estimada por análise pigmentar

(HPLC-CHEMTAX) evidenciou uma mudança entre uma dominância de haptófitas, no vórtice mais jovem, para uma dominância de *Prochlorococcus*, nas estruturas mais antigas. A dinâmica dos vórtices influencia na disponibilidade de nutrientes e luz que desempenha um papel fundamental na distribuição vertical do fitoplâncton. A idade das estruturas também se apresentou como um fator importante a ser considerado na distribuição da comunidade fitoplanctônica, pois à medida que essas estruturas evoluem (i.e., se deslocam em sua trajetória e interagem com as águas do entorno), adquirem mais semelhanças com o ambiente externo no que diz respeito à biomassa e composição fitoplanctônica. Por fim, podemos destacar que a transição dos vórtices entre uma região do sistema de ressurgência altamente produtiva e as águas de um oceano aberto oligotrófico se reflete na distribuição da biomassa fitoplanctônica e nas características de suas comunidades. A interação entre os vórtices das Agulhas e a diversidade do fitoplâncton no oceano Atlântico Sul foi evidenciada pela comparação entre o desenvolvimento do fitoplâncton no vórtice mais jovem (próximo a região de liberação destas estruturas) em relação ao vórtice mais antigo. A discussão desses processos contribuiu para o entendimento de como a estrutura das comunidades fitoplanctônicas podem ser modificadas em ambientes de condições oligotróficas.

7.2 Grupos do fitoplâncton fortalecem a captação de CO₂ pelo oceano Atlântico Sul

A variabilidade espacial de grupos fitoplanctônicos e do FCO₂ em situações de condições ambientais distintas, e com a influência de diferentes

sistemas dinâmicos no oceano Atlântico Sul foi discutida (Capítulo V). A maior parte do oceano Atlântico Sul é subsaturada em relação ao CO₂, propiciando que a região atue como um sumidouro desse gás de efeito estufa. No entanto, há diferenças relevantes em relação à magnitude desses fluxos e aos grupos fitoplanctônicos dominantes quando consideradas as diferentes províncias biogeoquímicas do oceano Atlântico Sul.

Na província denominada como BRAZ (dominada pelo sistema da corrente de contorno oeste – Corrente do Brasil), tivemos os menores fluxos de absorção de CO₂, com uma maior captação de CO₂ associada às variações de salinidade, apesar de uma dominância de diatomáceas. Nessa porção dominada pela corrente do Brasil, onde se registraram menores biomassas fitoplanctônicas, temos ainda uma grande influência da temperatura, porém a mistura de massas de água em determinadas áreas pode alterar os padrões de salinidade, temperatura e nutrientes, gerando mudanças na distribuição do fitoplâncton e no comportamento do FCO₂. A presença de áreas de ressurgência (e.g. Cabo Frio) e de fortes descargas de água doce (e.g. Estuários da Lagoa dos Patos e do Rio da Prata) são exemplos de regiões onde essas alterações foram observadas. Situação análoga foi observada na zona da confluência da corrente do Brasil (quente e pobre em nutrientes) com a corrente das Malvinas (águas frias e ricas em nutrientes). A distribuição zonal do fitoplâncton foi associada ao FCO₂, sendo os grupos mais adaptados a condições de altas temperaturas, maiores salinidades e baixas concentrações de nutrientes, como as cianobactérias (*Prochlorococcus* e *Synechococcus*) predominantes entre os 20°S e 30°S. Ao sul de 30°S, uma diminuição da temperatura e da salinidade, juntamente com o aumento da disponibilidade de nutrientes, favoreceram o

crescimento das diatomáceas. Com o aumento da biomassa associado às diatomáceas, tivemos fCO_2 mais intensos, porém estes não foram associados ao incremento na biomassa de diatomáceas, mas principalmente às variações de salinidade. A salinidade apresentou-se como um parâmetro bastante influenciador (direta ou indireta) da estrutura da comunidade fitoplanctônica nessa região e, simultaneamente, como um importante controlador da pCO_2 na superfície oceânica, associado com a intrusão de descarga continental tanto da Lagoa dos Patos quanto do Rio da Prata. A maioria dos grupos de fitoplâncton na província de BRAZ foram negativamente correlacionados com a salinidade. Entre estes, as diatomáceas apresentaram a correlação significativa mais alta, provavelmente devido à influência da entrada de água doce, rica em nutrientes, nesta região costeira bem misturada.

A porção central do giro anticiclônico subtropical do Atlântico Sul (província SATL) é uma região oligotrófica de oceano aberto, mas que apresentou influência significativa da biologia. A diferença de pressão parcial do CO_2 entre o oceano e a atmosfera, nesta região, foi alterada principalmente pela temperatura, mas também foi positivamente correlacionada com a salinidade, e negativamente associada com a biomassa fitoplanctônica (TChl *a*). Maiores concentrações de haptófitas, principalmente em 30°S, aumentaram a captação de CO_2 no sistema de giro central, promovendo elevadas taxas de absorção de CO_2 . Esse aumento considerável na absorção de CO_2 pode ser uma consequência da influência da Frente Subtropical do Atlântico Sul, que representa uma transição entre as águas subtropicais e subantárticas. Essas características frontais apresentam fortes gradientes meridionais de temperatura, salinidade e características biológicas.

Considerando a porção dominada pela corrente de contorno leste – Corrente de Benguela, na província denominada AFR, altas biomassas fitoplanctônicas com dominância dos grupos funcionais das haptófitas e diatomáceas foram associadas com uma forte captação de CO₂ atmosférico. Nesta região, a influência dos eventos de ressurgência associados à Corrente de Benguela pode estar associada a uma maior captação de CO₂ em 30°S. Mais ao sul dessa província, na região da retroflexão da corrente das Agulhas, onde os processos de mistura são favorecidos, uma menor estabilidade da coluna d'água promove uma maior disponibilidade de nutrientes para a zona eufótica. As haptófitas tiveram ocorrência dominante até 30°S, enquanto em 35°S as diatomáceas prevaleceram, provavelmente devido às maiores concentrações de nutrientes e aumento da mistura vertical, porém os maiores fluxos de captação de CO₂ atmosférico ocorreram em 30°S.

Por fim, possíveis cenários de mudanças climáticas, tais como aquecimento das águas superficiais e acidificação dos oceanos, e potenciais impactos no oceano Atlântico Sul foram discutidos com base no aumento das concentrações de CO₂ atmosférico. Mudanças na comunidade fitoplanctônica dominante, como resposta às mudanças climáticas, podem causar um impacto na captação de CO₂. O aumento na temperatura da superfície do mar pode diminuir a abundância de diatomáceas, por exemplo. O giro subtropical do Atlântico Sul pode se tornar mais oligotrófico, o que também resultaria em efeitos negativos sobre o fitoplâncton e, conseqüentemente, sobre a captação de CO₂. Na porção leste, onde as haptófitas foram dominantes, a maioria dos estudos apontam os coccolitoforídeos como sendo mais adaptados às condições de altos níveis de CO₂, porém esses organismos calcificantes podem ter um *feedback*

negativo sobre o CO_2 , reduzindo a sua captação pelos oceanos.

7.3 Contraste entre as plataformas continentais do sudoeste do oceano Atlântico Sul em relação a magnitude do FCO_2 e os grupos dominantes do fitoplâncton.

As plataformas continentais são ambientes dinâmicos que conectam os regimes costeiros e oceânicos, e que desempenham um papel importante na troca de dióxido de carbono (CO_2) entre o oceano e a atmosfera. O oceano costeiro é uma zona de transição constantemente influenciada por processos provenientes do continente e do oceano aberto adjacente, como por exemplo, entrada de descargas continentais, sistemas frontais, eventos de ressurgência, dinâmica das correntes oceânicas. O fitoplâncton é um componente chave para a compreensão do ciclo do carbono costeiro, contribuindo amplamente com a captação de CO_2 e a exportação de carbono por meio da bomba de carbono biológico. A ampla variabilidade espaço-temporal dos ambientes costeiros afeta a distribuição do fitoplâncton, sendo que a comunidade fitoplanctônica dominante em um ambiente natural é influenciada por variáveis ambientais ligadas a variações nos fluxos líquidos de CO_2 entre o oceano e a atmosfera (FCO_2).

No Oceano Atlântico Sudoeste entre 20°S – 50°S foram encontradas regiões contrastantes, marcadas por uma zona de transição a aproximadamente 35°S . Ao norte de 35°S , maiores temperaturas e salinidades da superfície do mar, combinadas com menor biomassa fitoplanctônica, favoreceram o domínio de cianobactérias. Nessas regiões, foi observado um comportamento de fonte

de CO₂ para atmosfera. Na zona de transição (35°S – 40°S), as variações de salinidade e temperatura promoveram uma mudança na estrutura da comunidade fitoplanctônica dominante e, conseqüentemente, mudaram o comportamento do FCO₂ de fonte para sumidouro de CO₂ atmosférico. Mais ao sul, entre 40°S e 50°S, menores temperaturas e salinidades, acompanhadas por maior biomassa fitoplanctônica, favoreceram o domínio das diatomáceas, que foram associadas a maiores taxas de absorção de CO₂.

O tamanho dos grupos do fitoplâncton dominantes pode influenciar na capacidade de absorção de CO₂ e, como vimos neste estudo, as cianobactérias, pertencentes ao picoplâncton, foram associadas a uma menor captação do CO₂, enquanto as diatomáceas, grupo bastante variável em relação à classe de tamanho, mas comumente associados ao microplâncton nas regiões de estudo, foram associadas a uma maior capacidade de captação de CO₂.

Compreender como a mudança no domínio do fitoplâncton afeta as taxas de absorção de CO₂ nesta região costeira do Oceano Atlântico Sul é essencial para alcançar um maior entendimento sobre a modulação do FCO₂ a longo prazo nas margens do Atlântico Sul ocidental.

7.4 Considerações finais e direcionamentos futuros

Em relação às hipóteses apresentadas e testadas no desenvolvimento desta Tese de Doutorado:

(i) a atividade biológica tem maior influência que os fatores físicos (e.g. temperatura, salinidade) na distribuição da $p\text{CO}_2^{\text{mar}}$ nas regiões de estudo.

(ii) determinados grupos funcionais do fitoplâncton favorecem uma maior

captação de CO₂ pelos oceanos nas diferentes províncias biogeoquímicas do Atlântico Sul.

Podemos concluir que a hipótese (i) foi aceita para a maioria das regiões estudadas do oceano Atlântico Sul, pois a atividade biológica teve influência significativa na distribuição da $p\text{CO}_2^{\text{mar}}$, exceto para áreas da porção oeste do Atlântico Sul, onde a temperatura e a salinidade, que têm também um papel importante na distribuição do fitoplâncton, exerceram forte controle no FCO₂. A hipótese (ii) também foi aceita, uma vez que foi detectada a influência de determinados grupos dominantes do fitoplâncton (e.g., haptófitas e diatomáceas) favorecendo uma maior captação de CO₂ nas diferentes regiões de estudo, em detrimento de grupos menores, como as cianobactérias, associados a menores magnitudes de FCO₂.

Em suma, os processos físicos que afetam o fitoplâncton nas diferentes regiões estudadas (zonas de plataforma sob influência dinâmica distintas e de oceano aberto) e geram variabilidade nos processos biogeoquímicos foram amplamente discutidos ao longo da Tese. A presença de vórtices anticiclônicos de mesoescala, bem como a mistura de massas de água com diferentes propriedades hidrográficas, foram os principais condicionantes que geraram respostas dinâmicas distintas na distribuição e composição dos grupos de fitoplâncton, que em determinadas ocasiões puderam ser associados à variabilidade do FCO₂. Sendo assim, foram considerados como importantes mecanismos moduladores na caracterização de áreas oceânicas como zonas emissoras ou absorvedores do CO₂.

As diatomáceas e as haptófitas foram os principais grupos associados às áreas de menor temperatura e salinidade, em superfície, bem como com

maior disponibilidade de nutrientes. Estes grupos favoreceram maiores fluxos de absorção de CO₂ em diversas regiões do oceano Atlântico Sul. Por outro lado, as células picoplantônicas de cianobactérias (*Prochlorococcus* e *Synechococcus*) estiveram mais relacionadas com as regiões oligotróficas de temperatura superficial maior. Neste caso, a presença destes organismos foi mais relacionada às regiões de emissão de CO₂ para a atmosfera.

A ideia de atribuir a captação de CO₂ aos grupos específicos do fitoplâncton é desafiadora, mas contribui para um melhor entendimento do ciclo biogeoquímico do carbono nos oceanos. Com a elaboração desta Tese, buscamos investigar o papel desempenhado por diferentes grupos do fitoplâncton na captação de CO₂ atmosférico em regiões do oceano Atlântico Sul, onde a biomassa fitoplanctônica foi significativamente relacionada à diferença de pCO₂ entre o oceano e a atmosfera. A fim de entender como os processos físicos e biológicos interagem, relacionamos os grupos dominantes às magnitudes dos FCO₂ encontrados no ambiente natural. Ou seja, tentamos compreender/elucidar como os grupos do fitoplâncton se distribuem em áreas costeiras e oceânicas do Oceano Atlântico Sul, e como se relacionam ao FCO₂, a partir de dados obtidos em diversas campanhas oceanográficas. Uma vez que as variáveis que interagem com o fitoplâncton também afetam a dinâmica do CO₂, o nosso desafio tendo em vista o amplo entendimento de todos os processos associados ao ciclo do carbono se tornou ainda mais complexo.

Novas investigações e estudos ainda são necessários para elucidar a complexa relação existente entre os principais grupos do fitoplâncton com o papel na modulação da captação do CO₂ em regimes locais e regionais distintos dos oceanos. As mudanças climáticas em curso têm o potencial de dobrar os

níveis de pressão parcial do CO₂ nos oceanos até o final desse século. Por outro lado, as mudanças nas comunidades fitoplanctônicas, principalmente devido ao aumento do CO₂ atmosférico e oceânico, afetarão a capacidade dos oceanos de mitigar os impactos da liberação crescente de CO₂ atmosférico decorrente das atividades humanas.

De acordo com os últimos relatórios climáticos, a força da bomba biológica provavelmente mudará no oceano futuro, em resposta às mudanças climáticas. No entanto, prever a direção de tal mudança é difícil devido à complexidade do problema. Numerosos contrastes surgem de comparações de diferentes áreas geográficas, ecossistemas, condições ambientais e organismos. Além disso, as alterações simultâneas do sistema carbonático oceânico, a disponibilidade de temperatura, luz e nutrientes, devido à mudança global, irá variar em diferentes regiões do oceano e, os mesmos, podem ter efeitos sinérgicos ou antagônicos no fitoplâncton.

Elevados níveis de CO₂ e de luz podem favorecer grupos fitoplanctônicos maiores, como as diatomáceas, resultando no aumento da exportação de carbono para o oceano profundo. Porém, isso vai depender da interação com outros processos como degradação microbiana e pastoreio, que podem retornar o CO₂ para a coluna d'água gerando uma retroalimentação positiva do CO₂. Por outro lado, o aquecimento do oceano e a consequente depleção de nutrientes favorecem o crescimento de grupos menores do fitoplâncton, como as cianobactérias picoplanctônicas, levando à redução da eficiência da bomba biológica do carbono. Como a eficiência da bomba biológica varia de acordo com a fisiologia do fitoplâncton e da estrutura da comunidade, é importante entender como os múltiplos estressores simultâneos (temperatura, intensidade da luz,

nutrientes e níveis de CO₂) afetam as taxas de crescimento e competição entre as espécies do fitoplâncton.

Ou seja, há ainda muitas incógnitas, e a falta de conhecimento de longo termo, tanto na distribuição de propriedades físico-químicas, como nas alterações do fitoplâncton e seus efeitos conjugados, acarretam maiores desafios ao pleno entendimento. Até o momento, poucos estudos investigaram os efeitos combinados de CO₂, temperatura e níveis de nutrientes no fitoplâncton. Experimentos *in situ* e em laboratório devem ser fomentados em escala multi-proxy (alterações de temperatura, salinidade, pH, níveis de CO₂) avaliando várias espécies de fitoplâncton e incorporando múltiplos tratamentos de estressores para compreender toda a gama de potencial efeitos. Além disso, a complexidade do papel que a cadeia alimentar marinha desempenha na bomba biológica, e sua alta variabilidade espacial e temporal, torna as generalizações globais difíceis. Estudos futuros devem abordar esta questão juntamente com os efeitos das atividades entre espécies, como a competição e a predação na bomba de carbono biológica.

Há ainda muitas limitações no entendimento de como o processo de acidificação dos oceanos afetará as comunidades fitoplanctônicas. A maioria dos estudos atuais investigaram as respostas em células fitoplanctônicas aclimatadas a mudanças nas condições ambientais ao longo de escalas de tempo muito curtas para que a evolução produza grandes mudanças. Ajustes são necessários para prever as mudanças na estrutura da comunidade fitoplanctônica com prazos mais longos de competição e transporte. Além disso, a evolução dos experimentos com fitoplâncton cultivado é um próximo passo importante na previsão de como os principais táxons do fitoplâncton

responderão às mudanças climáticas. Esses estudos são essenciais para obter uma ampla visão sobre a bomba de carbono biológico e a capacidade do oceano de atuar como um sumidouro de longo prazo para CO₂ atmosférico.

ANEXO I

Este anexo contém as seguintes figuras mencionadas no Capítulo IV :Figure S1; Figure S2; Figure S3. E as tabelas: Table S1; Table S2a; Table S2b; Table S2c e Table S3

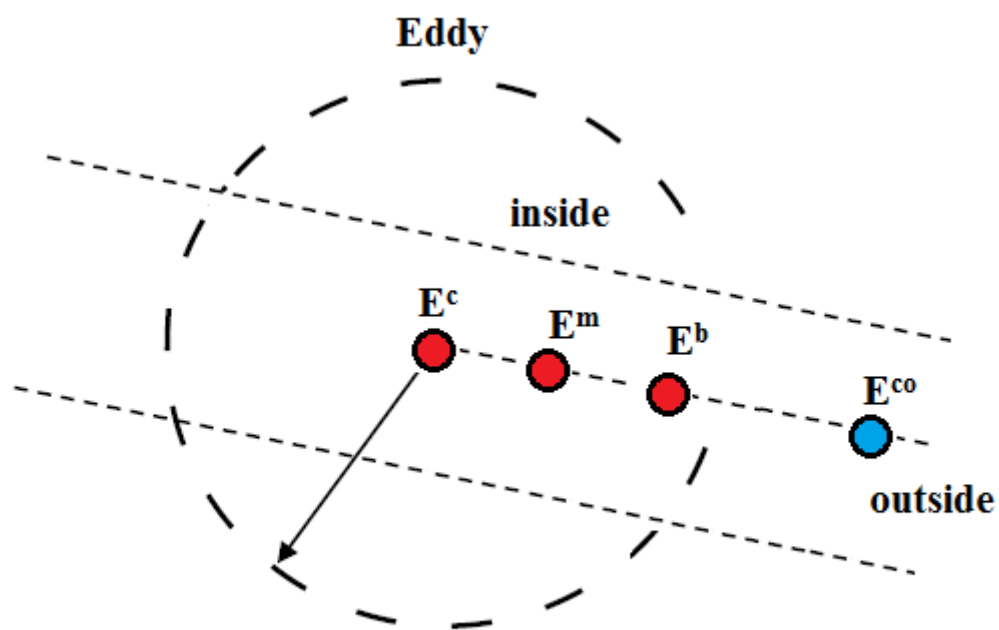


Figure S1. Scheme of sampling strategy for the eddies, where there are three stations inside (E^c - center station; E^m - median station; and E^b - border station) the eddy and one station outside (E^{co} - control station).

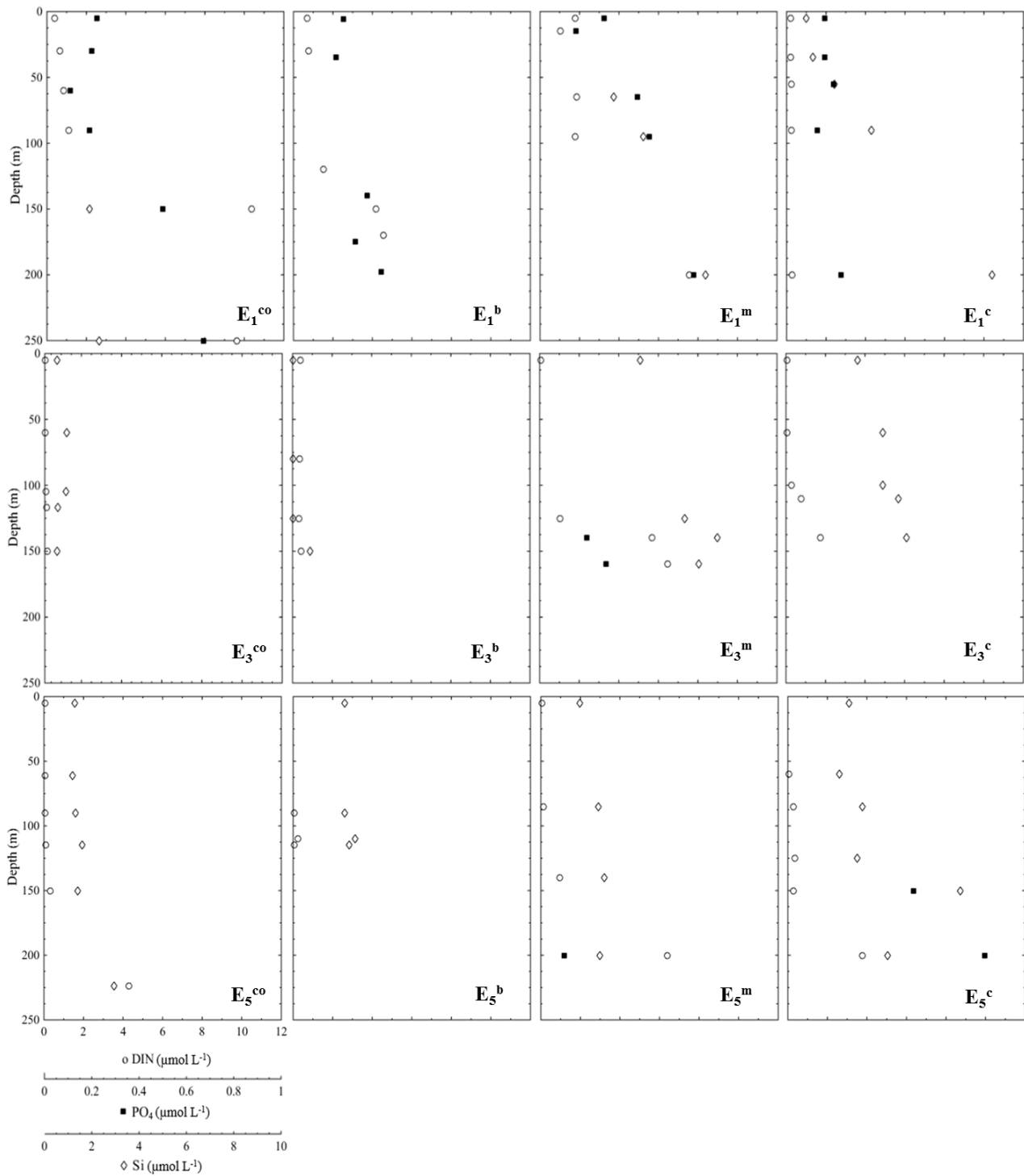


Figure S2. Distribution of nutrients ($\mu\text{mol L}^{-1}$) over depth for the three eddies sampled. Dissolved inorganic nitrogen ($\text{NO}_3^- + \text{NO}_2^-$) is represented by the white circles. Phosphate (PO_4^{3-}) is represented by the black squares, and silicic acid (Si) is represented by the white diamonds.

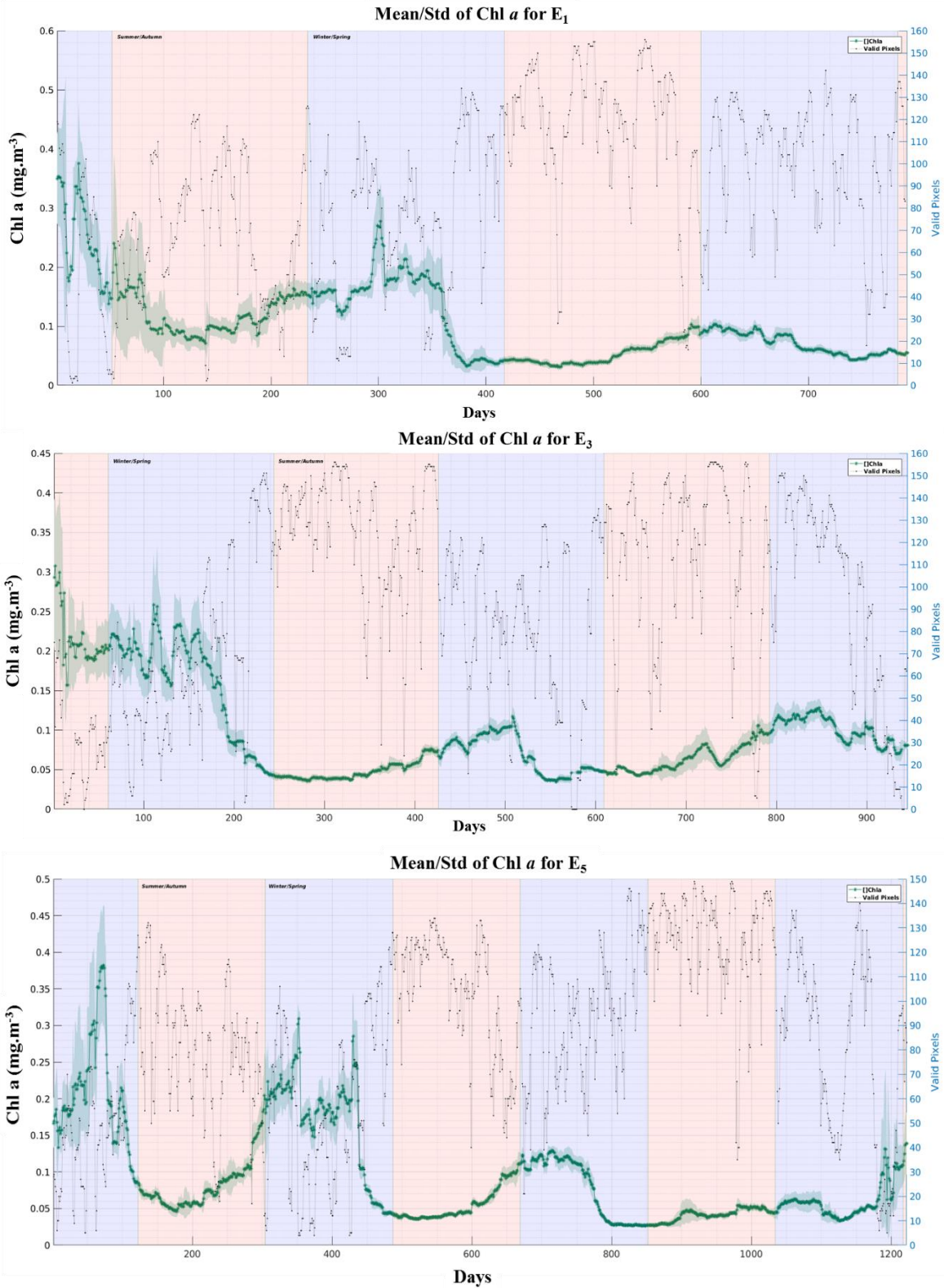


Figure S3. These graphs show the variability of chlorophyll a concentration along the eddies' lifetime (days). The standard deviation and the quantity of valid pixels used for the composite are also shown. To better support the data used, the number of values used in each composite are shown as it is important to note that even with 8 days of data used for the composite, cloud contamination can still persist in some instances for several days, which can lead to the overestimation/underestimation of certain means.

Table S1. Pigment ratios used in CHEMTAX analysis of pigment data: a) initial ratios before analysis; b) optimized ratios (for each depth interval) after analysis.

	Chl a	DVChl a	Viola	But	Fuco	Hex	Lut	Chl c3	Pras	Allo	Zea	Peri	Tchl b
(a) Input matrix													
Prasinophytes	1	0	0.054	0	0	0	0.021	0	0.245	0	0.058	0	0.704
Chlorophytes	1	0	0.049	0	0	0	0.171	0	0	0	0.032	0	0.315
Cryptophytes	1	0	0	0	0	0	0	0	0	0.379	0	0	0
Diatoms	1	0	0	0	0.623	0	0	0	0	0	0	0	0
Pelagophytes	1	0	0	0.658	0.779	0	0	0.230	0	0	0	0	0
Dinoflagellates	1	0	0	0	0	0	0	0	0	0	0	0.558	0
Haptophytes	1	0	0	0.054	0.265	0.421	0	0.174	0	0	0	0	0
Synechococcus	1	0	0	0	0	0	0	0	0	0	0.636	0	0
Prochlorococcus	1	1	0	0	0	0	0	0	0	0	0.389	0	0.994
(b) Output matrix													
0-50m													
	Chl a	DVChl a	Viola	But	Fuco	Hex	Lut	Chlc 3	Pras	Allo	Zea	Peri	Tchl b
Prasinophytes	1	0	0.067	0	0	0	0.036	0	0.035	0	0.083	0	1.524
Chlorophytes	1	0	0.124	0	0	0	0.024	0	0	0	0.044	0	0.301
Cryptophytes	1	0	0	0	0	0	0	0	0	0.512	0	0	0
Diatoms	1	0	0	0	0.730	0	0	0	0	0	0	0	0
Pelagophytes	1	0	0	0.935	0.412	0	0	0.316	0	0	0	0	0
Dinoflagellates	1	0	0	0	0	0	0	0	0	0	0	0.566	0
Haptophytes	1	0	0	0.203	0.080	1.036	0	0.318	0	0	0	0	0
Synechococcus	1	0	0	0	0	0	0	0	0	0	3.241*	0	0
Prochlorococcus	0	1	0	0	0	0	0	0	0	0	0.531	0	0.260
50-100m													
	Chla	DVChla	Viola	But	Fuco	Hex	Lut	Chlc 3	Pras	Allo	Zea	Peri	Tchl b
Prasinophytes	1	0	0.077	0	0	0	0.029	0	0.159	0	0.080	0	1.393
Chlorophytes	1	0	0.086	0	0	0	0.070	0	0	0	0.030	0	0.588
Cryptophytes	1	0	0	0	0	0	0	0	0	0.414	0	0	0
Diatoms	1	0	0	0	0.815	0	0	0	0	0	0	0	0
Pelagophytes	1	0	0	1.103	0.122	0	0	0.398	0	0	0	0	0
Dinoflagellates	1	0	0	0	0	0	0	0	0	0	0	0.798	0
Haptophytes	1	0	0	0.097	0.053	1.115	0	0.285	0	0	0	0	0
Synechococcus	1	0	0	0	0	0	0	0	0	0	3.732*	0	0
Prochlorococcus	0	1	0	0	0	0	0	0	0	0	0.393	0	0.155
100-200m													
	Chla	DVChla	Viola	But	Fuco	Hex	Lut	Chlc 3	Pras	Allo	Zea	Peri	Tchl b
Prasinophytes	1	0	0.065	0	0	0	0.026	0	0.299	0	0.075	0	0.872
Chlorophytes	1	0	0.098	0	0	0	0.077	0	0	0	0.037	0	0.380
Cryptophytes	1	0	0	0	0	0	0	0	0	0.550	0	0	0
Diatoms	1	0	0	0	1.017	0	0	0	0	0	0	0	0
Pelagophytes	1	0	0	1.333	0.306	0	0	0.330	0	0	0	0	0
Dinoflagellates	1	0	0	0	0	0	0	0	0	0	0	0.675	0
Haptophytes	1	0	0	0.213	0.043	0.788	0	0.357	0	0	0	0	0
Synechococcus	1	0	0	0	0	0	0	0	0	0	3.899*	0	0
Prochlorococcus	0	1	0	0	0	0	0	0	0	0	0.267	0	1.457

*CHEMTAX analysis showed zea/chl a ratios (3.2-3.9) higher than usually reported (0.2-2.5) [Higgins *et al.* 2011] for *Synechococcus*. We attribute these higher values to the fact that this is a minor group in terms of biomass and the CHEMTAX approach, in these cases, tends to lead to elevated ratios.

Table S2 a. Phytoplankton pigment mean concentration (ng L⁻¹) for each E₁ station and, in the last column, the mean for the eddy.

Symbol	Description	E ₁ ^{co}	E ₁ ^b	E ₁ ^m	E ₁ ^c	E ₁ mean
Chl a	Chlorophyll a	0.087	0.109	0.179	0.195	0.142
DV Chl a	Divinyl chlorophyll a	0.037	0.037	0.047	0.060	0.045
Chl b	Chlorophyll b	0.035	0.028	0.040	0.048	0.038
Chlc2	Chlorophyll c 2	0.018	0.012	0.026	0.030	0.021
Chl c3	Chlorophyll c 3	0.021	0.028	0.042	0.045	0.034
Fuco	Fucoxanthin	0.005	0.009	0.017	0.018	0.012
But	19'-butanoyloxyfucoxanthin	0.030	0.041	0.054	0.068	0.048
Hex	19'-hexanoyloxyfucoxanthin	0.053	0.059	0.074	0.082	0.067
Diad	Diadinoxanthin	0.006	0.006	0.013	0.013	0.009
Lut	Lutein	0.001	0.001	0.001	0.001	0.001
Pras	Prasincoxanthin	0.000	0.000	0.000	0.000	0.000
Allo	Alloxanthin	0.000	0.000	0.001	0.001	0.000
Diato	Diatoxanthin	0.000	0.000	0.000	0.000	0.000
Zea	Zeaxanthin	0.034	0.025	0.030	0.038	0.032
Car	βε-carotene + ββ-carotene	0.007	0.006	0.010	0.014	0.009
Peri	Peridinin	0.003	0.003	0.004	0.004	0.003
Viola	Violaxanthin	0.002	0.001	0.002	0.002	0.002
Pheide a	Pheophorbide a	0.005	0.006	0.011	0.009	0.008
Phe a	Pheophytin a	0.003	0.003	0.007	0.005	0.004
Chlide a	Chlorophyllide a	0.003	0.004	0.003	0.006	0.004

Table S2 b. Phytoplankton pigment mean concentration (ng L⁻¹) for each E₃ station and, in the last column, the mean for the eddy.

Symbol	Description	E ₃ ^{co}	E ₃ ^b	E ₃ ^m	E ₃ ^c	E ₃ mean
Chl a	Chlorophyll a	0.059	0.052	0.072	0.077	0.065
DV Chl a	Divinyl chlorophyll a	0.057	0.047	0.062	0.063	0.057
Chl b	Chlorophyll b	0.060	0.036	0.077	0.069	0.061
Chl c2	Chlorophyll c 2	0.008	0.007	0.010	0.011	0.009
Chl c3	Chlorophyll c 3	0.014	0.011	0.019	0.018	0.015
Fuco	Fucoxanthin	0.010	0.003	0.004	0.005	0.005
But	19'-butanoyloxyfucoxanthin	0.020	0.017	0.024	0.024	0.021
Hex	19'-hexanoyloxyfucoxanthin	0.024	0.023	0.034	0.038	0.030
Diad	Diadinoxanthin	0.009	0.003	0.003	0.004	0.005
Lut	Lutein	0.000	0.000	0.000	0.000	0.000
Pras	Prasincoxanthin	0.000	0.000	0.000	0.000	0.000
Allo	Alloxanthin	0.000	0.000	0.000	0.000	0.000
Diato	Diatocoxanthin	0.000	0.000	0.000	0.000	0.000
Zea	Zeaxanthin	0.040	0.036	0.039	0.041	0.039
Car	βε-carotene + ββ-carotene	0.007	0.009	0.013	0.013	0.010
Peri	Peridinin	0.003	0.002	0.003	0.003	0.003
Viola	Violaxanthin	0.001	0.001	0.002	0.002	0.001
Pheide a	Pheophorbide a	0.004	0.003	0.005	0.006	0.005
Phe a	Pheophytin a	0.004	0.003	0.005	0.005	0.004
Chlide a	Chlorophyllide a	0.002	0.001	0.002	0.002	0.002

Table S2 c. Phytoplankton pigment mean concentration (ng L⁻¹) for each E₅ station and, in the last column, the mean for the eddy.

Symbol	Description	E ₅ ^{co}	E ₅ ^b	E ₅ ^m	E ₅ ^c	E ₅ mean
Chl a	Chlorophyll a	0.058	0.039	0.055	0.052	0.051
DV Chl a	Divinyl chlorophyll a	0.055	0.037	0.050	0.037	0.044
Chl b	Chlorophyll b	0.069	0.045	0.075	0.054	0.061
Chl c2	Chlorophyll c 2	0.008	0.006	0.008	0.007	0.007
Chl c3	Chlorophyll c 3	0.014	0.009	0.015	0.013	0.013
Fuco	Fucoxanthin	0.003	0.003	0.004	0.004	0.003
But	19'-butanoyloxyfucoxanthin	0.020	0.015	0.020	0.018	0.018
Hex	19'-hexanoyloxyfucoxanthin	0.028	0.018	0.026	0.023	0.024
Diad	Diadinoxanthin	0.003	0.003	0.004	0.003	0.003
Lut	Lutein	0.000	0.000	0.000	0.000	0.000
Pras	Prasinoxanthin	0.000	0.000	0.000	0.000	0.000
Allo	Alloxanthin	0.000	0.000	0.000	0.000	0.000
Diato	Diatoxanthin	0.000	0.000	0.000	0.000	0.000
Zea	Zeaxanthin	0.032	0.023	0.024	0.025	0.026
Car	βε-carotene + ββ-carotene	0.012	0.009	0.012	0.009	0.010
Peri	Peridinin	0.002	0.002	0.002	0.002	0.002
Viola	Violaxanthin	0.000	0.001	0.001	0.000	0.001
Pheide a	Pheophorbide a	0.004	0.004	0.004	0.002	0.003
Phe a	Pheophytin a	0.003	0.003	0.004	0.003	0.003
Chlide a	Chlorophyllide a	0.002	0.001	0.003	0.001	0.002

Table S3. Percentage contribution of each phytoplankton group to the total chlorophyll a (TChl = Chl a + DV Chl a) for each eddy station at the depths sampled.

STN	Dep(m)	Chl a	DV Chla	TChl a	Pras	Chloro	Crypto	Diato	Pelago	Dino	Hapto	Syn	Proc	%
E₁^{co}	5	0.04	0.04	0.08	8.82	2.02	0.00	0.02	7.93	4.01	25.46	1.95	49.78	100.00
	30	0.13	0.04	0.17	9.95	6.63	0.01	0.04	11.80	3.82	38.22	4.58	24.94	100.00
	60	0.10	0.03	0.13	6.25	12.83	0.00	0.00	18.95	1.95	35.85	1.31	22.86	100.00
	90	0.08	0.04	0.12	5.80	12.74	0.01	0.62	12.04	3.45	31.85	3.08	30.41	100.00
Mean		0.09	0.04	0.12	7.71	8.56	0.00	0.17	12.68	3.31	32.85	2.73	32.00	100.00
E₁^b	5	0.12	0.04	0.16	7.69	1.67	0.00	0.57	16.90	3.47	43.93	0.63	25.13	100.00
	30	0.09	0.03	0.11	6.57	5.02	0.01	1.40	15.66	4.12	41.77	0.69	24.76	100.00
	120	0.12	0.04	0.16	0.59	7.49	0.00	2.94	9.98	2.83	46.44	3.73	26.00	100.00
	Mean		0.11	0.04	0.15	4.95	4.73	0.00	1.64	14.18	3.47	44.05	1.68	25.30
E₁^m	5	0.17	0.04	0.21	7.73	2.37	0.09	4.61	15.93	5.65	42.47	0.99	20.16	100.00
	15	0.19	0.05	0.24	7.87	2.99	1.45	4.09	16.50	3.97	42.26	0.64	20.23	100.00
	65	0.19	0.05	0.24	4.03	9.20	1.33	4.28	22.18	2.49	34.78	1.01	20.70	100.00
	95	0.17	0.05	0.21	4.75	8.37	0.07	4.85	21.47	2.08	35.07	1.25	22.10	100.00
Mean		0.18	0.05	0.23	6.10	5.73	0.73	4.46	19.02	3.55	38.65	0.97	20.80	100.00
E₁^c	5	0.20	0.07	0.27	7.91	2.25	1.27	3.43	16.69	2.41	39.70	1.61	24.72	100.00
	35	0.18	0.06	0.24	8.87	1.63	1.45	2.16	16.41	3.53	40.28	0.35	25.33	100.00
	55	0.18	0.05	0.23	4.24	8.71	0.06	3.19	24.74	2.80	33.58	0.95	21.72	100.00
	90	0.22	0.06	0.28	4.14	8.66	1.88	3.94	24.12	2.36	31.33	1.07	22.49	100.00
Mean		0.19	0.06	0.25	6.29	5.31	1.17	3.18	20.49	2.78	36.22	0.99	23.56	100.00
E₃^{co}	5	0.03	0.03	0.07	0.83	0.41	0.14	3.49	4.83	5.97	19.87	14.65	49.82	100.00
	60	0.04	0.04	0.09	1.08	9.88	0.00	3.27	6.49	3.47	15.77	10.25	49.78	100.00
	105	0.06	0.06	0.12	0.46	4.83	0.00	17.96	11.77	5.09	3.31	5.87	50.71	100.00
	120	0.10	0.11	0.21	0.47	3.81	0.00	0.36	6.48	3.47	29.86	3.13	52.44	100.00
	150	0.06	0.04	0.09	0.32	0.78	0.05	0.62	12.69	3.94	44.49	0.04	37.06	100.00
Mean		0.06	0.06	0.12	0.63	3.94	0.04	5.14	8.45	4.39	22.66	6.79	47.96	100.00
E₃^b	5	0.04	0.03	0.07	1.61	6.02	0.05	2.78	5.77	6.15	20.77	10.53	46.33	100.00
	80	0.05	0.05	0.10	1.34	7.81	0.03	1.65	8.03	2.57	19.97	8.04	50.56	100.00
	125	0.05	0.05	0.10	0.81	7.67	0.00	0.83	3.94	4.23	24.15	8.43	49.94	100.00
	150	0.07	0.05	0.13	0.20	0.65	0.05	0.10	12.76	3.20	38.60	1.15	43.30	100.00
Mean		0.05	0.05	0.10	0.99	5.53	0.03	1.34	7.63	4.04	25.87	7.04	47.53	100.00
E₃^m	5	0.03	0.03	0.06	0.00	12.32	0.00	3.00	4.09	8.31	16.47	9.82	45.99	100.00
	60	0.04	0.04	0.08	1.47	10.33	0.00	2.67	5.29	4.05	17.16	9.69	49.34	100.00
	110	0.14	0.13	0.27	2.21	6.18	0.00	0.46	6.30	2.72	30.37	2.84	48.92	100.00
	140	0.08	0.05	0.13	1.51	9.34	0.00	0.16	11.89	2.42	35.99	0.08	38.62	100.00
Mean		0.07	0.06	0.13	1.30	9.54	0.00	1.57	6.89	4.38	25.00	5.61	45.71	100.00
E₃^c	5	0.05	0.05	0.10	0.00	10.71	0.00	2.18	3.75	4.40	19.20	8.43	51.34	100.00
	60	0.05	0.04	0.10	1.14	9.08	0.05	3.40	5.87	3.70	22.96	7.46	46.34	100.00
	110	0.12	0.09	0.21	2.55	7.47	0.00	0.90	6.47	3.36	32.93	2.42	43.90	100.00
	140	0.09	0.06	0.15	0.76	4.58	0.02	0.10	11.08	2.08	38.58	1.09	41.72	100.00
Mean		0.08	0.06	0.14	1.11	7.96	0.02	1.64	6.79	3.39	28.42	4.85	45.82	100.00
E₅^{co}	5	0.03	0.02	0.06	0.98	7.96	0.00	4.25	5.37	8.96	18.96	11.62	41.89	100.00
	115	0.08	0.09	0.17	0.10	0.55	0.05	0.02	8.41	2.46	35.75	1.70	50.95	100.00
Mean		0.06	0.05	0.11	0.54	4.26	0.03	2.13	6.89	5.71	27.35	6.66	46.42	100.00
E₅^b	5	0.02	0.02	0.04	0.00	12.50	0.00	4.06	4.29	6.94	18.57	12.64	41.00	100.00
	140	0.05	0.06	0.11	0.80	5.42	0.00	0.18	9.47	3.20	28.31	1.48	51.14	100.00
Mean		0.04	0.04	0.08	0.40	8.96	0.00	2.12	6.88	5.07	23.44	7.06	46.07	100.00
E₅^m	5	0.03	0.01	0.04	0.74	15.34	0.00	4.74	4.14	10.22	16.35	13.78	34.67	100.00
	140	0.08	0.09	0.17	0.45	3.16	0.94	0.38	9.20	1.42	33.66	0.02	50.77	100.00
Mean		0.05	0.05	0.10	0.59	9.25	0.47	2.56	6.67	5.82	25.01	6.90	42.72	100.00
E₅^c	5	0.03	0.01	0.04	0.00	13.78	0.02	6.66	4.43	8.54	22.01	15.20	29.36	100.00
	60	0.03	0.02	0.05	1.05	10.98	0.00	6.43	5.94	7.17	19.09	12.87	36.47	100.00
	125	0.09	0.09	0.18	0.11	0.49	0.04	0.78	9.19	2.16	35.07	1.81	50.34	100.00
	150	0.05	0.03	0.08	0.53	1.50	0.11	0.00	14.31	0.07	50.65	0.02	32.81	100.00
Mean		0.05	0.04	0.09	0.42	6.69	0.04	3.47	8.47	4.49	31.70	7.48	37.25	100.00

ANEXO II

Este anexo contém as figuras: Figure S1 e Figure S2 mencionadas no Capítulo V e as seguintes tabelas: Table S1; Table S2; Table S3a, Table S3b, Table S3c, Table S3d.

Table S1. Pigment Ratios used in CHEMTAX analysis of pigment data: a) initial ratios before analysis. b) optimized ratios (for each depth interval) after analysis.

Pigments	Chl a	DVChl a	Viola	But	Fuco	Hex	Lut	Chl c3	Pras	Allo	Zea	Peri	Tchl b
(a) Input matrix													
Prasinophytes	1	0	0.054	0	0	0	0.021	0	0.245	0	0.058	0	0.704
Chlorophytes	1	0	0.049	0	0	0	0.171	0	0	0	0.032	0	0.315
Cryptophytes	1	0	0	0	0	0	0	0	0	0.379	0	0	0
Diatoms	1	0	0	0	0.623	0	0	0	0	0	0	0	0
Pelagophytes	1	0	0	0.658	0.779	0	0	0.230	0	0	0	0	0
Dinoflagellates	1	0	0	0	0	0	0	0	0	0	0	0.558	0
Haptophytes	1	0	0	0.054	0.265	0.421	0	0.174	0	0	0	0	0
Synechococcus	1	0	0	0	0	0	0	0	0	0	0.636	0	0
Prochlorococcus	1	1	0	0	0	0	0	0	0	0	0.389	0	0.994
(b) Output matrix													
H40 and TAI 2009 20°S and 30°S													
Prasinophytes	1	0	0.078	0	0	0	0.023	0	0.050	0	0.061	0	0.696
Chlorophytes	1	0	0.076	0	0	0	0.387	0	0	0	0.042	0	0.153
Cryptophytes	1	0	0	0	0	0	0	0	0	0.522	0	0	0
Diatoms	1	0	0	0	0.626	0	0	0	0	0	0	0	0
Pelagophytes	1	0	0	1.175	0.795	0	0	0.210	0	0	0	0	0
Dinoflagellates	1	0	0	0	0	0	0	0	0	0	0	0.876	0
Haptophytes	1	0	0	0.070	0.173	0.834	0	0.174	0	0	0	0	0
Synechococcus	1	0	0	0	0	0	0	0	0	0	1.239	0	0
Prochlorococcus	0	1	0	0	0	0	0	0	0	0	0.474	0	0.107
(c) Output matrix													
TAII 2011_1													
Prasinophytes	1	0	0.074	0	0	0	0.025	0	0.356	0	0.066	0	0.662
Chlorophytes	1	0	0.074	0	0	0	0.084	0	0	0	0.034	0	0.540
Cryptophytes	1	0	0	0	0	0	0	0	0	0.484	0	0	0
Diatoms	1	0	0	0	0.680	0	0	0	0	0	0	0	0
Pelagophytes	1	0	0	0.889	0.139	0	0	0.383	0	0	0	0	0
Dinoflagellates	1	0	0	0	0	0	0	0	0	0	0	0.770	0
Haptophytes	1	0	0	0.050	0.061	1.061	0	0.121	0	0	0	0	0
Synechococcus	1	0	0	0	0	0	0	0	0	0	0.893	0	0
Prochlorococcus	0	1	0	0	0	0	0	0	0	0	0.590	0	0.149
(d) Output matrix													
TAII 2011_2													
Prasinophytes	1	0	0.069	0	0	0	0.023	0	0.247	0	0.071	0	0.846
Chlorophytes	1	0	0.068	0	0	0	0.163	0	0	0	0.048	0	0.395
Cryptophytes	1	0	0	0	0	0	0	0	0	0.420	0	0	0
Diatoms	1	0	0	0	0.560	0	0	0	0	0	0	0	0
Pelagophytes	1	0	0	0.355	0.615	0	0	0.470	0	0	0	0	0
Dinoflagellates	1	0	0	0	0	0	0	0	0	0	0	0.721	0
Haptophytes	1	0	0	0.151	0.097	0.702	0	0.040	0	0	0	0	0
Synechococcus	1	0	0	0	0	0	0	0	0	0	2.453	0	0
Prochlorococcus	0	1	0	0	0	0	0	0	0	0	0.358	0	0.121
(e) Output matrix													
A10 2011													
Prasinophytes	1	0	0.075	0	0	0	0.024	0	0.074	0	0.083	0	1.070
Chlorophytes	1	0	0.097	0	0	0	0.133	0	0	0	0.040	0	0.348
Cryptophytes	1	0	0	0	0	0	0	0	0	0.616	0	0	0
Diatoms	1	0	0	0	0.593	0	0	0	0	0	0	0	0
Pelagophytes	1	0	0	0.966	0.248	0	0	0.235	0	0	0	0	0
Dinoflagellates	1	0	0	0	0	0	0	0	0	0	0	0.894	0
Haptophytes	1	0	0	0.060	0.053	0.730	0	0.175	0	0	0	0	0
Synechococcus	1	0	0	0	0	0	0	0	0	0	1.413	0	0
Prochlorococcus	0	1	0	0	0	0	0	0	0	0	0.495	0	0.122
(f) Output matrix													
FORSA 2015													
Prasinophytes	1	0	0.067	0	0	0	0.036	0	0.035	0	0.083	0	1.524
Chlorophytes	1	0	0.124	0	0	0	0.024	0	0	0	0.044	0	0.301
Cryptophytes	1	0	0	0	0	0	0	0	0	0.512	0	0	0
Diatoms	1	0	0	0	0.730	0	0	0	0	0	0	0	0
Pelagophytes	1	0	0	0.935	0.412	0	0	0.316	0	0	0	0	0
Dinoflagellates	1	0	0	0	0	0	0	0	0	0	0	0.566	0
Haptophytes	1	0	0	0.203	0.080	1.036	0	0.318	0	0	0	0	0
Synechococcus	1	0	0	0	0	0	0	0	0	0	3.241	0	0
Prochlorococcus	0	1	0	0	0	0	0	0	0	0	0.531	0	0.260

*CHEMTAX analysis showed some zea/chl a ratios higher than usually reported (0.2-2.5) (Higgins et al., 2011) for Synechococcus. We attribute these higher values to the fact that this is a minor group and the CHEMTAX approach tend to lead to elevated ratios.

Supplementary material

Table S2. Average percentage contribution of each phytoplankton group (prasino- prasinophytes, chloro- chlorophytes, crypto- cryptophytes, diato- diatoms, pelago- pelagophytes, dino- dinoflagellates, hapto- haptophytes, syn- *Synechococcus* and pro- *Prochlorococcus*) to the total chlorophyll *a* for each cruise.

		prasino%	chloro%	crypto%	diato%	pelago %	dino%	hapto%	syn%	pro%
BRZ	H40 2009	4.11	3.56	0,34	19.46	2.82	2.60	12.52	28.88	25.72
	TAI 2009_20°S	7.73	0.67	0.28	4.12	1.36	2.03	15.78	28.57	39.46
	TAII 2011_1	2.03	6.81	1.33	42.95	6.50	5.67	16.57	12.18	5.95
	TAII 2011_2	3.87	3.69	2.16	35.55	12.85	3.38	26.65	5.23	6.62
	A10	1.08	2.26	0.14	13.34	3.34	2.09	16.78	29.30	31.67
	Mean		3.76±2.55	3.40±2.26	0.85±0.87	23.08±15.95	5.37±4.58	3.15±1.51	17.66±5.31	20.83±11.34
SATL	H40 2009	1.17	4.30	0.01	8.50	2.82	2.80	12.14	35.26	33.01
	TAI 2009_30°S	8.39	4.83	0.55	3.20	4.58	3.89	15.40	31.06	28.11
	TAI 2009_20°S	9.98	6.94	0.92	6.50	3.46	2.89	14.99	35.69	18.65
	TAII 2011_1	2.24	8.90	0.48	7.86	13.83	2.44	37.62	16.62	10.01
	TAII 2011_2	1.74	2.56	0.17	8.97	5.36	4.90	31.83	19.02	25.44
	A10	3.04	3.58	0.05	4.98	6.21	2.51	23.70	21.96	33.97
	FORSA 2015	3.03	7.28	0.13	3.32	7.84	6.25	25.31	8.49	38.35
Mean		4.23±3.48	5.48±2.27	0.33±0.33	6.19±2.40	6.30±3.72	3.67±1.44	23.00±9.47	24.01±10.31	26.79±9.79
AFR	TAI 2009_30°S	13.98	2.36	2.10	8.25	6.94	4.57	48.69	8.65	4.46
	TAI 2009_20°S	13.82	2.73	1.86	20.32	4.97	6.26	37.72	11.54	0.77
	TAII 2011_2	3.87	3.69	2.16	35.55	12.85	3.38	26.65	5.23	6.62
	A10	10.34	5.06	1.30	9.54	9.09	10.03	41.02	8.64	4.98
Mean		10.50±4.73	3.46±1.20	1.86±0.39	18.42±12.64	8.46±3.38	6.06±2.90	38.52±9.15	8.52±2.58	4.21±2.47

Supplementary material

Table S3. Correlation matrices **a.** Using all data stations (n=311) gathered for this study; **b.** Using only Brazil province (BRZ) stations data (n=31); **c.** Using only South Atlantic Gyre province (SATL) stations data (n=237); **d.** Using only African province (AFR) stations data (n=43). Variables used in this correlation were: physico-chemical-biological parameters (temperature in °C, salinity, pCO₂^{sw} in µatm, NpCO₂^{sw} in µatm, DpCO₂ in µatm, wind in m.s⁻¹ and TChl *a* in mg.m⁻³) phytoplankton groups (prasino- prasinophytes, chloro- chlorophytes, crypto- cryptophytes, diato- diatoms, pelago- pelagophytes, dino- dinoflagelates, hapto- haptophytes, Syn- *Synechococcus* and Pro- *Prochlorococcus*).

a.

Correlations using all stations data (n=311)

Numbers marked in red mean significant correlations at $p < 0.05$

Variable	Mean	Std. dev.	Temp.	Sal.	pCO ₂ ^{sw}	NpCO ₂ ^{sw}	ΔpCO ₂ ^{sw}	wind	TChl <i>a</i>
Temperature	19.368	3.087	1	0.559	0.577	-0.396	0.552	0.037	-0.269
Salinity	35.864	0.716	0.559	1	0.115	-0.438	0.108	-0.104	-0.331
pCO₂^{sw}	351.974	17.163	0.577	0.115	1	-0.007	0.977	-0.014	-0.672
NpCO₂^{sw}	352.346	23.431	-0.396	-0.438	-0.007	1	-0.038	-0.043	-0.071
ΔpCO₂^{sw}	-32.720	18.404	0.552	0.108	0.977	-0.038	1	-0.065	-0.629
wind	6.059	2.440	0.037	-0.104	-0.014	-0.043	-0.065	1	0.148
TChl <i>a</i>	0.234	0.415	-0.269	-0.331	-0.672	-0.071	-0.629	0.148	1
prasino	0.015	0.033	-0.153	-0.226	-0.483	0.184	-0.467	0.207	0.668
chloro	0.010	0.016	-0.330	-0.342	-0.230	0.008	-0.243	0.201	0.347
crypto	0.003	0.013	-0.157	-0.267	-0.542	-0.087	-0.513	0.124	0.819
diatoms	0.046	0.266	-0.133	-0.231	-0.525	-0.136	-0.482	0.003	0.811
pelago	0.016	0.023	-0.490	-0.322	-0.498	0.021	-0.493	0.213	0.580
dino	0.014	0.060	-0.170	-0.204	-0.280	0.110	-0.263	0.038	0.581
hapto	0.072	0.145	-0.293	-0.270	-0.552	-0.006	-0.536	0.252	0.697
syn	0.033	0.034	-0.061	-0.135	-0.243	0.041	-0.249	0.166	0.369
pro	0.029	0.026	0.072	0.187	0.082	-0.139	0.059	0.050	-0.221

b.

Correlations using BRAZ stations data (n=31)

Numbers marked in red mean significant correlations at $p < 0.05$

Variable	Mean	Std. dev.	Temp.	Sal.	pCO ₂ ^{sw}	NpCO ₂ ^{sw}	ΔpCO ₂ ^{sw}	wind	TChl <i>a</i>
Temperature	22.741	2.642	1	0.702	-0.076	-0.224	-0.305	0.184	-0.544
Salinity	35.515	1.565	0.701	1	-0.516	-0.547	-0.476	0.368	-0.718
pCO ₂ ^{sw}	373.764	8.597	-0.076	-0.516	1	0.382	0.885	0.185	0.026
NpCO ₂ ^{sw}	334.930	24.787	-0.224	-0.547	0.382	1	0.073	-0.450	0.164
ΔpCO ₂ ^{sw}	-7.969	9.769	-0.305	-0.476	0.885	0.073	1	0.357	0.041
wind	8.114	2.207	0.184	0.368	0.185	-0.450	0.357	1	-0.435
TChl <i>a</i>	0.231	0.177	-0.544	-0.718	0.026	0.164	0.041	-0.434	1
prasino	0.007	0.007	0.097	-0.284	-0.006	0.408	-0.235	-0.585	0.451
chloro	0.010	0.017	-0.607	-0.669	0.051	0.091	0.106	-0.225	0.908
crypto	0.002	0.006	-0.478	-0.651	0.086	0.188	0.087	-0.307	0.889
diatoms	0.07	0.118	-0.614	-0.810	0.175	0.227	0.197	-0.425	0.956
pelago	0.009	0.009	-0.744	-0.555	-0.166	-0.017	-0.017	-0.181	0.757
dino	0.010	0.020	-0.505	-0.588	-0.031	0.079	0.005	-0.235	0.896
hapto	0.035	0.024	-0.550	-0.541	-0.179	0.038	-0.075	-0.307	0.846
syn	0.044	0.023	0.125	0.045	-0.223	-0.018	-0.271	-0.298	0.214
pro	0.040	0.023	0.756	0.709	-0.250	-0.245	-0.384	0.195	-0.525

c.

Correlations using SATL stations data (n=237)

Numbers marked in red mean significant correlations at $p < 0.05$

Variable	Mean	STd dev	Temp.	Sal.	pCO ₂ ^{sw}	NpCO ₂ ^{sw}	ΔpCO ₂ ^{sw}	wind	TChl <i>a</i>
Temperature	19.213	3.019	1	0.777	0.688	-0.416	0.644	-0.104	-0.432
Salinity	35.987	0.536	0.777	1	0.274	-0.622	0.285	-0.148	-0.306
pCO ₂ ^{sw}	352.485	11.557	0.688	0.274	1	0.022	0.951	-0.086	-0.533
NpCO ₂ ^{sw}	351.183	19.358	-0.416	-0.622	0.022	1	0.003	0.098	-0.074
ΔpCO ₂ ^{sw}	-32.550	12.795	0.644	0.285	0.951	0.003	1	-0.208	-0.520
wind	5.549	2.224	-0.104	-0.148	-0.086	0.098	-0.208	1	0.313
TChl <i>a</i>	0.140	0.146	-0.432	-0.305	-0.533	-0.074	-0.520	0.313	1
prasino	0.005	0.008	-0.083	-0.064	-0.301	-0.047	-0.302	0.221	0.563
chloro	0.009	0.017	-0.337	-0.278	-0.346	-0.051	-0.377	0.318	0.817
crypto	0.000	0.003	-0.150	-0.103	-0.324	-0.116	-0.329	0.068	0.686
diatoms	0.010	0.024	-0.219	-0.160	-0.379	-0.047	-0.409	0.139	0.635
pelago	0.014	0.022	-0.494	-0.353	-0.548	-0.060	-0.568	0.345	0.924
dino	0.005	0.011	-0.178	-0.156	-0.306	0.082	-0.365	0.157	0.336
hapto	0.043	0.065	-0.480	-0.362	-0.540	-0.010	-0.539	0.339	0.945
syn	0.028	0.021	-0.210	-0.135	-0.377	-0.118	-0.407	0.247	0.740
pro	0.031	0.027	-0.089	0.005	-0.182	0.005	-0.201	0.111	-0.052

d.

Correlations using AFR stations data (n=43)

Numbers marked in red mean significant correlations at $p < 0.05$

Variable	Mean	Std. dev.	Temp.	Sal.	pCO ₂ ^{sw}	NpCO ₂ ^{sw}	ΔpCO ₂ ^{sw}	wind	TChl <i>a</i>
Temperature	17.786	1.747	1	0.658	0.180	0.159	0.125	0.412	-0.339
Salinity	35.438	0.238	0.657	1	0.495	0.246	0.448	0.349	-0.746
pCO ₂ ^{sw}	333.454	25.844	0.180	0.495	1	0.685	0.996	-0.013	-0.870
NpCO ₂ ^{sw}	371.313	30.133	0.159	0.246	0.685	1	0.684	-0.364	-0.563
ΔpCO ₂ ^{sw}	-51.497	26.432	0.125	0.447	0.996	0.684	1	-0.081	-0.842
wind	7.392	2.509	0.412	0.349	-0.013	-0.363	-0.081	1	-0.141
TChl <i>a</i>	0.753	0.898	-0.339	-0.746	-0.870	-0.563	-0.842	-0.141	1
prasino	0.073	0.060	-0.014	-0.398	-0.395	-0.127	-0.406	0.078	0.508
chloro	0.015	0.012	-0.053	-0.022	-0.059	-0.006	-0.035	-0.366	0.118
crypto	0.019	0.029	-0.149	-0.645	-0.670	-0.564	-0.660	0.030	0.774
diatoms	0.227	0.684	-0.319	-0.592	-0.797	-0.488	-0.764	-0.193	0.847
pelago	0.034	0.027	-0.325	-0.411	-0.302	-0.255	-0.245	-0.363	0.535
dino	0.064	0.152	-0.363	-0.539	-0.222	-0.013	-0.20	-0.161	0.523
hapto	0.257	0.301	-0.088	-0.414	-0.471	-0.481	-0.476	0.151	0.531
Syn	0.053	0.071	0.160	-0.100	-0.163	0.117	-0.172	-0.065	0.186
Pro	0.010	0.012	-0.140	0.336	0.324	-0.108	0.348	-0.176	-0.388

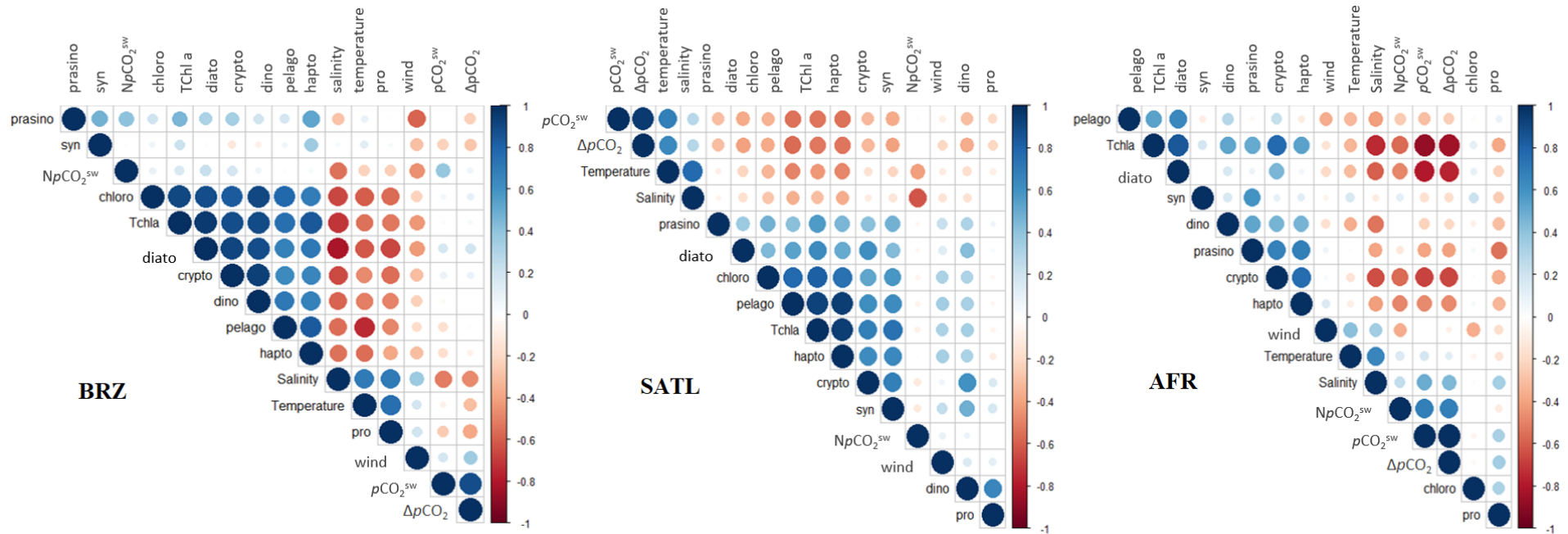


Figure S1. Correlations between physical-chemical and biological parameters. The physical-chemical parameters used in this correlation were: Temperature, salinity, wind, pCO_2^{sw} , $NpCO_2^{sw}$ and ΔpCO_2 and the biological: Tchl a, and the phytoplankton groups (prasino - prasinophytes, chloro-chlorophytes, crypto-cryptophytes, diato-diatoms, pelago- pelagophytes, dino- dinoflagellates, hacto- hactophytes, syn- *Synechococcus* and pro- *Prochlorococcus*) biomass for each province (BRZ, SATL and AFR).

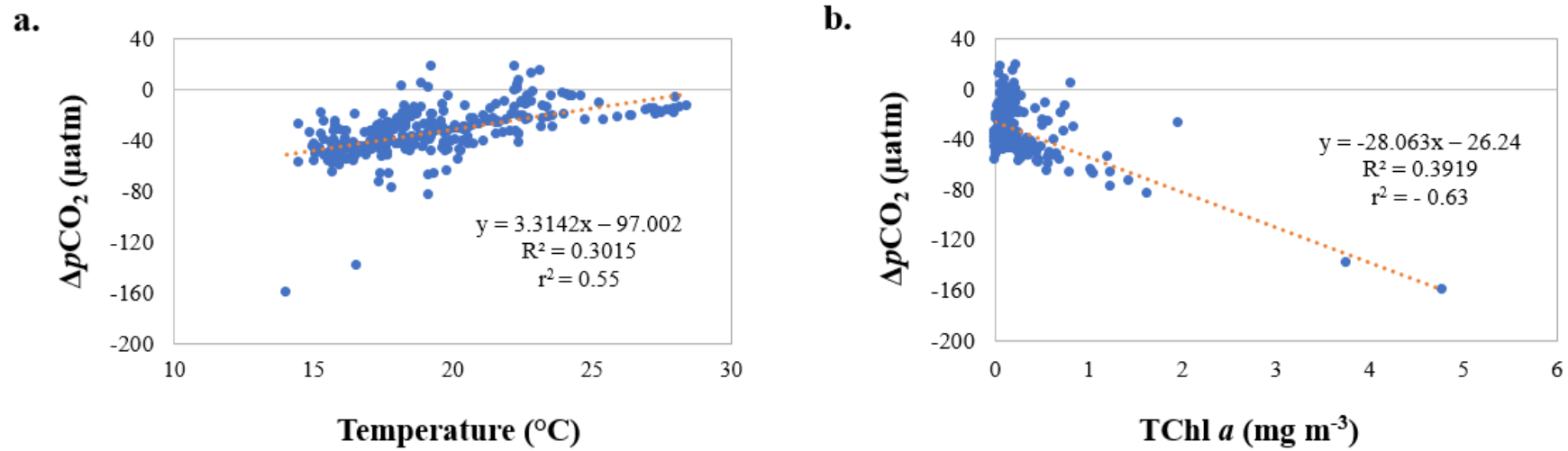


Figure S2. Basin-wide correlation of **(a)** sea surface temperature vs. $\Delta p\text{CO}_2$ (i.e. difference between CO_2 partial pressures in ocean and atmosphere) and **(b)** Total chlorophyll *a* (TChl *a*) vs. $\Delta p\text{CO}_2$.

Capítulo VIII: Referências Bibliográficas

Acha EM, Mianzan HW, Guerrero RA, Favero M, Bava J (2004), Marine fronts in the continental shelves of austral South America: Physical and ecological processes, *J. Mar. Syst.* 44:83– 105.

Aidar E, Gaeta, AS, Giancesella-Galvão SMF, Kutner MBB, Teixeira C. (1993) Ecossistema costeiro subtropical: nutrientes dissolvidos, fitoplâncton e clorofila-a e suas relações com as condições oceanográficas na região de Ubatuba, SP. Publicação Especial do Instituto Oceanográfico, 10, 9-43.

Aiken J, Pradhan Y, Barlow R, Lavender S, Poulton A, Holligan P, Hardman-Mountford N (2009) Phytoplankton pigments and functional types in the Atlantic Ocean: a decadal assessment, 1995–2005. *Deep-Sea Res. II.* 56:899–917.

Aiken J, Rees N, Hooker S, *et al.* (2000) The Atlantic meridional transect: overview and synthesis of data. *Prog. Oceanogr.* 45: 257-312.

Alexander H, Rouco M, Haley ST, Wilson ST, Karl DM and Dyhrman ST (2015) Functional group-specific traits drive phytoplankton dynamics in the oligotrophic ocean. *Proc. Natl. Acad. Sci. USA* 112, E5972–E5979. doi: 10.1073/pnas.1518165112

Alvain S, Le C, Bopp L, Racault M, Beaugrand G, Dessailly D and Buitenhuis ET (2013) Remote Sensing of Environment Rapid climatic driven shifts of diatoms at high latitudes. *Remote Sensing of Environment* 132:195–201. doi: 10.1016/j.rse.2013.01.014

Amin SA, Parker MS, Armbrust EV (2012) Interactions between diatoms and bacteria. *Microbiol. Mol. Biol. Rev.* 76(3):667. doi:10.1128/MMBR.00007-12.

Aminot A, Chaussepied M (1983) Manuel des analyses chimiques en milieu marin. Editions Jouve, CNEXO, Paris, 395 p.

Angel MV, Fasham MJR (1983) Eddies and Biological Processes. In: Robinson A.R. (eds) *Eddies in Marine Science. Topics in Atmospheric and Oceanographic Sciences.* Springer, Berlin, Heidelberg

- Angel-benavides IM, Pilo G, Dias, FB and Garcia, CAE (2016) Influência de vórtices de mesoescala na concentração de clorofila da confluência Brasil-Malvinas: mecanismos inferidos por sensoriamento remoto. *Braz. J. Aquat. Sci. Technol.*, 20(1):10–20. doi:10.14210/bjast.v20n1
- Araujo, MLV, Mendes CRB, Tavano VM, Garcia CAE and Baringer, MO (2017) Contrasting patterns of phytoplankton pigments and chemotaxonomic groups along 30°S in the subtropical South Atlantic Ocean. *Deep Sea Res. I: Oceanographic Research Papers*, 120:112–121. doi:10.1016/j.dsr.2016.12.004
- Arrigo KR, Robinson DH, Worthen DL, Dunbar RB, DiTullio GR, VanWoert M. and Lizotte MP (1999) Phytoplankton Community Structure and the Drawdown of Nutrients and CO₂ in the Southern Ocean. *Science* 283:365–367. doi:10.1126/science.283.5400.365
- Arrigo, KR (2005). Marine microorganisms and global nutrient cycles. *Nature (Lond.)* 437(7057): 349-355. doi:10.1038/nature04158
- Arruda R, Calil PHR, Bianchi AA, Doney SC, Gruber N, Lima I, Turi G (2015) Air-sea CO₂ fluxes and the controls on ocean surface pCO₂ seasonal variability in the coastal and open-ocean southwestern Atlantic Ocean: a modeling study. *Biogeosc.* 12, 5793–5809. doi:10.5194/bg-12-5793-2015.
- Azevedo JLL, Nof D, Mata MM (2012) Eddy-train encounters with a continental boundary: a South Atlantic case study. *J. Phys. Oceanogr.* 42, 1548–1565.
- Bach LT, Hernández-Hernández N, Taucher J, Spisla C, Sforna C, Riebesell U, Arístegui J (2019) Effects of Elevated CO₂ on a Natural Diatom Community in the Subtropical NE Atlantic. *Front. in Mar. Sci.* 6:75 doi :0.3389/fmars.2019.00075.
- Badger MR, Andrews TJ, Whitney SM, Ludwig M, Yellowlees DC, Leggat W, Price GD (1998) The diversity and coevolution of Rubisco, plastids, pyrenoids, and chloroplast-based CO₂-concentrating mechanisms in algae. *Canadian Journal of Botany* 76(6):1052-1071. doi:10.1139/b98-074.
- Barlow R, Gibberd MJ, Lamont T, Aiken J, Holligan P (2016) Chemotaxonomic phytoplankton patterns on the eastern boundary of the Atlantic Ocean. *Deep-Sea Res. I: Oceanographic Research Papers*, 111:73–78. doi:10.1016/j.dsr.2016.02.011
- Barlow R, Lamont T, Gibberd M, Airs R, Jacobs L, Britz K (2017) Phytoplankton communities and acclimation in a cyclonic eddy in the southwest Indian Ocean. *Deep. Res. I* 124, 18–30. doi:10.1016/j.dsr.2017.03.013
- Barroso HS, Becker H, Melo VMM (2016) Influence of river discharge on phytoplankton structure and nutrient concentrations in four tropical semiarid estuaries. *Braz Jour of Ocean* 64(1):37-48 doi:10.1590/S1679-87592016101406401.
- Barton AD, Dutkiewicz S, Flierl G, Bragg J, Follows MJ (2010) Patterns of Diversity in Marine Phytoplankton *Science* 327: 1509 DOI: 10.1126/science.1184961
- Basu S, Mackey, KRM (2018) Phytoplankton as key mediators of the biological carbon pump: Their responses to a changing climate. *Sustainability (Switzerland)*. MDPI AG. doi:10.3390/su10030869
- Bauer JE, W-J Cai, Raymond PA, Bianchi TS, Hopkinson CS, Regnier PAG (2013) The changing carbon cycle of the coastal ocean. *Nature* 504:63-70. doi:10.1038/nature12857
- Beal LM, Chereskin TK, Lenn YD, Elipot S (2006) The Sources and Mixing Characteristics of the Agulhas Current. *J. Phys. Oceanogr.* 36:2060–2074. doi:10.1175/JPO2964.1
- Beal LM, De Ruijter WPM, Biastoch A, Zahn R & SCOR/WCRP/IAPSO Working Group 136 (2016) On the role of the Agulhas system in ocean circulation and climate *Nature* 472(7344):429-436 doi: 10.1038/nature09983
- Baugrand G, Edwards M, Legendre L (2010) Marine biodiversity, ecosystem functioning, and carbon cycles (2010) *PNAS* 107(22):10120-4. doi: 10.1073/pnas.0913855107
- Behrenfeld MJ, Boss E, Siegel DA and Shea DM (2005) Carbon-based ocean productivity and phytoplankton physiology from space. *Glob Biogeo Cycles*19(1):1–14. doi: 10.1029/2004GB002299

- Bennington V, McKinley GA, Dutkiewicz S, Ullman D (2009) What does chlorophyll variability tell us about export and air–sea CO₂ flux variability in the North Atlantic? *Global Biogeochemical Cycles*, 23, GB3002 doi:10.1029/2008GB003241.
- Bergo NM, Signori CN, Amado AM, Brandini FP, Pellizari VH (2017) The partitioning of carbon biomass among the Pico- and nano-plankton community in the South Brazilian bight during a strong summer intrusion of south atlantic central water. *Front. Mar. Sci.* 4:238. doi: 10.3389/fmars.2017.00238
- Bianchi A A, L. Bianucci, A. R. Piola, D. R. Pino, I. Schloss, A. Poisson, and C. F. Balestrini (2005), Vertical stratification and air-sea CO₂ fluxes in the Patagonian shelf, *J. Geophys. Res.*, 110, C07003, doi:10.1029/2004JC002488
- Bianchi AA, Pino DR, Perlender HGI, Osiroff AP, Segura V, Lutz V, Clara ML, Balestrini, CF and Piola AR (2009) Annual balance and seasonal variability of sea–air CO₂ fluxes in the Patagonia Sea: their relationship with fronts and chlorophyll distribution, *J. Geophys. Res.* 114, C03018. doi:10.1029/2008JC004854.
- Biaostoch A, Beal LM, Casal TGD, Lutjeharms JRE (2009) Variability and coherence of the Agulhas Undercurrent in a high-resolution ocean general circulation model. *J. Phys. Oceanogr.* 39, 2417–2435 doi:
- Bibby TS, Gorbunov MY, Wyman KW, Falkowski PG (2008) Photosynthetic community responses to upwelling in mesoscale eddies in the subtropical North Atlantic and Pacific Oceans. *Deep. Res. Part II Top. Stud. Oceanogr.* 55:1310–1320. doi:10.1016/j.dsr2.2008.01.014
- Bibby TS, Moore CM (2011) Silicate:nitrate ratios of upwelled waters control the phytoplankton community sustained by mesoscale eddies in sub-tropical North Atlantic and Pacific. *Biogeosciences* 8:657–666. doi:10.5194/bg-8-657-2011
- Biller SJ, Berube PM, Lindell D, Chisholm SW (2014). function of collective diversity. *Nature Publishing Group*, 13(1): 13–27. doi: 10.1038/nrmicro3378
- Bopp L, Aumont O, Cadule P, Alvain S, Gehlen M (2005) Response of diatoms distribution to global warming and potential implications: A global model study. *Geophys Res Lett* 32:L19606. doi:10.1029/2005GL023653
- Bopp L, Resplandy L, Orr JC, Doney SC, Dunne JP, Gehlen M, Halloran P, et al (2013) Multiple stressors of ocean ecosystems in the 21st century: projections with CMIP5 models, *Biogeosciences*, 10, 6225–6245, doi:10.5194/bg-10-6225-2013.
- Borges AV, Delille B, Frankignoulle M (2005) Budgeting sinks and sources of CO₂ in the coastal ocean: Diversity of ecosystems counts, *Geophys. Res. Lett.* 32: L14601. doi:10.1029/2005GL023053.
- Boyd PW (2015) Toward quantifying the response of the oceans' biological pump to climate change. *Front. Mar. Sci.* 2:77. doi: 10.3389/fmars.2015.00077
- Braga ES, Chiozzini VC, Berbel GBB, Maluf JCC, Aguiar VMC, Charo M, Molina D, Romero SI, Eichler BB (2008) Nutrient distributions over the Southwestern South Atlantic continental shelf from Mar del Plata (Argentina) to Itajaí (Brazil): winter-summer aspects. *Cont. Shelf Res.* 28: 1649–1661.
- Brandini F, Michelazzo LS, Freitas GR, Campos G, Chuqui M, Jovane L (2019) Carbon Flow for Plankton Metabolism of Saco do Mamanguá Ria, Bay of Ilha Grande, a Subtropical Coastal Environment in the South Brazil Bight. *Front. Mar Sci* 6:584. doi:10.3389/fmars.2019.00584
- Brandini FP, Boltovskoy D, Piola A, Kocmur S, Röttgers R, Abreu PC, Mendes LR (2000) Multiannual trends in fronts and distribution of nutrients and chlorophyll in the southwestern Atlantic (30–62° S). *Deep-Sea Res I: Oceanographic Research Papers* 47:1015–1033 DOI 10.1016/S0967-0637(99)00075-8.
- Brandini FP, Nogueira M, Simião M, Carlos Ugaz Codina J, Almeida Noernberg M, Pereira F, Nogueira M, Simião M, Carlos J, Codina U, Almeida M. (2014) Deep chlorophyll maximum and plankton community response to oceanic bottom intrusions on the continental shelf in the South Brazilian Bight. *Cont Shelf Res* 89:61–75 DOI 10.1016/j.csr.2013.08.002
- Brandini, FP (1990). Hydrography and characteristics of the phytoplankton in shelf and oceanic

- waters off southeastern Brazil during winter (July/August 1982) and summer (February/March 1984). *Hydrobiologia* 196, 111–148. doi: 10.1007/BF00006105
- Burrage D, Wesson J, Martinez C, Pérez T, Möller Jr. O, Piola, A (2008) Patos Lagoon outflow within the Rio de la Plata plume using an airborne salinity mapper: Observing an embedded plume. *Cont Shelf Res* 28:1625–1638.
- Cabré A, Marinov I, Bernardello R, Bianchi D (2015) Oxygen minimum zones in the tropical Pacific across CMIP5 models: mean state differences and climate change trends *Biogeosciences*, 12:5429–5454. doi:10.5194/bg-12-5429-2015
- Cai W-J (2011) Estuarine and coastal ocean carbon paradox: CO₂ sinks or sites of terrestrial carbon incineration? *Annu. Rev. Mar. Sci.* 3:123–145 doi:10.1146/annurev-marine-120709-142723
- Cai W-J, Dai M, Wang Y (2006), Air-sea exchange of carbon dioxide in ocean margins: A province-based synthesis, *Geophys. Res. Lett.*, 33, L12603, doi:10.1029/2006GL026219.
- Cai W-J. (2003) Riverine inorganic carbon flux and rate of biological uptake in the Mississippi River plume. *Geophys. Res. Lett.* 30:1032
- Campos EJD, Velhote D, Silveira ICA (2000) Shelf break upwelling driven by Brazil Current cyclonic meanders, *Geophys. Res. Lett.* 27:751–754.
- Cao Z, Dai M, Zheng N, Wang D, Li Q, Zhai W, Meng F, Gan J (2011) Dynamics of the carbonate system in a large continental shelf system under the influence of both a river plume and coastal upwelling. *J. Geophys. Res.* 116:G02010. doi: 10.1029/2010JG001596
- Cao L, Zhang H (2017) The role of biological rates in the simulated warming effect on oceanic CO₂ uptake, *J. Geophys. Res. Biogeosci.*, 122, 1098-1106, doi:10.1002/2016JG003756.
- Cao Z, Yang W, Zhao Y, Guo X, Yin Z, Du C, Zhao H, Dai M (2020) Diagnosis of CO₂ dynamics and fluxes in global coastal oceans *National Science Review* 7(4)786–797. Doi:10.1093/nsr/nwz105
- Capone D, Hutchins D (2013) Microbial biogeochemistry of coastal upwelling regimes in a changing ocean. *Nature Geosci* 6:711–717. Doi:10.1038/ngeo1916
- Carstensen J, Chierici M, Gustafsson BG, Gustafsson E (2018) Long-term and seasonal trends in estuarine and coastal carbonate systems. *Glob Biogeo Cycles* 32:497–513. doi: 10.1002/2017GB005781
- Carvalho-Borges M De, Orselli IBM, Luiza M, Ferreira, DC, Kerr R (2018) Seawater acidification and anthropogenic carbon distribution on the continental shelf and slope of the western South Atlantic Ocean. *Journal Mar Sys* 187: 62–81. doi:10.1016/j.jmarsys.2018.06.008
- Castelão RM, Barth JA (2006) Upwelling around Cabo Frio, Brazil: The importance of wind stress curl. *Geophys. Res. Lett.* 33: L03602- L03605 doi:10.1029/2005GL025182.
- Castro BM, Brandini FP, Pires-Vanin AMS, Miranda LB (2006) Multidisciplinary oceanographic processes on the western Atlantic continental shelf between 4°N and 34°S. *The Sea*. 11:209–251.
- Castro, BM Miranda LB (1998), Physical oceanography of the western Atlantic Continental Shelf located between 4°N and 34°S coastal segment (4, w). *The Sea*, 11, 209-251.
- Cavender-Bares KK, Karl DM, Chisholm SW (2001) Nutrient gradients in the western North Atlantic Ocean: Relationship to microbial community structure and comparison to patterns in the Pacific Ocean. *Deep-Sea Res I* 48:2373–2395. doi: 10.1016/s0967-0637(01)00027-9
- Cermeño P, Dutkiewicz S, Harris RP, Follows M, Schofield O, Falkowski PG (2008). The role of nutricline depth in regulating the ocean carbon cycle. *PNAS* 105(51), 20344–20349. doi:10.1073/pnas.0811302106
- Chang Y-L, Miyazawa Y, Oey L-Y, Kodaira T, Huang S (2017) The formation processes of phytoplankton growth and decline in mesoscale eddies in the western North Pacific Ocean. *J Geophys. Res. Ocean* 122:4444–4455. doi:10.1002/2017JC012722
- Chelton DB, Behrenfeld MJ, Strutton PG (2014) Regional variations in the influence of mesoscale eddies on near-surface chlorophyll. *J. Geophys. Res. Oceans* 119:8195–8220.

doi:10.1002/2014JC010111.

Chelton DB, Schlax, MG, Samelson, RM (2011) Global observations of nonlinear mesoscale eddies. *Prog. Oceanogr.* 91:167–216. doi:10.1016/j.pocean.2011.01.002

Chen C-TA, Andreev A, Kim K-R, Yamamoto M (2004) Roles of continental shelves and marginal seas in the biogeochemical cycles of the North Pacific Ocean. *J. Oceanogr.* 60:17–44.

Chen C-TA, Borges AV (2009) Reconciling opposing views on carbon cycling in the coastal ocean: continental shelves as sinks and near-shore ecosystems as sources of atmospheric CO₂. *Deep-Sea Res II* 2009; 56: 578–90 doi:10.1016/j.dsr2.2009.01.001

Chen C-TA, Huang T-H, Chen Y-C, Bai Y, He X, Kang Y (2013) Air–sea exchanges of CO₂ in the world's coastal seas. *Biogeosciences* 10:6509–6544. doi:10.5194/bg-10-6509-2013

Chen YLL, Chen HY, Karl DM, Takahashi M (2004) Nitrogen modulates phytoplankton growth in spring in the South China Sea. *Cont. Shelf Res.* 24:527–541.

Chen YLL, Chen HY, Lin II, Lee MA, Chang J (2007) Effects of cold eddy on phytoplankton production and assemblages in Luzon strait bordering the South China Sea. *J. Oceanogr.* 63: 671–683. doi:10.1007/s10872-007-0059-9

Chenillat F, Franks PJS, Combes V (2016) Biogeochemical properties of eddies in the California Current System *Geo Res Lett* 43:5812–5820. doi:10.1002/2016GL068945.

Ciavatta S, Brewin RJW, Skákala J, Polimene L, de Mora L, Artioli Y, Allen JI (2018) Assimilation of Ocean-Color Plankton Functional Types to Improve Marine Ecosystem Simulations. *J Geo Res: Oceans* 123(2), 834–854. doi:10.1002/2017JC013490

Ciotti AM, Odebrecht C, Fillmann G, Jr OM (1995) Freshwater outflow and Subtropical Convergence influence on phytoplankton biomass on the southern Brazilian Continental shelf. *Cont Shelf Res*15(14):1737–1756. doi: 10.1016/0278-4343(94)00091-Z

Ciotti, AM, Garcia CAE, Jorge D (2010) Temporal and meridional variability of Satellite-estimates of surface chlorophyll concentration over the Brazilian continental shelf. *Pan-American Journal of Aquatic Sciences*, 5(2): 236-253.

Claustre H, Babin M, Merien D, Ras J, Prieur L, Dallot S et al (2005) Towards a taxon-specific parameterization of bio-optical models of primary production: a case study in the North Atlantic. *J. Geophys. Res.* 110:C07S12. doi: 10.1029/2004JC002634

Collins S, Rost B, Rynearson TA (2014) Evolutionary potential of marine phytoplankton under ocean acidification. *Evol. Appl.* 7:140–155. doi: 10.1111/eva.12120

Condie S, Condie R, Bates A (2016) Retention of plankton within ocean eddies. *Glob. Ecol. Biogeogr.* 25:1264–1277. doi:10.1111/geb.12485

Cotti-Rausch, B.E., Lomas, M.W., Lachenmyer, E.M., Goldman, E.A., Bell, D.W., Goldberg, S.R., Richardson, T.L. (2016). Mesoscale and sub-mesoscale variability in phytoplankton community composition in the Sargasso Sea. *Deep Sea Research Part I: Oceanographic Research Papers* (110) 106-122. doi:10.1016/j.dsr.2015.11.008.

Cotti-Rausch, B.E., Lomas, M.W., Lachenmyer, E.M., Baumann, E.G., Richardson, T. L. (2020) Size-fractionated biomass and primary productivity of Sargasso Sea phytoplankton. *Deep Sea Research Part I: Oceanographic Research Papers*,156,103141. doi:10.1016/j.dsr.2019.103141.

Coupe P, Matsuoka A, Ruiz-Pino D, Gosselin M, Marie D, Tremblay JE, Babin M (2015) Pigment signatures of phytoplankton communities in the Beaufort Sea. *Biogeosciences* 12: 991–1006. doi:10.5194/bg-12-991-2015

Craig SE, Thomas H, Jones CT, Li WKW, Greenan BJW, Shadwick EH, Burt WJ (2015) The effect of seasonality in phytoplankton community composition on CO₂ uptake on the Scotian Shelf. *J Mar Sys.* 147:52-60. doi: 10.1016/j.jmarsys.2014.07.006

Craig SE, Thomas H, Jones CT, Li WKW, Greenan BJW, Shadwick EH, Burt WJ (2013) Temperature and phytoplankton cell size regulate carbon uptake and carbon overconsumption in the ocean. *Biogeosciences Discuss.* 10:11255–11282. doi: 10.5194/bgd-10-11255-2013

- Cullen JJ, Franks PJS, Karl DM, Longhurst A (2002) Physical Influences on Marine Ecosystem Dynamics. *The Sea*, Vol. 12; Allan R. Robinson, James J. McCarthy, ed., New York: John Wiley and Sons, Inc.
- de Boyer Montégut C, Madec G, Fischer AS, Lazar A, Iudicone D (2004) Mixed layer depth over the global ocean: An examination of profile data and a profile-based climatology. *J. Geophys. Res. C Ocean*. 109:1–20. doi:10.1029/2004JC002378
- Demarcq H, Barlow R, Hutchings L (2007). Application of a chlorophyll index derived from satellite data to investigate the variability of phytoplankton in the Benguela ecosystem, *African J Mar Sci* 29(2): 271-282. doi: 10.2989/AJMS.2007.29.2.11.194
- Demir-Hilton E, Sudek S, Cuvelier M (2011) Global distribution patterns of distinct clades of the photosynthetic picoeukaryote *Ostreococcus*. *ISME J* 5, 1095–1107 doi:10.1038/ismej.2010.209
- de Souza AGQ, Kerr R, Azevedo JLL (2018) On the influence of Subtropical Mode Water on the South Atlantic Ocean, *J Mar Sys* 185:13-24. doi:10.1016/j.jmarsys.2018.04.006.
- Dvořák P, Casamatta DA, Hašler P, Jahodářová E, Norwich AR, Pouličková A (2017) Diversity of the Cyanobacteria. In: Hallenbeck P. (eds) *Modern Topics in the Phototrophic Prokaryotes*. Springer, Cham. doi:10.1007/978-3-319-46261-5_1
- Dickson AG (1981) An exact definition of total alkalinity and a procedure for the estimation of alkalinity and total inorganic carbon from titration data. *Deep Sea Res. Part A. Oceanogr. Res. Papers* 28 (6): 609-623
- Dickson AG (2010) The carbon dioxide system in seawater: equilibrium chemistry and measurements U. Riebesell, V.J. Fabry, L. Hansson, J.-P. Gattuso (Eds.) *Guide to Best Practices for Ocean Acidification Research and Data Reporting*, Publications Office of the European Union Luxembourg (2010), p. 260
- Dickson AG, Sabine CL, Christian JR (Eds.) *Guide to best practices for ocean CO2 measurements*. PICES Special Publication 3, p.191, 2007.
- Doney SC, Busch DS, Cooley SR, Kroekert KJ (2020) The Impacts of Ocean Acidification on Marine Ecosystems and Reliant Human Communities *Annual Review of Environment and Resources* 2020 45:1
- Dong S, Goni G, Bringas F (2015) Temporal variability of the south Atlantic Meridional overturning circulation between 20°S and 35°S. *Geoph Res Lett* 42:7655-7662. Doi: 10.1002/2015GL065603
- Dufresne A, Garczarek L, Partensky F (2005) Accelerated evolution associated with genome reduction in a free-living prokaryote. *Genome Biol* 6, R14. doi:10.1186/gb-2005-6-2-r14
- Duncombe Rae CM (1991) Agulhas retroflection rings in the South Atlantic Ocean: an overview. *South African J. Mar. Sci.* 11:327–344. doi:10.2989/025776191784287574
- Durall C, Lindblad P (2015) Mechanisms of carbon fixation and engineering for increased carbon fixation in cyanobacteria. *Algal Research* 11:263–270 doi: 10.1016/j.algal.2015.07.002
- Durgadoo JV, Rühls S, Biastoch A, Böning CWB (2017) Indian Ocean sources of Agulhas Leakage. *J Geophys Res: Ocean* 3481–3499. doi:10.1002/2016JC012676
- Dutkiewicz S, Morris JJ, Follows MJ, Scott J, Levitan O, Dyhrman ST, Berman-Frank I (2015) Impact of ocean acidification on the structure of future phytoplankton communities. *Nat. Clim. Chang.* 5:1002–1006.
- Eden C, Dietze H (2009) Effects of mesoscale eddy/wind interactions on biological new production and eddy kinetic energy. *J. Geophys. Res. Ocean.* 114:1–13. doi:10.1029/2008JC005129
- Endo H, Ogata H, Suzuki K (2018) Contrasting biogeography and diversity patterns between diatoms and haptophytes in the central Pacific Ocean. *Sci Rep* 8, 10916 (2018) doi:10.1038/s41598-018-29039-9
- Enochs IC, Manzello DP, Jones PR, Stamates SJ and Carsey TP (2019) Seasonal Carbonate Chemistry Dynamics on Southeast Florida Coral Reefs: Localized Acidification Hotspots From Navigational Inlets. *Front. Mar. Sci.* 6:160. doi: 10.3389/fmars.2019.00160

- Eyre BD, Ferguson AJP (2005) Benthic metabolism and nitrogen cycling in a sub-tropical east Australian estuary (Brunswick)—temporal variability and controlling factors. *Limnol Oceanogr* 50:81–96
- Falkowski P.G., Laws E.A., Barber R.T., Murray J.W. (2003) Phytoplankton and Their Role in Primary, New, and Export Production. In: Fasham M.J.R. (eds) *Ocean Biogeochemistry. Global Change — The IGBP Series* (closed). Springer, Berlin, Heidelberg. https://doi.org/10.1007/978-3-642-55844-3_5
- Fay AR, McKinley, GA (2017) Correlations of surface ocean pCO₂ to satellite chlorophyll on monthly to interannual timescales. *Global Biogeochem. Cycles* 31: doi: 10.1002/2016GB005563.
- Feely RA, Alin SR, Newton J, Sabine CL, Warner M, Devol A, Krembs C, Maloy C (2010) The combined effects of ocean acidification, mixing, and respiration on pH and carbonate saturation in an urbanized estuary. *Estuarine, Coastal Shelf Sci.* 88:442–49 *Estuarine Coastal and Shelf Science* doi: 10.1016/j.ecss.2010.05.004
- Feely RA, Sabine CL, Takahashi T, Wanninkhof R (2001) Uptake and storage of carbon dioxide in the ocean: The global CO₂ survey. *Oceanography* 14(4):18–32, doi:10.5670/oceanog.2001.03.
- Fernandes LF, Brandini FP (2004) Diatom associations in shelf waters off Paraná State, Southern Brazil: annual variation in relation to environmental factors. *Brazilian Journal of Oceanography*, 52(1), 19-34. doi: 10.1590/S1679-87592004000100003
- Ferreira A, Stramski D, Garcia CAE, Garcia VMT, Ciotti AM, Mendes CRB (2013) Variability in light absorption and scattering of phytoplankton in Patagonian waters: Role of community size structure and pigment composition, *J. Geophys. Res. Oceans* 118. doi:10.1002/jgrc.20082.
- Finkel ZV, Beardall J, Flynn KJ, Quigg A, Rees TAV, Raven JA (2010). Phytoplankton in a changing world: Cell size and elemental stoichiometry. *Journal Plank Res* 32(1):119–137. doi:10.1093/plankt/fbp098
- Finkel ZV, Sebbo J, Feist-Burkhardt S. *et al.* (2007) A universal driver of macroevolutionary change in the size of marine phytoplankton over the Cenozoic. *Proc. Natl Acad. Sci. USA*, 104, 20416–20420
- Flombaum P, Gallegos JL, Gordillo RA, Rincón J, Zabala LL, Jiao N (2013) Present and future global distributions of the marine Cyanobacteria *Prochlorococcus* and *Synechococcus*. *PNAS* 110:9824–9829 doi:10.1073/pnas.1307701110.
- Friedlingstein P, Jones MW, O'Sullivan M, Andrew RM, Hauck J, Peters GP, Peters W, et al (2019) Global Carbon Budget. *Earth Syst. Sci. Data*, 11 (4), 1783–1838 doi:10.5194/essd-11-1783-2019
- Gao W, Wang Z, Zhang K (2017) Controlling effects of mesoscale eddies on thermohaline structure and in situ chlorophyll distribution in the western North Pacific. *J. Mar. Syst.* 175:24–35. doi:10.1016/j.jmarsys.2017.07.002
- Garcia CAE, Sarma YVB, Mata MM, Garcia VMT (2004) Chlorophyll variability and eddies in the Brazil-Malvinas Confluence region. *Deep Sea Res. II* 51:159– 172.
- Garcia VMT, Garcia CAE, Mata MM, Pollery RC, Piola AR, Signorini SR, McClain CR, Iglesias-Rodriguez MD (2008) Environmental factors controlling the phytoplankton blooms at the Patagonia shelf-break in spring. *Deep-Sea Res I: Oceanographic Research Papers*, 55(9), 1150–1166. doi:10.1016/j.dsr.2008.04.011.
- Gaube P, Chelton DB, Strutton PG, Behrenfeld MJ (2013) Satellite observations of chlorophyll, phytoplankton biomass, and Ekman pumping in nonlinear mesoscale eddies. *J. Geophys. Res. Ocean.* 118, 6349–6370. doi:10.1002/2013JC009027
- Gayoso AM, Podestá GP (1996) Surface hydrography and phytoplankton of the Brazil-Malvinas currents confluence, *Journal of Plankton Research*, 18(6): 941–951. doi:10.1093/plankt/18.6.941
- Gérikas Ribeiro C, dos Santos AL, Marie D, Pellizari VH, Brandini FP, Vaultot D (2016) Pico and nanoplankton abundance and carbon stocks along the Brazilian Bight *PeerJ* 4:e2587. doi:10.7717/peerj.2587
- Godrijan J, Drapeau D, Balch WM (2020). Mixotrophic uptake of organic compounds by

- coccolithophores. *Limnology and Oceanography* 00:(1–12). Doi:10.1002/lno.11396.
- Gonçalves-Araujo R, De Souza MS, Mendes CRB, Tavano VM, Pollery RC, Garcia CAE (2012) Brazil-Malvinas confluence: effects of environmental variability on phytoplankton community structure. *J. Plankton Res.* 34:399–415. doi: 10.1093/plankt/fbs013
- Goncalves-Araujo R, De Souza MS, Tavano VM, Garcia CAE (2015) Influence of oceanographic features on spatial and interannual variability of phytoplankton in the Bransfield Strait, Antarctica. *J Mar Sys* 142 :1-15. doi: 10.1016/j.jmarsys.2014.09.007
- Goncalves-Araujo R, De Souza MS, Mendes CRB, Tavano VM, Garcia CAE (2016) Seasonal change of phytoplankton (spring vs. summer) in the southern Patagonian shelf, Cont Shelf Res 124:142-152. doi:10.1016/j.csr.2016.03.023.
- González-Dávila M, Santana-Casiano JM, Ucha IR (2009) Seasonal variability of fCO₂ in the Angola-Benguela region. *Prog Ocean* 83(1–4):124–133. doi:10.1016/j.pocean.2009.07.033
- Gregor L, Monteiro PMS (2013) Is the southern benguela a significant regional sink of CO₂? *South African Journal of Science* 109(5–6): 1–5. Doi:10.1590/SAJS.2013/20120094
- Gruber N (2015) Ocean biogeochemistry: Carbon at the coastal interface *Nature* 517(7533) DOI: 10.1038/nature14082
- Guenther M, Gonzalez-Rodriguez E, Carvalho WF, Rezende CE, Mugrabe G., Valentin JL (2008) Plankton trophic structure and particulate organic carbon production during a coastal downwelling-upwelling cycle. *Mar. Ecol. Prog. Ser.* 363:109-119
- Guerra LAA, Paiva AM, Chassignet EP (2018) On the translation of Agulhas rings to the western South Atlantic Ocean. *Deep-Sea Res. I* 2018, 139, 104–113.
- Guidi L, Chaffron S, Bittner L, Eveillard D, Larhlimi A, Roux S, Darzi Y, et al (2016) Plankton networks driving carbon export in the oligotrophic ocean. *Nature* 532:465–470 DOI 10.1038/nature16942.
- Guidi L, Stemmann L, Jackson GA (2009). Effects of phytoplankton community on production, size and export of large aggregates: A world-ocean analysis. 54(6), 1951–1963.
- Haidar AT, Thierstein HR (2001) Coccolithophore dynamics off Bermuda (N. Atlantic). *Deep-Sea Res. II*, 48 (2001), pp. 1925-1956.
- Hammer, Øyvind, Harper DAT, Ryan PD, (2001) Past: Paleontological Statistics Software Package for Education and Data Analysis. *Palaeontologia Electronica*, vol. 4, issue 1, art. 4: 9pp., 178kb.
- Hardman-Mountford NJ, Richardson AJ, Agenbag JJ, Hagen E, Nykjaer L, Shillington FA, Villacastin C. (2003). Ocean climate of the South East Atlantic observed from satellite data and wind models. *Progress in Oceanography*, 59(2–3), 181–221 doi:10.1016/j.pocean.2003.10.001
- Hartmann M, Grob C, Tarran GA, Martin AP, Burkill PH, Scanlan DJ, Zubkov MV (2012) Mixotrophic basis of Atlantic oligotrophic ecosystems. *PNAS* 109: 5756–5760 doi:10.1073/pnas.1118179109
- He Q, Zhan H, Cai S, Li Z (2016) Eddy effects on surface chlorophyll in the northern South China Sea: mechanism investigation and temporal variability analysis. *Deep. Res. Part I Oceanogr. Res. Pap.* 112:25–36. doi:10.1016/j.dsr.2016.03.004.
- Higgins H, Wright S, Schluter L (2011) Quantitative interpretation of chemo-taxonomic pigment data. In: Roy, S., Llewellyn, C., Egeland, E., Johnsen, G. (Eds.), *Phytoplankton Pigments: Characterization, Chemotaxonomy and Applications in Oceanography*. Cambridge University Press, Cambridge, pp. 257–313.
- Hilligsøe KM (2011) Linking phytoplankton community size composition with temperature, plankton food web structure and sea–air CO₂ flux. *Deep-Sea Res. I* 58: 826–838
- Huang B, Hu J, Xu H, Cao Z, Wang D (2010) Phytoplankton community at warm eddies in the northern South China Sea in winter 2003/2004. *Deep. Res. Part II Top. Stud. Oceanogr.* 57, 1792–1798. doi:10.1016/j.dsr2.2010.04.005
- Hutchings L, van der Lingen CD, Shannon LJ, Crawford RJM, Verheye HMS, Bartholomae CH,

- van der Plas AK et al (2009) The Benguela Current: An ecosystem of four components (2009). *Progress in Oceanography*, 53:15–32. doi:10.1016/j.pocean.2009.07.046
- Iglesias-Rodriguez MD, Halloran PR, Rickaby REM, Hall IR, Colmenero-Hidalgo E, Gittins JR, Boessenkool KP (2008). Phytoplankton Calcification in a High-CO₂ World. *Science*, 320(5874), 336–340. Doi:10.1126/science.1154122
- Islabão CA, Mendes CRB, Detoni AMS, Odebrecht C (2017) Phytoplankton community structure in relation to hydrographic features along a coast-to-off shore transect on the SW Atlantic Continental Shelf. *Continental Shelf Research*, 151:30–39. doi:10.1016/j.csr.2017.10.003
- Ito RG, Garcia CAE, Tavano VM (2016) Net sea-air CO₂ fluxes and modelled pCO₂ in the southwestern subtropical Atlantic continental shelf during spring 2010 and summer 2011. *Cont Shelf Res* 119:68–84. doi:10.1016/j.csr.2016.03.013
- Ito RG, Schneider B, Thomas H (2005) Distribution of surface fCO₂ and air-sea fluxes in the Southwestern subtropical Atlantic and adjacent continental shelf. *J Mar Sys* 56(3–4):227–242. doi:10.1016/j.jmarsys.2005.02.005
- Jeffrey SW (1974) Profiles of photosynthetic pigments in the ocean using thin-layer chromatography. *Mar. Biol.* 26, 101–110. doi:10.1007/BF00388879
- Jeffrey SW, Hallegraeff GM (1980). Studies of phytoplankton species and photosynthetic pigments in a warm core eddy of the East Australian Current. I. Summer populations. *Mar. Ecol. Prog. Ser.* 3, 285–294.
- Jeffrey SW, Wright SW, Zapata M (2011). Microalgal classes and their signature pigments. In S. Roy, C. Llewellyn, E. S. Egeland, and G. Johnsen (Eds.), *Phytoplankton Pigments* (pp. 3–77). Doi:10.1017/CBO9780511732263.004
- Jensen L, Erik, M, Richardson K. (2017) Using species distribution modelling to predict future distributions of phytoplankton: Case study using species important for the biological pump. *Marine Ecology* 1–12. Doi:10.1111/maec.12427
- Ji X, Jolanda MHV, Dedmer B. Van de Waal, Björn R, Jef (2020) Phenotypic Plasticity of Carbon Fixation Stimulates Cyanobacterial Blooms at Elevated CO₂. *Science Advances* 6 (8): eaax2926. doi:10.1126/sciadv.aax2926.
- Jiang LQ, Cai, W-J, Wang Y, Bauer JE (2013) Influence of terrestrial inputs on continental shelf carbon dioxide. *Biogeosciences* 10 (2), 839–849.
- Jiang, L-Q, Cai W-J, Wanninkhof R, Wang Y-C, Lüger H (2008) Air–sea CO₂ fluxes on the U.S. South Atlantic Bight: Spatial and seasonal variability, *J. Geophys. Res.*, 113, C07019, doi:10.1029/2007JC004366, 2008.
- Jorgensen et al 2006 Jørgensen, B.B., 2006. Bacteria and marine biogeochemistry. In: Schulz, H.D., Zabel, M. (Eds.), *Marine Geochemistry*. Springer, Berlin, pp. 169–206.
- Kahl LC, Bianchi AA, Osiroff AP, Pino DR, Piola AR (2017) Distribution of sea-air CO₂ fluxes in the Patagonian Sea: seasonal, biological and thermal effects. *Cont. Shelf Res.* 143:18–28. doi:10.1016/j.csr.2017.05.011
- Kahru, M., Mitchell, B.G., Gille, S.T., Hewes, C.D., Holm-Hansen, O., 2007. Eddies enhance biological production in the Weddell-Scotia Confluence of the Southern Ocean. *Geophys. Res. Lett.* 34. doi:10.1029/2007GL030430
- Kemp, A.E.S. and Villareal, T.A. (2018). The case of the diatoms and the muddled mandalas: Time to recognize diatom adaptations to stratified waters, *Progress in Oceanography*, 167, 138–149. doi:10.1016/j.pocean.2018.08.002.
- Kerr R, da Cunha LC, Kikuchi RKP, Horta PA, Ito RG, Muler MN, Copertino MS et al (2016). The Western South Atlantic Ocean in a High-CO₂ World: Current Measurement Capabilities and Perspectives. 740–752. doi:10.1007/s00267-015-0630-x
- Kerr R, Orselli IBM, Lencina-Avila JM, Eidt RT, Mendes CRB, da Cunha LC, Goyet C *et al.* Carbonate system properties in the Gerlache Strait, Northern Antarctic Peninsula (February 2015): I. Sea–Air CO₂ fluxes. *Deep–Sea Research Part II* (2017), doi:10.1016/j.dsr2.2017.02.008
- Kohfeld *et al.* Role of Marine Biology in Glacial-Interglacial CO₂ Cycles. *Science*, 308, 74–78,

2005

Körtzinger, A (2003) A significant sink of CO₂ in the tropical Atlantic Ocean associated with the Amazon River plume. *Geophysical Research Letters*.

Körtzinger A, Send U, Lampitt RS, Hartman S, Wallace DWR, Karstensen J, Villagarica MG, Llinás O, DeGrandpre MD (2008) The seasonal pCO₂ cycle at 49N/16.5W in the northeastern Atlantic Ocean and what it tells us about biological productivity. *J Geophys Res Ocean* 113: C04020 doi:10.1029/2007JC004347.

Krumhardt KM, Lovenduski NS, Freeman NM, Bates NR (2016). Apparent increase in coccolithophore abundance in the subtropical North Atlantic from 1990 to 2014. *Biogeosciences*, 13, 1163–1177. doi:10.5194/bg-13-1163-2016

Laiolo L, McInnes AS, Matear R, Doblin MA (2016) Key Drivers of Seasonal Plankton Dynamics in Cyclonic and Anticyclonic Eddies off East Australia. *Front Mar Sci* 3:1–14. doi:10.3389/fmars.2016.00155

Lamont T, Barlow RG, Brewin RJW (2019) Long-term trends in phytoplankton chlorophyll a and size structure in the Benguela Upwelling System. *J Geophys Res: Ocean* 124:1170– 1195.

Laruelle GG, Cai W, Hu X, Gruber N, Mackenzie FT, Regnier P (2018) Continental shelves as a variable but increasing global sink for atmospheric carbon dioxide. *Nat Commun* 9, 454. Doi:10.1038/s41467-017-02738-z

Laruelle GG, Dürr HH, Slomp CP, Borges AV (2010) Evaluation of sinks and sources of CO₂ in the global coastal ocean using a spatially-explicit typology of estuaries and continental shelves, *Geophys. Res. Lett.* 37:L15607. doi:10.1029/2010GL043691.

Laruelle GG, Landschützer P, Gruber N, Tison J-L, Delille B, Regnier P (2017) Global high-resolution monthly pCO₂ climatology for the coastal ocean derived from neural network interpolation. *Biogeosciences* 14:4545–4561. doi:10.5194/bg-14-4545-2017

Laruelle GG, Dürr HH, Lauerwald R, Hartmann J, Slomp CP, Goossens N, Regnier PAG (2013) Global multi-scale segmentation of continental and coastal waters from the watersheds to the continental margins. *Hydrol. Earth Syst. Sci.* 17::2029–2051. doi:10.5194/hess-17-2029-2013

Lauderdale JM, Dutkiewicz S, Williams RG, Follows MJ (2016) Quantifying the drivers of ocean-atmosphere CO₂ fluxes. *Global Biogeochem. Cycles* 30:983–999. doi:10.1002/2016GB005400.

Le Quéré C, Andres RJ, Boden T, Conway T, Houghton, RA, House, JI, Marland G et al (2013) The global carbon budget 1959–2011. *Earth Syst. Sci. Data* 5:165–185. doi:10.5194/essd-5-165-2013

Le Quéré C, Andrew RM, Canadell JG, Sitch S, Korsbakken JI, Peters GP, Manning A C, et al (2016) Global Carbon Budget 2016, *Earth Syst. Sci. Data*, 8, 605–649, doi:10.5194/essd-8-605-2016, 2016.

Le Quéré C, Raupach M, Canadell J, Marland G, Bopp L, Ciais P, Conway TJ et al (2009) Trends in the sources and sinks of carbon dioxide. *Nature Geosci* 2: 831–836. Doi: 10.1038/ngeo689, 2009.

Le Quéré C, Rödenbeck C, Buitenhuis ET, Conway TJ, Langenfelds R, Gomez A, Labuschagne C, et al. (2007) Saturation of the Southern Ocean CO₂ Sink Due to Recent Climate Change. *Science* 316:1735-1737. Doi: 10.1126/science.1136188

Lee M-M, Williams RG (2000) The role of eddies in the isopycnal transfer of nutrients and their impact on biological production. *J. Mar. Res.* 58, 895–917. doi:10.1357/002224000763485746

Lee S-K, Park W, Van Sebille E, Baringer MO, Wang C, Enfield DB, Yeager S, Kirtman BP (2011), What caused the significant increase in Atlantic ocean heat content since the mid-20th century? *Geophys. Res. Lett.*, 38, L17607, doi:10.1029/2011GL048856. Lefèvre N, Taylor A (2002) Estimating pCO₂ from sea surface temperatures in the Atlantic gyres, *Deep Sea Res., Part I*, 49(3), 539–554.

Lefèvre N., Moore, GF (2000). Distribution of the CO₂ partial pressure along an Atlantic meridional transect. *Progress in Oceanography*, 45. 401–413.

Lehahn Y, D'Ovidio F, Lévy M, Amitai Y, Heifetz E (2011) Long range transport of a quasi isolated

- chlorophyll patch by an Agulhas ring. *Geophys. Res. Lett.* 38:1–6. doi:10.1029/2011GL048588
- Lencina-Avila JM, Ito RG, Garcia CAE, Tavano VM (2016) Sea-air carbon dioxide fluxes along 35°S in the South Atlantic Ocean. *Deep-Sea Res I: Ocean Res Pap* 115:175–187. doi:10.1016/j.dsr.2016.06.004
- Leonardos N, Geider RJ (2005) Elevated atmospheric carbon dioxide increases organic carbon fixation by *Emiliania huxleyi* (Haptophyta), under nutrient-limited high-light conditions, *J. Phycol.* 41:1196–1203.
- Lévy M, Iovino D, Resplandy L, Klein P, Madec G, Tréguier AM, Masson S, Takahashi K (2012) Large-scale impacts of submesoscale dynamics on phytoplankton: Local and remote effects. *Ocean Model.* 43–44, 77–93. doi:10.1016/j.ocemod.2011.12.003
- Lévy M. (2003) Mesoscale variability of phytoplankton and of new production: Impact of the large-scale nutrient distribution. *J. Geophys. Res.* 108, 3358. doi:10.1029/2002JC001577
- Lewis E, Wallace DWR (1998) Program developed for CO₂ systems calculations. In: ORNL/CDIAC 105. Oak Ridge, Tennessee, Carbon Dioxide Information Analysis Center, Oak Ridge National Laboratory US Department of Energy.
- Li J, Qi Y, Jing Z, Wang J (2014) Enhancement of eddy-Ekman pumping inside anticyclonic eddies with wind-parallel extension: Satellite observations and numerical studies in the South China Sea. *J. Mar. Syst.* 132:150–161. doi:10.1016/j.jmarsys.2014.02.002
- Li WKW (2002) Macroecological patterns of phytoplankton in the northwestern North Atlantic Ocean. *Nature* 419: 154–157. doi:10.1038/nature00994
- Li WKW, McLaughlin FA, Lovejoy C, Carmack EC (2009) Smallest algae thrive as the Arctic Ocean freshens. *Science* 326, 539. doi: 10.1126/science.1179798
- Lima C, Mendes R, Tavano V, Detoni A, Secchi E. (2019). Chemotaxonomy-based mapping of phytoplankton communities in the subtropical Southwestern Atlantic Ocean, with emphasis on the marine cyanobacterium *Trichodesmium*. *Progress in Oceanography* 172: 77–88. doi:10.1016/j.pocean.2019.01.008
- Liss PS, Merlivat L (1986) Air-sea gas exchange rates. Introduction and synthesis. In: *The Role of Air-Sea Exchange in Geochemical Cycling*, edited by P. B. Menard, pp. 113–127. D. Reidel, Norwell, Mass., 1986.
- Litchman E, de Tezanos Pinto, P., Edwards KF, Klausmeier CA, Kremer CT, Thomas MK (2015) Global biogeochemical impacts of phytoplankton: A trait-based perspective. *Journal of Ecology*, 103(6), 1384–1396. Doi:10.1111/1365-2745.12438
- Litchman E, Klausmeier C, Yoshiyama K (2009) Contrasting size evolution in marine and freshwater diatoms *PNAS* 106(8):2665–70 doi: 10.1073/pnas.0810891106
- Liu F, Yin K, He L, Tang S, Yao J (2018) Influence on phytoplankton of different developmental stages of mesoscale eddies off eastern Australia. *J. Sea Res.* 137:1–8. doi:10.1016/j.seares.2018.03.004
- Liu H, Probert I, Uitz J, Claustre H, Aris-Brosou S, Frada M, Not F, de Vargas C (2009) Extreme diversity in noncalcifying haptophytes explains a major pigment paradox in open oceans. *Proc. Natl. Acad. Sci.* 106, 12803–12808. doi:10.1073/pnas.0905841106
- Lohbeck KT, Riebesell U, Reusch TBH (2012). Adaptive evolution of a key phytoplankton species to ocean acidification. *Nature Geoscience*, 5(5), 346–351. doi:10.1038/ngeo1441
- Longhurst A, Sathyendranath S, Platt T, Caverhill C (1995) An estimate of global primary production in the ocean from satellite radiometer data. *J Plankton Res* 17:1245–1271.
- Longhurst AR (2006) *Ecological Geography of the Sea*, 2nd Edn. San Diego, CA: Academic Press, doi: 10.1016/B978-012455521-1/50012-7
- Lopez H, Goni G, Dong S (2017) A reconstructed South Atlantic Meridional Overturning Circulation time series since 1870. *Geoph Res Lett* 44(7):3309–3310. Doi: 10.1002/2017GL073227
- Lutjeharms JRE (2007) Three decades of research on the greater Agulhas Current To cite this

- version: Three decades of research on the greater Agulhas Current. *Ocean Science* 3:129–147.
- Lutjeharms J. and Stockton (1987). P. Kinematics of the upwelling front off southern Africa. *South African Journal of Marine Science*, 5, pp. 35-49.
- Lutjeharms J, Meeuwis J (1987). The extent and variability of Southeast Atlantic upwelling. *South African Journal Marine Science*, 5 (1987), pp. 51-62
- Machu E, Garçon V (2001) Phytoplankton seasonal distribution from SeaWiFS data in the Agulhas Current system. *J. Mar. Res.* 59:795–812. doi:10.1357/002224001762674944
- Mackey KR, Paytan A, Caldeira K, Grossman AR, Moran D, McIlvin M, Saito MA (2013), Effect of temperature on photosynthesis and growth in marine *Synechococcus* spp., *Plant Physiol.*, 163(2):815-29. doi: 10.1104/pp.113.221937
- Mackey KRM, Morris JJ, Morel FMM, Kranz SA (2015) Response of photosynthesis to ocean acidification. *Oceanography* 28:74–91.
- Mackey MD, Mackey DJ, Higgins HW, Wright SW (1996) CHEMTAX - A program for estimating class abundances from chemical markers: Application to HPLC measurements of phytoplankton. *Mar. Ecol. Prog. Ser.* 144:265–283. doi:10.3354/meps144265
- Marañón E, Behrendfeld MJ, Gonzalez N, Mouriño B, Zubkov MV (2003). High variability of primary production in oligotrophic waters in the Atlantic Ocean: uncoupling from phytoplankton biomass and size structure. *Mar Ecol Prog Series MEPS* 257:1-11. doi:10.3354/meps257001
- Marañón E, Cermeño P, Latasa M, Tadonléké R (2012) Temperature, resources, and phytoplankton size structure in the ocean. *Limnol. Oceanogr.* 57:1266–68
- Marañón E, Holligan PM, Varela M (2000) Basin-scale variability of phytoplankton biomass and growth in the Atlantic Ocean, *Deep-Sea Res.* 47: 825-857
- Marañón E, Lorenzo MP, Cermeño P, Mouriño-Carbalido B (2018) Nutrient limitation suppresses the temperature dependence of phytoplankton metabolic rates. *ISME J* 12, 1836–1845 (2018). <https://doi.org/10.1038/s41396-018-0105-1>
- Marañón E. (2005) Phytoplankton growth rates in the Atlantic subtropical gyres. *Limnol Ocean.* 50:299–310. doi:10.4319/lo.2005.50.1.0299
- Marañón E. (2015) Cell size as a key determinant of phytoplankton metabolism and community structure. *Annu Rev Mar Sci.* 7:241–64. doi: 0.1146/annurev-marine-010814-015955
- Margalef, R. (1978). Life-forms of phytoplankton as survival alternatives in an unstable environment. *Oceanol. Acta* 1, 493–509.
- Marques WC, Fernandes EH, Monteiro IO, Möller OO (2009) Numerical modeling of the Patos Lagoon coastal plume, Brazil. *Continental Shelf Research*, 29, 556-571.
- Marques WC, Matano RP, Palma ED, Piola AR (2010) The influence of the Brazil and Malvinas currents on the Southwestern Atlantic Shelf circulation *Ocean Sci.*, 6:983-995 doi:10.5194/os-6-983-2010
- McGillicuddy D *et al.*, (2007). Eddy/wind interactions stimulate extraordinary mid-ocean plankton blooms. *Science* 316 (5827), 1021–1026.
- McGillicuddy DJ (2015) Formation of Intrathermocline Lenses by Eddy–Wind Interaction. *J. Phys. Oceanogr.* 45, 606–612. doi:10.1175/JPO-D-14-0221.1
- McGillicuddy DJ (2016) Mechanisms of Physical-Biological-Biogeochemical Interaction at the Oceanic Mesoscale, *Annual Review of Marine Science*. doi:10.1146/annurev-marine-010814-015606
- McManus G, Dawson R (1994) Phytoplankton pigments in the deep chlorophyll maximum of the Caribbean Sea and the western tropical Atlantic Ocean. *Mar. Ecol. Prog. Ser.* 113, 199–206. doi:10.3354/meps113199
- Mendes CR, Cartaxana P, Brotas V (2007) HPLC determination of phytoplankton and microphytobenthos pigments: comparing resolution and sensitivity of a C18 and a C8. *Oceanography: methods*. Doi:10.4319/lom.2007.5.363

- Mendes CRB, Tavano VMT, Leal MC, Souza MS, Brotas V, Garcia CAE (2012) Dynamics of phytoplankton communities during late summer around the tip of the Antarctic Peninsula. *Deep-Sea Res I* 65:1–14.
- Mendes CRB, Tavano VMT, Leal MC, Souza MS, Brotas V, Garcia CAE (2013) Shifts in the dominance between diatoms and cryptophytes during three late summers in the Bransfield Strait (Antarctic Peninsula) *Polar Biol* 36:537–547. doi: 10.1007/s00300-012-1282-4.
- Meredith MP, Watkins JL, Murphy EJ, Cunningham NJ, Wood AG, Korb R, Whitehouse MJ, et al (2003) An anticyclonic circulation above the Northwest Georgia Rise, Southern Ocean. *Geophys. Res. Lett.* 30:1–5. doi:10.1029/2003GL018039
- Millero FJ. 2007. The marine inorganic carbon cycle. *Chem. Rev.* 107:308–41
- Montes-Hugo MM, Doney SC, Ducklow HW, Fraser W, Martinson D, Stammerjohn SE, Schofiels O (2009) Recent Changes in Phytoplankton Communities Associated with Rapid Regional Climate Change Along the Western Antarctic Peninsula. *Science* v. 323, 1470-1473. DOI: 10.1126/science.1164533
- Moore JK, Abbott MR (2000) Phytoplankton chlorophyll distributions and primary production in the Southern Ocean. *J. Geophys. Res.: Ocean.* 105:28709-28722 doi: 10.1029/1999JC000043
- Moore LR, Rocap G, Chisholm SW (1998) Physiology and molecular phylogeny of coexisting *Prochlorococcus* ecotypes. *Nature* 393:464–467. doi: 10.1038/30965
- Morales CE, Anabalón V, Bento JP, Hormazabal S, Cornejo M, Correa-Ramírez MA, Silva N, (2017) Front-Eddy Influence on Water Column Properties, Phytoplankton Community Structure, and Cross-Shelf Exchange of Diatom Taxa in the Shelf-Slope Area off Concepción (~36–37°S). *J. Geophys. Res. Ocean.* 122, 8944–8965. doi:10.1002/2017JC013111
- Morán XAG, López-Urrutia A, Calvo-Díaz A, Li WKW (2010). Increasing importance of small phytoplankton in a warmer ocean. *Global Change Biology*, 16(3), 1137–1144. Doi:10.1111/j.1365-2486.2009.01960.x
- Moreau S, Penna AD, Lloret J, Patel R, Langlais C, Boyd, PW, Matear RJ, Phillips HE, Trull TW, Tilbrook B, Lenton A, Strutton PG (2017) Eddy-induced carbon transport across the Antarctic Circumpolar Current. *Global Biogeochem. Cycles* 1–19. doi:10.1002/2017GB005669
- Moser GAO, Piedras FR, Oaquim, A. B. J., Souza, D. S., Leles, S. G., de Lima, D. T., *et al.* (2017). Tidal effects on phytoplankton assemblages in a near-pristine estuary: a trait-based approach for the case of a shallow tropical ecosystem in Brazil. *Mar. Ecol.* 38:4. doi: 10.1111/maec.12450
- Moser, G. A., Castro, N., Takanoashi, R., Fernandes, A., Pollery RC, Tenenbaum D (2016). The influence of surface low-salinity waters and cold subsurface water masses on picoplankton and ultraplankton distribution in the continental shelf off Rio de Janeiro, SE Brazil. *Cont. Shelf Res.* 120, 82–95. doi: 10.1016/j.csr.2016.02.017
- Mouw, C. B., Barnett, A., McKinley, G. A., Gloege, L., and Pilcher, D. (2016). Phytoplankton Size Impact on Export Flux in the Global Ocean. *Global Biogeochemical Cycles.* <https://doi.org/10.1002/2015GB005355>
- Muelbert JH, Acha M, Mianzán HW, Guerrero RA, Reta R, Braga ED, Garcia VM, Berasategui AD, Gómez-Erache M, Ramírez F (2008). Biological, physical and chemical properties at the Subtropical Shelf Front Zone in the SW Atlantic Continental Shelf. *Continental Shelf Research* 28:1662– 1673. doi:10.1016/j.csr.2007.08.011
- Niencheski LF, Windom HL (1994), Nutrient flux and budget in Patos Lagoon estuary, *Science of The Total Environment*, Volume 149, Issues 1–2,53-60. doi:10.1016/0048-9697(94)90004-3.
- Nightingale PD, Liss PS Schlosser P (2000) Measurements of airsea gas transfer during an open ocean algal bloom, *Geophys. Res. Lett.*, 27, 2117 – 2120.
- Ning X, Peng X, Le F, Hao Q, Sun J, Liu C, Cai, Y(2008). Nutrient limitation of phytoplankton in anticyclonic eddies of the northern South China Sea. *Biogeosciences Discuss.* 5, 4591–4619. doi:10.5194/bgd-5-4591-2008
- NOAA National Centers for Environmental Information, State of the Climate: Global Climate Report for Annual 2017, published online January 2018, retrieved on August 21, 2020 from <https://www.ncdc.noaa.gov/sotc/global/201713>.

- Not F, Latasa M, Scharek R, Viprey M, Karleskind P, Balagué V, Ontoria-Oviedo I, Cumino A, Goetze E, Vaultot D, Massana R (2008) Protistan assemblages across the Indian Ocean, with a specific emphasis on the picoeukaryotes. *Deep. Res. Part I Oceanogr. Res. Pap.* 55, 1456–1473. doi:10.1016/j.dsr.2008.06.007
- Oliveira RR, Pezzi LP, Souza, RB, Santini MF, Cunha LC, Pacheco FS (2019) First measurements of the ocean-atmosphere CO₂ fluxes at the Cabo Frio upwelling system region, Southwestern Atlantic Ocean. *Cont Shelf Res* 181:135-142. doi:10.1016/j.csr.2019.05.008
- Oliver MJ, Irwin AJ (2008). Objective global ocean biogeographic provinces. *Geoph Res Lett*, 35(15):1–6. doi:10.1029/2008GL034238
- Orselli, IBM, Kerr R, Ito RG, Tavano VM, Mendes CR, Garcia CAE (2018a) How fast is the Patagonian shelf-break acidifying? *J Mar Sys*, 178, 1-14.
- Orselli IBM, Kerr R, Azevedo JLL, Galdino F, Araujo M, Garcia CAE (2018b) The sea-air CO₂ net fluxes in the South Atlantic Ocean and the role played by Agulhas eddies. *Prog Oceanogr* 170:40–52. doi:10.1016/j.pocean.2018.10.006
- Orselli IBM, Goyet C, Kerr R, Azevedo JLL de, Araujo M, Galdino F, Garcia CAE (2019). The Effect of Agulhas Eddies on Absorption and Transport of Anthropogenic Carbon in the South Atlantic Ocean. *Climate*, 7(6), 84. <https://doi.org/10.3390/cli7060084>
- Oschlies A (2002) Can eddies make ocean deserts bloom? *Global Biogeochem. Cycles* 16, 53-1-53–11. doi:10.1029/2001GB001830
- Paasche E (2002) A review of the coccolithophorid *Emiliana huxleyi* (Prymnesiophyceae), with particular reference to growth, coccolith formation, and calcification-photosynthesis interactions. *Phycologia*, 40:503–529.
- Padin XA, Velo A, Gago J, Gilcoto M, Alvarez M, Pardo PC, Marinas DI (2010) Air-Sea CO₂ fluxes in the Atlantic as measured during boreal spring and autumn. *Biogeosciences* 7(5):1587–1606. doi:10.5194/bg-7-1587-2010
- Painter SC, Poulton AJ, Allen JT, Pidcock R, Balch WM (2010) The COPAS-08 expedition to the Patagonian Shelf: Physical and environmental conditions during the 2008 coccolithophore bloom, *Cont Shelf Res* 30(18): 1907– 1923.
- Passow U, Carlson CA (2012) The biological pump in a high CO₂ World. *MEPS* 470:249-271 doi: 10.3354/meps09985
- Person R, Aumont O, Lévy M (2018) The Biological Pump and Seasonal Variability of pCO₂ in the Southern Ocean: The Biological Pump and Seasonal Variability of pCO₂ in the Southern Ocean: Exploring the Role of Diatom Adaptation to Low Iron HAL Id : hal-01959020. (December). <https://doi.org/10.1029/2018JC013775>
- Peterson RG, Stramma L (1991) Upper-level circulation in the South Atlantic Ocean. *Prog Oceanogr* 26: 1-73.
- Pezzi LP, Souza RB, Acevedo O, Wainer I, Mata MM, Garcia CAE, Camargo R (2009) Multi-year measurements of the Oceanic and Atmospheric Boundary Layers at the Brazil-Malvinas Confluence Region. *J Geoph Res*, v. 114, p. D19103, doi:10.1029/2008JD011379.
- Pierrot D, Lewis E, Wallace D (2006). CO₂SYS Dos Program Developed for CO₂ System Calculations. ORNL/CDIAC-105. Oak Ridge, TN: Carbon Dioxide Information Analysis Center; Oak Ridge National Laboratory; US Department of Energy.
- Pierrot D, Neil C, Sullivan K, Castle R, Wanninkhof R, Lueger H (2009). Recommendations for autonomous underway pCO₂ measuring systems and data reduction routines. *Deep Sea Res. II* 56, 512–522. doi: 10.1016/j.dsr2.2008.12.005
- Pilo GS, Mata MM, Azevedo JLL (2015) Eddy surface properties and propagation at Southern Hemisphere. 629–641. <https://doi.org/10.5194/os-11-629-2015>
- Piola AR, Matano RP, Palma ED, Möller Jr OO (2005). The influence of the Plata River discharge on the western South Atlantic Shelf The influence of the Plata River discharge on the western South Atlantic shelf. (January), 1–5. doi:10.1029/2004GL021638
- Piola ARN, Martínez Avellaneda, R. A. Guerrero, F. P. Jardón, E. D. Palma, and S. I. Romero

- (2010), Malvinas-slope water intrusions on the northern Patagonia continental shelf, *Ocean Sci.*, 6(1), 345–359.
- Piola AR, Möller Jr., O.O., Guerrero, R.A. and Campos, E.J.D. (2008). Variability of the Subtropical Shelf front off eastern South America: winter 2003 and summer 2004. *Continental Shelf Research* 28 (2008), doi: 10.1016/j.csr.2008.03.013.
- Pittera J, Humily F, Thorel M, Grulois D, Garczarek L, Six C (2014), Connecting thermal physiology and latitudinal niche partitioning in marine *Synechococcus*. *The ISME Journal*, 8(6):1221-36. doi: 10.1038/ismej.2013.228
- Poulton AJ, Holligan PM, Charalampopoulou A, Adey TR (2017) Coccolithophore ecology in the tropical and subtropical Atlantic Ocean: New perspectives from the Atlantic meridional transect (AMT) programme. *Prog Oceanogr*, 158:150-170. Doi: 10.1016/j.pocean.2017.01.003
- PROENÇA, L.A.O., 2006. Algal blooms in coastal zones: examples of harmful impacts from the Brazilian coast. *Journal of Coastal Research*, SI 39 (Proceedings of the 8th International Coastal Symposium), 76 - 78. Itajaí, SC, Brazil, ISSN 0749-0208.
- R Core Team (2014). R: A language and environment for statistical computing. Vienna, Austria: R Foundation for Statistical Computing. Retrieved from <https://www.R-project.org/>
- R DEVELOPMENT CORE TEAM, version 2.10.0, 2009. The R Foundation for statistic computing.
- Raven JA (1987) The role of vacuoles. *New Phytologist* 106, 357–422.
- Reinfelder JR (2011) Carbon concentrating mechanisms in eukaryotic marine phytoplankton. *Annu. Rev. Mar. Sci.* 3: 291–315. doi: 10.1146/annurev-marine-120709-142720
- Reygondeau G, Longhurst A, Martinez E, Beaugrand G, Antoine D, Maury O (2013) Dynamic biogeochemical provinces in the global ocean. *Glob Biogeo Cycles*, 27(4):1046–1058. doi:10.1002/gbc.20089
- Richardson TL, Jackson GA (2007) Small phytoplankton and carbon export from the surface ocean. *Science* 315(5813): 838-40. doi:10.1126/science.1133471
- Riebesell U, Körtzinger A, Oschlies A (2009). Sensitivities of marine carbon fluxes to ocean change. *Proceedings of the National Academy of Sciences of the United States of America*, 106(49):20602–20609. Doi:10.1073/pnas.0813291106
- Rivero-Calle S, Gnanadesikan A, Castillo CE, Del Balch WM, Guikema, SD (2015) Multidecadal increase in North Atlantic coccolithophores and the potential role of rising CO₂. 350(6267), 9824–9829.
- Rixen T, Ittekkot V (2005) Nitrogen deficits in the Arabian Sea, implications from a three component mixing analysis. *Deep-Sea Res II* 52: 1879–91.
- Robbins LL, Hansen ME, Kleypas JA, Meylan SC (2010): CO₂calc: a user-friendly seawater carbon calculator for Windows, Max OS X, and iOS (iPhone), U.S. Geological Survey Open-File Report, 2010–1280, 1–17, <http://pubs.usgs.gov/of/2010/1280/>
- Rodrigues RR, Lorenzetti JA (2001) A numerical study of the effects of bottom topography and coastline geometry on the southeast Brazilian coastal upwelling. *Cont. Shelf. Res.*, 21, 371–394.
- Rodríguez F, Varela M, Fernández E, Zapata M (2003) Phytoplankton and pigment distributions in an anticyclonic slope water oceanic eddy (SWODDY) in the southern Bay of Biscay. *Mar. Biol.* 143, 995–1011. doi:10.1007/s00227-003-1129-1
- Roobaert A, Laruelle GG, Landschützer P, Regnier P (2019) Uncertainty in the global oceanic CO₂ uptake induced by wind forcing: quantification and spatial analysis, *Biogeosciences*, 15:1701–1720. doi:10.5194/bg-15-1701-2018
- Rosgaard L, de Porcellinis adn AJ, Jacobsen JH, Frigaard NU, Sakuragi Y (2012) Bioengineering of carbon fixation, biofuels, and biochemicals in cyanobacteria and plants. *Journal of Biotechnology* 162:134–147. doi: 10.1016/j.jbiotec.2012.05.006.
- Sabine CL, Feely RA, Gruber N, Key RM, Lee K, Bullister JL, Rios AF et al (2004). The oceanic sink for anthropogenic CO₂. *Science*, 305(5682): 367–371. Doi:10.1126/science.1097403

- Saeck EA, O'Brien KR, Weber TR, Buford MQ (2013) Changes to chronic nitrogen loading from sewage discharges modify standing stocks of coastal phytoplankton. *Marine Pollution Bulletin* 71:159-167.
- Sambrotto RN (2014) Ocean chemistry: biogeochemical regime in focus. *Nature Geosciences* 7(12):862-863.
- Santana-Casiano JM, González-Dávila, M., and Ucha, I. R. (2009). Carbon dioxide fluxes in the Benguela upwelling system during winter and spring: A comparison between 2005 and 2006. *Deep Sea Research Part II: Topical Studies in Oceanography*, 56(8–10), 533–541. Doi:10.1016/j.dsr2.2008.12.010
- Sarmiento JL, Gruber N. (2002). Sinks for anthropogenic carbon. *Physics Today*, 55(8), 30. <https://doi.org/10.1063/1.1510279>
- Sarthou G, Timmermans KR, Blain S, Tréguer P (2005) Growth physiology and fate of diatoms in the ocean: a review *Journal of Sea Research* 53:25–42 doi: 10.1016/j.seares.2004.01.007
- Schiebel R, Zeltner A, Treppke UF, Waniek JJ, Bollmann J, Rixen T, Hemleben, C. (2004) Distribution of diatoms, coccolithophores and planktic foraminifera in the Arabian Sea. *PANGAEA*, doi:10.1594/PANGAEA.736805
- Schloss IR, Ferreyra GA, Ferrario ME, Almandoz GO, Codina R, Bianchi AA, Poisson A (2007) Role of plankton communities in sea-air variations in pCO₂ in the SW Atlantic Ocean. *MEPS* 332:93–106. doi:10.3354/meps332093
- Schlüter L, Henriksen P, Nielsen TG, Jakobsen HH (2011) Phytoplankton composition and biomass across the southern Indian Ocean. *Deep. Res. Part I Oceanogr. Res. Pap.* 58: 546–556. doi:10.1016/j.dsr.2011.02.007
- Schouten MW, de Ruijter WPM, van Leeuwen PJ, Lutjeharms JRE (2000) Translation, decay and splitting of Agulhas rings in the southeastern Atlantic Ocean. *J. Geophys. Res. Ocean.* 105: 21913–21925. doi:10.1029/1999JC000046
- Schuster U, McKinley GA, Bates N, Chevallier F, Doney SC, Fay AR, Watson AJ (2013) An assessment of the Atlantic and Arctic sea–air CO₂ Fluxes, 1990–2009. *Biogeosciences* 10(1): 607–627. Doi:10.5194/bg-10–607.
- Shadwick EH, Thomas H (2011) Carbon dioxide in the coastal ocean: a case study in the Scotian Shelf region, In: *The Ocean Year Book Volume 25*, Martinus Nijhoff, Boston
- Shannon LV (1985) The Benguela ecosystem. 1. Evolution of the Benguela. physical features and processes. In *Oceanography and Marine Biology. An Annual Review* 23. Barnes. M. (Ed.). Aberdeen; University Press: 105–182.
- Siegel DA, Peterson P, McGillicuddy DJ, Maritorena S, Nelson NB (2011) Bio-optical footprints created by mesoscale eddies in the Sargasso Sea. *Geophys. Res. Lett.* 38, 1–6. doi:10.1029/2011GL047660
- Sigman DM, Boyle EA (2000) Glacial/interglacial variations in atmospheric carbon dioxide, *Nature* 407(6806): 859–869.
- Signorini SR, Häkkinen S, Gudmundsson K, Olsen A, Omar AM, Olafsson J, Reverdin G (2012) The role of phytoplankton dynamics in the seasonal and interannual variability of carbon in the subpolar North Atlantic – a modeling study 683–707. doi:10.5194/gmd-5-683-2012
- Signorini SR, McClain CR (2009) Effect of uncertainties in climatologic wind, ocean pCO₂, and gas transfer algorithms on the estimate of global sea-air CO₂ flux. *Global Biogeochem Cycles* 23:1–14. Doi:10.1029/2008GB003246
- Signorini SR, Franz BA, McClain CR (2015) Chlorophyll variability in the oligotrophic gyres: mechanisms, seasonality and trends. *Front Mar Sci* 2:1–11. Doi:10.3389/fmars.2015.00001
- Silveira ICA, Brown WS, Flierl GR (2000) Dynamics of the North Brazil Current Retroflexion Region from the WESTRAX Observations. *JGR* 105(C12): 28,559-583.
- Simon N, Cras A-L, Foulon E, Lemée R (2009) Diversity and evolution of marine phytoplankton C. R. *Biologies* 332:159–170 doi:10.1016/j.crv.2008.09.009

- Smayda TJ, Trainer VL (2010) Progress in Oceanography Dinoflagellate blooms in upwelling systems: seeding, variability, and contrasts with diatom bloom behaviour. *Prog. Oceanogr.* 85: 92–107. doi: 10.1016/j.pocean.2010.02.006.
- Soares I, Möller Jr O (2001) Low-frequency currents and water mass spatial distribution on the southern Brazilian shelf. *Continental Shelf Research*, 21: 1785-1814.
- Sommer U, Paul C, Moustaka-Gouni M (2015) Warming and ocean acidification effects on phytoplankton-from species shifts to size shifts within species in a mesocosm experiment. *PLoS ONE* 2015, 10.
- Souza MS, Mendes CRB, Tavano VM, Brotas V, Pollery RC (2011) Phyto-plankton community during a Coccolithophorid bloom in the Patagonian shelf: Microscopic and HPLC pigment analyses, *Journal of the Marine Biological Association of the UK* 92(01):13–27 doi: 10.1017/S0025315411000439
- Souza AG, Kerr RK, Azevedo JLL (2018) On the influence of Subtropical Mode Water on the South Atlantic Ocean, *Journal of Marine Systems*, 185. doi:10.1016/j.jmarsys.2018.04.006
- Swan CM, Vogt M, Gruber N, Laufkoetter C (2016) A global seasonal surface ocean climatology of phytoplankton types based on CHEMTAX analysis of HPLC pigments. *Deep-Sea Research Part I: Oceanographic Research Papers*, 109:137–156. doi:10.1016/j.dsr.2015.12.002
- Sweeney C, Gloor E, Jacobson AR, Key RM, McKinley G, Sarmiento JL, Wanninkhof R (2007) Constraining global air-sea gas Exchange for CO₂ with recent bomb 14C measurements. *Global Biogeochemical Cycles* 21(2). Doi: 10.1029/2006GB002784
- Takahashi T, Feely RA, Weiss F, Wanninkhof RH, Chipman DW, Stewart C, Timothy TT (1997) Global air-sea flux of CO₂: An estimate based on measurements of sea – air pCO₂ difference. *PNAS* 94(16):892–8299. Doi:10.1073/pnas.94.16.8292
- Takahashi T, Sutherland SC, Sweeney C, Poisson A, Metzl N, Tilbrook B, Nojiri Y et al (2002) Global sea – air CO₂ flux based on climatological surface ocean pCO₂, and seasonal biological and temperature effects. *Deep Sea Research Part II: Topical Studies in Oceanography*, 49(9–10): 1601–1622. Doi:10.1016/S0967-0645(02)00003-6
- Takahashi T, Sutherland SC, Wanninkhof R, Sweeney C, Feely RA, Chipman DW, de Baar HJ W (2009) Climatological mean and decadal change in surface ocean pCO₂, and net sea-air CO₂ flux over the global oceans. *Deep-Sea Research Part II: Topical Studies in Oceanography* 56(8–10):554–577. doi:10.1016/j.dsr2.2008.12.009
- Takao S, Nakaoka S-I, Hashihama F, Shimada K, Yoshikawa-Inoue H, Hirawake T, Kanda J, Hashida G, Suzuki K (2020) Effects of phytoplankton community composition and productivity on sea surface pCO₂ variations in the Southern Ocean *Deep-Sea Research I* 160:103263 doi: 10.1016/j.dsr.2020.103263
- Taucher J, Oschlies A (2011) Can we predict the direction of marine primary production change under global warming? *Geophys. Res. Lett.*, 38, L02603, doi:10.1029/2010gl045934.
- Taucher J, Jones J, James A, Brzezinski MA, Carlson CA, Riebesell U, Passow U (2015) Combined effects of CO₂ and temperature on carbon uptake and partitioning by the marine diatoms *Thalassiosira weissflogii* and *Dactyliosolen fragilissimus*. *Limnology and ocean* 60(3):901–919. doi:10.1002/lno.10063
- Tenenbaum DR, Menezes M, Viana SdeC, Mendes MCdeQ, Eduardo J, Hatherly MMF (2006) Dinoflagelados e tintinídeos da região central da Zona Econômica Exclusiva brasileira: guia de identificação. Museu Nacional, Rio de Janeiro. Os Dinoflagelados. In *Dinoflagelados e Tintinídeos da região central da Zona Econômica Exclusiva brasileira: Guia de identificação* (D.R. Tenenbaum ed.). Rio de Janeiro: Museu Nacional- Universidade Federal do Rio de Janeiro, p. 35-163.
- Ter Braak CJF, Prentice IC (1988) A theory of gradient analysis. *Adv. Ecol. Res.* 18:271–317. doi: 10.1016/S0065-2504(08)60183-X.
- Terlouw GJ, Knor LACM, De Carlo EH, Drupp PS, Mackenzie FT, Li YH, Sutton AJ, Plueddemann AJ and Sabine CL (2019) Hawaii Coastal Seawater CO₂ Network: A Statistical Evaluation of a Decade of Observations on Tropical Coral Reefs. *Front. Mar. Sci.* 6:226. doi: 10.3389/fmars.2019.00226

- Thomas H, Bozec Y, Elkalay K, de Baar HJW, Borges AV, Schiettecatte L-S (2005) Controls of the surface water partial pressure of CO₂ in the North Sea *Biogeosciences*, 2, 323–334, 2005
- Tilburg CE (2002) Ocean color variability in the Tasman Sea. *Geophys. Res. Lett.* 29:1–4. doi:10.1029/2001GL014071
- Tortell PD, DiTullio GR, Sigman DM, Morel FMM (2002) CO₂ effects on taxonomic composition and nutrient utilization in an Equatorial Pacific phytoplankton assemblage *Mar. Ecol. Prog. Ser.* 236:37–43. Doi: 10.3354/meps236037
- Troost TA, Kooi BW, Kooijman SA (2005) Ecological specialization of mixotrophic plankton in a mixed water column. *Am. Nat.* 166, E45–E61.
- Tsunogai S, Watanabe S, Sato T (1999) Is there a “continental shelf pump” for the absorption of atmospheric CO₂? *Tellus B*, 51: 701-712. doi:10.1034/j.1600-0889.1999.t01-2-00010.x
- Uitz J, Claustre H, Gentili B, Stramski D (2010) Phytoplankton class-specific primary production in the world's oceans: Seasonal and interannual variability from satellite observations *Glob Biogeo Cycles* 24:GB3016. doi:10.1029/2009GB003680
- Ulibarrena J, Conzonno VH (2015) Mechanisms involved in the proliferation and distribution of phytoplankton in the Patagonian Sea, Argentina, as revealed by remote sensing studies. *Environ Earth Sci* 74: 439–449. Doi:10.1007/s12665-015-4052-0
- Unrein F, Gasol J, Not F (2013) Mixotrophic haptophytes are key bacterial grazers in oligotrophic coastal waters. *ISME J* 8, 164–176 doi:10.1038/ismej.2013.132
- Vaillancourt RD, Marra J, Seki MP, Parsons ML, Bidigare, RR (2003) Impact of a cyclonic eddy on phytoplankton community structure and photosynthetic competency in the subtropical North Pacific Ocean. *Deep. Res. Part I Oceanogr. Res. Pap.* 50:829–847. doi:10.1016/S0967-0637(03)00059-1
- Van Foreest D, Shillington F, Legeckis R (1984) Large scale, stationary, frontal features in the Benguela Current system, *Cont Shelf Res* 3:465-474
- Villac MC, Cabral-Noronha VA, Oliveira Pinto T (2008) The phytoplankton biodiversity of the coast of the state of São Paulo, Brazil. *Biota Neotrop.* 8:151–173. doi: 10.1590/s1676-06032008000300015
- VLIZ (2009) Longhurst Biogeographical Provinces, <http://www.vliz.be/vmcddata/vlimar/downloads.php>, 2009.
- Volk T, Hoffert MI (1985) Ocean carbon pumps: Analysis of relative strengths and efficiencies in ocean-driven atmospheric CO₂ changes. In E. T. Sundquist, & W. S. Broecker (Eds.), *The Carbon Cycle and Atmospheric CO₂: Natural Variations Archean to Present* (pp. 99–110). Washington, DC: American Geophysical Union.
- Wanninkhof R (2014) Relationship between wind speed and gas exchange over the ocean revisited. *Limnology and Oceanography: Methods*, 12:351–362. Doi:10.1029/92JC00188
- Wanninkhof R, Barbero L, Byrne R, Cai W-J, Huang WJ, Zhang JZ, Baringer M, and Langdon C (2015) Ocean acidification along the Gulf Coast and East coast of the USA. *Cont Shelf Res* 98:54-71. doi: 10.1016/j.csr.2015.02.008.
- Wanninkhof, RH (1992) Relationship between wind speed and gas exchange over the ocean. *Journal Geophysical Research*, v.97, p.7373-7382, 1992.
- Watermann F, Hillebrand H, Gerdes G, Krumbein WE, Sommer U (1999) Competition between benthic cyanobacteria and diatoms as influenced by different grain sizes and temperatures *MEPS* 187:77-87. *JSTOR*, www.jstor.org/stable/24853356.
- Watson AJ, LISS PS (1998) Marine biological controls on climate via the carbon and sulphur geochemical cycles. *Philosophical transaction of the royal society B: biological sciences* 353: 41-51.
- Wei T, Simko V (2017). R package "corrplot": Visualization of a Correlation Matrix (Version 0.84). Available from <https://github.com/taiyun/corrplot>
- Weiss RF (1974) Carbon dioxide in water and seawater: the solubility of a non-ideal gas. *Mar.*

Chem., 2: 203-215.

Williams, PJLB, Thomas DN Reynolds CS [Eds.] 2002. *Phytoplankton Productivity: Carbon Assimilation in Marine and Freshwater Ecosystems*. Blackwell Science, Inc., Oxford, U.K. 400 pp. ISBN: 0-632- 05711-4

Williams RG (2011) Oceanography: Ocean eddies and plankton blooms. *Nat. Geosci.* 4, 739–740. doi:10.1038/ngeo1307

Worden AZ, Nolan JK, Palenik B (2004) Assessing the dynamics and ecology of marine picophytoplankton: The importance of the eukaryotic component. *Limnol. Oceanogr.* 49: 168–179. doi:10.4319/lo.2004.49.1.0168

Wright SW, Ishikawa A, Marchant HJ, Davidson AT, Van Den Enden RL, Nash GV (2009) Composition and significance of picophytoplankton in Antarctic waters. *Polar Biol.* 32, 797–808. doi:10.1007/s00300-009-0582-9

Wright SW, van den Enden RL, Pearce I, Davidson AT, Scott FJ, Westwood KJ (2010) Phytoplankton community structure and stocks in the Southern Ocean (30-80°E) determined by CHEMTAX analysis of HPLC pigment signatures. *Deep. Res. Part II Top. Stud. Oceanogr.* 57, 758–778. doi:10.1016/j.dsr2.2009.06.015

Wu Y, Campbell DA, Irwin AJ, Suggett DJ, Finkel ZV (2014) Ocean acidification enhances the growth rate of larger diatoms. *59(3)*, 1027–1034. <https://doi.org/10.4319/lo.2014.59.3.1027>

Xue L, Cai W-J (2020) Total alkalinity minus dissolved inorganic carbon as a proxy for deciphering ocean acidification mechanisms. *Mar Chem* 222:103791 doi: 10.1016/j.marchem.2020.10379

Zapata M, Rodríguez F, Garrido JL (2000) Separation of chlorophylls and carotenoids from marine phytoplankton: A new HPLC method using a reversed phase C8 column and pyridine-containing mobile phases. *Mar. Ecol. Prog. Ser.* 195: 29–45. doi:10.3354/meps195029

Zeebe RE (2011) Where are you heading Earth? (Commentary) *Nature Geoscience*, 4, 416-417, 2011

Zeebe RE, Wolf-Gladrow DA (2008) Carbon dioxide, dissolved (ocean). *Encyclopedia of Paleoclimatology and Ancient Environments*, Ed. V. Gornitz, Kluwer Academic Publishers, Earth Science Series, 2008.

Zeng J, Nojiri Y, Landschützer P, Telszewski M, Nakaoka S (2014) A Global Surface Ocean f CO₂ Climatology Based on a Feed-Forward Neural Network. *American Meteorological Society*, 31, 1838–1849. <https://doi.org/10.1175/JTECH-D-13-00137.1>

Zhang H, Cao L (2016) Simulated effect of calcification feedback on atmospheric CO₂ and ocean acidification. *Nature Publishing Group*, 1–10. doi:10.1038/srep20284

Zondervan I, Zeebe RE, Rost B, Riebesell U (2001) Decreasing marine biogenic calcification: A negative feedback on rising atmospheric pCO₂. *Global Biogeochem. Cycles* 15(2):507 – 516.

Zwirgmaier K, Jardillier L, Ostrowski M, Mazard S, Garczarek L, Vaultot D (2008). Global phylogeography of marine *Synechococcus*, and *Prochlorococcus* reveals a distinct partitioning of lineages among oceanic biomes. *Environ. Microbiol.* 10:147–161.